# 4
# Special Tensors

In this chapter we will discuss the more important tensors and tensor properties. We begin with zero-rank tensors and work our way through tensors of higher rank. The sequence is essentially chosen according to physical aspects.

## 4.1
## Zero-Rank Tensors

We investigate two types of zero-rank tensors, namely, the intrinsic isotropic properties, such as, e.g., the specific heat at constant hydrostatic pressure, the specific weight and the chemical composition, on the one hand and the spatial mean values of anisotropic properties as well as all other scalar invariants on the other hand. We also look at all differential quotients of these properties with respect to scalar quantities, such as hydrostatic pressure, temperature, and electric potential.

In order to achieve a certain degree of completeness in the discussion of the more important experimental methods, let us consider the comparatively simple measurement methods for the specific weight [1] and the specific heat.

One obtains a precision value of the *specific weight* with a sufficiently accurate measurement of the crystallographic metric given by

$$\rho = \frac{Z \cdot \text{molar weight}}{V \cdot L},$$

where $Z$ is the number of stoichiometric units in the unit cell, $V$ the volume of the elementary cell and $L$ Avogadro's number $6.0222 \times 10^{23}$ molecules per mole. $V$ can normally be determined to a fraction of one-tenth of a percent from high-precision measurements of the lattice constants and thus also the specific weight. Very small crystals with dimensions of about 0.1 mm are suitable for these measurements.

**1**) In practice, the difference between the specific weight and density does not play a role when the weights used for measurement are calibrated in mass units (g).

*Physical Properties of Crystals*. Siegfried Haussühl.

ISBN: 978-3-527-40543-5

Today, such precision measurements are possible within about an hour with the aid of an automatic diffractometer as long as the crystals are homogenous and their chemical composition is reliably known. If problems occur, or if a higher precision is required, one must employ the methods of direct density determination. Here we will discuss the buoyancy method that, especially with large crystals with a weight of at least 10 g, allows the highest accuracy with a relative error of less than $10^{-5}$. If possible, the specimen should be large. It should not possess inclusions and its surface should be smooth and free of impurities. The specimen is first weighed in air and then in a homogenous, practically nonsolvent liquid. It is important to ensure that the surface is completely wetted (no gas bubbles). Let both weights be $G_A$ and $G_L$. The crystal is again weighed in air to check that no loss has occurred due to dissolution. The actual weight $G$ is determined from $G_A$ after the addition of the buoyancy in air, or the buoyancy in the liquid, respectively:

$$G = G_A + \rho_A V_B = G_L + \rho_L V_B.$$

Thus

$$\rho = \frac{G}{V_B} = \frac{G_A}{G_A - G_L}(\rho_L - \rho_A) + \rho_A.$$

$V_B$ is the volume of the body, $\rho_L$ and $\rho_A$ are the specific weights of the liquid and the air, respectively ($\rho_A$ at 293 K and normal pressure is about 1.21 g per liter). In practice, it has been found expedient to use a calibrated standard liquid that remains unchanged over many years, e.g., xylene or petrol. Crystal samples of known density, such as quartz or LiF, are suitable for the measurement of $\rho_L$. For many materials water does not come into consideration, despite its well-known density, because of its good solvent power and the necessity to degas it by boiling before each measurement. Therefore, it is only suitable in special cases. If a pure liquid, with sufficiently low solubility, cannot be found, one can, as a last resort, use a saturated solution of the given crystal.

Measurements with the suspension method, where a liquid composed of two components is mixed such that a specimen just floats in the mixture, as well as pycnometer measurements for powder specimens usually yield inaccurate values, so that these methods are not normally taken into consideration.

Excellent commercial equipment is available for the measurement of the *specific heat* under constant pressure. For precision measurements, as required, e.g., in the determination of the transition enthalpy, an exact and highly sensitive temperature measurement is decisive. Thermistors (semiconductors) where the resistance exhibits an extremely high temperature dependence are well proven for this task. These elements must be calibrated by the experimentalist. This is done appropriately with the help of calibrated quartz thermometers, where the temperature dependence of the resonant frequencies of

$\alpha$-quartz plates is used for the temperature measurement. Temperature differences of up to $10^{-4}$ K can be measured, fulfilling essentially all requirements for a highly precise measurement of the specific heat, provided the crystals are of sufficient size and quality, with weights of at least 0.05 g.

Of the few pseudo scalars playing a role in practical work, we mention the optical activity of isotropic media which will be discussed in more detail in Section 4.3.6.7.

## 4.2
## First-Rank Tensors

### 4.2.1
### Symmetry Reduction

As we have already seen, odd-rank polar tensors vanish in centro-symmetric point symmetry groups. Also in all acentric point symmetry groups, containing the subgroup 22 (22, 42, $\bar{4}2$, 62, 23, 43, $\bar{4}3$), the existence of a first-rank polar tensor is impossible, as is evident from Table 3.2. We also know the effect of 2, $\bar{2}$, and $\bar{2}\bar{2}$ from Table 3.2. Consequently, we have only to check the three- and four-fold rotation axes and rotation–inversion axes and their combinations with 2, $\bar{2}$ and $\bar{2}\bar{2}$. We place these rotation axes parallel to $\boldsymbol{e}_3$. With

$$\boldsymbol{R}_{\pm 3 \| \boldsymbol{e}_3} = \begin{pmatrix} -1/2 & \pm\sqrt{3}/2 & 0 \\ \mp\sqrt{3}/2 & -1/2 & 0 \\ 0 & 0 & 1 \end{pmatrix}$$

one finds $t_1' = t_1 = -1/2\, t_1 \pm \sqrt{3}/2\, t_2$, thus $t_1 = t_2 = 0$. $+$ applies to a clockwise (right) rotation, and $-$ to a counter-clockwise (left) rotation. $t_3' = t_3$ remains as the only independent component. In PSG 32 and $3/\mathrm{m} \equiv \bar{6}$, the two-fold axis and the symmetry plane, respectively, also destroy the existence of $t_3$. All $t_i$ vanish for $\bar{3}$ (Laue-class!).

With

$$\boldsymbol{R}_4 = \begin{pmatrix} 0 & 1 & 0 \\ \bar{1} & 0 & 0 \\ 0 & 0 & 1 \end{pmatrix}$$

one gets $t_1' = t_1 = t_2$, $t_2' = t_2 = -t_1$, and thus $t_1 = t_2 = 0$, which is already a consequence of the two-fold axis parallel to 4. On the other hand $t_3' = t_3$ exists.

In $\bar{4}$ with

$$\boldsymbol{R}_{\bar{4}} = \begin{pmatrix} 0 & \bar{1} & 0 \\ 1 & 0 & 0 \\ 0 & 0 & \bar{1} \end{pmatrix}$$

we have $t_3 = 0$.

With first-rank pseudo tensors, the inversion center provides no reduction. $\bar{2}$ parallel to $\boldsymbol{e}_i$ (symmetry plane perpendicular to $\boldsymbol{e}_i$) only allows the existence of $t_i$. The same component is also preserved by a rotation about $\boldsymbol{e}_i$. Thus first-rank pseudo tensors have the same form in all symmetry groups of type n/m.

Finally, let us discuss the effect of cylindrical symmetry. Here, the rotation through an arbitrary angle $\varphi$ about a fixed axis, running, e.g., parallel to $\boldsymbol{e}_3$, gives rise to a symmetry-equivalent situation. The transformation matrix is

$$\boldsymbol{R}_{\infty} = \begin{pmatrix} \cos\varphi & \sin\varphi & 0 \\ -\sin\varphi & \cos\varphi & 0 \\ 0 & 0 & 1 \end{pmatrix}.$$

Thus $t_1' = t_1 = \cos\varphi\, t_1 + \sin\varphi\, t_2$ for each value of $\varphi$, in other words $t_1 = t_2 = 0$. However, the component $t_3$ does not vanish.

The result of these considerations is noted in Table 4.1. It should be stressed that a polar vector, except in triclinic and monoclinic system, always takes on a distinct orientation, namely that of the given principal axis. The ten PSGs with nonvanishing first-rank polar tensors are called *pyroelectric groups* (1, 2, m, mm, 3, 3m, 4, 4m, 6, 6m).

### 4.2.2 Pyroelectric and Related Effects

As a concrete example we discuss the *pyroelectric effect*. If one heats certain crystals, e.g., tourmaline, in which the effect was first observed, opposite electric charges are generated at certain opposed face elements $\Delta F$. Within a certain temperature interval, one observes, to a first approximation, a linear relationship between the change in charge density and the temperature difference. We describe the electric polarization accompanying a change in charge $\Delta Q$ by the vector

$$\Delta \boldsymbol{P} = K \frac{\Delta Q}{\Delta F} \boldsymbol{f};$$

$\boldsymbol{f}$ is the unit vector of the face normal on $\Delta F$, $K$ is the constant of the given system of measurement (in the MKS system: $K = 1$, in the CGS system: $K = 4\pi$). We compare this quantity to the electric moment $\boldsymbol{M} = KQ\boldsymbol{x}$, where $\boldsymbol{x}$

**Table 4.1** Non-vanishing components of first-rank tensors in the 32 point symmetry groups ($\boldsymbol{t} = t_i \boldsymbol{e}_i$).

| PSG | Polar tensor | Pseudo tensor | PSG | Polar tensor | Pseudo tensor |
|---|---|---|---|---|---|
| 1 | $t_1, t_2, t_3$ | $t_1, t_2, t_3$ | $6 \parallel \boldsymbol{e}_3$ | $t_3$ | $t_3$ |
| $\bar{1}$ | – | $t_1, t_2, t_3$ | 62 | – | – |
| $2 \parallel \boldsymbol{e}_3$ or $\boldsymbol{e}_2$ | $t_3$ or $t_2$ | $t_3$ or $t_2$ | 6m | $t_3$ | – |
| $\mathrm{m} \equiv \bar{2} \parallel \boldsymbol{e}_3$ or $\boldsymbol{e}_2$ | $t_1, t_2$ or $t_1, t_3$ | $t_3$ or $t_2$ | 6/m | – | $t_3$ |
| $2/\mathrm{m} \parallel \boldsymbol{e}_3$ or $\boldsymbol{e}_2$ | – | $t_3$ or $t_2$ | $\bar{6}$ | – | $t_3$ |
| 22 | – | – | $\bar{6}$m | – | – |
| $\bar{2}2 \equiv$ mm2, $2 \parallel \boldsymbol{e}_3$ | $t_3$ | – | 6/mm | – | – |
| 2/mm | – | – | 23 | – | – |
| $3 \parallel \boldsymbol{e}_3$ | $t_3$ | $t_3$ | m3 | – | – |
| 32 | – | – | 43 | – | – |
| 3m | $t_3$ | – | $\bar{4}$3m | – | – |
| $\bar{3}$ | – | $t_3$ | 4/m3 | – | – |
| $\bar{3}$m | – | – | $\infty \parallel \boldsymbol{e}_3$ | $t_3$ | $t_3$ |
| $4 \parallel \boldsymbol{e}_3$ | $t_3$ | $t_3$ | $\infty 2$ | – | – |
| 42 | – | – | $\infty$m | $t_3$ | – |
| 4m | $t_3$ | – | $\infty/\mathrm{m}$ | – | $t_3$ |
| 4/m | – | $t_3$ | $\bar{\infty}$ | – | $t_3$ |
| $\bar{4}$ | – | $t_3$ | $\bar{\infty}$m | – | – |
| $\bar{4}$m | – | – | $\infty/$mm | – | – |
| 4/mm | – | – | | | |

specifies the distance vector of the center of charge on the opposite faces. A rectangular parallelepiped probe with edges $x_i$ parallel to the Cartesian basic vectors $\boldsymbol{e}_i$ then has an electric moment with the components

$$\Delta M_i = K \Delta Q_i x_i,$$

where the charges on the opposed faces are $+\Delta Q_i/2$ and $-\Delta Q_i/2$. The electric moment per volume element is then

$$\frac{\Delta M_i}{\Delta V} = K \frac{\Delta Q_i x_i}{x_i x_j x_k} = K \frac{\Delta Q_i}{\Delta F_i} = \Delta P_i \quad \text{with} \quad \Delta F_i = x_j x_k \quad (i \neq j, k).$$

A change in the electric moment per volume element caused by a change in temperature should be recognized as a change in the electric polarization $\Delta \boldsymbol{P}$.

Thus we describe the pyroelectric properties of a crystal by the relation

$$\Delta P_i = \pi_i \Delta T + \rho_i (\Delta T)^2 + \sigma_i (\Delta T)^3 + \cdots,$$

where the tensors $\{\pi_i\}$, $\{\rho_i\}$, $\{\sigma_i\}$ $\cdots$ give the pyroelectric effect to first-, second-, third- and further-order approximations.

This definition also provides a simple measurement procedure, an aspect, which should be carefully noted with the introduction of any new property. For the practical realization of the measurement of the pyroelectric effect, it is

appropriate to use a plane-parallel thin plate with a rather large diameter-to-thickness ratio. The plate is to be metallized on both sides, where the boundary parts remain free for the purpose of insulation of both electrodes. One now measures the change in charge density after a change in temperature, e.g., with the aid of a commercial charge amplifier or via the electric voltage produced at the electrodes. Note, however, that the dielectric constant of the plate in the direction of the normals must be considered (see Section 4.3.3).

Hence, one directly obtains the longitudinal component of the pyroelectric effect in the direction $\boldsymbol{e}_i'$ of the plate normals. It is

$$\pi_1' = u_{1i}\pi_i.$$

The reference face $F = \pi_i x_i$, a plane perpendicular to the vector $\boldsymbol{\pi} = \pi_i \boldsymbol{e}_i$, represents the longitudinal effect through

$$\pi_1' = F/|\boldsymbol{x}|;$$

on the other hand $F$ is equal to the scalar product of $\boldsymbol{\pi}$ and $\boldsymbol{x}$, thus $\pi_i' = |\boldsymbol{\pi}| \cos\zeta$, where $\zeta$ is the angle between the normals on the reference face (parallel to $\boldsymbol{\pi}$) and $\boldsymbol{x}$. From this, one recognizes the decrease of the pyroelectric effect with increasing deviation from the direction of the maximum effect. Any other form of the test object, e.g., a partially metallized sphere, would result in a complicated relationship between measured quantity and tensor property.

The determination of the pyroelectric effect is possible in all PSGs, except 1 and m, by means of a single measurement along the respective principal axis in which $\boldsymbol{\pi}$ also lies. In PSG 1 we carry out the measurement of the longitudinal effect along three noncoplanar directions $\boldsymbol{e}_j' = u_{ji}\boldsymbol{e}_i$ and get the following system of equations for the determination of the three components $\pi_i$:

$$\begin{aligned}
\pi_1' &= u_{1i}\pi_i, \\
\pi_2' &= u_{2i}\pi_i, \\
\pi_3' &= u_{3i}\pi_i
\end{aligned}$$

(here, the directions $\boldsymbol{e}_i'$ need not be chosen to be orthogonal). The solution is:

$$\boldsymbol{\pi} = \frac{1}{D}\begin{vmatrix} \pi_1' & u_{12} & u_{13} \\ \pi_2' & u_{22} & u_{23} \\ \pi_3' & u_{32} & u_{33} \end{vmatrix}\boldsymbol{e}_1 - \frac{1}{D}\begin{vmatrix} \pi_1' & u_{11} & u_{13} \\ \pi_2' & u_{21} & u_{23} \\ \pi_3' & u_{31} & u_{33} \end{vmatrix}\boldsymbol{e}_2 + \frac{1}{D}\begin{vmatrix} \pi_1' & u_{11} & u_{12} \\ \pi_2' & u_{21} & u_{22} \\ \pi_3' & u_{31} & u_{32} \end{vmatrix}\boldsymbol{e}_3.$$

$D$ is the determinant of the matrix $(u_{ij})$. In PSG $m$, two measurements in directions within the symmetry plane will be sufficient.

The pyroelectric effect consists of two parts: the primary or true pyroelectric effect resulting from a change in the arrangement of dipole moments and the secondary effect, resulting from a change in charge density due to thermal

expansion (see Section 4.3.11). All crystals with large pyroelectric effects, such as triglycine sulfate $(NH_2CH_2COOH)_3H_2SO_4$, and its analogs, where $H_2SO_4$ is substituted by $H_2SeO_4$ or $H_2BeF_4$, and in addition $LiNbO_3$ and $Pb_5Ge_3O_{11}$ also show ferroelectric properties (see Section 4.3.4). Pyroelectric constants of some important crystal species are listed in Table 12.5 (annex).

In the last few years pyroelectric crystals have found special interest in the construction of highly sensitive radiation detectors in all spectral regions, especially for high energy radiation. With the aid of very small crystal plates it is possible to count individual photons (even in the visible spectral range) and from the magnitude of the pyroelectric effect to measure the energy of the photons (energy discrimination). A further application is possible in connection with the conversion of thermal energy into electrical energy when the charges appearing due to a temperature change are collected and stored. For example, the natural day–night temperature variations, which can be artificially modulated by suitable control processes, offer a simple and cheap inducing source. The efficiency, i.e., that fraction of the required heat input per heating cycle, that can be converted into electrical energy, is at present still under 1%. If one could succeed in finding crystals with substantially larger effects, a broad commercial utilization of the pyroelectric effect to generate electrical energy would be conceivable, provided production and processing costs are sufficiently low.

Further examples of first-rank tensors are the piezoelectric effect under hydrostatic pressure $\Delta p$ as well as both analogous magnetic effects:

$B_i = \beta_i \Delta T$ pyromagnetic effect and
$B_i = \gamma_i \Delta p$ piezomagnetic effect.

$\{\beta_i\}$ and $\{\gamma_i\}$ are pseudo tensors, of which at present no reliable results are known.

## 4.3
## Second-Rank Tensors

### 4.3.1
### Symmetry Reduction

First we want to gain a general view of the form of the polar tensors and the pseudo tensors in all point symmetry groups. We choose the Cartesian reference system according to the convention introduced in Section 2.2. With the polar tensors of even rank it is sufficient to discuss only the 11 Laue groups due to their centrosymmetric behavior. Pseudo tensors of even rank vanish in the Laue groups. In the enantiomorphic PSGs they take on the same form as

**Table 4.2** Non-vanishing components of second-rank tensors in standard setting.

| PSG | Polar tensor | Pseudo tensor |
|---|---|---|
| 1 | $t_{ij},\ i,j=1,2,3$ | $t_{ij},\ i,j=1,2,3$ |
| $\bar{1}$ | $t_{ij},\ i,j=1,2,3$ | – |
| $2 \parallel e_2$ | $t_{11}, t_{22}, t_{33}, t_{13}, t_{31}$ | $t_{11}, t_{22}, t_{33}, t_{13}, t_{31}$ |
| $\bar{2} \parallel e_2$ | $t_{11}, t_{22}, t_{33}, t_{13}, t_{31}$ | $t_{12}, t_{21}, t_{23}, t_{32}$ |
| $2/\mathrm{m} \parallel e_2$ | $t_{11}, t_{22}, t_{33}, t_{13}, t_{31}$ | – |
| 22 | $t_{11}, t_{22}, t_{33}$ | $t_{11}, t_{22}, t_{33}$ |
| mm2 | $t_{11}, t_{22}, t_{33}$ | $t_{12}, t_{21}$ |
| 2/mm | $t_{11}, t_{22}, t_{33}$ | – |
| $3 \parallel e_3$ | $t_{11}=t_{22}, t_{33}, t_{12}=-t_{21}$ | $t_{11}=t_{22}, t_{33}, t_{12}=-t_{21}$ |
| 32 | $t_{11}=t_{22}, t_{33}$ | $t_{11}=t_{22}, t_{33}$ |
| 3m | $t_{11}=t_{22}, t_{33}$ | $t_{12}=-t_{21}$ |
| $\bar{3}$ | $t_{11}=t_{22}, t_{33}, t_{12}=-t_{21}$ | – |
| $\bar{3}$m | $t_{11}=t_{22}, t_{33}$ | – |
| $4 \parallel e_3$ | $t_{11}=t_{22}, t_{33}, t_{12}=-t_{21}$ | $t_{11}=t_{22}, t_{33}, t_{12}=-t_{21}$ |
| 42 | $t_{11}=t_{22}, t_{33}$ | $t_{11}=t_{22}, t_{33}$ |
| 4m | $t_{11}=t_{22}, t_{33}$ | $t_{12}=-t_{21}$ |
| 4/m | $t_{11}=t_{22}, t_{33}, t_{12}=-t_{21}$ | – |
| $\bar{4}$ | $t_{11}=t_{22}, t_{33}, t_{12}=-t_{21}$ | $t_{11}=-t_{22}, t_{12}=t_{21}$ |
| $\bar{4}$m, $2 \parallel e_1$ | $t_{11}=t_{22}, t_{33}$ | $t_{11}=-t_{22}$ |
| 4/mm | $t_{11}=t_{22}, t_{33}$ | – |
| $6 \parallel e_3, \infty \parallel e_3$ | $t_{11}=t_{22}, t_{33}, t_{12}=-t_{21}$ | $t_{11}=t_{22}, t_{33}, t_{12}=-t_{21}$ |
| $62, \infty 2$ | $t_{11}=t_{22}, t_{33}$ | $t_{11}=t_{22}, t_{33}$ |
| $6\mathrm{m}, \infty\mathrm{m}$ | $t_{11}=t_{22}, t_{33}$ | $t_{12}=-t_{21}$ |
| $6/\mathrm{m}, \infty/\mathrm{m}$ | $t_{11}=t_{22}, t_{33}, t_{12}=-t_{21}$ | – |
| $\bar{6}, \overline{\infty}$ | $t_{11}=t_{22}, t_{33}, t_{12}=-t_{21}$ | – |
| $\bar{6}\mathrm{m}, \overline{\infty}\mathrm{m}$ | $t_{11}=t_{22}, t_{33}$ | – |
| $6/\mathrm{mm}, \infty/\mathrm{mm}$ | $t_{11}=t_{22}, t_{33}$ | – |
| 23 | $t_{11}=t_{22}=t_{33}$ | $t_{11}=t_{22}=t_{33}$ |
| m3 | $t_{11}=t_{22}=t_{33}$ | – |
| 43 | $t_{11}=t_{22}=t_{33}$ | $t_{11}=t_{22}=t_{33}$ |
| $\bar{4}3$ | $t_{11}=t_{22}=t_{33}$ | – |
| 4/m3 | $t_{11}=t_{22}=t_{33}$ | – |
| isotropic without $\bar{1}$ | $t_{11}=t_{22}=t_{33}$ | $t_{11}=t_{22}=t_{33}$ |
| isotropic with $\bar{1}$ | $t_{11}=t_{22}=t_{33}$ | – |

the polar tensors. Thus we have to study only the 11 enantiomorph PSG's (1, 2, 22, 3, 32, 4, 42, 6, 62, 23, 43) for all even-rank tensors and, in addition, the remaining ten non-Laue groups (m, 2m = mm, 3m, 4m, $\bar{4}$, $\bar{4}$m, 6m, $\bar{6}$, $\bar{6}$m, $\bar{4}$3) for even-rank pseudo tensors.

We now show the symmetry reduction for the most important PSG's. The reader can handle all other cases with ease. A complete survey of all second-rank tensors is given in Table 4.2. For better clarity, it is often useful to write the components of a second-rank tensor in matrix notation, thus

$$\{t_{ij}\} = \begin{pmatrix} t_{11} & t_{12} & t_{13} \\ t_{21} & t_{22} & t_{23} \\ t_{31} & t_{32} & t_{33} \end{pmatrix}.$$

**Monoclinic System (PSG 2, m = $\bar{2}$, 2/m)**

The effect of two-fold rotation axes and rotation–inversion axes parallel to $\boldsymbol{e}_i$ for polar tensors of even rank was previously discussed in Section 3.8.2. The result is: the indices $i$ may only occur with even numbers.

We choose the standard setting $\boldsymbol{e}_2 \parallel \boldsymbol{a}_2$ parallel to the two-fold rotation axis or rotation–inversion axis, respectively (normal on the mirror plane). Thus for polar tensors there exists only the following five components containing the index 2 even numbered: $t_{11}$, $t_{22}$, $t_{33}$, $t_{13}$ and $t_{31}$. With a symmetric tensor we have $t_{13} = t_{31}$ (four independent components). For a pseudo-tensor $\{t_{ij}\}$ in PSG 2 there exists no difference to a polar tensor. This is not the case in PSG m. Using the transformation condition for pseudo tensors we have

$$t'_{ii} = t_{ii} = -t_{ii}, \quad t'_{12} = t_{12}, \quad t'_{21} = t_{21}, \quad t'_{13} = t_{13} = -t_{13},$$
$$t'_{31} = t_{31} = -t_{31} \quad \text{as well as} \quad t'_{23} = t_{23} \quad \text{and} \quad t'_{32} = t_{32}.$$

Thus all tensor components vanish in PSG m except $t_{12}$, $t_{21}$, $t_{23}$, and $t_{32}$. Polar tensors and pseudo tensors show complementary forms in PSG m.

**Orthorhombic System (PSG 22, mm, 2/mm)**

In the standard setting $\boldsymbol{e}_i \parallel \boldsymbol{a}_i$ only such components exist in PSG 22 where the indices 1 and 2 (and hence 3) occur an even number of times, namely $t_{11}$, $t_{22}$, and $t_{33}$.

In PSG mm one gets for the pseudo tensors in the standard setting ($\boldsymbol{e}_1$ and $\boldsymbol{e}_2$ perpendicular to the symmetry planes) only the two nonvanishing components $t_{12}$ and $t_{21}$.

**Trigonal System (PSG 3, 32, 3m, $\bar{3}$, $\bar{3}$m)**

The three-fold rotation axis or rotation–inversion axis may run parallel to $\boldsymbol{e}_3$. The respective symmetry operations are

$$\boldsymbol{R}_{\pm 3 \parallel e_3} = \begin{pmatrix} -1/2 & \pm\sqrt{3}/2 & 0 \\ \mp\sqrt{3}/2 & -1/2 & 0 \\ 0 & 0 & 1 \end{pmatrix}$$

and

$$\boldsymbol{R}_{\pm \bar{3} \parallel e_3} = \begin{pmatrix} 1/2 & \mp\sqrt{3}/2 & 0 \\ \pm\sqrt{3}/2 & 1/2 & 0 \\ 0 & 0 & \bar{1} \end{pmatrix}.$$

The signs $+$ and $-$ designate a clockwise or anti-clockwise rotation, respectively.

The conditions for polar tensors in the case of a three-fold rotation axis are

$$t'_{11} = t_{11} = 1/4\, t_{11} + 3/4\, t_{22} \mp \sqrt{3}/4(t_{12} + t_{21})$$
$$t'_{22} = t_{22} = 3/4\, t_{11} + 1/4\, t_{22} \pm \sqrt{3}/4(t_{12} + t_{21})$$
$$t'_{23} = t_{23} = -1/2\, t_{23} \mp \sqrt{3}/2\, t_{13}$$
$$t'_{13} = t_{13} = -1/2\, t_{13} \pm \sqrt{3}/2\, t_{23}$$

(and analogous equations for $t'_{32}$ and $t'_{31}$),

$$t'_{33} = t_{33}.$$

The result must be independent of the direction of rotation. Thus the terms with alternating signs vanish. For the PSG's 3 and $\bar{3}$ it follows that $(t_{12} + t_{21}) = t_{23} = t_{13} = t_{32} = t_{31} = 0$. Consequently, the following tensor components exist: $t_{11} = t_{22}$, $t_{33}$, and $t_{12} = -t_{21}$.

The PSG 32 with the two-fold axis parallel to $\boldsymbol{e}_1$ (standard setting) also requires $t_{12} = t_{21} = 0$ (index 1 must occur even numbered!). If $\boldsymbol{e}_1$ is not placed along the two-fold axis, but anywhere perpendicular to the three-fold axis, one obtains the same result.

Pseudo tensors of PSG 3m must simultaneously satisfy the conditions for PSG 3 and PSG m. Hence only the components $t_{12}$ and $t_{21}$ remain with $t_{12} = -t_{21}$.

#### Tetragonal System (PSG 4, 4/m, 42, 4m, $\bar{4}$, $\bar{4}$m, 4/mm)

The symmetry operations of the four-fold rotation axis or rotation–inversion axis parallel to $\boldsymbol{e}_3$ are

$$\boldsymbol{R}_{\pm 4 \| \boldsymbol{e}_3} = \begin{pmatrix} 0 & \pm 1 & 0 \\ \mp 1 & 0 & 0 \\ 0 & 0 & 1 \end{pmatrix} \quad \text{and} \quad \boldsymbol{R}_{\pm \bar{4} \| \boldsymbol{e}_3} = \begin{pmatrix} 0 & \mp 1 & 0 \\ \pm 1 & 0 & 0 \\ 0 & 0 & \bar{1} \end{pmatrix}.$$

Since the operations 4 and $\bar{4}$ also contain a two-fold axis parallel to $\boldsymbol{e}_3$, it suffices to consider only the tensor components containing the index 3 even numbered, namely $t_{11}$, $t_{22}$, $t_{33}$, $t_{12}$, and $t_{21}$. For polar tensors of PSG 4 the transformation gives

$$t'_{11} = t_{11} = t_{22}, \quad t'_{22} = t_{22} = t_{11}, \quad t'_{33} = t_{33} \quad \text{and} \quad t'_{12} = t_{12} = -t_{21}.$$

Accordingly, only three independent components exist: $t_{11} = t_{22}$, $t_{33}$, and $t_{12} = -t_{21}$. 2 or $\bar{2} \equiv$ m parallel to $\boldsymbol{e}_1$ causes $t_{12}$ to vanish.

Pseudo tensors of PSG 4m fulfill the conditions for PSG 4 as well as for PSG mm. Hence only $t_{12} = -t_{21}$ remain as nonvanishing components. Pseudo tensors of PSG $\bar{4}$ are subject to the conditions $t_{11} = -t_{22}$, $t_{33} = 0$, $t_{12} = t_{21}$,

$t_{23} = t_{13} = t_{32} = t_{31} = 0$. The PSG $\bar{4}$m ($\equiv \bar{4}2$m) contains the subgroup 22, thus of those components existing in PSG $\bar{4}$ only $t_{11} = -t_{22} \neq 0$ remain. If we chose the base vectors $\boldsymbol{e}'_1$ and $\boldsymbol{e}'_2$ perpendicular to the symmetry planes, only the components $t'_{12}$ and $t'_{21}$ with $t'_{12} = t'_{21}$ would exist.

#### Hexagonal System (PSG 6, 6/m, 62, 6m, $\bar{6}$, $\bar{6}$m, 6/mm)

Since a six-fold axis is equivalent to two- and three-fold axes with the same orientation, the symmetry reduction can be considerably simplified. In PSG 6, the conditions for the subgroups 2 and 3 in the case of polar tensors result in the following independent components: $t_{11} = t_{22}$, $t_{33}$, $t_{12} = -t_{21}$. In PSG 62, $t_{12}$ vanishes with $\boldsymbol{e}_1$ parallel to the two-fold axis (index 1 odd-numbered occurence).

For pseudo tensors of PSG 6m, the symmetry plane perpendicular to $\boldsymbol{e}_1$ demands: $t_{ii} = 0$, $t_{12} = -t_{21}$. Pseudo tensors in PSG $\bar{6} \equiv 3/\mathrm{m}$ and $\bar{6}$m do not exist, because the subgroup m (normals of the symmetry plane parallel to $\boldsymbol{e}_3$) only allows components to exist containing the index 3 once. The three-fold axis does not allow such components, as we have seen.

#### Cubic System (PSG 23, m3, $\bar{4}3$, 43, m3m)

The three-fold axis common to all cubic PSG's is represented by

$$\boldsymbol{R}_{3\|[111]} = \begin{pmatrix} 0 & 1 & 0 \\ 0 & 0 & 1 \\ 1 & 0 & 0 \end{pmatrix}.$$

Since all cubic PSG's contain the subgroup 22, only the components $t_{ii}$ can appear. These are transformed into each other by the three-fold axis so that only one independent component $t_{11} = t_{22} = t_{33}$ is possible. With polar tensors, addition of further symmetry operations does not result in new conditions. The pseudo tensors vanish totally in PSG $\bar{4}3$, because the operation $\bar{4}$ with the condition $t_{11} = -t_{22}$ contradicts the relation $t_{11} = t_{22} = t_{33}$.

Furthermore, all cubic crystals behave like isotropic substances with respect to second-rank tensor properties. In particular, a pure longitudinal effect exists in all directions.

The case of the cylindrical symmetry groups is homologous to the situation in the corresponding PSG's of the hexagonal system (see Exercise 4).

### 4.3.2
### Tensor Quadric, Poinsots Construction, Longitudinal Effects, Principal Axes' Transformation

The quadric $t_{ij}x_ix_j = F$ is fixed by the six independent quantities $t_{11}$, $t_{22}$, $t_{33}$, $t_{12} + t_{21}$, $t_{13} + t_{31}$, $t_{23} + t_{32}$. They completely represent the symmetrical part of a second-rank tensor. As we shall see, almost all important second-

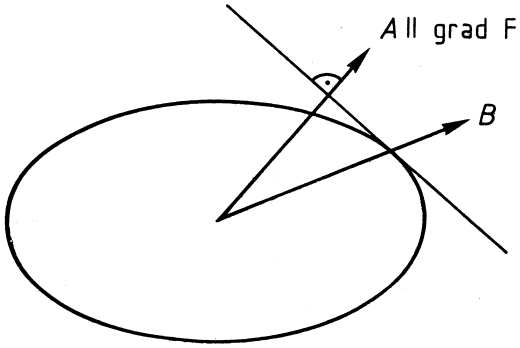


**Figure 4.1** Poinsot construction. The tangent plane to the ellipsoid stands perpendicular to the plane of projection.

rank tensors are symmetric. The representation quadric provides an instructive geometric visualization of the tensor in a way which cannot be achieved with higher rank tensors. In the following, we assume a certain knowledge concerning the form of these second-order surfaces (ellipsoids, hyperboloids, paraboloids, spheres, cylinders, and their degeneracies). Let the tensor $\{t_{ij}\}$ operate on the vectors $\boldsymbol{A}$ and $\boldsymbol{B}$ according to $A_i = t_{ij}B_j$. With symmetric tensors, one can then recognize the position of the vector $\boldsymbol{A}$ with known $\boldsymbol{B}$ from the quadric with the help of the *Poinsot construction*. Let the vector $\boldsymbol{B}$, starting at the origin of the coordinate system, intercept the quadric at point $P$ (Fig. 4.1). We imagine the tangent plane drawn at this point on the quadric. The normal on this tangent plane then runs parallel to the wanted vector $\boldsymbol{A}$. The proof for this relationship is as follows: We first consider the differential $\Delta F = (dF/dx_i)\,\Delta x_i$, the first-order approximation of the Taylor expansion of $F$ with respect to the coordinates $x_i$. We can write $\Delta F$ as a scalar product:

$$\Delta F = \operatorname{grad} F \cdot \Delta \boldsymbol{x} = (\operatorname{grad} F)_i \Delta x_i,$$

where $\operatorname{grad} F$ (read "Gradient F") denotes the vector $(dF/dx_i)\,\boldsymbol{e}_i$. If the end point of the vector $\boldsymbol{x} + \Delta\boldsymbol{x}$ also lies in the quadric, then $\Delta\boldsymbol{x}$ is parallel to the tangential plane, thus $\Delta F = 0$ and hence the scalar product $\operatorname{grad} F \cdot \Delta\boldsymbol{x} = 0$. Therefore $\operatorname{grad} F$ is perpendicular to the quadric and thus runs parallel to the normal on the tangent plane. From $F = t_{ij}x_ix_j$ one gets $dF/dx_i = 2t_{ij}x_j$. Because $\boldsymbol{x} = c\boldsymbol{B}$ ($c$ is a constant) we have $(\operatorname{grad} F)_i = 2ct_{ij}B_j = 2cA_i$, thus $\operatorname{grad} F = 2c\boldsymbol{A}$.

A second important property of the quadric is to read for every direction the corresponding longitudinal effect. As shown in Section 3.10, for any arbitrary direction $\boldsymbol{e}'_i$, the corresponding longitudinal effect is $t'_{ii} = F|\boldsymbol{x}|^{-2}$. The vector $\boldsymbol{x}$ runs from the origin, in the direction $\boldsymbol{e}'_i$, to point $P$ on the quadric.

The complete measurement of symmetric second-rank tensors or the symmetric part of second-rank tensors is possible with the help of longitudinal effects. These possess the advantage that they can be easily measured in practice with sufficient accuracy. Let us demonstrate the procedure on the general example of a symmetric tensor in the triclinic system. The tensor is represented in the crystal-physical reference system by the basic vectors $\boldsymbol{e}_i$. The measurement of the longitudinal effect along $\boldsymbol{e}_i$ leads directly to the components $t_{ii}$ ($t_{11}$, $t_{22}$, $t_{33}$). Further measurements of longitudinal effects along the bisectors of any two basic vectors, that is, in the direction $\boldsymbol{e}'_{i\pm} = \sqrt{2}/2(\boldsymbol{e}_j \pm \boldsymbol{e}_k)$ with $i \neq j, k$ and $i, j, k$ cyclic, deliver the longitudinal effects

$$t'_{ii\pm} = \tfrac{1}{2}(t_{jj} + t_{kk}) \pm t_{jk}$$

(application of the transformation formula). The unknown components $t_{jk}$ are found from

$$t'_{ii+} - t'_{ii-} = 2t_{jk}.$$

The sums $t'_{ii+} + t'_{ii-} = t_{jj} + t_{kk}$ allow a control of the first series of measurements. Hence, all six independent components can be determined. Since the three principal components $t_{11}$, $t_{22}$, and $t_{33}$ are already known from the measurements along $\boldsymbol{e}_i$, only a few measurements are needed in the direction of the bisectors to obtain $t_{jk}$. In another version, only the longitudinal effects along the six different bisectors are used. Of course, one can also choose longitudinal effects in other directions. The evaluation is then less transparent. We will come to concrete examples later. The measurement of the asymmetric part of a second-rank tensor is not possible without the inclusion of transverse effects.

A transformation of the reference system can bring a second-order surface into a special position in which all geometric parameters are directly evident. This is the *principal axes' transformation*. In such a principal axes' reference system, the longitudinal effects along the basic vectors of the reference system take on extreme values. An equivalent statement is that in the direction of the basic vectors pure longitudinal effects appear, i.e., no transverse effects occur when the inducing quantities act along these basic vectors. The condition for a pure longitudinal effect in the tensor relation $A_i = t_{ij}B_j$ is $A_i = \lambda B_i$, where $\lambda$ is the corresponding longitudinal effect (eigenvalue). Hence one obtains three equations $A_i = \lambda B_i = t_{ij}B_j$ for $i = 1, 2, 3$ or $(t_{ij} - \lambda\delta_{ij})B_j = 0$, where $\delta_{ij}$ is the Kronecker symbol.

For the calculation of the extreme values of the longitudinal effect, which are connected with the square of the radius vector $\boldsymbol{x}$ of the quadric $F = t_{ij}x_ix_j$, we construct, according to the rules of variational calculus, an auxiliary function $H = F - \lambda\boldsymbol{x}^2$, which also takes on an extreme value, as long as $F$ remains constant. That is, the end point of $\boldsymbol{x}$ lies on the quadric and in addition, $\boldsymbol{x}^2$

itself takes on an extreme value. $\lambda$ is still an open factor, not dependent on $\boldsymbol{x}$, a so-called Lagrangian multiplier. The condition for an extreme value is then $\partial H/\partial x_i = 0$, thus

$$\frac{\partial H}{\partial x_i} = \frac{\partial F}{\partial x_i} - \lambda 2x_i = 2t_{ij}x_j - 2\lambda x_i = 0 \;\text{ for }\; i = 1,2,3,$$

where we here assume $\{t_{ij}\}$ to be a symmetric tensor. We write this system of three linear equations in the form $(t_{ij} - \lambda\delta_{ij})x_j = 0$. These conditions are identical with those of a pure longitudinal effect. The system with $\boldsymbol{x} \neq 0$ only has a solution when the associated determinant vanishes, that is

$$\begin{vmatrix} t_{11}-\lambda & t_{12} & t_{13} \\ t_{12} & t_{22}-\lambda & t_{23} \\ t_{13} & t_{23} & t_{33}-\lambda \end{vmatrix} = 0.$$

We obtain a third-order equation in $\lambda$, the so-called characteristic equation. It is an invariant, as one recognizes from the transformation behavior of determinants. In particular, the coefficients of the characteristic equation are also scalar invariants of the tensor, i.e., quantities that assume the same value in any arbitrary Cartesian reference system. The characteristic equation possesses three solutions specified by $\lambda_1$, $\lambda_2$, and $\lambda_3$. Written out, the characteristic equation is

$$-\lambda^3 + \lambda^2(t_{11}+t_{22}+t_{33}) - \lambda(-t_{23}^2 + t_{22}t_{33} - t_{13}^2 + t_{11}t_{33} - t_{12}^2 + t_{11}t_{22}) + |t_{ij}| = 0,$$

where $|t_{ij}|$ stands for the determinant of the matrix of the tensor components. From the alternative writing of the characteristic equation in the form $(\lambda_1 - \lambda)(\lambda_2 - \lambda)(\lambda_3 - \lambda) = 0$ we see that the three invariants have the following form:

$$\begin{aligned} I_1 &= t_{11}+t_{22}+t_{33} &&= \lambda_1+\lambda_2+\lambda_3, \\ I_2 &= t_{11}t_{22}+t_{22}t_{33}+t_{11}t_{33}-t_{12}^2-t_{13}^2-t_{23}^2 &&= \lambda_1\lambda_2+\lambda_2\lambda_3+\lambda_1\lambda_3, \\ I_3 &= |t_{ij}| &&= \lambda_1\lambda_2\lambda_3. \end{aligned}$$

The solution of the characteristic equation can be quickly found with the aid of an iteration method using the prescription $A_i^{(n+1)} = t_{ij}A_j^{(n)}$ which produces the new vector $\boldsymbol{A}^{(n+1)}$ of the next iteration step from the vector $\boldsymbol{A}^{(n)}$. For increasing $n$, $\boldsymbol{A}^{(n+1)}$ more closely approaches a direction with an extreme radius vector of the quadric, as one can read from the Poinsot construction. With this method, one obtains the direction for the maximum longitudinal effect. In practice, this is today naturally carried out with the help of a personal computer, which gives the solutions in a few seconds. For each eigenvalue $\lambda$

one obtains the direction of the associated basic vector (eigenvector) from the system of equations according to

$$x_1 : x_2 : x_3 =$$
$$[(t_{22} - \lambda)(t_{33} - \lambda) - t_{23}^2] : [(t_{23}t_{13} - t_{12}(t_{33} - \lambda)] : [t_{12}t_{23} - t_{13}(t_{22} - \lambda)].$$

This follows from the representation of our system of equations in the form of scalar products of the vector $\boldsymbol{x}$ with the vectors $\boldsymbol{C}_i$, having the components $C_{ij} = t_{ij} - \lambda\delta_{ij}$. We have $\boldsymbol{C}_i \cdot \boldsymbol{x} = 0$ for $i = 1, 2, 3$, i.e., $\boldsymbol{x}$ is perpendicular to the vectors $\boldsymbol{C}_i$ and thus runs parallel to one of the vector products of two of these vectors $\boldsymbol{C}_i$. The above proportionality results from $\boldsymbol{x} \parallel \boldsymbol{C}_2 \times \boldsymbol{C}_3$. The directions of the extreme values are mutually perpendicular. This is recognized as follows: Let $\lambda'$ and $\lambda''$ be two arbitrary eigenvalues of the characteristic equation and $\boldsymbol{x}'$ and $\boldsymbol{x}''$ the associated eigenvectors. We then have the equations

$$t_{ij}x_j' - \lambda' x_i' = 0, \quad t_{ij}x_j'' - \lambda'' x_i'' = 0.$$

We multiply the $i$th equation of the first system with $x_i''$, the second with $x_i'$, sum the three equations and get

$$t_{ij}x_j'x_i'' - \lambda' x_i'x_i'' = 0 \quad \text{and} \quad t_{ij}x_j''x_i' - \lambda'' x_i''x_i' = 0.$$

We form the difference of these expressions and note that

$$t_{ij}x_j'x_i'' = t_{ij}x_j''x_i' \qquad (\text{because } t_{ij} = t_{ji});$$

thus

$$(\lambda' - \lambda'')x_i'x_i'' = 0.$$

If $\lambda' \neq \lambda''$, it follows that

$$x_i'x_i'' = \boldsymbol{x}' \cdot \boldsymbol{x}'' = 0;$$

therefore the eigenvectors $\boldsymbol{x}'$ and $\boldsymbol{x}''$ are mutually perpendicular. If we place the basic vectors of our Cartesian reference system parallel to these eigenvectors, the transverse components $t_{ij}'$ $(i \neq j)$ vanish and the relationship between the vectors $\boldsymbol{A}$ and $\boldsymbol{B}$ is $A_i = t_{ii}'B_i$ with $t_{ii}' = \lambda_i$. This means that the physical efficacy of a symmetric second-rank tensor is fully described by the three eigenvalues (also called principal values) when, in addition, the position of the principal axes (eigenvectors) of the tensor in the crystal-physical system is known.

The symmetry properties of crystals also determine of course, according to Neumann's principle, the form and position of the quadric in the crystal. For example, the quadric of all second-rank tensors with a three-, four-

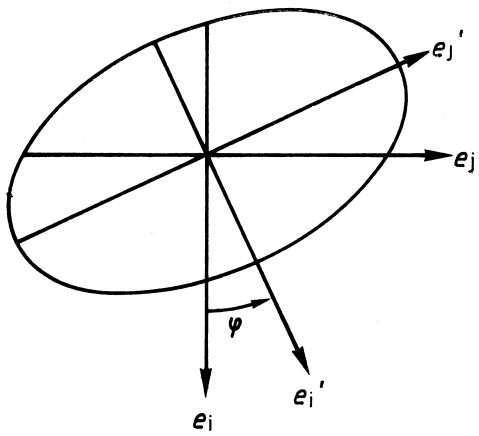


**Figure 4.2** Principal axes transformation within a plane perpendicular to $e_k$.

or six-fold rotation- or rotation–inversion axis possesses rotational symmetry with just this symmetry axis as the rotation axis. In the orthorhombic system, the principal axes of the quadric run parallel to the basic directions of the orthorhombic system (parallel to the two-fold rotation- or rotation–inversion axes respectively). Furthermore, the arrangement of the crystals, as based on the specifications in Table 4.2, corresponds in all systems, except the triclic and monoclinic, to the principal axes' system of second-rank tensors.

Of special practical importance is the *plane principal axis transformation*. We consider a cut through the quadric perpendicular to the basic vector $\boldsymbol{e}_k$. An example of such a cut is represented by the ellipse in Fig. 4.2. The other two basic vectors $\boldsymbol{e}'_i$ and $\boldsymbol{e}'_j$ shall be placed parallel to the principal axes of the given sectional plane by a rotation of an angle $\varphi$ (positive in the clockwise direction looking along $\boldsymbol{e}_k$!) about $\boldsymbol{e}_k$. The transformation formulae are

$$\boldsymbol{e}'_i = \cos\varphi\,\boldsymbol{e}_i + \sin\varphi\,\boldsymbol{e}_j, \quad \boldsymbol{e}'_j = -\sin\varphi\,\boldsymbol{e}_i + \cos\varphi\,\boldsymbol{e}_j, \quad \boldsymbol{e}'_k = \boldsymbol{e}_k.$$

The principal axis position is reached when the tensor components $t'_{ij}$ $(i \neq j)$ vanish. For a symmetric tensor we get by tensor transformation

$$\begin{aligned} t'_{ii} &= \cos^2\varphi\, t_{ii} + \sin^2\varphi\, t_{jj} + 2\sin\varphi\cos\varphi\, t_{ij} \\ t'_{jj} &= \sin^2\varphi\, t_{ii} + \cos^2\varphi\, t_{jj} - 2\sin\varphi\cos\varphi\, t_{ij} \\ t'_{ij} &= -\sin\varphi\cos\varphi\, t_{ii} + \sin\varphi\cos\varphi\, t_{jj} + (\cos^2\varphi - \sin^2\varphi)t_{ij} \end{aligned}$$

(with $t_{ij} = t_{ji}$).

With $2\sin\varphi\cos\varphi = \sin 2\varphi$ and $\cos^2\varphi - \sin^2\varphi = \cos 2\varphi$, we have from the condition $t'_{ij} = 0$ the angle of rotation

$$\tan 2\varphi = \frac{2t_{ij}}{t_{ii} - t_{jj}}.$$

From this and with the help of the relations

$$\cos^2\varphi = \frac{1+\cos 2\varphi}{2} \quad \text{and} \quad \sin^2\varphi = \frac{1-\cos 2\varphi}{2}$$

one finds

$$t'_{ii} = \frac{t_{ii}+t_{jj}}{2} + \frac{t_{ij}}{\sin 2\varphi},$$
$$t'_{jj} = \frac{t_{ii}+t_{jj}}{2} - \frac{t_{ij}}{\sin 2\varphi}.$$

It is also interesting that with each arbitrary rotation about the axis $\boldsymbol{e}_k$ the sum of the principal components remains constant: $t'_{ii} + t'_{jj} = t_{ii} + t_{jj}$. In the monoclinic system, plane and general principal axes' transformations are identical, if $\boldsymbol{e}_k$ is laid parallel to 2 or $\bar{2}$, respectively. Examples will follow in the following sections.

### 4.3.3
### Dielectric Properties

An electric field induces in matter a charge displacement described by the electric polarization $\boldsymbol{P}$ which we introduced previously. The electric field is represented by the vector of the electric field strength. This points into the direction of the force $\boldsymbol{K}$ experienced by a positive electric point charge $q$ in the electric field according to $\boldsymbol{K} = q\boldsymbol{E}$. The relationship between the electric charge density and the electric field strength in a plate capacitor leads us to the vector of the electric displacement. One plate of the capacitor with the surface $F$ and charge $Q$ possesses a charge density of $Q/F$ (ignoring boundary effects). The vector $\boldsymbol{D} = K\frac{Q}{F}\boldsymbol{e}$ perpendicular to the plate, where $\boldsymbol{e}$ specifies the surface normal of the plate, is in this case the vector of electric displacement. $K$ is a constant dependent on the system of units (MKSA system: $K = 1$; cgs system: $K = 4\pi$). The field strength $\boldsymbol{E}$ takes on the same direction. Inside the capacitor the field strength is practically constant, so that the potential difference of a unit charge on one plate in relation to the charge on the opposite plate is

$$U = \int_{x_1}^{x_2} \boldsymbol{E}\cdot d\boldsymbol{x} = |\boldsymbol{E}|d,$$

where $d$ is the distance between the plates. The electric voltage $U$ at the capacitor determines the field strength. The charge $Q$ and thus the magnitude

of the electric displacement is proportional to the applied voltage, as one can demonstrate experimentally as well as by a simple consideration of electrostatics. Accordingly, in vacuum $\boldsymbol{D}$ and $\boldsymbol{E}$ are parallel, hence $\boldsymbol{D} = \epsilon_0 \boldsymbol{E}$. The quantity $\epsilon_0$ is called the absolute dielectric constant. Its numerical value in the MKSA system is

$$\epsilon_0 = \frac{1}{4\pi \cdot c^2} 10^7 = 8.854 \times 10^{-12} \mathrm{AsV^{-1}m^{-1}}$$

($c$ is the velocity of light in vacuum $2.998 \times 10^8 \mathrm{ms^{-1}}$); in the cgs system

$$\epsilon_0 = 1 \quad \text{(dimensionless)}.$$

If we now place an isotropic medium between the plates, $\boldsymbol{D}$ and $\boldsymbol{E}$ remain parallel. The total electric displacement is determined by the contribution of the polarization of the medium and we have the relationship $\boldsymbol{D} = \epsilon_0 \boldsymbol{E} + \boldsymbol{P}$. Since, to a first approximation, $\boldsymbol{P}$ may be considered as proportional to the electric field, we can write $\boldsymbol{D} = \epsilon \boldsymbol{E}$ with $\boldsymbol{P} = (\epsilon - \epsilon_0)\boldsymbol{E}$. We call $\epsilon$ the absolute dielectric constant of the given isotropic medium. It is useful to refer $\epsilon$ to the value of the vacuum constant $\epsilon_0$. $\epsilon_{\mathrm{rel}} = \epsilon/\epsilon_0$ is the relative dielectric constant (DC). Sometimes it is advantageous to use the relation $\boldsymbol{P} = \chi \epsilon_0 \boldsymbol{E}$. $\chi$ is called the electric susceptibility. With the above relation we have $\chi = \epsilon_{\mathrm{rel}} - 1$.

In anisotropic media, instead of $\boldsymbol{D} = \epsilon \boldsymbol{E}$ we must introduce the general vector function $D_i = \epsilon_{ij} E_j$. $\{\epsilon_{ij}\}$ is the *dielectric tensor*. $\{\epsilon_{ij}\}$ is symmetric, as one can recognize from the energy density $W_{\mathrm{el}}$ of the electric field in a plate capacitor.

A change in the electric displacement $\Delta D_i$ leads to a reversible change of the energy density

$$\Delta W_{\mathrm{el}} = E_i \Delta D_i = \epsilon_{ij} E_i \Delta E_j;$$

hence

$$\frac{\partial W_{\mathrm{el}}}{\partial E_j} = \epsilon_{ij} E_i.$$

The total energy density is

$$W_{\mathrm{el}} = \int E_i dD_i = \int E_i \epsilon_{ij} dE_j = \frac{1}{2} \epsilon_{ij} E_i E_j.$$

Because

$$\frac{\partial^2 W_{\mathrm{el}}}{\partial E_j \partial E_i} = \frac{\partial^2 W_{\mathrm{el}}}{\partial E_i \partial E_j}$$

we have $\epsilon_{ij} = \epsilon_{ji}$.

The measurement of the dielectric properties takes place preferably with the help of the longitudinal effect of thin crystal plates which fill the inner space of a plate capacitor. The capacitance of a simple plate capacitor is described to a good approximation by $C = \epsilon_{\text{rel}} C_0$. $C_0$ is the capacitance of the evacuated capacitor. It is expedient to measure the capacitance as a frequency determining term of a high frequency oscillator via a bridge circuit. In order to keep the highly interfering depolarization phenomena at the boundary regions of the specimens small, the diameter-to-thickness ratio of the plates should be at least 10.

The plate capacitor is realized by metallization of the large surfaces of a thin plane-parallel crystal plate (coated with a conducting silver paste or vacuum evaporated by silver or gold). In this case $C = \epsilon_{\text{rel}} \epsilon_0 F/d$, where $d$ and $F$ refer to the thickness and area of the plate, respectively. If the weight $G$ of the plate and the density $\rho$ are known, one obtains very accurate values for $F = V/d = G/\rho d$ ($V$ being the volume of the plate).

For many purposes, the *immersion method* (Fig. 4.3a) achieves sufficient accuracy. The specimen, in the form of a thin plate, is placed in a cylindrical measurement cell. The isolated main electrode should be nearly fully covered by the specimen. The remaining space in the cell is filled, bubble free,

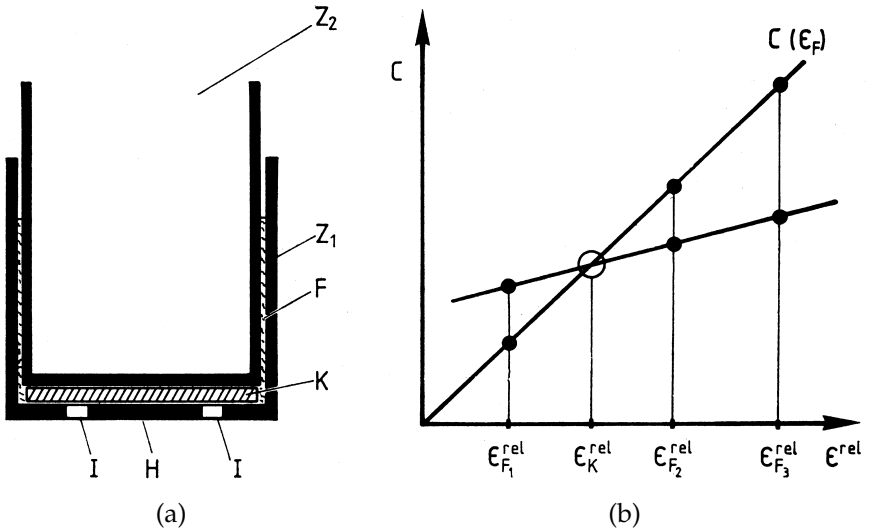


**Figure 4.3** (a) Immersion cell for the measurement of the dielectric constant of thin plates (longitudinal effect along the plate normal). H main electrode, I isolation, K crystal plate, F immersion liquid, $Z_1$ external cylinder, $Z_2$ internal cylinder. $Z_1$ and $Z_2$ represent the base electrode. (b) Graphic evaluation of the data obtained by the immersion method. $C$ is the measured capacity of the arrangement in arbitrary units.

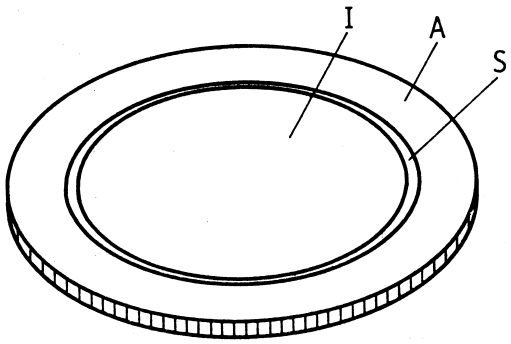


**Figure 4.4** Arrangement of the electrodes for the measurement of the longitudinal dielectric constant of thin plates. I main electrode, A outside or guard electrode, and S free gap.

with a liquid of known dielectric constant. Using a bridge circuit, one now measures the capacitance of this capacitor, filled with crystal and liquid and only with liquid, respectively. The knowledge of the absolute capacitance is not necessary; rather it suffices to read a reproducible setting of the variable plate capacitor in the bridge circuit. This procedure is carried out with several liquids. The liquids are selected such that the effective dielectric constant of the specimen lies between those of the liquids. One now plots the measured readings of the compensation capacitor against the known dielectric constants of the liquids and gets to a good approximation a straight line (Fig. 4.3b). In all measurements, the cell is to be adjusted to the thickness of the specimen. Now the measured values for the specimen are plotted as a function of the dielectric constants of the liquids. The line connecting the points may show a slight curvature. The abscissa of the intersection point of both curves yields the wanted longitudinal effect.

If the specimens are homogenous, an accuracy of up to 1 per mille can be achieved with this method without further precautions when the values for the liquids are sufficiently well known. In this case, the specimens need not be prepared with conducting electrodes. Within limits, reasonable values can also be obtained using plates of ill-defined geometry with pieces broken off and unequal thickness. This applies, in particular, to cubic crystals with their isotropic behavior.

If one requires higher accuracy, as, e.g., for the measurement of the pressure- or temperature dependence of the dielectric properties, a method using a guard electrode is recommended in which nearly all interferences due to boundary effects are suppressed (see Fig. 4.4). An arrangement for highly precise measurements was described by Andeen *et al.* (1971). This so-called *substitution method* with a three-electrode arrangement works on a principle

similar to the immersion method. The capacitance $C$ is measured between the main electrode and the base electrode, whereby, in magnitude and phase, the same alternating voltage present at the main electrode is applied to the guard electrode, separated by a small gap from the main electrode. As a consequence, a largely parallel and homogenous electric field forms in the region of the crystal above the main electrode. Altogether, one requires the following four measurements: 1. Filling with air:

$$C_1 = \epsilon_0 \epsilon_\mathrm{A} F/d_0,$$

2. filling with crystal plate and air:

$$1/C_2 = (d_0 - d_1)/(\epsilon_0 \epsilon_A F) + d_1/(\epsilon_0 \epsilon'_{\mathrm{rel},11} F),$$

3. filling with liquid:

$$C_3 = \epsilon_0 \epsilon_\mathrm{Fl} F/d_0,$$

4. filling with crystal and liquid:

$$1/C_4 = (d_0 - d_1)/(\epsilon_0 \epsilon_\mathrm{Fl} F) + d_1/(\epsilon_0 \epsilon'_{\mathrm{rel},11} F),$$

where $\epsilon_0$ is the absolute dielectric constant of the vacuum, $\epsilon_\mathrm{A}$, $\epsilon_\mathrm{Fl}$, $\epsilon'_{\mathrm{rel},11}$ are the relative dielectric constants of air, the liquid, and the crystal along the plate normal $\boldsymbol{e}'_1$. $d_0$ is the separation between main and base electrode, $d_1$ is the thickness of the plane-parallel crystal plate, and $F$ is the effective area of the main electrode. The capacitances in cases 2 and 4 result from the formula of capacitances in serial connection ($1/C = 1/C_a + 1/C_b$). The four relations allow the elimination of $d_0$, $d_1$, $\epsilon_\mathrm{Fl}$, and $F$.

The wanted dielectric constant of the plate (longitudinal effect) is then

$$\epsilon'_{\mathrm{rel},11} = \frac{1 - C_3/C_1 + C_3/C_2 - C_3/C_4}{C_1/C_2 - C_3/C_4} \epsilon_\mathrm{A}.$$

For $\epsilon_\mathrm{A}$ one can write, to a sufficient approximation, the value 1.000 53 for 293 K and atmospheric pressure.

Up to now we assumed that the dielectric tensor possesses real components. Let us give a short comment on the general case of a complex dielectric constant. It only plays a role in time-dependent processes. Let the components $\epsilon_{ij}$ be represented as $\epsilon_{ij} = \epsilon'_{ij} + i\epsilon''_{ij}$, where $\epsilon'_{ij}$ and $\epsilon''_{ij}$ are real quantities.

We imagine a periodic electric field $\boldsymbol{E} = \boldsymbol{E}_0 e^{2\pi i \nu t}$ producing an electric displacement $\boldsymbol{D} = \boldsymbol{D}_0 e^{2\pi i \nu t - i\delta}$ in a crystal. $\nu$ is the frequency and $\delta$ the phase difference of both waves. For simplicity, we consider the situation of a pure longitudinal effect with $\boldsymbol{D} = \epsilon \boldsymbol{E}$, where $\epsilon = \epsilon' + i\epsilon''$. We then have

$$\frac{D_0}{E_0} e^{-i\delta} = (\epsilon' + i\epsilon'')$$

and hence

$$\epsilon'' = \frac{-D_0}{E_0}\sin\delta \quad \text{and} \quad \tan\delta = \frac{-\epsilon''}{\epsilon'}$$

(because $e^{-i\delta} = \cos\delta - i\sin\delta$).

We now calculate the dielectric loss per second, the dissipated energy

$$L = \frac{1}{T_0}\int_0^{T_0} \boldsymbol{I}\cdot\boldsymbol{E}dt.$$

$T_0$ is the period of oscillation.

Here we require the relation between the current density vector $\boldsymbol{I}$ and the electric field strength as expressed in Ohm's law (see Section 4.3.7).

We have $I_i = (s'_{ij} + is''_{ij})E_j$, where the conductivity may also be described by a complex tensor quantity. In the case of a pure longitudinal effect , one has $\boldsymbol{I} = (s' + is'')\boldsymbol{E}$. Furthermore, the current density is proportional to the time derivative of the electric displacement, thus

$$\boldsymbol{I} = K^{-1}\frac{d\boldsymbol{D}}{dt} = K^{-1}(\epsilon' + i\epsilon'')\frac{d\boldsymbol{E}}{dt}.$$

As a result we have $s' = -K^{-1}\cdot 2\pi\nu\epsilon''$ and $s'' = K^{-1}\cdot 2\pi\nu\epsilon'$. $K$ is the constant of the chosen system of units.

Only the real part is relevant for the calculation of the dissipated energy. Hence we obtain

$$L = \frac{1}{T_0}\int_0^{T_0} s'E_0^2\cos^2 2\pi\nu t dt = \frac{1}{2}E_0^2 s' = K^{-1}\pi\nu D_0 E_0\sin\delta.$$

Thus, a fraction of the energy of the electric field, proportional to $\sin\delta$, is continuously converted into ohmic heat. The measurement of $\sin\delta$ follows directly from the comparison of the phase position of $\boldsymbol{E}$ and the displacement current or by a comparison of the reactive power and effective power.

As an example, we discuss the measurement of the dielectric tensor on triclinic lithium hydrogenoxalate-hydrate ($LiHC_2O_4\cdot H_2O$), PSG 1. Table 4.3 presents the measured longitudinal effects for altogether eight different directions.

The crystal-physical reference system is connected to the crystallographic reference system used by Thomas (1972) according to the convention described in Section 2.2.

The measurements were made on circular plates with diameters of about 20 mm and thicknesses of about 1.5 mm. The immersion liquids used were m-xylene ($\epsilon_{rel}$ =2.37), chlorobenzene ($\epsilon_{rel}$ =5.71), and ethyl dichloride ($\epsilon_{rel}$ = 10.65). A plate of NaCl with $\epsilon_{rel}$ =5.87 was used for control. The data are valid for 20°C.

**Table 4.3** Dielectric measurements on triclinic $LiHC_2O_4 \cdot H_2O$ at 293 K. Values of the longitudinal effect $\epsilon'_{rel,11}$ along the direction $e'_1 = u_{1i}e_i$ (plate normal) for a frequency of 10 MHz.

| Nr. | $u_{11}$ | $u_{12}$ | $u_{13}$ | $\epsilon'_{rel,11}$ |
|---|---|---|---|---|
| 1 | 1 | 0 | 0 | 6.77 |
| 2 | 0 | 1 | 0 | 5.43 |
| 3 | 0 | 0 | 1 | 4.91 |
| 4 | 0 | $\sqrt{2}/2$ | $\sqrt{2}/2$ | 4.70 |
| 5 | 0 | $\sqrt{2}/2$ | $-\sqrt{2}/2$ | 5.33 |
| 6 | −0.6996 | 0.7145 | 0 | 6.58 |
| 7*) | −0.4591 | 0.1662 | 0.873 | 3.89 |
| 8 | −0.2767 | 0.8035 | 0.5263 | 4.71 |

*) Normal on the cleavage face $(\bar{1}01)$

Measurements 1, 2, and 3 directly yield $\epsilon_{rel,11}$, $\epsilon_{rel,22}$, and $\epsilon_{rel,33}$. From 4 and 5 and using the relation mentioned in Section 4.3.2 one gets $\epsilon_{rel,23} = -0.41$; similarly, from 6 $\epsilon_{rel,12} = -0.54$. Applying the general formula for the longitudinal effect of measurement in direction 7 $\epsilon_{rel,13} = +1.73$ is obtained. The longitudinal effect in direction 8, calculated from these values of the dielectric constants, is in good agreement with the experimental value.

Through a principal axes' transformation one finds the principal values

$$\epsilon'_{rel,11} = 8.10, \quad \epsilon'_{rel,22} = 5.26\,; \text{ and } \epsilon'_{rel,33} = 3.75.$$

The associated eigenvectors, referred to the crystal-physical reference system are

$$\begin{aligned} \boldsymbol{e}'_1 &= 0{,}822\boldsymbol{e}_1 - 0{,}246\boldsymbol{e}_2 + 0{,}514\boldsymbol{e}_3, \\ \boldsymbol{e}'_2 &= -0{,}232\boldsymbol{e}_1 - 0{,}968\boldsymbol{e}_2 - 0{,}094\boldsymbol{e}_3, \\ \boldsymbol{e}'_3 &= 0{,}520\boldsymbol{e}_1 - 0{,}044\boldsymbol{e}_2 - 0{,}853\boldsymbol{e}_3. \end{aligned}$$

We thus find a distinct anisotropy with an absolute maximum in a direction close to the cleavage surface and a minimum slightly perpendicular to the cleavage plane $(\bar{1}01)$ (see Table 4.3). We will return to these anisotropy effects when discussing other properties.

A simple model has proved successful for the interpretation of the dielectric properties of isotropic media. It merely takes into account the polarizability of quasi-spherically shaped lattice particles as invariant quantities in the local electric field. The local electric field is composed of the external field and the field produced by the polarized dielectric. The local electric field is approximately given by $\boldsymbol{E}_{loc}$

$$\boldsymbol{E}_{loc} = \boldsymbol{E} + \frac{1}{3\epsilon_0}\boldsymbol{P}.$$

Let an isotropic lattice particle contribute the amount $\boldsymbol{p}_j = \alpha_j \boldsymbol{E}_{loc}$ to the total polarization, under the assumption that the local field has about the same

strength for each atomistic lattice particle within the medium; $\alpha_j$ is the polarizability of the $j$th particle. The total polarization $\boldsymbol{P}$ is then

$$\boldsymbol{P} = \boldsymbol{E}_{\text{loc}} \sum_j N_j \alpha_j,$$

where $N_j$ represents the number of the $j$th particle per volume unit. Taking into account the relation $\boldsymbol{P} = (\epsilon - \epsilon_0)\boldsymbol{E}$, one finds

$$\frac{\epsilon_{\text{rel}} - 1}{\epsilon_{\text{rel}} + 2} = \frac{1}{3\epsilon_0} \sum_j N_j \alpha_j.$$

If one is dealing with a substance composed of equal particles, as, e.g., with molecular crystals, one obtains the *Clausius–Mosotti formula*

$$\frac{\epsilon_{\text{rel}} - 1}{\epsilon_{\text{rel}} + 2} = \frac{L\rho}{3\epsilon_0 M} \alpha,$$

where $L = 6.022 \times 10^{23} \text{mol}^{-1}$ denotes Avogadro's number, $M$ the molar weight, $\rho$ the density, and $\alpha$ the polarizability of the molecule. Let $N$ be the number of molecules per volume element, then $\rho L = NM$. The quantity

$$\frac{\epsilon_{\text{rel}} - 1}{\epsilon_{\text{rel}} + 2} \frac{M}{\rho} = \frac{L}{3\epsilon_0} \alpha$$

is termed the molar polarization.

It enables us to experimentally determine the polarizability of simple compounds from the dielectric constant. If one knows the polarizability of the lattice particles, then with the help of the general formula, one can also estimate the mean dielectric constant of these materials. An important aspect here is the law of addition of polarizability, which, however, does not take into account the mutual interaction of the lattice particles nor the anisotropy of the polarizability.

### 4.3.4 Ferroelectricity

The temperature dependence of the polarizability and thus also of the dielectric constants of many isotropic substances may be described, according to Debye's approach, approximately by $\alpha = \alpha_0 + \bar{\boldsymbol{p}}^2/3kT$. $\bar{\boldsymbol{p}}$ is a mean value of the dipole moment, $k$ is Boltzmann's constant. If $\bar{\boldsymbol{p}} \neq 0$ and $\partial\alpha_0/\partial T$ is sufficiently small, then the polarizability and hence the dielectric constants decrease weakly with increasing temperature, as one recognizes from $\partial\epsilon_{\text{rel}}/\partial\alpha$ according to the Clausius–Mosotti relation. On the other hand, in crystals with vanishing $\bar{\boldsymbol{p}}$ one often observes, over a wide temperature range, a slight, approximately uniform increase of $\epsilon_{\text{rel}}$ with increasing temperature.

A totally different behavior of the temperature dependence is observed in certain crystal species, such as potassium calcium tartrate-dihydrate (Rochelle salt), triglycine sulfate, $BaTiO_3$, or $KH_2PO_4$. An example is shown in Fig. 4.5. When approaching a certain transition temperature, extremely large dielectric constants (DC) are observed, in some cases several powers of ten higher than in normal substances, where DC values rarely surmount the value of 50 (see Tables 12.6, 12.7). In addition, one also finds a rapid decrease of the DC with increasing frequency. In many cases, the temperature dependence of the susceptibility can be approximately represented by a *Curie–Weiss law* of the type

$$\chi = \frac{C_0}{T - T_0},$$

where $C_0$ is the Curie–Weiss constant and $T_0$ the Curie temperature.

One just about always sees a hysteresis, i.e., the electric polarization follows the electric field with a certain delay up to the transition point of saturation. Often one also sees a remenance, i.e., the polarization remains unchanged by a change in the direction of the electric field. From the analogy to ferromagnetic properties, this anomalous dielectric behavior was given the name *ferroelectricity*. In the meantime, several hundred ferroelectric substances are known, which even between themselves exhibit very different dielectric properties. Some materials, such as $BaTiO_3$, Rochelle salt, and $NH_4H_2PO_4$ (ADP) as well as their structural derivatives have found wide technical application not only because of their dielectric properties but also because of their piezoelectric properties (see Section 4.4.1).

The atomistic interpretation of ferroelectricity presumes that the crystals possess permanent dielectric dipoles belonging to individual particle or particle complexes. An external electric field can order these dipoles in a parallel direction. The temperature change works against this order. Below a certain temperature $T_0$, most ferroelectrics self-order these dipoles in parallel directions within domains. Thus these domains possess a primary electric moment and belong to one of the ten pyroelectric point symmetry groups (see Section 4.2.2). The different domains can be considered as electric twins. Above the temperature $T_0$, the domains vanish and the distribution of the dipoles is static (paraelectric phase). When the pyroelectric easy-axis direction vanishes, the crystal takes on a higher symmetry group which must be a supergroup of the symmetry group of the ferroelectric phase. The total moment per volume element due to the parallel ordering of the dipoles is called spontaneous polarization. This normally occurs along a distinct crystallographic direction.

If the dipoles order themselves in a regular sequence of alternating sign, one talks about *antiferroelectricity* analogous to the situation with antiferromagnetic effects.

### 4.3.5
### Magnetic Permeability

Although the origin of magnetism is quite different certain magnetic phenomena can be described analogously to electrostatic ones. The magnetic quantity

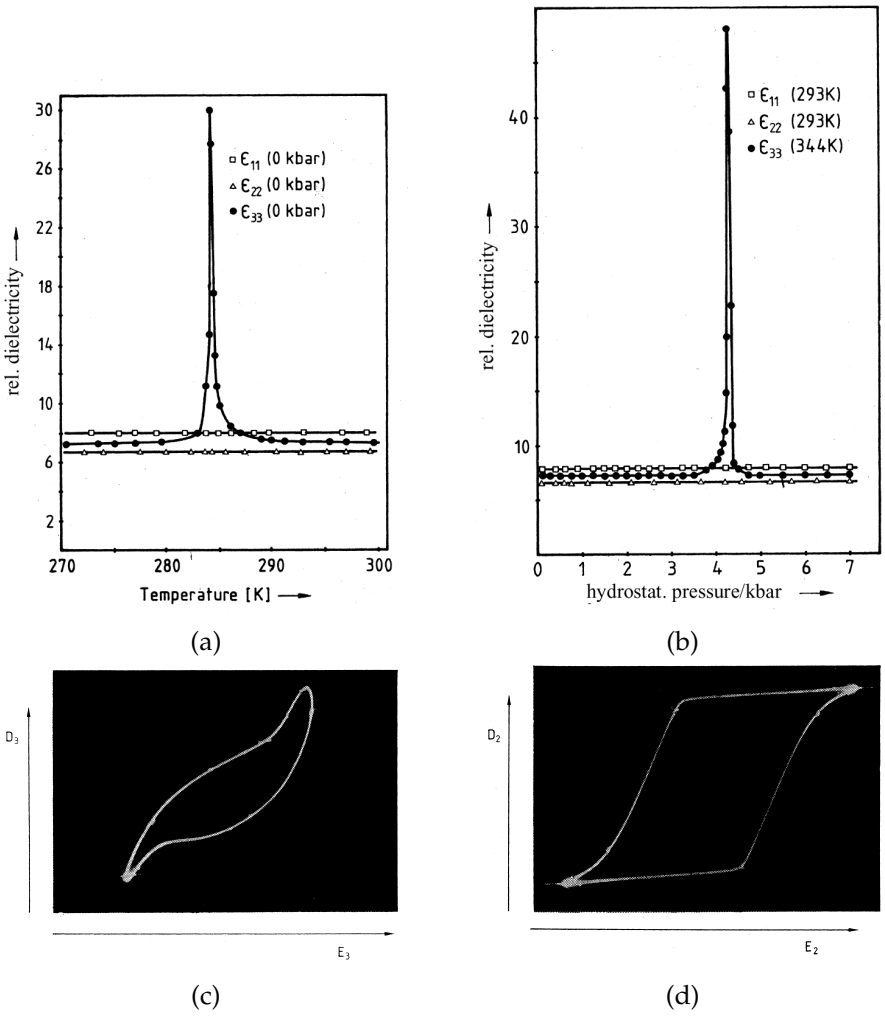


**Figure 4.5** Dependence of the dielectric constants on temperature (a) and hydrostatic pressure (b) in $Li_2Ge_7O_{15}$ (paraelectric phase: PSG mmm, ferroelectric phase: PSG mm2; Preu & Haussühl, 1982). $\epsilon_{33}$ exhibits a steep anomalous increase at the phase transition. (c) and (d) ferroelectric hysteresis of polarization and external electric field in $C(NH_2)_3Al(SO_4)_2 \cdot 6H_2O$ (GASH) and triglycine sulfate (TGS) in the ferroelectric phase (PSG 3m and 2, respectively; $E \parallel 3$ and $\parallel 2$, respectively). The oscillograms have been recorded at 293 K employing the arrangement suggested by Schubring et al. (1964). GASH shows the rather rare case of an asymmetric hysteresis loop.

corresponding to the electric field strength is the magnetic field strength $\boldsymbol{H}$ pointing into the direction of the force $\boldsymbol{F}$ which the magnetic field exerts on an imaginary magnetic point-like north pole of strength $p$:

$$\boldsymbol{F} = p\boldsymbol{H}.$$

The field strength at an arbitrary position around a bar magnet points in the direction of the field lines leaving the north pole and ending in the south pole. The quantity $p$ corresponds to the electric charge as in the definition of the electric field strength. Since no isolated point-like magnetic poles exist, the effect of the magnetic field is demonstrated simply by considering the force exerted by a magnetic field on a small bar magnet of magnetic moment $\mathcal{M} = p\boldsymbol{l}$. $\boldsymbol{l}$ is a vector pointing from the imaginary point-like south pole of the magnet to the point-like north pole. The north pole is pulled in the direction of the magnetic field while the south pole experiences a corresponding repulsion. The resulting torque $\boldsymbol{M}$, perpendicular to $\boldsymbol{H}$ and to the magnetic moment $\mathcal{M}$ has the magnitude $|\boldsymbol{H}||\boldsymbol{l}||\sin\varphi|$, where $\varphi$ is the angle between $\boldsymbol{l}$ and $\boldsymbol{H}$. Thus $\boldsymbol{M} = \mathcal{M} \times \boldsymbol{H}$ (Fig. 4.6).

If we now place a body in a magnetic field, the magnetic moments of the atoms or molecules also experience a torque which may lead to an alignment of the magnetic moments. The total magnetic moment of the body per volume element is called the magnetization $\boldsymbol{C}$. This corresponds to the vector of the electric polarization. In weak magnetic interactions one expects a linear relationship between the magnetic field $\boldsymbol{H}$ and the magnetization, thus $C_i = \chi_{ij}\mu_0 H_j$. $\{\chi_{ij}\}$ is the *tensor of magnetic susceptibility* and $\mu_0$ is the permeability of the vacuum. By analogy to the electric case, we introduce a further quantity, the magnetic induction $\boldsymbol{B}$, corresponding to the vector of the electric displacement. The definition is

$$B_i = \mu_{ij}H_j = \chi_{ij}\mu_0 H_j + \mu_0 H_i = (\chi_{ij} + \delta_{ij})\mu_0 H_j.$$

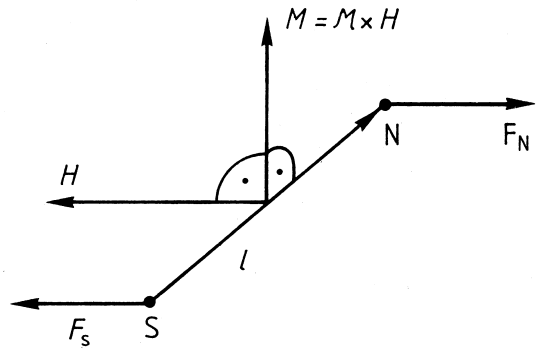


**Figure 4.6** Body torque $M$, which is exerted on a bar magnet $\mathcal{M} = p\boldsymbol{l}$ in a magnetic field $\boldsymbol{H}$.

$\{\mu_{ij}\}$ is the *tensor of the magnetic permeability*.

The tensors $\{\chi_{ij}\}$ and $\{\mu_{ij}\}$ are of polar character because $\boldsymbol{H}$ as well as $\boldsymbol{C}$ and hence $\boldsymbol{B}$ are pseudo tensors (axial vectors). The latter is a consequence of the 2. Maxwell equation

$$\operatorname{rot} \boldsymbol{H} = \boldsymbol{I} + \frac{1}{c}\frac{\partial \boldsymbol{D}}{\partial t};$$

$\boldsymbol{I}$ specifies the electric current density (Ampère's law). Since $\boldsymbol{I}$ and $\boldsymbol{D}$ are polar vectors, rot $\boldsymbol{H}$ must also be polar (see Section 3.7).

Essentially, one distinguishes three groups of magnetic behavior.

1. *Diamagnetism:* Primarily, the given substances possess no magnetic moment. In a magnetic field, a weak magnetization is induced opposing the field. The magnetization is only slightly temperature dependent. Diamagnetic substances are repelled by a magnetic field, the $\chi$-values are negative (of the order $10^{-6}$). Typical representatives are most salts of the A subgroup of the periodic table with inorganic anions. Bismuth possesses a particularly large effect.

2. *Paramagnetism:* The magnetization induced by the field is aligned parallel to the field. The magnetization is more strongly temperature dependent than in the case of diamagnetism. Atoms or molecules in the medium possess a magnetic moment. Paramagnetic substances are attracted towards the magnetic field. The $\chi$-values are positive (of the order $10^{-5}$). Typical representatives are the transition elements, in particular those of the iron group and the rare earths as well as their salts.

3. *Ferromagnetism:* The magnetic moments possess, within certain temperature ranges, opposite orientations, e.g., parallel or antiparallel arrangements (ferro, antiferromagnetism) or a combination of both (ferrimagnetism). Due to the cooperative alignment of the magnetic moments, the magnetization is much stronger than in the case of paramagnetism. If all moments are aligned parallel, no further increase in magnetization is possible (saturation). From this we recognize that the linear relationship $B_i = \mu_{ij}H_j$ is not sufficient for ferromagnetic substances. Rather, the components $\mu_{ij}$ are quite complicated functions of $\boldsymbol{H}$.

In addition, hysteresis effects also occur, i.e., the magnetization lags behind the external magnetic field. The persistence of the magnetization after switching off the external magnetic field is called remanence. Hysteresis is a characteristic phenomenon of ferromagnetism, analogous to the situation of ferroelectricity. In some iron alloys the $\chi$-values can rise up to $10^6$. Typical ferromagnetics are iron, nickel, cobalt, and rare earth metals as well as the alloys of these elements. Furthermore, ferromagnetic properties appear in certain compounds of otherwise nonferromagnetic transition elements such as CrTe or MnP.

The measurement of magnetic properties is based on the magnetization generated in the magnetic field. For ferromagnetic substances with large val-

ues of susceptibility simple arrangements are sufficient. For example, one can measure the change of magnetic induction inside a cylindrical coil after inserting the probe in a way that is similar to measuring the change in capacitance of a capacitor. The resulting torque experienced by a magnetometer needle is a direct measure of the change in $\boldsymbol{B}$. Calibration with known probes then allows the determination of the susceptibility. The measurement of the inductance of a coil allows a simple and reliable determination of the frequency dependence of the susceptibility.

With diamagnetic and paramagnetic substances, the sensitivity of this method is too low. In order to detect the expected anisotropy in noncubic crystals it is necessary to generate, as far as possible, purely longitudinal effects of magnetization, i.e., the magnetic field and the magnetization should be aligned parallel through the whole probe. We now consider the simplest case of a dia- or paramagnetic crystal without primary magnetic moment. A small probe in a magnetic field experiences a magnetic moment of $\mathcal{M} = V\chi_{\text{eff}}\mu_0\boldsymbol{H} = p\boldsymbol{l}$. $V$ is the volume of the probe and $\chi_{\text{eff}}$ is the longitudinal effect of the susceptibility in the direction of the magnetic field. In the case of an inhomogenous magnetic field we imagine $\boldsymbol{H}$ represents a mean value over the volume of the probe. Let the magnetic field possess the strength $\boldsymbol{H}_1$ at the south pole and the strength $\boldsymbol{H}_2$ at the north pole, with $\boldsymbol{H}_2 \parallel \boldsymbol{H}_1 \parallel \boldsymbol{l}$. The resulting force on the probe is then

$$\boldsymbol{F} = p(\boldsymbol{H}_2 - \boldsymbol{H}_1) = p|\boldsymbol{l}|\frac{(\boldsymbol{H}_2 - \boldsymbol{H}_1)}{|\boldsymbol{l}|} \approx V\chi_{\text{eff}}\mu_0|\boldsymbol{H}|\frac{d\boldsymbol{H}}{dx},$$

where $(\boldsymbol{H}_2 - \boldsymbol{H}_1)/|\boldsymbol{l}|$ is replaced by the differential quotient $d\boldsymbol{H}/dx$ for the transition to infinitesimal $\boldsymbol{l}$. $x$ is the coordinate along the vector of the magnetization. For practical measurements it is desirable to achieve, as far as possible, a constant value of $d\boldsymbol{H}/dx$ over the whole probe. A particularly simple arrangement is again the cylindrical coil, in which one suspends a cylindrical probe symmetric to the coil axis. A large part of the probe remains outside the coil in order to make the region of the inhomogenous field as effective as possible (Fig. 4.7).

If one works with a cylindrical probe of length $L$ and cross-section $Q$ and sets up the magnetic field so that $d\boldsymbol{H}/dx$ is constant over each cross-section perpendicular to the cylindrical axis, then one can calculate the total force on the probe according to

$$|\boldsymbol{F}| = \int_V \chi_{\text{eff}}\mu_0|\boldsymbol{H}|\left|\frac{d\boldsymbol{H}}{dx}\right| dV = \frac{Q}{2}\chi_{\text{eff}}\mu_0|\boldsymbol{H}^2 - \boldsymbol{H}_0^2|,$$

where $dV$ is replaced by $Q\,dx$. $\boldsymbol{H}$ and $\boldsymbol{H}_0$ are the field strengths at the top and bottom ends of the probe respectively, and can be measured with calibrated probes. The force $\boldsymbol{F}$ due to the vertical field gradients $d\boldsymbol{H}/dx$ of the cylindrical

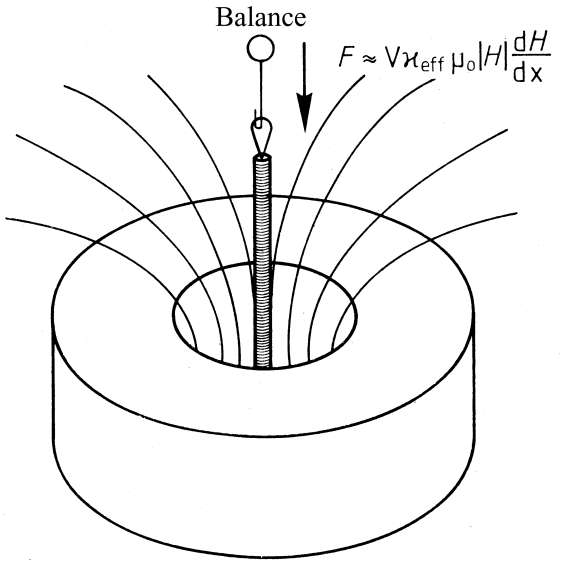


**Figure 4.7** Measurement of the magnetization of a cylindrical probe in an inhomogeneous magnetic field.

coil is measured by weighing, in the case of horizontal field gradients with the aid of a torsion balance.

### 4.3.6 Optical Properties: Basic Laws of Crystal Optics

The optical properties of crystals are essentially determined by their dielectric behavior. In view of the fundamental importance of these properties for practical crystal optics, e.g., in polarization microscopy as well as for many crystal-physical effects, in particular higher order optical effects (e.g., electro-optics, piezo-optics, nonlinear optics) and spectroscopic phenomena, we must carefully discuss some of the basic laws of crystal optics in this section. We will restrict ourselves mainly to the phenomena of wave propagation, which is coupled with the vibrations of the electric displacement vector $\boldsymbol{D}$. These are easier to handle theoretically than energy propagation.

Let us first consider the case of a nonabsorbing (electrically nonconducting) and centrosymmetric medium. The material properties are given by the dielectric tensor and the tensor of the magnetic permeability, hence by the relations $D_i = \epsilon_{ij} E_j$ and $B_i = \mu_{ij} H_j$, whereby all quantities are to be understood as frequency-dependent functions. Other material properties which interact with electromagnetic waves, as represented by light rays, are excluded for the present. In a further simplification we assume that the tensor $\{\mu_{ij}\}$ at the high frequencies of the optical range is quasi-isotropic and for all crystals, de-

scribed to sufficient accuracy by the vacuum value $\mu_0$ according to $B_i = \mu_0 H_i$. This is also in agreement with experimental observations.

The electrical processes of light propagation obey the fundamental equations of electrodynamics (*Maxwell's equations*, which in the cgs system are (with $\mu_0 = 1$):

$$\begin{aligned}
&\text{rot}\,\boldsymbol{E} = -\frac{1}{c}\frac{\partial \boldsymbol{H}}{\partial t} \quad \text{(induction law)}\\
&\text{rot}\,\boldsymbol{H} = \frac{1}{c}\frac{\partial \boldsymbol{D}}{\partial t} \quad \text{(Ampères law of current density and magnetic field)}\\
&\text{div}\,\boldsymbol{D} = 0 \quad \text{(no free charge density; otherwise div } \boldsymbol{D} = 4\pi\rho', \\
&\qquad\qquad\qquad\qquad \text{where } \rho' \text{ specifies the electric charge density)}\\
&\text{div}\,\boldsymbol{H} = 0 \quad \text{(no magnetic charges exist).}
\end{aligned}$$

$c$ is the velocity of light, and $t$ the time. The reader is referred to a standard physics textbook for the derivation of Maxwell equations. The most important experimental situation is the propagation of a plane wave, which to a good approximation occurs when the dimensions of the homogenous medium perpendicular to the direction of propagation are far greater than the wavelength of the given radiation. For the magnetic field we take a plane wave of the form

$$\boldsymbol{H} = \boldsymbol{H}_0 e^{2\pi i(\boldsymbol{k}\cdot\boldsymbol{x} - \nu t)}.$$

$\boldsymbol{k}$ is the propagation vector, perpendicular to the wave front with length $|\boldsymbol{k}| = 1/\lambda$. $\lambda$ is the wavelength, $\nu$ the frequency. With $\text{rot}\,\boldsymbol{v} = \nabla \times \boldsymbol{v}$ and the differential operator

$$\nabla = \boldsymbol{e}_j \frac{\partial}{\partial x_j} \quad \text{(summed over j!)}$$

we obtain from Ampères law

$$\text{rot}\,\boldsymbol{H} = 2\pi i \boldsymbol{k} \times \boldsymbol{H} = \frac{1}{c}\frac{\partial \boldsymbol{D}}{\partial t}.$$

Hence, it follows that $\boldsymbol{H}$ and $\boldsymbol{D}$ possess the same time and space dependence, thus

$$\boldsymbol{D} = \boldsymbol{D}_0 e^{2\pi i(\boldsymbol{k}\cdot\boldsymbol{x} - \nu t)} \quad \text{and hence only} \quad \frac{\partial \boldsymbol{D}}{\partial t} = -2\pi i \nu \boldsymbol{D}.$$

Because $D_i = \epsilon_{ij} E_j$ and $B_i = \mu_{ij} H_j$ we also have

$$\boldsymbol{E} = \boldsymbol{E}_0 e^{2\pi i(\boldsymbol{k}\cdot\boldsymbol{x} - \nu t)} \quad \text{and} \quad \boldsymbol{B} = \boldsymbol{B}_0 e^{2\pi i(\boldsymbol{k}\cdot\boldsymbol{x} - \nu t)}.$$

We recognize further that $\boldsymbol{D}$ is perpendicular to $\boldsymbol{k}$ and $\boldsymbol{H}$ and the vectors $\boldsymbol{k}$, $\boldsymbol{D}$, $\boldsymbol{H}$ form a right-handed system. From

$$\text{div}\,\boldsymbol{H} = \frac{\partial H_j}{\partial x_j} = 2\pi i k_j H_j = 2\pi i \boldsymbol{k} \cdot \boldsymbol{H} = 0$$

follows that $\boldsymbol{k}$ and $\boldsymbol{H}$ are orthogonal. This means the waves of $\boldsymbol{D}$ and $\boldsymbol{H}$ are always of pure transversal type.

To which conditions are now $\boldsymbol{D}$ and $\boldsymbol{E}$ subject? Differentiation with respect to time gives, from Ampères law,

$$\frac{\partial^2 \boldsymbol{D}}{\partial t^2} = c \operatorname{rot} \frac{\partial \boldsymbol{H}}{\partial t}$$

and after inserting $\partial \boldsymbol{H}/\partial t$, we get from the induction law

$$\frac{\partial^2 \boldsymbol{D}}{\partial t^2} = -c^2 \operatorname{rot} \operatorname{rot} \boldsymbol{E}.$$

Using the expansion rule, we find

$$\begin{aligned} \operatorname{rot} \operatorname{rot} \boldsymbol{E} = \nabla \times (\nabla \times \boldsymbol{E}) &= \nabla(\nabla \cdot \boldsymbol{E}) - \nabla^2 \boldsymbol{E} \\ &= \operatorname{grad} 2\pi i \boldsymbol{k} \cdot \boldsymbol{E} - \sum_j \frac{\partial^2 \boldsymbol{E}}{\partial x_j^2} = -4\pi^2 (\boldsymbol{k} \cdot \boldsymbol{E}) \boldsymbol{k} + 4\pi^2 \boldsymbol{k}^2 \boldsymbol{E}. \end{aligned}$$

Thus we have

$$\frac{\partial^2 \boldsymbol{D}}{\partial t^2} = -4\pi^2 \nu^2 \boldsymbol{D} = c^2 4\pi^2 \{(\boldsymbol{k} \cdot \boldsymbol{E}) \boldsymbol{k} - \boldsymbol{k}^2 \boldsymbol{E}\},$$

hence

$$\frac{\nu^2}{c^2} \boldsymbol{D} = \boldsymbol{k}^2 \boldsymbol{E} - (\boldsymbol{k} \cdot \boldsymbol{E}) \boldsymbol{k}.$$

After introducing the unit vector in the propagation direction $\boldsymbol{g} = \boldsymbol{k}/|\boldsymbol{k}|$, we obtain the wave equation

$$\frac{v^2}{c^2} \boldsymbol{D} = \boldsymbol{E} - (\boldsymbol{g} \cdot \boldsymbol{E}) \boldsymbol{g},$$

where $\nu\lambda = v$ is the propagation velocity of the wave.

If one eliminates $\boldsymbol{D}$ by $D_i = \epsilon_{ij} E_j$, one obtains a system of three linear equations for $E_i$. The system only has solutions for $\boldsymbol{E} \neq 0$ when its determinant vanishes. We then obtain, for any arbitrary propagation direction $\boldsymbol{g}$, an equation for $v^2/c^2 = 1/n^2$. The ratio $n$ of the velocity of light $c$ in vacuum and propagation velocity $v$ in the medium is known as the *refractive power* or *refractive index*. The equation referred to is therefore also called the *index equation*.

Assume now the axes of our Cartesian reference system have been chosen parallel to the principal axes of the dielectric tensor, where we have $D_j = \epsilon_{jj} E_j$ and $\epsilon_{ij} = 0$ for $i \neq j$. We can then replace $E_j$ by $D_j/\epsilon_{jj}$ in the above equation and for each component write

$$D_j \left\{ \frac{v^2}{c^2} - \frac{1}{\epsilon_{jj}} \right\} = -(\boldsymbol{g} \cdot \boldsymbol{E}) g_j.$$

In the directions of the principal axes we have $\boldsymbol{D} \parallel \boldsymbol{E}$, thus because $\boldsymbol{g} \cdot \boldsymbol{D} = 0$ we also have $\boldsymbol{g} \cdot \boldsymbol{E} = 0$; in addition we have $1/\epsilon_{jj} = v^2/c^2$, in case $D_j \neq 0$. We then obtain for the accompanying propagation velocity $v_j$

$$v_j^2 = \frac{c^2}{\epsilon_{jj}}.$$

The quantities $c/v_j = n_j$ are the *principal refractive indices*. For these $n_j = \sqrt{\epsilon_{jj}}$ is true in the system of units selected here. Especially for the vacuum $n = 1 = \sqrt{\epsilon_0}$ and thus $n_j = \sqrt{\epsilon_{\mathrm{rel},jj}}$ (*Maxwell's relation* for $\mu = 1$).

Consider now the general case where $\boldsymbol{E}$ does not run parallel to $\boldsymbol{D}$. From the above equation, we have for an arbitrary $\boldsymbol{g}$

$$D_1 : D_2 : D_3 = \frac{g_1}{v_1^2 - v^2} : \frac{g_2}{v_2^2 - v^2} : \frac{g_3}{v_3^2 - v^2},$$

where $v$ is the velocity of the wave propagating in direction $\boldsymbol{g}$.

For the determination of $v^2$ as a function of $\boldsymbol{g}$ we form $\boldsymbol{D} \cdot \boldsymbol{g} = 0$ and obtain

$$\frac{g_1^2}{v_1^2 - v^2} + \frac{g_2^2}{v_2^2 - v^2} + \frac{g_3^2}{v_3^2 - v^2} = 0,$$

resulting in a second-order equation in $v^2$

$$\sum_{i=1,2,3} g_i^2 (v_j^2 - v^2)(v_k^2 - v^2) = 0 \qquad (j = i+1,\ k = i+2 \bmod 3).$$

For an arbitrary direction $\boldsymbol{g}$, this equation yields two intrinsic values $v'^2$ and $v''^2$, which in general, are different. A total of four solutions exist $v = \pm v'$ and $v = \pm v''$. The propagation velocities in the direction $\boldsymbol{g}$ and in the opposite direction $-\boldsymbol{g}$ are equal in magnitude. How are now the accompanying vectors $\boldsymbol{D}'$ and $\boldsymbol{D}''$ oriented to $v'$ and $v''$? They are mutually perpendicular as seen by forming the scalar product $\boldsymbol{D}' \cdot \boldsymbol{D}''$. We have

$$\begin{aligned} \boldsymbol{D}' \cdot \boldsymbol{D}'' &= \sum_j Q' Q'' \frac{g_j^2}{(v_j^2 - v'^2)(v_j^2 - v''^2)} \\ &= \frac{Q' Q''}{(v'^2 - v''^2} \sum_j \left[ \frac{g_j^2}{(v_j^2 - v'^2)} - \frac{g_j^2}{(v_j^2 - v''^2)} \right] \quad = \quad 0, \end{aligned}$$

provided $v'^2 \neq v''^2$.

$Q'$ and $Q''$ are factors determining the length of $\boldsymbol{D}'$ and $\boldsymbol{D}''$; the terms in the square brackets vanish individually. The case $v'^2 = v''^2$ leaves the position of $\boldsymbol{D}'$ and $\boldsymbol{D}''$ open (degeneracy!). Furthermore, $\boldsymbol{D}'$ and $\boldsymbol{D}''$ lie parallel to

the half axes of the sectional ellipse cut out of the tensor quadric $F = a_{ij}x_ix_j$ (ellipsoid) by the central plane perpendicular to the propagation direction $\boldsymbol{g}$, characterized by $\boldsymbol{g} \cdot \boldsymbol{x} = 0$ and containing the center of the ellipsoid.

The components $a_{ij}$ establish the connection of $\boldsymbol{E}$ and $\boldsymbol{D}$ according to $E_j = a_{jk}D_k$. They are called *polarization constants*. As proof we calculate the directions in which the radius vector of the sectional ellipse takes on an extreme value; these directions coincide with the directions of the major and minor half axes of the ellipse. Similar to the principal axes' transformation, the conditions for extreme values here are: $\boldsymbol{x}^2 =$ extremum, auxiliary condition $\boldsymbol{g} \cdot \boldsymbol{x} = 0$ (ellipse lies in the plane perpendicular to $\boldsymbol{g}$) and $a_{ij}x_ix_j = F$ (ellipse belongs to the tensor quadric). Again we assume that our coordinate system is the principal axes' system of the dielectric tensor. We then have $a_{jj} = 1/\epsilon_{jj}$, $a_{jk} = 0$ for $j \neq k$. The tensor quadric is then $\sum_j x_j^2/\epsilon_{jj} = F$ and with $n_j^2 = \epsilon_{jj}$ and $F = 1$

$$\sum_j \frac{x_j^2}{n_j^2} = 1.$$

In this form it is called the *indicatrix*. We now introduce an auxiliary function $H$, which also takes on an extreme value:

$$H = \sum_j x_j^2 - \lambda_1 \boldsymbol{g} \cdot \boldsymbol{x} - \lambda_2 \left( \sum_j x_j^2/n_j^2 - 1 \right).$$

The conditions $\partial H/\partial x_j = 0$ give for $j = 1, 2, 3$

$$2x_j - \lambda_1 g_j - 2\lambda_2 x_j/n_j^2 = 0.$$

We multiply the $j$th equation with $x_j$, sum over $j = 1, 2, 3$, and obtain

$$\sum_j 2x_j^2(1 - \lambda_2/n_j^2) - \lambda_1 \sum_j g_j x_j = 0.$$

The second term vanishes because $\boldsymbol{g} \cdot \boldsymbol{x} = 0$. Therefore

$$\sum_j x_j^2 = \lambda_2 \sum_j x_j^2/n_j^2, \quad \text{hence} \quad \lambda_2 = \sum_j x_j^2 = \boldsymbol{x}^2.$$

We recognize the meaning of $\boldsymbol{x}^2$ as follows: by scalar multiplication of the wave equation with $\boldsymbol{D}$ one gets

$$\boldsymbol{D}^2/n^2 = \boldsymbol{E} \cdot \boldsymbol{D} - (\boldsymbol{g} \cdot \boldsymbol{E})(\boldsymbol{g} \cdot \boldsymbol{D}).$$

The last term vanishes. Furthermore,

$$\boldsymbol{D}^2/n^2 = \boldsymbol{E} \cdot \boldsymbol{D} = \sum_j a_{jj} D_j^2,$$

and thus

$$1/n^2 = \sum_j a_{jj} D_j^2 / \boldsymbol{D}^2 = a'_{11},$$

where $a'_{11}$ represents the longitudinal effect along $\boldsymbol{e}'_1 = \boldsymbol{D}/|\boldsymbol{D}|$. On the other hand this is obtained from the radius vector of the tensor quadric according to $a'_{11} = F/\boldsymbol{x}^2$. With $F = 1$ we have $\boldsymbol{x}^2 = n^2$, i.e., the lengths of the major and minor half axes of the sectional ellipse are equal to the refractive indices of both possible waves propagating along $\boldsymbol{g}$. From the above system of equations, one obtains for the coordinates of the half axes

$$2x_j = \lambda_1 g_j \Big/ \left(1 - \frac{n^2}{n_j^2}\right)$$

and thus

$$x_1 : x_2 : x_3 = \frac{g_1}{1 - n^2/n_1^2} : \frac{g_2}{1 - n^2/n_2^2} : \frac{g_3}{1 - n^2/n_3^2}.$$

This ratio is identical to the relation derived above for $D_1 : D_2 : D_3$. This is recognized when one substitutes the refractive indices by the corresponding velocities. Hence the directions of vibrations $\boldsymbol{D}'$ and $\boldsymbol{D}''$ run parallel to the half axes of the sectional ellipse.

We summarize these results to the *basic law of crystaloptics* for nonconducting centrosymmetric crystals:

For each propagation direction $\boldsymbol{g}$ in a crystal there exist two linear polarized waves, whose $\boldsymbol{D}$-vectors (directions of vibration)) run parallel to the half axes of the associated sectional ellipse of the indicatrix. The associated refractive indices are equal to the lengths of these half axes. If the refractive indices $n'$ and $n''$ belonging to $\boldsymbol{g}$ are equal, then the sectional ellipse is in the form of a circle and the direction of vibrations within the plane of the circle is not fixed (degenerate).

Thus the propagation of light in a crystal is determined only by the form and position of the indicatrix. We can divide the centrosymmetric crystals into the following optical classes (see also Section 4.3.6.4):

1. *Optically isotropic:* cubic crystals. The indicatrix is a sphere. The position of the $\boldsymbol{D}$-vectors is not fixed.

2. *Optically uniaxial:* trigonal, tetragonal, and hexagonal crystals. The indicatrix is an ellipsoid of revolution; the axis of revolution runs parallel to the three-, four-, or six-fold axis.

3. *Optically biaxial:* orthorhombic, monoclinic, and triclinic crystals. The indicatrix is a triaxial ellipsoid. In orthorhombic crystals the principal axes of the indicatrix lie parallel to the orthorhombic basic vectors. In monoclinic crystals the distinct monoclinic basic vector $\boldsymbol{a}_2$ (parallel to a two-fold axis or

to a normal on the symmetry plane) must run parallel to one principal axis of the indicatrix. In triclinic crystals the indicatrix is not fixed by any symmetry considerations. (The term "biaxial" refers to the existence of two directions called *optic axes*, in which the sectional ellipse takes on the form of a circle; see Section 4.3.6.4).

As we have seen, the vector of the electric displacement $\boldsymbol{D}$, also within the crystal, is perpendicular to the propagation direction $\boldsymbol{k}$ of the electromagnetic wave and to the vector of the magnetic field strength $\boldsymbol{H}$. In crystals, as opposed to isotropic media, the vector of the electric field strength $\boldsymbol{E}$ usually deviates from $\boldsymbol{D}$. However, $\boldsymbol{E}$ is also perpendicular to $\boldsymbol{H}$, as one recognizes from the Maxwell equation $\mathrm{rot}\,\boldsymbol{E} = -\frac{1}{c}\partial\boldsymbol{H}/\partial t$ after introducing the expression for plane waves. Hence the three vectors $\boldsymbol{D}$, $\boldsymbol{E}$, and $\boldsymbol{k}$ lie in the plane perpendicular to the magnetic field $\boldsymbol{H}$. The position of $\boldsymbol{E}$ with given $\boldsymbol{k}$ and $\boldsymbol{D}$ is obtained by the Poinsot construction (see Section 4.3.2) in the plane perpendicular to $\boldsymbol{H}$. For this purpose we draw the ellipse cut out by the plane perpendicular to $\boldsymbol{H}$ and passing through the center of the tensor quadric (Fig. 4.8). $\boldsymbol{E}$ is then perpendicular to the tangent of this ellipse at the intercept point of the vector $\boldsymbol{D}$ (tensor quadric $F = a_{ij}x_ix_j$, $E_i = a_{ij}D_j$). For our description thus far we have given preference to the $\boldsymbol{D}$-vector because it allows a simpler representation of the crystal-optic properties.

The flow of energy of the electromagnetic wave is described by the Poynting vector $\boldsymbol{S} = (c/4\pi)\boldsymbol{E} \times \boldsymbol{H}$. $\boldsymbol{S}$ shows the direction of the ray $\boldsymbol{s}$ along which the electromagnetic energy (per second and unit area) propagates. In the Poinsot construction we can now draw directly the position of $\boldsymbol{S}$, namely perpendicular to $\boldsymbol{H}$ and $\boldsymbol{E}$ (see Fig. 4.8).

Ray vector $\boldsymbol{s}$ and propagation vector $\boldsymbol{k}$ thus stand in a close geometrical relationship from which one can derive a set of interesting rules which we are unable to pursue here. The phenomenon of double refraction is taken up in Exercise 5 (see Section 4.3.2).

#### 4.3.6.1 **Reflection and Refraction**

An electromagnetic wave, incident on a boundary surface, causes two phenomena: reflection and refraction. Both phenomena may be considered as sufficiently well known for the case of isotropic media. *Law of reflection:* Angle of incidence $\alpha_\mathrm{I}$ = Angle of reflection $\alpha_\mathrm{Ir}$,

$$\textit{Snellius' law of refraction:} \quad \frac{\sin\alpha_\mathrm{I}}{\sin\alpha_\mathrm{II}} = \frac{v_\mathrm{I}}{v_\mathrm{II}} = \frac{n_\mathrm{II}}{n_\mathrm{I}},$$

where $v_\mathrm{I}$ and $v_\mathrm{II}$ are the wave velocities in media I and II (Fig. 4.9). In order to also calculate the intensities of the reflected and refracted waves we draw upon the boundary conditions for the quantities $\boldsymbol{H}$, $\boldsymbol{D}$, and $\boldsymbol{E}$. We imagine a plane boundary surface of a crystal II being struck by a wave with the wave

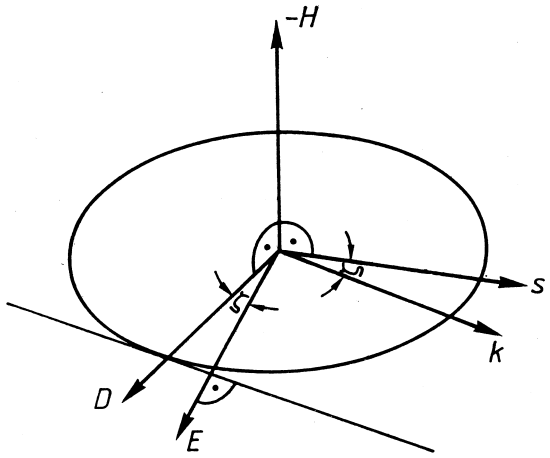


**Figure 4.8** Construction of ray vector $s$ ($\parallel$ Poynting vector) according to the Poinsot construction from the position of $\boldsymbol{D}$ and $\boldsymbol{k}$ within the plane perpendicular to the magnetic field $\boldsymbol{H}$.

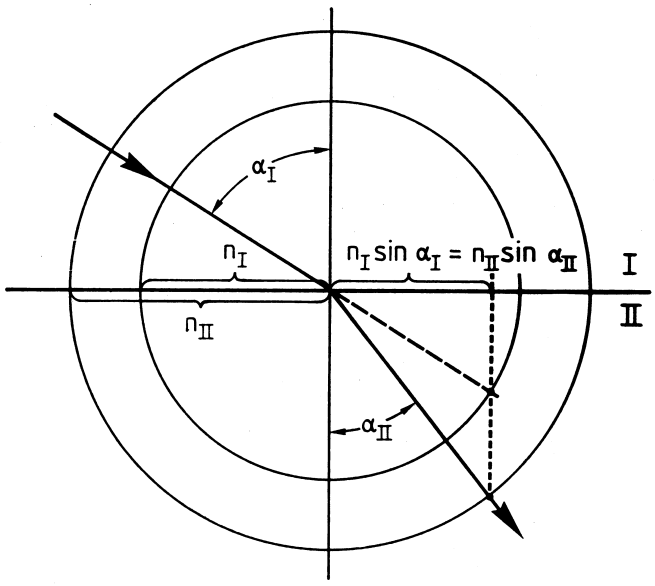


**Figure 4.9** Refraction at the boundary surface of two isotropic media I and II.

normal $\boldsymbol{k}_\mathrm{I}$ coming from an external isotropic medium I. The plane spanned by the normal on the boundary surface and $\boldsymbol{k}_\mathrm{I}$ is called the incidence plane. At first, let the direction of vibration of $\boldsymbol{D}_\mathrm{I}$ be arbitrary. In general, the tangential components of $\boldsymbol{E}$ and $\boldsymbol{H}$, i.e., the projection of $\boldsymbol{E}$ or $\boldsymbol{H}$ on the boundary sur-

face, pass through the boundary surface continuously, in other words, without spontaneous change. The reason for this behavior is that the closed line integral $\oint \boldsymbol{E} \cdot d\boldsymbol{x}$ vanishes since the path of integration outward runs along one border of the boundary surface and returns along the other border. We then have

$$E_{\mathrm{tg}}(\mathrm{I})\Delta x - E_{\mathrm{tg}}(\mathrm{II})\Delta x = 0,$$

hence $E_{\mathrm{tg}}(\mathrm{I}) = E_{\mathrm{tg}}(\mathrm{II})$; $\Delta x$ is the path of integration along the border. The contributions from crossing the boundary surface twice can be neglected. The same applies to $\boldsymbol{H}$. In contrast to $\boldsymbol{E}$ and $\boldsymbol{H}$, the normal components of the vectors of the electric displacement $\boldsymbol{D}$ and of the magnetic induction $\boldsymbol{B}$ pass continuously through the boundary surface. As proof, we make use of the condition $\operatorname{div} \boldsymbol{D} = 0$ (for nonconducting media) and integrate over a thin plate whose parallel surfaces enclose the boundary surface on both sides. According to Gauss's law, the volume integral is

$$\int_{\mathrm{Plate}} \operatorname{div} \boldsymbol{D} dV = \int_{\mathrm{Surface}} \boldsymbol{D} \cdot d\boldsymbol{f},$$

where $dV$ is a volume element of the plate and $d\boldsymbol{f}$ is the normal on a surface element of area $|d\boldsymbol{f}|$. For the limiting value of an arbitrarily thin plate one obtains

$$\int_{\mathrm{Surface}} \boldsymbol{D} \cdot d\boldsymbol{f} = D_{\mathrm{In}}\Delta f - D_{\mathrm{IIn}}\Delta f;$$

$\Delta f$ is the surface of one side of the plate. Since $\operatorname{div} \boldsymbol{D} = 0$ we have $D_{\mathrm{In}} = D_{\mathrm{IIn}}$. Analogously for $\boldsymbol{B}$ we have $B_{\mathrm{In}} = B_{\mathrm{IIn}}$. With the help of these conditions the relations at the boundary surface can now be elucidated.

Let the three participating waves, namely the incident wave from medium I, the wave reflected back into medium I and the wave refracted into medium II be specified by their propagation vectors $\boldsymbol{k}_{\mathrm{I}}$, $\boldsymbol{k}_{\mathrm{Ir}}$, and $\boldsymbol{k}_{\mathrm{II}}$ (Fig. 4.10). Let the basic vectors of a Cartesian reference system be selected such that $\boldsymbol{e}_1$ and $\boldsymbol{e}_2$ lie in the boundary surface, whereby $\boldsymbol{e}_1$ is perpendicular to the plane of incidence. $\boldsymbol{e}_3$ points in the direction of the normal on the boundary surface.

In the following, we discuss the important case of an isotropic medium I adjacent to an anisotropic medium II. At first we prove that $\boldsymbol{k}_{\mathrm{I}}$, $\boldsymbol{k}_{\mathrm{Ir}}$, and $\boldsymbol{k}_{\mathrm{II}}$ lie in the plane of incidence. We imagine the electric field strength $\boldsymbol{E}$ is resolved into components perpendicular and parallel to the plane of incidence ($\boldsymbol{E}_{\mathrm{tg}} \parallel \boldsymbol{e}_1$, $\boldsymbol{E}_{\perp} \cdot \boldsymbol{e}_1 = 0$). As we shall see, both components behave differently with respect to reflection and refraction.

In the case $\boldsymbol{E}_{\mathrm{I}} \parallel \boldsymbol{e}_1$ we also have $\boldsymbol{D}_{\mathrm{I}} \parallel \boldsymbol{e}_1$, and furthermore $\boldsymbol{H}_{\mathrm{I}} \cdot \boldsymbol{e}_1 = 0$ and $\boldsymbol{H} \parallel \boldsymbol{B}$. From $\boldsymbol{D}_{\mathrm{I}} \parallel \boldsymbol{D}_{\mathrm{Ir}}$ and $\boldsymbol{D}_{\mathrm{Ir}} \cdot \boldsymbol{k}_{\mathrm{Ir}} = 0$ we note that $\boldsymbol{k}_{\mathrm{Ir}}$ also lies in the plane of incidence. The condition $D_{\mathrm{In}} = D_{\mathrm{IIn}}$ means here that $\boldsymbol{D}_{\mathrm{II}}$ lies in the boundary

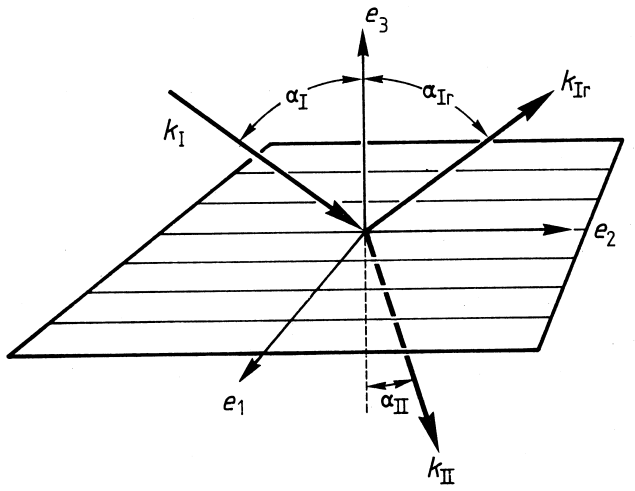


**Figure 4.10** Propagation vectors in reflection and refraction on a boundary surface.

surface. $\boldsymbol{H}_{\mathrm{II}}$ remains in the plane of incidence as a consequence of $H_{\mathrm{IItg}} = H_{\mathrm{Itg}}$. Because $\boldsymbol{H}_{\mathrm{II}} \cdot \boldsymbol{D}_{\mathrm{II}} = 0$ we also have $\boldsymbol{D}_{\mathrm{II}}$ perpendicular to the plane of incidence. Hence $\boldsymbol{k}_{\mathrm{II}}$ lies in the plane of incidence ($\boldsymbol{D}_{\mathrm{II}} \cdot \boldsymbol{k}_{\mathrm{II}} = 0$!).

In the case $\boldsymbol{E}_{\mathrm{I}} \cdot \boldsymbol{e}_1 = 0$, $\boldsymbol{H}_{\mathrm{I}}$ and hence $\boldsymbol{B}_{\mathrm{I}}$ are perpendicular to the plane of incidence ($\boldsymbol{H}_{\mathrm{I}} \parallel \boldsymbol{e}_1$). In medium I we have $\boldsymbol{H}_{\mathrm{I}} \parallel \boldsymbol{H}_{\mathrm{Ir}}$. Because $\boldsymbol{H}_{\mathrm{Ir}} \cdot \boldsymbol{k}_{\mathrm{Ir}} = 0$, $\boldsymbol{k}_{\mathrm{Ir}}$ must lie in the plane of incidence. The condition $B_{\mathrm{In}} = B_{\mathrm{IIn}}$ requires that $\boldsymbol{B}_{\mathrm{II}}$ lies in the boundary surface and hence also $\boldsymbol{H}_{\mathrm{II}}$. Conservation of the tangential component of $\boldsymbol{H}$, thus, $H_{\mathrm{I}} = H_{\mathrm{IItg}}$ ($H_{\mathrm{I}} = H_{\mathrm{Itg}}$!), means that we have $\boldsymbol{H}_{\mathrm{II}} \parallel \boldsymbol{H}_{\mathrm{I}}$ and that $\boldsymbol{k}_{\mathrm{II}}$ also lies in the plane of incidence ($\boldsymbol{H}_{\mathrm{II}} \cdot \boldsymbol{k}_{\mathrm{II}} = 0$!).

For the following derivation of the formulae for the amplitude of the reflected and refracted waves we assume that both media are isotropic.

**A. $E$ perpendicular to the plane of incidence, $H$ in the plane of incidence**

Let the incident wave be given by

$$\boldsymbol{E}_{\mathrm{I}} = \boldsymbol{E}_{\mathrm{I}0} e^{2\pi i(\boldsymbol{k}_{\mathrm{I}} \cdot \boldsymbol{x} - \nu t)},$$

the reflected wave by

$$\boldsymbol{E}_{\mathrm{Ir}} = \boldsymbol{E}_{\mathrm{Ir}0} e^{2\pi i(\boldsymbol{k}_{\mathrm{Ir}} \cdot \boldsymbol{x} - \nu t)},$$

and the refracted wave by

$$\boldsymbol{E}_{\mathrm{II}} = \boldsymbol{E}_{\mathrm{II}0} e^{2\pi i(\boldsymbol{k}_{\mathrm{II}} \cdot \boldsymbol{x} - \nu t)}.$$

The $\boldsymbol{k}$'s are of the form $\boldsymbol{k} = k_2\boldsymbol{e}_2 + k_3\boldsymbol{e}_3$. Because of the continuity of $E_{\mathrm{tg}}$ we then have for $x_3 = 0$:

$$E_{\mathrm{I}0}e^{2\pi i k_{\mathrm{I}2}x_2} + E_{\mathrm{Ir}0}e^{2\pi i k_{\mathrm{Ir}2}x_2} = E_{\mathrm{II}0}e^{2\pi i k_{\mathrm{II}2}x_2}.$$

This condition can only be satisfied for arbitrary $\boldsymbol{E}_{\mathrm{I}}$ and $\boldsymbol{k}_{\mathrm{I}}$ when the exponential factors are equal, hence $k_{\mathrm{I}2} = k_{\mathrm{Ir}2} = k_{\mathrm{II}2}$. This means, the tangential component of the propagation vector remains conserved. Because

$$k_{\mathrm{I}2} = |\boldsymbol{k}_{\mathrm{I}}|\sin\alpha_{\mathrm{I}}, \quad k_{\mathrm{Ir}2} = |\boldsymbol{k}_{\mathrm{Ir}}|\sin\alpha_{\mathrm{Ir}}, \quad \text{and} \quad k_{\mathrm{II}2} = |\boldsymbol{k}_{\mathrm{II}}|\sin\alpha_{\mathrm{II}}$$

one obtains for both conditions

$$\alpha_{\mathrm{I}} = \alpha_{\mathrm{II}}(\text{law of reflection}) \quad \text{and}$$
$$\frac{\sin\alpha_{\mathrm{I}}}{\sin\alpha_{\mathrm{II}}} = \frac{|\boldsymbol{k}_{\mathrm{II}}|}{|\boldsymbol{k}_{\mathrm{I}}|} = \frac{n_{\mathrm{II}}}{n_{\mathrm{I}}}(\text{law of refraction}).$$

Furthermore, we have $E_{\mathrm{I}0} + E_{\mathrm{Ir}0} = E_{\mathrm{II}0}$. A second condition is gained from the continuity of the tangential component of $\boldsymbol{H}$. Since $\boldsymbol{k}$, $\boldsymbol{E}$, and $\boldsymbol{H}$ form a right-handed system, one finds for $x_3 = 0$

$$-\cos\alpha_{\mathrm{I}}H_{\mathrm{I}0}e^{2\pi i k_{\mathrm{I}2}x_2} + \cos\alpha_{\mathrm{I}}H_{\mathrm{Ir}0}e^{2\pi i k_{\mathrm{Ir}2}x_2} = -\cos\alpha_{\mathrm{II}}H_{\mathrm{II}0}e^{2\pi i k_{\mathrm{II}}2x_2}.$$

This also applies in the case that medium II is anisotropic and two refracted waves arise, because the exponential factors must be equal in each case. Now in order to connect this condition and the one above, it is necessary to use the relationship between the amplitudes of the electric and magnetic field strengths of an electromagnetic wave. From the induction law

$$\mathrm{rot}\,\boldsymbol{E} = -\frac{1}{c}\frac{\partial \boldsymbol{H}}{\partial t} \quad \text{we get} \quad \boldsymbol{k}\times\boldsymbol{E} = \frac{\nu}{c}\cdot\boldsymbol{H}.$$

For the absolute values in isotropic media one gets

$$|\boldsymbol{H}| = |\boldsymbol{E}||\boldsymbol{k}|(c/\nu) \quad \text{and with} \quad |\boldsymbol{k}|/\nu = 1/v \quad (\text{because } \lambda\nu = v),$$
$$|\boldsymbol{H}| = \frac{c}{v}|\boldsymbol{E}| = n|\boldsymbol{E}|.$$

Thereby we convert the condition for the tangential component of $\boldsymbol{H}$ into

$$n_{\mathrm{I}}\cos\alpha_{\mathrm{I}}(-E_{\mathrm{I}0} + E_{\mathrm{Ir}0}) = -n_{\mathrm{II}}\cos\alpha_{\mathrm{II}}E_{\mathrm{II}0}.$$

Together with $E_{\mathrm{I}0} + E_{\mathrm{Ir}0} = E_{\mathrm{II}0}$ and with $n_{\mathrm{II}}/n_{\mathrm{I}} = \sin\alpha_{\mathrm{I}}/\sin\alpha_{\mathrm{II}}$, one obtains for $\boldsymbol{E}$ perpendicular to the plane of incidence the *first Fresnel formula*

$$E_{\mathrm{I}0} : E_{\mathrm{II}0} : E_{\mathrm{Ir}0} = \sin(\alpha_{\mathrm{I}} + \alpha_{\mathrm{II}}) : (\sin(\alpha_{\mathrm{I}} + \alpha_{\mathrm{II}}) + \sin(\alpha_{\mathrm{II}} - \alpha_{\mathrm{I}})) : \sin(\alpha_{\mathrm{II}} - \alpha_{\mathrm{I}}).$$

**B. $E$ in the plane of incidence, $H$ perpendicular to the plane of incidence.**
We can proceed analogously to the previous derivation when we correspondingly exchange $\boldsymbol{E}$ and $\boldsymbol{H}$. Preserving the tangential component of $\boldsymbol{H}$ and $\boldsymbol{E}$, respectively, gives

$$H_{\mathrm{Itg}} + H_{\mathrm{Irtg}} = H_{\mathrm{IItg}} \qquad (\text{here } \boldsymbol{H} = \boldsymbol{H}_{\mathrm{tg}}\,!) \quad \text{and}$$
$$E_{\mathrm{Itg}} = \cos\alpha_{\mathrm{I}} E_{\mathrm{I}0} e^{2\pi i k_{\mathrm{I}2} x_2} - \cos\alpha_{\mathrm{I}} E_{\mathrm{Ir}0} e^{2\pi i k_{\mathrm{Ir}2} x_2} = \cos\alpha_{\mathrm{II}} E_{\mathrm{II}0} e^{2\pi i k_{\mathrm{II}2} x_2}.$$

If we again substitute the amplitudes of the magnetic field strength by those of the electric field strength and use the addition theorem of trigonometric functions we get for $\boldsymbol{E}$ in the plane of incidence the *second Fresnel formula*

$$E_{\mathrm{I}0} : E_{\mathrm{II}0} : E_{\mathrm{Ir}0} = \tan(\alpha_{\mathrm{I}} + \alpha_{\mathrm{II}}) : \left\{ \frac{\tan(\alpha_{\mathrm{I}} + \alpha_{\mathrm{II}})}{\cos(\alpha_{\mathrm{I}} - \alpha_{\mathrm{II}})} + \frac{\tan(\alpha_{\mathrm{II}} - \alpha_{\mathrm{I}})}{\cos(\alpha_{\mathrm{I}} + \alpha_{\mathrm{II}})} \right\} : \tan(\alpha_{\mathrm{I}} - \alpha_{\mathrm{II}}).$$

With the aid of the Fresnel formulae we can now calculate the intensity of the reflected and refracted waves for the case of isotropic media by constructing the respective Poynting vectors and also take into account the change of the ray cross-section. The cross-section $q_{\mathrm{II}}$ in medium II is

$$q_{\mathrm{II}} = q_{\mathrm{I}} \cos\alpha_{\mathrm{II}} / \cos\alpha_{\mathrm{I}},$$

where $q_{\mathrm{I}}$ is the cross-section of the incident ray. Moreover, the energy conservation of course holds. This is guaranteed by the Fresnel equations, as one can easily check ($|\boldsymbol{S}_{\mathrm{I}}| = |\boldsymbol{S}_{\mathrm{Ir}}| + |\boldsymbol{S}_{\mathrm{II}}|$).

We have for the intensity $I_{\mathrm{Ir}}$ of the reflected wave in the case $\boldsymbol{E}$ perpendicular to the plane of incidence

$$\frac{I_{\mathrm{Ir}}}{I_{\mathrm{I}}} = \left( \frac{\sin(\alpha_{\mathrm{I}} - \alpha_{\mathrm{II}})}{\sin(\alpha_{\mathrm{I}} + \alpha_{\mathrm{II}})} \right)^2 = \left( \frac{1 - \dfrac{n_{\mathrm{II}}}{n_{\mathrm{I}}} \dfrac{\cos\alpha_{\mathrm{II}}}{\cos\alpha_{\mathrm{I}}}}{1 + \dfrac{n_{\mathrm{II}}}{n_{\mathrm{I}}} \dfrac{\cos\alpha_{\mathrm{II}}}{\cos\alpha_{\mathrm{I}}}} \right)^2$$

using $\sin\alpha_{\mathrm{I}} / \sin\alpha_{\mathrm{II}} = n_{\mathrm{II}} / n_{\mathrm{I}}$.

The result for perpendicular incidence ($\alpha_\mathrm{I} = 0$) is

$$\frac{I_\mathrm{Ir}}{I_\mathrm{I}} = \left(\frac{1 - n_\mathrm{II}/n_\mathrm{I}}{1 + n_\mathrm{II}/n_\mathrm{I}}\right)^2 .$$

For the reflection at a plate of refractive index 1.50 adjacent to vacuum or air one thus obtains only the small fraction of about 4%. On the other hand, one observes for glancing incidence ($\alpha_\mathrm{I} = 90°$) independent of $n_\mathrm{II}/n_\mathrm{I}$ $\frac{I_\mathrm{Ir}}{I_\mathrm{I}} = 1$, hence the full reflection of the incident wave. From the second Fresnel formula one gets the same result for both these limiting cases. The course of $I_\mathrm{Ir}/I_\mathrm{I}$ between both limiting values is, however, different for both directions of vibration. In particular, as a consequence of the second formula for $\boldsymbol{E}$ in the plane of incidence, the amplitude of the reflected wave

$$I_\mathrm{Ir} = I_\mathrm{I}\left(\frac{\tan\alpha_\mathrm{II} - \alpha_\mathrm{I})}{\tan(\alpha_\mathrm{II} + \alpha_\mathrm{I})}\right)^2 \quad \text{vanishes,}$$

as $(\alpha_\mathrm{II} + \alpha_\mathrm{I})$ approaches 90°, that is, the reflected and refracted waves are perpendicular to one another.

If one substitutes in the law of refraction $\sin\alpha_\mathrm{I}/\sin\alpha_\mathrm{II} = n_\mathrm{II}/n_\mathrm{I}$ the angle $\alpha_\mathrm{II}$ by $(90 - \alpha_\mathrm{I})$, we get Brewster's law for the vanishing of the reflected wave $\tan\alpha_\mathrm{I} = n_\mathrm{II}/n_\mathrm{I}$. Because of the conservation of energy, the whole intensity of the incident wave goes into the refracted wave. If the incident wave is composed of light with arbitrary directions of vibration then the ray reflected under the Brewester angle contains only the direction of vibration perpendicular to the plane of incidence. This is the simplest method to produce polarized light.

A further phenomena is the case of *total reflection*. If $n_\mathrm{II} < n_\mathrm{I}$, there exists a limiting angle for $\alpha_\mathrm{I}$, above which no refracted wave can occur. The condition is $\alpha_{II} = 90°$ and thus $\sin\alpha'_\mathrm{I} = n_\mathrm{II}/n_\mathrm{I}$. A method to determine refractive indices is based on the measurement of the angle $\alpha'_\mathrm{I}$ of the total reflection.

We now return to refraction when a light wave is incident upon an anisotropic medium. According to the above, with a known plane of incidence, we merely have to take into account the condition for the preservation of the tangential component of the propagation vector of the incident wave. With the help of the index surface we establish which refractive indices in the plane of incidence are consistent with the condition $k_\mathrm{Itg} = k_\mathrm{IItg}$. The index surface is a double-shelled centrosymmetric surface, constructed such that the lengths of the radius vectors $\boldsymbol{x}$ are equal to the refractive indices of the given directions of propagation, hence $x_i = ng_i$. In the principal axes' reference system of the indicatrix, one obtains the index surface from the velocity equation derived above for a given direction of propagation $\sum_i g_i^2/(v_i^2 - v^2) = 0$, when we write $v = c/n$, $v_i = c/n_i$, $x_i = ng_i$, and $\boldsymbol{x}^2 = n^2$. The result is the equation for

the index surface:

$$\sum_i \frac{x_i^2 n_i^2}{\sum_j x_j^2 - n_i^2} = 0$$

or after multiplication with the common denominator and separation of a factor $\sum_i x_i^2$

$$(x_1^2 n_1^2 + x_2^2 n_2^2 + x_3^2 n_3^2)(x_1^2 + x_2^2 + x_3^2) - x_1^2 n_1^2 (n_2^2 + n_3^2) \\ - x_2^2 n_2^2 (n_3^2 + n_1^2) - x_3^2 n_3^2 (n_1^2 + n_2^2) + n_1^2 n_2^2 n_3^2 = 0.$$

The index surface of an isotropic medium, hence also cubic crystals, is a sphere of radius $n$. In optical uniaxial crystals (one principal symmetry axis 3,4, or 6), the index surface consists of a sphere $x_1^2 + x_2^2 + x_3^2 = n_1^2 = n_2^2$ and the ellipsoid $x_1^2/n_3^2 + x_2^2/n_3^2 + x_3^2/n_1^2 = 1$, as is seen by setting $n_1 = n_2$. With these crystals of trigonal, tetragonal, and hexagonal symmetry we have accordingly for each direction of propagation a wave with the fixed refractive index $n_1$. This wave is called the ordinary wave. If $n_1 < n_3$, the crystal is said to be optical positive (optical positive character) and in the other case $n_1 > n_3$ optical negative. We will return to the diagnostic value of this classification and the general definition of the optical character later.

Now to construct the refracted wave, we place the center of the index surface on the intercept line of the boundary surface and the plane of incidence. The curves of intersection of the plane of incidence with the index surface are cut, in medium II, by the line parallel to the axis of incidence at an interval of $n_\mathrm{I} \sin \alpha_\mathrm{I} = (c/\nu) k_\mathrm{Itg}$ (Fig. 4.11). The lines from the center of the index surface to the intersection points give the propagation direction of the wave refracted in medium II. Therefore, the condition for the conservation of the tangential component of $\boldsymbol{k}_\mathrm{I}$ and hence the law of refraction is fulfilled:

$$n_\mathrm{I} \sin \alpha_\mathrm{I} = (c/\nu) k_\mathrm{Itg} = (c/\nu) k_\mathrm{IItg} = n_\mathrm{II} \sin \alpha_\mathrm{II}.$$

In anisotropic media, two waves appear in the general case, except in total reflection.

The associated ray vectors are obtained with the aid of the Poinsot construction. For this purpose, the directions of vibrations of both refracted waves must be constructed. This occurs with the help of the indicatrix and the sectional ellipses perpendicular to both propagation vectors $\boldsymbol{k}'_\mathrm{II}$ and $\boldsymbol{k}''_\mathrm{II}$ analogous to Fig. 4.8. Besides wave double refraction, one also observes ray double refraction. In the case of perpendicular incidence of the wave we have $\alpha_\mathrm{I} = \alpha_\mathrm{II} = 0$, i.e., the refracted waves keep the direction of the incident wave, although they possess different propagation velocities and different directions of vibration of the $\boldsymbol{D}$-vector. Hence we observe no wave double refraction. If

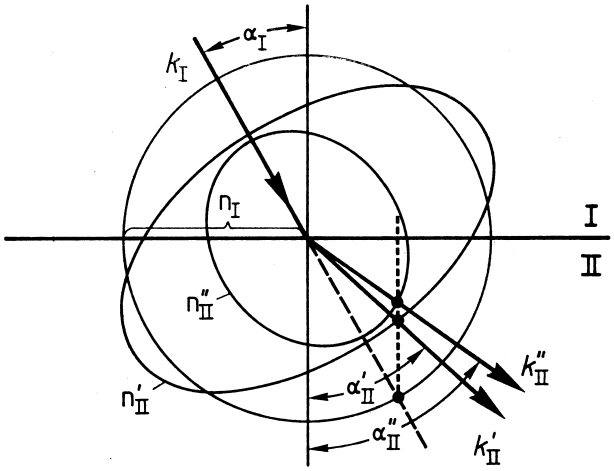


**Figure 4.11** Construction of the refraction at the transition from an isotropic medium I into a double-refracting medium II. Intersection of the incident plane with the double-shelled index surface. Conservation of the tangential component of $\boldsymbol{k}_{\mathrm{I}}$.

the principal axes of the indicatrix lie oblique to the axis of incidence, then with perpendicular incidence, we also have ray double refraction. When constructing the refracted waves at the reverse side of the plate we merely have to take into account the conservation of the tangential component of the $\boldsymbol{k}$-vectors as before.

Fig. 4.12 shows the separation of rays through a plane-parallel plate under perpendicular incidence. This arrangement also allows, in a simple manner, the production of linearly polarized light.

We now calculate the angle of ray double refraction at perpendicular incidence. The position of both $\boldsymbol{D}$-vectors results from the condition

$$D_1 : D_2 : D_3 = g_1 n_1^2/(n^2 - n_1^2) : g_2 n_2^2/(n^2 - n_2^2) : g_3 n_3^2/(n^2 - n_3^2),$$

where for $n$ we set the values $n'$ and $n''$ from the index equation for the given direction of propagation.

With the notation $E_i = a_{ij} D_j$ one finds the directions of the associated $\boldsymbol{E}$-vectors ($a_{ij}$ are the polarization constants; in the principal axes' system $a_{ii} = 1/n_i^2$ and $a_{ij} = 0$ for $i \neq j$). Both ray vectors $\boldsymbol{s}'$ and $\boldsymbol{s}''$ are given by $\boldsymbol{s}' \parallel \boldsymbol{E}' \times \boldsymbol{H}'$ and $\boldsymbol{s}'' \parallel \boldsymbol{E}'' \times \boldsymbol{H}''$, whereby the vectors $\boldsymbol{H}'$ and $\boldsymbol{H}''$ run parallel to $\boldsymbol{D}''$ and $\boldsymbol{D}'$ respectively. Thus, one finds for the angle of ray double refraction $\zeta$, with the help of the scalar product $\boldsymbol{s}' \cdot \boldsymbol{s}''$:

$$\cos\zeta = \frac{(\boldsymbol{E}' \times \boldsymbol{H}') \cdot (\boldsymbol{E}'' \times \boldsymbol{H}'')}{|\boldsymbol{E}' \times \boldsymbol{H}'||\boldsymbol{E}'' \times \boldsymbol{H}''|} \qquad \text{(see also Exercise 11).}$$

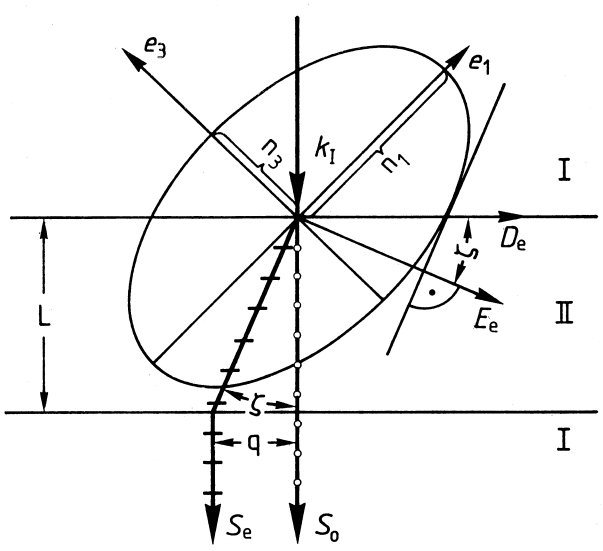


**Figure 4.12** Ray double refraction and ray separation on a plane-parallel plate of an optical uniaxial crystal at perpendicular incidence (the indicatrix is a rotation ellipsoid!). The ordinary ray $s_o$ (direction of vibration perpendicular to the plane of incidence) experiences no refraction. The direction of vibration of the extraordinary ray $s_e$ lies within the plane of incidence. $s_e$ itself runs within the crystal parallel to the trace of the tangent of the indicatrix at the piercing point of $\boldsymbol{D}_e$ (Poinsot construction). The ray separation after refraction at the reverse side is $q = L \tan\zeta$ ($L$ thickness of plate).

#### 4.3.6.2 **Determining Refractive Indices**

Besides the possibilities discussed above (e.g., total reflection or reflection coefficients using the Fresnel formulae), the practical determination of refractive indices is mainly made by deflection through a prism. In isotropic media, minimal deflection allows very exact measurements, whereby the light ray runs symmetric to the prism. Furthermore, the adjustment of the minimal deflection is, to a first approximation, noncritical with respect to small deviations from the exact position for minimal deflection (see Exercise 12).

On the other hand, for anisotropic crystals, perpendicular incidence has proven rather successful, because here no wave double refraction takes place, i.e., the wave normals of both possible waves in the crystal run parallel to the normal on the front prism face (Fig. 4.13a). Hence, we know with high reliability the direction of the wave normals in the crystal. Let the prism angle be $\varphi$. Because $\sin\alpha_\mathrm{I}/\sin\alpha_\mathrm{II} = n_\mathrm{II}/n_\mathrm{I}$ and $\alpha_\mathrm{II} = \varphi$ one obtains for the deflection angle $\alpha = \alpha_\mathrm{I} - \varphi$ and thus $\sin(\alpha+\varphi)/\sin\varphi = n_\mathrm{II}/n_\mathrm{I}$. The deflection angle can be directly determined with the help of a goniometer, where a detector system is moved on the periphery of a circle, or by the aid of length measurements (Fig. 4.13b).

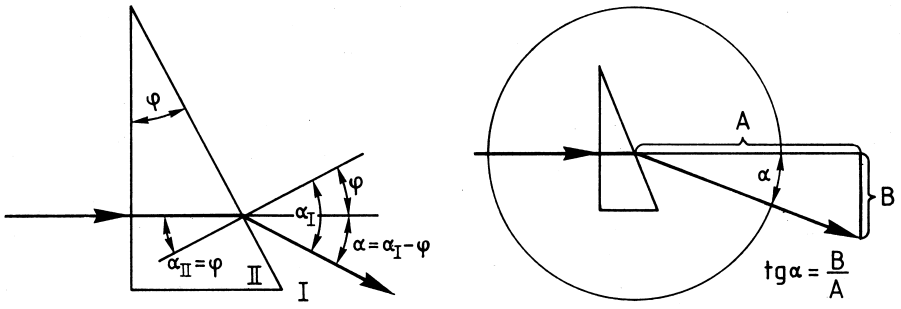


**Figure 4.13** (a) Prism method with perpendicular incidence. (b) Measurement of the deflection angle by a goniometer or by the aid of a measurement of the lengths $A$ and $B$.

We now discuss the general case of the measurement of the complete set of refractive indices of a triclinic crystal. We start with the crystal-physical reference system and prepare three prisms with the refractive edge $\boldsymbol{e}_j$ ($j = 1,2,3$) and a face perpendicular to $\boldsymbol{e}_i$, the respective transmission direction at perpendicular incidence (Fig. 4.14). In a first step, we determine for each transmission direction $\boldsymbol{e}_i$ the directions of vibrations of both possible $\boldsymbol{D}$-vectors, $\boldsymbol{D}'$ and $\boldsymbol{D}''$. This is performed best on a thin, plane-parallel crystal plate by the aid of polarization microscope under crossed polarizers. If the direction of vibration of $\boldsymbol{D}'$ or $\boldsymbol{D}''$ agrees with the transmission direction of the first or second polarizer, the plate appears completely dark after the second polarizer: Extinction position (see Section 4.3.6.3). Let the angle between $\boldsymbol{e}_j$ and the transmission direction of the first polarizer in the extinction position be $\psi_i$, whereby the fixed position of the respective vectors as shown in Fig. 4.14 is to be maintained. In order to avoid confusion, the indices $i, j, k$ are to be chosen in a cyclic sequence. In a second step we measure the deflection angles $\alpha_i'$ and $\alpha_i''$ for each of the three transmission directions. From these we obtain the associated refractive indices $n_i'$ und $n_i''$. The assignment of the extinction angle $\psi_i$ to $\boldsymbol{D}'$ is to be controlled by the aid of a polarizer placed in front of the prism. The polarizer is rotated until the intensity of the respective ray (deflection angle $\alpha'$) vanishes. $\boldsymbol{D}'$ is then perpendicular to the transmission direction of the polarizer. We now have available a total of nine quantities, namely $\psi_i$, $n_i'$ and $n_i''$ ($i = 1,2,3$), for the determination of the six coefficients $a_{ij}$ of the indicatrix. The sectional ellipse perpendicular to $\boldsymbol{e}_i$ is given in the crystal-physical system by

$$a_{jj}x_j^2 + a_{kk}x_k^2 + 2a_{jk}x_jx_k = 1$$

(do not sum!; $x_i = 0$ in the equation $a_{ij}x_ix_j = 1$!).

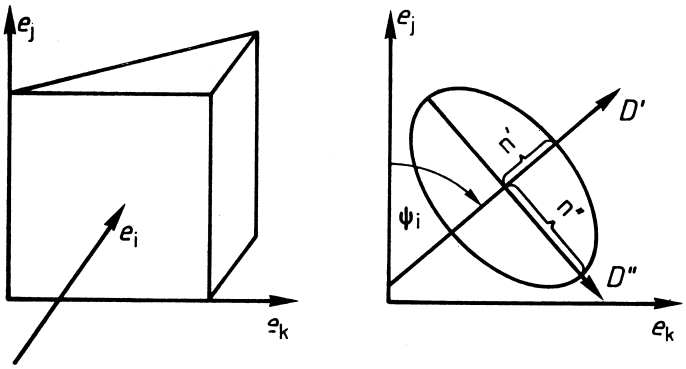


**Figure 4.14** Measurement of indices of refraction on triclinic crystals by the prism method with perpendicular incidence. Pay attention to the sense of rotation of the angle $\psi_i$ when applying the inverse transformation.

A plane principal axes' transformation

$$\begin{aligned} \boldsymbol{e}'_i &= \boldsymbol{e}_i \\ \boldsymbol{e}'_j &= \cos\psi_i \boldsymbol{e}_j + \sin\psi_i \boldsymbol{e}_k \\ \boldsymbol{e}'_k &= -\sin\psi_i \boldsymbol{e}_j + \cos\psi_i \boldsymbol{e}_k \end{aligned}$$

transforms the equation of the sectional ellipse into $a'_{jj}x'^2_j + a'_{kk}x'^2_k = 1$. We have $a'_{jj} = 1/n'^2_i$ and $a'_{kk} = 1/n''^2_i$.

We find the necessary coefficients with the help of the inverse transformation (see Section 4.3.2)

$$\begin{aligned} a_{jj} &= \cos^2\psi_i a'_{jj} + \sin^2\psi_i a'_{kk}; \\ a_{kk} &= \sin^2\psi_i a'_{jj} + \cos^2\psi_i a'_{kk}; \\ a_{jk} = a_{kj} &= \tfrac{1}{2}(a'_{jj} - a'_{kk})\sin 2\psi_i. \end{aligned}$$

One then obtains the three principal coefficients $a_{11}$, $a_{22}$, and $a_{33}$, each twice, independent of one another and thus we have a good control of the reliability of the measurement.

In a third step we perform a general principal axes' transformation and find the principal refractive indices $n_1$, $n_2$, and $n_3$ as well as the associated directions of vibrations of the $\boldsymbol{D}$-vectors. With this method one can achieve, without special measures, an accuracy of about $10^{-4}$ for the principal refractive indices, when the specimens are homogenous and adequately oriented and prepared. The dimensions of the prisms play an important role with respect to the quality of the preparation, particularly with soft crystals. The edge lengths

of the prisms should not be essentially smaller than 6 mm and the prism angles should be selected to be as large as possible up to just about the limit for total reflection.

The determination of the indicatrix of crystals of higher symmetry is substantially easier. For example, with optical uniaxial crystals one needs only one prism, in which the entrance face of the light ray contains the respective principal symmetry axis.

#### 4.3.6.3 Plane-Parallel Plate between Polarizers at Perpendicular Incidence

In the practical application of crystal optics, the plane-parallel plate is the most important standard preparation in polarization microscopy as well as in technical components. This also applies to the investigation of higher optical effects (electro-optics, piezo-optics). The transmission takes place almost exclusively in perpendicular incidence. Here we derive the intensity formula for the transmitted ray dependent on the position of the direction of vibration.

A linear polarized wave emerging from the first polarizer $P_1$ strikes the crystal plate. There it is split into components parallel to the directions of vibrations of the associated sectional ellipse. After passing through a thickness $L$ both waves leave the plate and unify themselves to an elliptically polarized wave. This means, that we have a wave composed of two plane-polarized partial waves with the same propagation vector (and hence the same frequency), however, with different directions of vibration and phase (time difference of the maximum amplitude). A second polarizer $P_2$ transmits only that component, whose direction of vibration corresponds to the transmission direction of $P_2$. From the square of the amplitude of this component we then obtain a measure for the intensity of the transmitted light.

We introduce the following notations for the calculation (Fig. 4.15):

- Normal on the boundary surface: $\boldsymbol{e}_3$,
- Direction of vibration of the first polarizer $P_1$: $\boldsymbol{e}_1$,
- Directions of vibration of the sectional ellipse (directions of major and minor semiaxis): $\boldsymbol{e}'$ and $\boldsymbol{e}''$,
- Direction of vibration of the second polarizer $P_2$: $\boldsymbol{e}_1'$,
- Angle between $\boldsymbol{e}_1$ and $\boldsymbol{e}'$: $\phi$,
- Angle between $\boldsymbol{e}_1$ and $\boldsymbol{e}_1'$: $\psi$.

We describe the incident wave by $\boldsymbol{D} = D_0 e^{2\pi i(\boldsymbol{k}\cdot\boldsymbol{x}-\nu t)}\boldsymbol{e}_1$, whereby $\boldsymbol{k} = k_3\boldsymbol{e}_3$.

When the wave enters the crystal ($x_3 = 0$), $\boldsymbol{D}$ it is split into components parallel to $\boldsymbol{e}'$ and $\boldsymbol{e}''$,

$$D_0\boldsymbol{e}_1 = D_0'\boldsymbol{e}' + D_0''\boldsymbol{e}'' \quad \text{with} \quad D_0' = D_0\cos\varphi, \quad D_0'' = -D_0\sin\varphi.$$

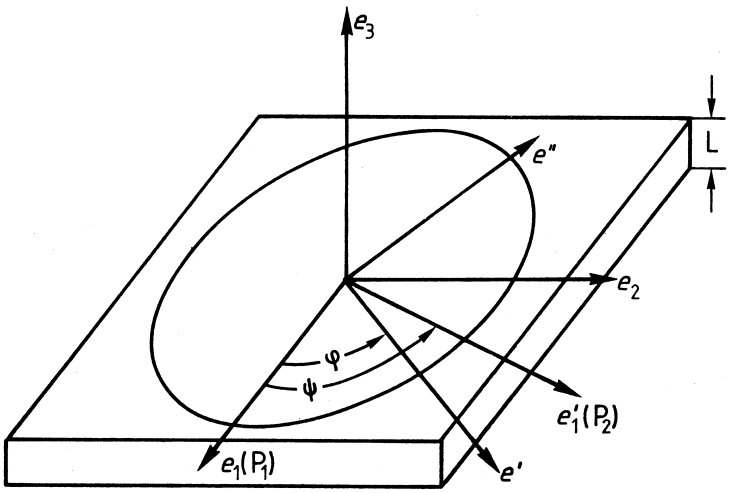


**Figure 4.15** Plane-parallel plate between two polarizers $P_1$ and $P_2$.

After passing through a distance $x_3 = L$ both partial waves combine on the top side of the plate to

$$\boldsymbol{D} = D_0 \cos\varphi e^{2\pi i(k_3' L - \nu t)} \boldsymbol{e}' - D_0 \sin\varphi e^{2\pi i(k_3'' L - \nu t)} \boldsymbol{e}''.$$

After reentering in air or vacuum, respectively, we have

$$\boldsymbol{D} = D_0 \cos\varphi e^{2\pi i M} \boldsymbol{e}' - D_0 \sin\varphi e^{2\pi i(M+d)} \boldsymbol{e}'' \quad \text{with}$$
$$M = L/\lambda' + (x_3 - L)/\lambda_0 - \nu t$$

and $d = L(n'' - n')/\lambda_0$, whereby $\lambda_0$ means the wavelength in air or vacuum ($n = \lambda_0/\lambda$!), respectively.

Because

$$\boldsymbol{e}' = \cos(\psi - \varphi)\boldsymbol{e}_1' - \sin(\psi - \varphi)\boldsymbol{e}_2',$$
$$\boldsymbol{e}'' = \sin(\psi - \varphi)\boldsymbol{e}_1' + \cos(\psi - \varphi)\boldsymbol{e}_2' \quad (\text{with } \boldsymbol{e}_2' \cdot \boldsymbol{e}_1' = 0)$$

we obtain for the amplitude of the wave transmitted through the second polarizer

$$D_{\|P_2} = D_0 \cos\varphi \cos(\psi - \varphi) e^{2\pi i M} - D_0 \sin\varphi \sin(\psi - \varphi) e^{2\pi i(M+d)}.$$

If we ignore reflection losses at both boundary surfaces, we obtain for the time average of the transmitted intensity $I$ the following value:

$$I = I_0 \cos^2\varphi \cos^2(\psi - \varphi)(1 - \tan\varphi \tan(\psi - \varphi) e^{2\pi i d})(1 - \tan\varphi \tan(\psi - \phi) e^{-2\pi i d}).$$

Here we have used the fact that the time average of the intensity is proportional to the square of the magnitude of the complex amplitude of $\boldsymbol{D}$, hence $I = qD_{\parallel P_2}\bar{D}_{\parallel P_2}$, and $I_0$, the intensity of the primary wave, is to be correspondingly represented by $I_0 = qD_0\bar{D}_0$. $q$ is a proportionality factor.

With the help of the relations

$$\begin{aligned} e^{is} + e^{-is} &= 2\cos s, \quad \cos s = 1 - 2\sin^2(s/2), \\ \sin(u+v) &= \sin u \cos v + \sin v \cos u \quad \text{and} \\ \cos(u+v) &= \cos u \cos v - \sin u \sin v \end{aligned}$$

we can write the intensity formula in a much simpler form:

$$I = I_0(\cos^2\psi + \sin 2\varphi \sin 2(\psi - \varphi)\sin^2 \pi d).$$

The quantity $d = L(n'' - n')/\lambda_0$ is called the optical path difference, measured in wavelengths (for air or vacuum, respectively). Of special practical importance is the case of crossed polarizers $\psi = 90^\circ$.

Here

$$I = I_0 \sin^2 2\varphi \sin^2 \pi d.$$

This relationship is the basis of polarization microscopy as well as of the quantitative measurement of the optical path difference and its variation under external conditions. If $\boldsymbol{e}'$ is parallel or perpendicular to $\boldsymbol{e}_1$ or $\boldsymbol{e}'_1 = \boldsymbol{e}_2$, the directions of vibrations of the polarizers, then $I$ vanishes completely ($\varphi = 0$ or $90^\circ$; extinction position). In the so-called diagonal position $\varphi = 45^\circ$ (and odd multiples thereof), $I$ takes on a maximum. The factor $\sin^2 \pi d$ causes a strong dependence on the wavelength of the primary radiation. If one works with white light, then those regions of the spectrum are attenuated or extinguished for which $\pi d = m\pi$ ($m$ integer), hence $d = m$ or $\lambda_0 = L(n'' - n')/m$. As a consequence, one observes the characteristic color phenomena, from which the experienced polarization microscopist, at least in the range of small values of $m$, can draw quantitative conclusions about the existing path difference.

If one places an arrangement of several crystal plates with parallel directions of vibration between the polarizers, the path differences $d_i$ add according to $d = \sum_i d_i$. The application of the so-called compensators is based on this fact. Compensators are crystal plates whose effective path difference can be varied within certain limits by changing the active thickness (quartz-wedge compensator, Fig. 4.16) or by rotating a plate perpendicular to the transmission direction (rotatory compensator).

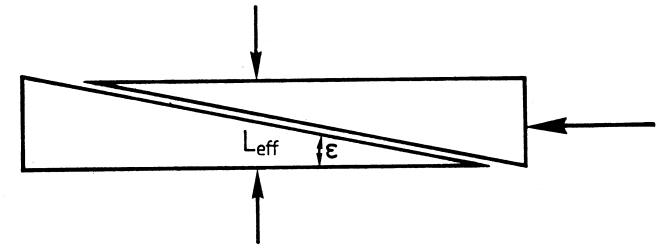


**Figure 4.16** Quartz-wedge compensator. The effective thickness $L_{\text{eff}}$ can be varied by translation of the wedges. In order to achieve high resolution the edge angle $\varepsilon$ should be chosen to be sufficiently small. The wedges possess the same orientation. The optic axis is oriented within the outside faces of the plate.

#### 4.3.6.4 **Directions of Optic Isotropy: Optic Axes, Optic Character**

In each crystal there exist directions having a circle as the sectional ellipse. The associated directions of vibration of the $\boldsymbol{D}$-vectors are, in this case, not fixed by the sectional ellipse. The refractive indices of all waves with this propagation direction are the same. We call these directions of isotropy of wave propagation *optic axes*. We consider the case of an arbitrary indicatrix in the principal axes' system:

$$\sum_i x_i^2/n_i^2 = 1 \quad \text{with} \quad n_1 < n_2 < n_3.$$

If we vary the position of the propagation directions perpendicular to $\boldsymbol{e}_2$, then one principal axis, respectively, of the sectional ellipse remains unaltered, namely that parallel to $\boldsymbol{e}_2$ with a length of $n_2$. The other principal axis changes its position between the values $n_1$ and $n_3$. Since $n_2$ lies between these values, there exists one direction in which $n' = n'' = n_2$.

Let the given propagation directions form an angle $V$ with the direction $\boldsymbol{e}_3$ (Fig. 4.17). We thus have $\cos V = x_1/n_2$.

The condition for the circular section is

$$x_1^2 + x_3^2 = n_2^2 \quad \text{and} \quad x_1^2/n_1^2 + x_3^2/n_3^2 = 1.$$

After eliminating $x_3$ we find

$$\cos V = \frac{x_1}{n_2} = \pm\frac{n_1}{n_2}\sqrt{\frac{n_3^2 - n_2^2}{n_3^2 - n_1^2}} = \pm\sqrt{\frac{\dfrac{n_3^2}{n_2^2} - 1}{\dfrac{n_3^2}{n_1^2} - 1}}.$$

The angle $2V$ between both these equivalent optical axes is called the *axial angle*. We call the bisector of the smaller angle between the optical axes the *acute*

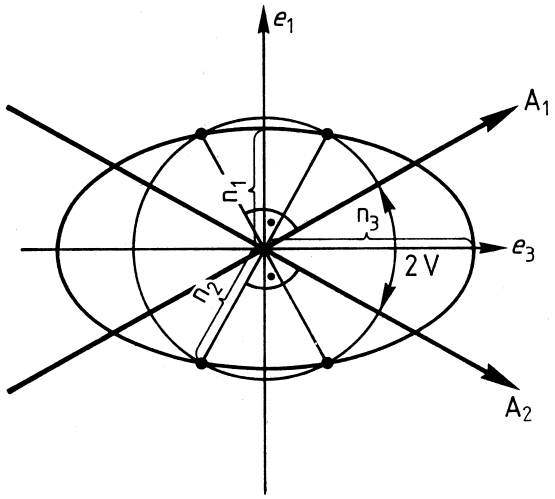


**Figure 4.17** Construction of the optic axes $A_1$ and $A_2$ in the plane perpendicular to the medium semiaxis $\boldsymbol{e}_2$ (axial plane). In the present case the acute bisectrix runs parallel to $\boldsymbol{e}_3$ (optically positive, if $n_3 > n_1$).

*bisectrix*, the other bisector is called the *obtuse bisectrix*. The plane spanned by both axes is called the axial plane, their normal (parallel $\boldsymbol{e}_2$) is called the optical binormal. We can now define the *optic character* in general:

*optically positive*, if acute bisectrix parallel to largest semiaxis $n_3$ (largest refractive index),

*optically negative*, if acute bisectrix parallel to shortest semiaxis $n_1$.

In crystals with a three-, four-, or six-fold principal axis, the indicatrix takes on the form of an ellipsoid of revolution. Both optical axes converge to one optical axis. Such crystals are therefore called optical uniaxial as opposed to the orthorhombic, monoclinic, and triclinic crystals which are referred to as optical biaxial.

The optic character is an important and easily accessible criterion for the diagnosic work. If a crystal plate, cut approximately perpendicular to an optic axis and aligned between crossed polarizers, is irradiated by a divergent beam of light, one can observe simultaneously the change of the path difference as a function of the deviation of the transmission direction from the optic axis (conoscopic imaging). With optic uniaxial crystals, the directions of identical path difference lie in cones around the optic axis and are identified by concentric rings around the piercing point of the optic axis. If one works with white light, one observes color phenomena which correspond to the progress of interference colors of a plane-parallel plate with increasing path difference. For this reason the curves are termed isochromates. Furthermore, the directions,

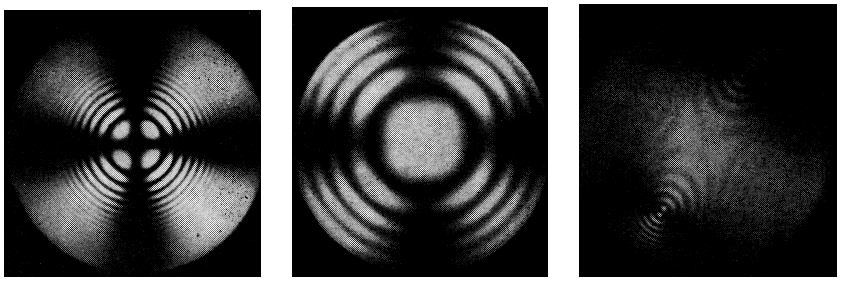

(a) (b) (c)

**Figure 4.18** Conoscopic images around optical axes taken under crossed polarizers. (a) uniaxial, not optically active ($C(NH_2)_3Al(SO_4)_2 \cdot 6H_2O$); (b) uniaxial, optical active (cesium tartrate); (c) biaxial, not optical active (calcium formiate, diagonal position).

in which the principal axes of the sectional ellipse run parallel to the directions of vibration of the polarizers, show extinction. These directions converge in the image field to dark lines called isogyres. In optical biaxial crystals, the isochromates and the isogyres deviate in a characteristic manner from the image of uniaxial crystals (Fig. 4.18). If one now places an auxiliary crystal, with a path difference of around a quarter of a wavelength, in the ray path, one observes in different directions addition or subtraction of the path difference and thus a characteristic change of the interference colors. One can immediately recognize the optical character from the increase or decrease of the effective path difference in the vicinity of an optical axis, dependent on the position of the major semiaxis of the sectional ellipse of the auxiliary crystal.

The characteristic axis images can also be used for a fast and convenient determination of the orientation of large crystals. For this purpose, one places the crystal to be investigated in a cuvette with a liquid possessing a refractive index roughly coincident with that of the crystal. Two polarizers are then placed in front and behind the cuvette in crossed position. With divergent white light coming directly from a light bulb in front of the first polarizer, the position of the optical axis(es) can be located, with high accuracy, within a few minutes by turning the crystal.

The optical axes play a role in the determination of the directions of vibration of the $\boldsymbol{D}$-vectors for an arbitrary propagation direction $\boldsymbol{g}$ with the aid of Fresnel's construction in a stereographic projection. We draw the optical axes $A_1$ and $A_2$ as well as the propagation vector $\boldsymbol{g}$ from the center of the indicatrix. The normals $L_1$ and $L_2$ on the planes spanned by $A_1$ and $\boldsymbol{g}$ as well as $A_2$ and $\boldsymbol{g}$ intercept the indicatrix in points possessing a distance $n_2$ from the center. This means, both normals lie symmetric to one of the semiaxes of the sectional ellipse (perpendicular to $\boldsymbol{g}$). The bisectors of the normals $L_1$ and

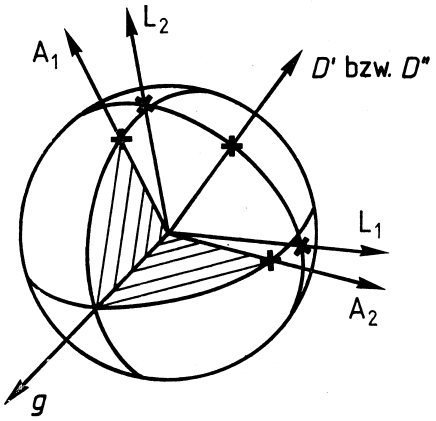


**Figure 4.19** Fresnel's construction of the directions of vibration $D'$ and $D''$, respectively, from the position of the propagation vector $g$ and the optical axes $A_1$ and $A_2$. The construction can be performed conveniently by the aid of the stereographic projection.

$L_2$ then deliver the associated directions of vibration (Fig. 4.19). In uniaxial crystals, the position of the directions of vibrations is particularly easy to recognize. The $\boldsymbol{D}$-vector of the extraordinary wave vibrates in the plane spanned by $\boldsymbol{g}$ and the optical axis (principal section), and the $\boldsymbol{D}$-vector of the ordinary wave vibrates perpendicular to the principal plane.

#### 4.3.6.5 Sénarmont Compensator for the Analysis of Elliptically Polarized Light

Any number of waves with a fixed frequency $\nu$ and a common direction of propagation $\boldsymbol{g}$, but with different directions of vibration and arbitrary phase combine in isotropic media to form an elliptically polarized wave. One can imagine this wave as composed of two linear polarized waves with mutually perpendicular directions of vibration and with a phase difference of 90°. This is recognized as follows. Let arbitrary waves $\boldsymbol{D}_j = \boldsymbol{D}_{j0} e^{2\pi i(\boldsymbol{k}\cdot\boldsymbol{x}-\nu t+\alpha_j)}$ with $\boldsymbol{D}_j \cdot \boldsymbol{k} = 0$ unite to the resultant $\boldsymbol{D} = \sum_j \boldsymbol{D}_j$. In a Cartesian reference system let $\boldsymbol{D}_{j0}$ be resolved into components

$$\boldsymbol{D}_{j0} = D_{j0} \cos\varphi_j \boldsymbol{e}_{\mathrm{I}} + D_{j0} \sin\varphi_j \boldsymbol{e}_{\mathrm{II}} \qquad (\boldsymbol{k} \parallel \boldsymbol{e}_{\mathrm{III}}).$$

We then have

$$\boldsymbol{D} = e^{2\pi i(\boldsymbol{k}\cdot\boldsymbol{x}-\nu t)} (\boldsymbol{D}_{\mathrm{I}0} e^{2\pi i\varphi_{\mathrm{I}}} + \boldsymbol{D}_{\mathrm{II}0} e^{2\pi i\varphi_{\mathrm{II}}}) = e^{2\pi iA} (\boldsymbol{D}_{\mathrm{I}0} + \boldsymbol{D}_{\mathrm{II}0} e^{2\pi i\delta}) = \boldsymbol{D}_{\mathrm{I}} + \boldsymbol{D}_{\mathrm{II}},$$

where

$$\boldsymbol{D}_{\mathrm{I}0}e^{2\pi i\varphi_{\mathrm{I}}} = \sum_j D_{j0}\cos\varphi_j e^{2\pi i\alpha_j}\boldsymbol{e}_{\mathrm{I}},$$
$$\boldsymbol{D}_{\mathrm{II}0}e^{2\pi i\varphi_{\mathrm{II}}} = \sum_j D_{j0}\sin\varphi_j e^{2\pi i\alpha_j}\boldsymbol{e}_{\mathrm{II}},$$
$$A = (\boldsymbol{k}\cdot\boldsymbol{x} - \nu t + \varphi_{\mathrm{I}}) \quad \text{and} \quad \delta = (\varphi_{\mathrm{II}} - \varphi_{\mathrm{I}})$$

The resultant of $\boldsymbol{D}$ to a certain value of $A$ is obtained from the real part of $\boldsymbol{D}$ in the directions $\boldsymbol{e}_{\mathrm{I}}$ and $\boldsymbol{e}_{\mathrm{II}}$. Thus

$$\mathrm{Re}(D_{\mathrm{I}}) = D_{\mathrm{I}} = D_{\mathrm{I}0}\cos 2\pi A \quad \text{and}$$
$$\mathrm{Re}(D_{\mathrm{II}}) = D_{\mathrm{II}} = D_{\mathrm{II}0}\cos 2\pi(A+\delta).$$

Elimination of $A$ using

$$\cos 2\pi(A+\delta) = \cos 2\pi A\cos 2\pi\delta - \sin 2\pi A\sin 2\pi\delta$$

gives

$$D_{\mathrm{II}}/D_{\mathrm{II}0} - D_{\mathrm{I}}/D_{\mathrm{I}0}\cos 2\pi\delta = -\sqrt{1-(D_{\mathrm{I}}/D_{\mathrm{I}0})^2}\sin 2\pi\delta.$$

After squaring we have

$$D_{\mathrm{I}}^2/D_{\mathrm{I}0}^2 + D_{\mathrm{II}}^2/D_{\mathrm{II}0}^2 - 2D_{\mathrm{I}}D_{\mathrm{II}}\cos 2\pi\delta/D_{\mathrm{I}0}D_{\mathrm{II}0} = \sin^2 2\pi\delta.$$

This is the equation of an ellipse. The resultant of $\boldsymbol{D}$ passes through the ellipse once per vibration. The position of the principal axes of the ellipse and the extreme values of $\boldsymbol{D}$ are calculated with the help of a plane principal axes' transformation. The result for an angle of rotation $\psi$ around $\boldsymbol{e}_{\mathrm{III}}$ is

$$\tan 2\psi = \frac{2D_{\mathrm{I}0}D_{\mathrm{II}0}\cos 2\pi\delta}{D_{\mathrm{I}0}^2 - D_{\mathrm{II}0}^2}.$$

The associated extreme values are $D'_{\mathrm{I}0}$ and $D''_{\mathrm{II}0}$. In the rotated reference system, the equation of the ellipse is $(D'_{\mathrm{I}}/D'_{\mathrm{I}0})^2 + (D'_{\mathrm{II}}/D'_{\mathrm{II}0})^2 = 1$. This means, the elliptic polarized wave can also be represented as a superposition of two linear polarized waves with mutually perpendicular directions of vibration. These exhibit a phase difference of 90°, as one recognizes from the equivalence of the equation of the ellipse in the principal axes' system with the parameter representation

$$D'_{\mathrm{I}} = D'_{\mathrm{I}0}\cos 2\pi A' \quad \text{and} \quad D''_{\mathrm{II}} = D'_{\mathrm{II}0}\sin 2\pi A'.$$

We use the Sénarmont compensator to analyze elliptic polarized light. This consists of a crystal plate with a path difference of $\lambda_0/4$ (e.g., a cleavage

lamella of mica or a quartz plate of corresponding thickness) and a polarizer, both of which can be rotated independently around their common normal. In order to analyze the incident elliptic polarized light, one rotates the $\lambda_0/4$-plate and the direction of vibration of the polarizer until complete extinction occurs. From the position of the directions of vibration of the semiaxes of the $\lambda_0/4$-plate and the direction of vibration of the polarizer one obtains the amplitude ratio $D'_{\mathrm{I}0}/D'_{\mathrm{II}0}$ and the position of the principal axes.

We explain the relation first for elliptically polarized light emerging from a double refracting crystal plate exposed to a linear polarized wave with a direction of vibration $\boldsymbol{e}_1$, which bisects the principal axes of the sectional ellipse (diagonal position). After leaving the plate, both waves have amplitudes

$$\boldsymbol{D}' = D_0 \frac{1}{\sqrt{2}} \cos 2\pi A \boldsymbol{e}' \quad \text{and} \quad \boldsymbol{D}'' = D_0 \frac{1}{\sqrt{2}} \cos 2\pi (A+d) \boldsymbol{e}''$$

with $d = L(n'' - n')/\lambda_0$.

$D_0$ is the amplitude of the incident wave. We now split both waves into components parallel and perpendicular to the direction of vibration of the polarizer according to

$$D_1 = \frac{D_0}{2} \cos 2\pi A + \frac{D_0}{2} \cos 2\pi (A+d)$$
$$D_2 = -\frac{D_0}{2} \cos 2\pi A + \frac{D_0}{2} \cos 2\pi (A+d).$$

With the aid of

$$\cos u + \cos v = 2 \cos \left( \frac{u+v}{2} \right) \cos \left( \frac{u-v}{2} \right) \quad \text{and}$$
$$\cos u - \cos v = -2 \sin \left( \frac{u+v}{2} \right) \sin \left( \frac{u-v}{2} \right)$$

we obtain

$$D_1 = D_0 \cos(\pi d) \cos 2\pi (A + d/2)$$
$$D_2 = -D_0 \sin(\pi d) \sin 2\pi (A + d/2).$$

This is the normal representation of an elliptically polarized wave (partial amplitudes vibrate mutually perpendicular and have a phase difference of 90°). If we now place the $\lambda_0/4$-plate in the ray path such that its directions of vibration correspond to those of $D_1$ and $D_2$, hence parallel and perpendicular to the direction of vibration of the polarizer, the phase difference changes by a further 90°. If the direction of vibration of the slower wave of the compensator lies parallel to $\boldsymbol{e}_1(n'')$, the phase difference of both partial waves increases to 180°. In the converse case, the phase difference vanishes ($\boldsymbol{e}_1(n')$). In each case,

we obtain a plane-polarized wave as a superposition of both partial waves. The position of the resultant

$$D_{\text{res}} = \mp D_0 \cos(\pi d)\boldsymbol{e}_1 - D_0 \sin(\pi d)\boldsymbol{e}_2$$

( $-$ for $n''$ of the compensator parallel to $\boldsymbol{e}_1$, $+$ for $n'$ perpendicular to $\boldsymbol{e}_1$, $n'' > n'$) can be determined with the help of the second rotatable polarizator, which is rotated to the extinction position. The angle $\psi$ between resultant and $\boldsymbol{e}_1$ is given by

$$\tan\psi = \varepsilon = \left(\frac{D_2}{D_1}\right)_{\text{res}} = \sin(\pi d)/\cos(\pi d) = \tan \pi d,$$

where $\varepsilon$ specifies the eccentricity of the ellipse. Hence, one can not only analyze the elliptically polarized light emerging from the crystal plate but also measure the path difference of the given crystal plate, if it lies in the range of up to one wavelength. This method finds its most important application in the measurement of induced changes of the path difference, such as, e.g., in electro-optic or piezo-optic effects (see Section 4.4.2). In order to improve the accuracy, further devices of similar type have been developed. With the aid of a left-quartz right-quartz double plate after Nakamura, the extinction position can be most precisely fixed.

Circular polarized light is present, when $|\varepsilon| = 1$, i.e., when both partial waves possess the same amplitude. One specifies elliptically polarized light as left or right rotating depending on the sense of rotation of the resultant on the ellipse. When facing in the propagation direction of the wave, one observes right-rotating light, if the sense of rotation is counterclockwise, otherwise left-rotating light. Often also the terms laev- and dextro-rotating are used.

#### 4.3.6.6 **Absorption**

In isotropic absorbing substances one notes that the relative change in intensity $\Delta I/I$ of a light ray is proportional to the infinitesimal thickness $\Delta x$ through which it passes, thus $\Delta I/I = -\mu\Delta x$. $\mu$ is the absorption coefficient. On integrating one finds $I = I_0 e^{-\mu L}$, that is, an exponential decline with thickness $L$ (*Lambert's absorption law*).

How can we describe this behavior in the material constants of wave propagation? If one introduces, instead of the refractive power $n$, which up to now was considered as a real quantity, a complex refractive index $n = n_0 + in_0\kappa$, where $n_0$ and $\kappa$ are real quantities, a wave propagating in the direction $\boldsymbol{e}_3$ attains the form

$$\boldsymbol{D} = \boldsymbol{D}_0 e^{2\pi i(nx_3/\lambda_0 - \nu t)} = \boldsymbol{D}_0 e^{-2\pi n_0\kappa x_3/\lambda_0} e^{2\pi i(n_0 x_3/\lambda_0 - \nu t)}.$$

The quantity $4\pi n_0\kappa/\lambda_0$ then corresponds to the absorption coefficient mentioned above ($I \sim |\boldsymbol{D}|^2$).

The phenomenological description of absorption in the framework of Maxwell's equations is provided by the relation between refractive index and the dielectric constant $\epsilon_{\mathrm{rel},jj} = n_j^2$ (Maxwell's relation, see Section 4.3.6). As was shown in 4.3.3, there exists a relationship between the real part of the electric conductivity and the imaginary part of the dielectric constant. Let $\epsilon_{ij} = \epsilon'_{ij} + i\epsilon''_{ij}$. If we set

$$\epsilon_{\mathrm{rel},ij} = n_{ij}^2, \quad \text{with} \quad n_{ij} = n_{ij0} + in_{ij0}\kappa_{ij},$$

we get by multiplying

$$\epsilon'_{\mathrm{rel},ij} = n_{ij0}^2(1 - \kappa_{ij}^2) \quad \text{and} \quad \epsilon''_{\mathrm{rel},ij} = 2\kappa_{ij}n_{ij0}^2.$$

The derivation of the basic equations for the propagation of plane waves runs analogously to the procedure for nonabsorbing media, whereby all quantities may now be complex. We will not display this here in detail, but will mention the most important results. The basic law of crystal optics takes the following form: In an absorbing medium, two elliptically polarized waves with $\boldsymbol{D}$-vectors perpendicular to the propagation direction can propagate in any direction. The major semiaxes of the elliptically polarized waves are mutually perpendicular; the ellipses possess the same eccentricity and their $\boldsymbol{D}$-vector moves in the same sense.

A derivation of this law is found, e.g., in Szivessy (1928). For the quantitative determination of the optical properties of absorbing crystals, two reference surfaces must be considered, the indicatrix, which reflects the real part of the dielectric tensor and a second surface for the absorption coefficient, which is also to be thought of as a second-order surface. In case the position of the indicatrix is fixed by symmetry conditions, then the absorption surface is also fixed by symmetry. One has to assign to each of the three principal refractive indices a principal absorption coefficient, with the help of which one can describe the complete optical behavior. In monoclinic and triclinic crystals, only one or none of the principal axes of both reference surfaces, respectively, coincide.

With weak absorption, as, e.g., in most crystals with low electric conductivity, the law of crystal optics is valid, to a sufficient degree, for nonabsorbing media. This means that for each direction of propagation, there exist two linear polarized vibrations with $\boldsymbol{D}$-vectors lying parallel to the principal axes of the sectional ellipse. However, the absorption coefficients of both waves are, in general, different. Such a crystal plate shows, in linear polarized white light, color phenomena dependent on the position of the direction of vibration of the polarizer. This phenomenon is called pleochroism. In many crystals, e.g., in certain varieties of tourmaline, the absorption for one of the two directions of vibration is so strong that such a crystal plate can be directly used for the

production of polarized light. Commercial polarization foils contain strongly pleochroitic, parallel oriented crystals, which already in thin films give rise to almost complete absorption in one of the two directions of vibration.

Fresnel's formulae can also be directly adopted for absorbing media when one allows complex indices of refraction. The law of refraction for light waves passing through the boundary surface from a nonabsorbing medium I into an absorbing medium II takes the form

$$\frac{\sin\alpha_{\mathrm{I}}}{\sin\alpha_{\mathrm{II}}} = \frac{n_{\mathrm{II}}}{n_{\mathrm{I}}} = \frac{n_{\mathrm{II0}}(1+i\kappa_{\mathrm{II}})}{n_{\mathrm{I}}}.$$

In the case of perpendicular incidence, we obtain from the amplitude ratio with $n_{\mathrm{I}} = 1$ (vacuum)

$$\frac{E_{\mathrm{Ir}}}{E_{\mathrm{I}}} = \frac{n_{\mathrm{II}}-1}{n_{\mathrm{II}}+1}$$

the reflectance

$$R = \left|\frac{n_{\mathrm{II}}-1}{n_{\mathrm{II}}+1}\right|^2 = \frac{(n_{\mathrm{II0}}-1)^2 + n_{\mathrm{II0}}^2\kappa_{\mathrm{II}}^2}{(n_{\mathrm{II0}}+1)^2 + n_{\mathrm{II0}}^2\kappa_{\mathrm{II}}^2}.$$

In strongly absorbing media ($\kappa \gg n_{\mathrm{II0}}$) $R$ approaches the value 1 (metallic reflection).

If the medium II is anisotropic, one observes, in general, even with perpendicular incidence, a dependence of the reflectance on the direction of vibration of the incident linear polarized light. This phenomenon is called reflection pleochroism. With oblique incidence such effects are even more prominent. One can determine the optic constants of such crystals from an analysis of the reflected light, which in absorbing media is usually elliptically polarized.

#### 4.3.6.7 **Optical Activity**

In certain acentric crystals, as e.g., quartz or $LiIO_3$, one observes a rotation of the direction of vibration of the $\boldsymbol{D}$-vector when a wave propagates in a certain direction. The rotation is proportional to the thickness of the medium traversed. This effect, which can also occur in cubic crystals and in liquids, is called *optical activity*. The phenomenological description of optical activity is achieved with the help of an extension of the relationship between $\boldsymbol{E}$ and $\boldsymbol{D}$ according to

$$D_i = \epsilon_{ij}E_j + g_{ijk}\frac{\partial E_j}{\partial x_k}.$$

What must be the nature of the tensor $\{g_{ijk}\}$ so that, corresponding to observation, it does not change the energy content of an electromagnetic wave

$$\boldsymbol{E} = \boldsymbol{E}_0 e^{2\pi i(\boldsymbol{k}\cdot\boldsymbol{x}-\nu t)}$$

by a reversal in propagation direction?

The electric energy density is calculated according to

$$W_{\mathrm{el}} = \sum_i \int E_i dD_i = \int \sum_{i,j} E_i \epsilon_{ij} dE_j + \int \sum_{i,j} E_i 2\pi i g_{ijk} k_k dE_j$$

with

$$\frac{dE_j}{dx_k} = 2\pi i k_k E_j.$$

The second term vanishes when $g_{ijk} = -g_{jik}$. $\{g_{ijk}\}$ must, therefore, be antisymmetric in the first two indices, if the energy density is to be independent of the direction of the propagation vector. If one substitutes $g_{ijk}$ by $\gamma_{lk}$ according to $\frac{2\pi}{\lambda} g_{ijk} = \gamma_{lk}$ or $-\gamma_{lk}$ with $l \neq i, j$ and $i$, $j$, $l$ cyclic or anticyclic in 1, 2, 3, respectively, one arrives at a clearer representation

$$g_{ijk} \frac{dE_j}{dx_k} = g_{ijk} \cdot 2\pi i k_k E_j = -i(\boldsymbol{G} \times \boldsymbol{E})_i,$$

whereby $\boldsymbol{G}$, the *gyration vector*, possesses the components $G_i = \gamma_{ij} g_j$. $\boldsymbol{g}$ is as previously, the unit vector in the direction $\boldsymbol{k}$. Thus we have $D_i = \epsilon_{ij} E_j - i(\boldsymbol{G} \times \boldsymbol{E})_i$. While $\{g_{ijk}\}$ represents, in both first index positions, an antisymmetric polar tensor, the tensor $\gamma_{ij}$ derived from this as well as the vector $\boldsymbol{G}$ are pseudo tensors. $\boldsymbol{G} \times \boldsymbol{E}$ delivers a polar vector because $\boldsymbol{D}$ and $\boldsymbol{E}$ are polar; hence $\boldsymbol{G}$ is a pseudo tensor. From symmetry, the prescribed form of the tensor in the point symmetry groups is found in Table 4.2. Recall that the existence of an inversion center lets all components $\gamma_{ij}$ vanish, in agreement with experimental findings.

We will now discuss at least some essentials of the propagation of plane electromagnetic waves in optically active crystals in order to be prepared for an understanding of higher order optical effects in a later section.

We get the index equation as follows. We proceed from the relation derived from Maxwell's equations

$$\frac{v^2}{c^2} D_j = E_j - (\boldsymbol{g} \cdot \boldsymbol{E}) g_j.$$

With

$$\frac{v^2}{c^2} = n^{-2}, \quad \epsilon_{\mathrm{rel},jj} = n_j^2 \quad \text{and} \quad D_i = \epsilon_{ij} E_j - i(\boldsymbol{G} \times \boldsymbol{E})_i.$$

The following equations are then valid in the principal axes' system of the real dielectric tensor:

$$E_j(n_j^2 - n^2(1 - g_j^2)) + E_{j+1}(n^2 g_j g_{j+1} + iG_{j+2}) + E_{j+2}(n^2 g_{j+2} g_j - iG_{j+1}) = 0 \quad \text{for} \quad j = 1, 2, 3.$$

This homogenous system of equations has a solution for $\boldsymbol{E} \neq 0$ only when its determinant vanishes. From this condition, and after appropriate collection, we obtain the index equation for optically active crystals

$$n^4\left(\sum_j n_j^2 g_j^2\right) - n^2\left(\sum_j n_j^2 n_{j+1}^2(1-g_{j+2}^2) - (\boldsymbol{g}\times\boldsymbol{G})^2\right) + n_1^2 n_2^2 n_3^2 - \sum_j n_j^2 G_j^2 = 0.$$

The coefficient for $n^6$ cancels out. A solution with given direction of propagation $\boldsymbol{g}$ requires the knowledge of the principal refractive indices and of the gyration vector. In the form

$$n^4 - n^2\frac{\sum_j n_j^2 n_{j+1}^2(1-g_{j+2}^2)}{\sum_j n_j^2 g_j^2} + \frac{n_1^2 n_2^2 n_3^2}{\sum_j n_j^2 g_j^2} = \frac{\sum_j n_j^2 G_j^2 - n^2(\boldsymbol{g}\times\boldsymbol{G})^2}{\sum_j n_j^2 g_j^2} = q^2$$

the left-hand side corresponds to the index equation without activity (see Section 4.3.6.1; with $x_i = ng_i$). Let the solutions be $n_0'$ and $n_0''$. Hence the index equation has the form $(n^2 - n_0'^2)(n^2 - n_0''^2) = q^2$. From this, one can find approximations for $n'$ and $n''$, both possible refractive indices for the direction of propagation $\boldsymbol{g}$, when one writes in $q^2$ for $n^2$ an approximate value, e.g., $n_0'^2$ or $n_0''^2$. Experiments have shown that in almost all crystals investigated so far, it suffices to calculate $q^2$ under the assumption $n_1 = n_2 = n_3 = n$. Then $q^2$ becomes

$$q_0^2 = (\boldsymbol{g}\cdot\boldsymbol{G})^2 \quad \text{because} \quad \boldsymbol{G}^2 - (\boldsymbol{g}\times\boldsymbol{G})^2 = (\boldsymbol{g}\cdot\boldsymbol{G})^2.$$

As a result, for $n'$ and $n''$ we have

$$n'^2, n''^2 = \frac{1}{2}\left\{n_0'^2 + n_0''^2 \pm \sqrt{(n_0'^2 - n_0''^2)^2 + 4q_0^2}\right\},$$

where

$$n' > n'' \quad \text{and} \quad n_0' > n_0''.$$

If one enters $n'$ and $n''$ into the basic equations and keeps the condition $n_1 = n_2 = n_3 = \bar{n}$ for the terms connected with the gyration vector, whereby $\bar{n}$ is a mean refractive index, one finds the following approximation law for the propagation of plane waves in optically active nonabsorbing crystals:

Two elliptically polarized transverse waves of the same ellipticity, but with opposite sense of rotation can propagate in any arbitrary direction $\boldsymbol{g}$. The associated refractive indices are $n'$ and $n''$. The major semiaxes of both ellipses of vibration are mutually perpendicular and lie parallel to the directions of vibration that would exist without optical activity in the given direction of propagation (see, e.g., Szivessy, p. 811).

**Table 4.4** Optic properties of optical active crystals of trigonal, tetragonal and hexagonal symmetry.

| PSG 3, 4, 6 ($n_1 = n_2$) | PSG 32, 42, 62 ($n_1 = n_2$) |
|---|---|
| $\gamma_{11} = \gamma_{22}, \gamma_{33}, \gamma_{12} = -\gamma_{21}$ | $\gamma_{11} = \gamma_{22}, \gamma_{33}$ |
| $\boldsymbol{g} = \boldsymbol{e}_3$: | |
| $G_k = \gamma_{k3} g_3$ | |
| $G_1 = G_2 = 0, G_3 = \gamma_{33}$ | $G_1 = G_2 = 0, G_3 = \gamma_{33}$ |
| $\boldsymbol{g} \cdot \boldsymbol{G} = \gamma_{33}; \boldsymbol{g} \times \boldsymbol{G} = 0$ | $\boldsymbol{g} \cdot \boldsymbol{G} = \gamma_{33}; \boldsymbol{g} \times \boldsymbol{G} = 0$ |
| Index equation (for both groups): | |
| $n^4 - 2n_1^2 n^2 + n_1^4 - \gamma_{33}^2 = 0,$ | |
| $n'^2 = n_1^2 + \gamma_{33}, n''^2 = n_1^2 - \gamma_{33}$ | |
| Basic equations: | |
| $D_1 = \epsilon_{11} E_1 + i\gamma_{33} E_2$ | |
| $D_2 = \epsilon_{11} E_2 - i\gamma_{33} E_1$ | |
| $D_3 = \epsilon_{33} E_3$ | |
| $\boldsymbol{g} = \boldsymbol{e}_1$: | |
| $G_1 = \gamma_{11}, G_2 = \gamma_{21}, G_3 = 0$ | $G_1 = \gamma_{11}, G_2 = G_3 = 0$ |
| $\boldsymbol{g} \times \boldsymbol{G} = \gamma_{21} \boldsymbol{e}_3$ | $\boldsymbol{g} \times \boldsymbol{G} = 0$ |
| $\boldsymbol{g} \cdot \boldsymbol{G} = \gamma_{11}$ | $\boldsymbol{g} \cdot \boldsymbol{G} = \gamma_{11}$ |
| Index equation: | |
| $n^4 - n^2 \left\{ n_1^2 + n_3^2 - \frac{1}{n_1^2} \gamma_{12}^2 \right\}$ | $n^4 - n^2(n_1^2 + n_3^2) + n_1^2 n_3^2 - \gamma_{11}^2 = 0$ |
| $+ n_1^2 n_3^2 - (\gamma_{11}^2 + \gamma_{12}^2) = 0$ | |
| With $n = n_1$ we have in both cases | |
| $n'^2$ resp. $n''^2 = (n_1^2 + n_3^2)/2 +$ resp. $-\frac{1}{2}\sqrt{(n_1^2 - n_3^2)^2 + 4\gamma_{11}^2}$ | |
| Basic equations: | |
| $D_1 = \epsilon_{11} E_1 - i\gamma_{21} E_3$ | |
| $D_2 = \epsilon_{11} E_2 + i\gamma_{11} E_3$ | |
| $D_3 = \epsilon_{33} E_3 - i\gamma_{11} E_2 + i\gamma_{21} E_1$ | |

The $\boldsymbol{D}$-vectors of these waves combine according to $\boldsymbol{D} = \boldsymbol{D}' + iu\boldsymbol{D}''$ for $n'$ and $\boldsymbol{D} = \boldsymbol{D}'' + iu\boldsymbol{D}'$ for $n''$, whereby $\boldsymbol{D}'$ and $\boldsymbol{D}''$, respectively, run parallel to the semiaxes of the sectional ellipse for missing optical activity and $|\boldsymbol{D}'| = |\boldsymbol{D}''|$. The ellipticity $u$ is dependent on the optic constants. In very rare cases of extremely large double refraction, one of course expects a certain deviation from this situation.

As an example, we now discuss the propagation of light parallel and perpendicular to the optic axis in crystals of the PSG 3, 4, 6, 32, 42, and 62. According to Table 4.4, the components $\gamma_{11} = \gamma_{22}$ and $\gamma_{33}$ as well as $\gamma_{12} = -\gamma_{21}$ exist for the case of pure rotation axes. In the PSG 32, 42, and 62, $\gamma_{12} = \gamma_{21} = 0$. Table 4.4 lists the relationships for both groups.

Besides the three material equations, we have available the following relationships $D_j = n^2 E_j - n^2 (\boldsymbol{g} \cdot \boldsymbol{E}) g_j$ from the Maxwell equations to determine the components of the $\boldsymbol{D}$-vectors. For the case $\boldsymbol{g} = \boldsymbol{e}_3$ we have $D_3 = 0$ because $\operatorname{div} \boldsymbol{D} = \boldsymbol{k} \cdot \boldsymbol{D} = 0$. If we introduce for $D_1$ and $D_2$ the values of the material

equations, we get

$$D_1 = \epsilon_{11}E_1 + i\gamma_{33}E_2 = n^2E_1$$
$$D_2 = \epsilon_{11}E_2 - i\gamma_{33}E_1 = n^2E_2.$$

Hence, with $\epsilon_{11} = n_1^2$ and the relationship $n^2 - n_1^2 = \pm\gamma_{33}$ we have: $E_1 = iE_2$ and $D_1 = iD_2$ for $n'$ as well as $E_2 = iE_1$ and $D_1 = -iD_2$ for $n''$.

The resulting waves $\boldsymbol{D}' = D_1\boldsymbol{e}_1 - iD_1\boldsymbol{e}_2$ and $\boldsymbol{D}'' = D_1\boldsymbol{e}_1 + iD_1\boldsymbol{e}_2$ represent two circular polarized waves, of which the first is left rotating and the second right rotating, when $\boldsymbol{g}$ points in the positive $\boldsymbol{e}_3$-direction.

If linear polarized light enters a plate cut perpendicular to the optic axis in perpendicular incidence, two circular polarized waves of opposite sense of rotation originate in the crystal and propagate with a velocity corresponding to the refractive indices $n'$ and $n''$. After traversing the thickness $L$ they immerse in the vacuum and interfere to a linear polarized wave, whose direction of vibration with respect to the primary wave is rotated by an angle $\varphi$.

The explanation is as follows: Let the primary wave be given by

$$\boldsymbol{D} = D_0e^{2\pi i(k_3x_3 - \nu t)}\boldsymbol{e}_1.$$

When entering the plate ($x_3 = 0$), it splits up into two circular polarized waves

$$\boldsymbol{D}_+ = (D_0/2)e^{2\pi i(k_3'x_3 - \nu t)}\boldsymbol{e}_1 - (iD_0/2)e^{2\pi i(k_3'x_3 - \nu t)}\boldsymbol{e}_2$$

and

$$\boldsymbol{D}_- = (iD_0/2)e^{2\pi i(k_3''x_3 - \nu t)}\boldsymbol{e}_2 + (D_0/2)e^{2\pi i(k_3''x_3 - \nu t)}\boldsymbol{e}_1.$$

For $x_3 = 0$, the necessary condition $\boldsymbol{D} = \boldsymbol{D}_+ + \boldsymbol{D}_-$ is fulfilled.

After traversing the thickness $L$, both circular polarized waves propagate with the same velocity.

The components vibrating in $\boldsymbol{e}_1$ and $\boldsymbol{e}_2$, respectively, are combined to give

$$D_1 = (D_0/2)e^{2\pi iA} + (D_0/2)e^{2\pi i(A+d)}$$
$$D_2 = (iD_0/2)e^{2\pi i(A+d)} - (iD_0/2)e^{2\pi iA},$$

where

$$A = k_3'L + k_3(x_3 - L) - \nu t \quad \text{for} \quad x_3 > L \quad \text{and}$$
$$d = (k_3'' - k_3')L.$$

The physically effective contents of $D_1$ and $D_2$ are the real parts

$$\mathrm{Re}(D_1) = D_0/2\big(\cos 2\pi A + \cos 2\pi(A+d)\big),$$
$$\mathrm{Re}(D_2) = D_0/2\big(\sin 2\pi A - \sin 2\pi(A+d)\big).$$

With the help of the relations

$$\cos u + \cos v = 2\cos\frac{u+v}{2}\cdot\cos\frac{u-v}{2} \quad \text{and}$$
$$\sin u - \sin v = 2\sin\frac{u-v}{2}\cdot\cos\frac{u+v}{2}$$

one gets

$$\mathrm{Re}(D_1) = D_0\cos\pi d\cdot\cos 2\pi\left(A+\frac{d}{2}\right) \qquad \text{and}$$
$$\mathrm{Re}(D_2) = D_0\sin\pi d\cdot\cos 2\pi\left(A+\frac{d}{2}\right).$$

Both components together form a linear polarized wave with the direction of vibration

$$\boldsymbol{e} = \cos\varphi\,\boldsymbol{e}_1 + \sin\varphi\,\boldsymbol{e}_2.$$

We have

$$\varphi = \pi(k_3'' - k_3')L = \frac{\pi(n''-n')L}{\lambda_0}.$$

$\varphi$ can be easily measured from the extinction position of a rotatable polarizer placed behind the crystal plate. With $\varphi$ one also has $\gamma_{33}$ because $n'^2 - n''^2 = 2\gamma_{33}$, hence

$$\gamma_{33} = (n''-n')(n''+n')/2 = \varphi\lambda_0(n'+n'')/2\pi L.$$

For $(n'+n'')$ we can write $2n_1$ as an approximation. The negative angle of rotation per mm thickness is termed the specific rotation: $\alpha = -180^\circ|n'-n''|/\lambda_0$ (unit, degree per mm).

The derived relations are also valid for cubic crystals of the PSG 23 and 43 as well as for optically active isotropic substances.

For the case $\boldsymbol{g} = \boldsymbol{e}_1$ we assume that $\gamma_{12}$ vanishes. Since $\boldsymbol{k}\cdot\boldsymbol{D} = 0$, $D_1 = 0$, and because $D_1 = \epsilon_{11}E_1$, $E_1 = 0$ and $\boldsymbol{g}\cdot\boldsymbol{E} = 0$. If one introduces in the dynamic basic equations $D_j = n^2E_j - n^2(\boldsymbol{g}\cdot\boldsymbol{E})g_j$ for $D_j$ the values of the material equations, one gets

$$D_2 = \epsilon_{11}E_2 + i\gamma_{11}E_3 = n^2E_2$$
$$D_3 = \epsilon_{33}E_3 - i\gamma_{11}E_2 = n^2E_3.$$

From these one also finds here a fixed ratio of $E_3/E_2$, namely

$$E_3/E_2 = (n^2-n_1^2)/i\gamma_{11} = -i\gamma_{11}/(n^2-n_3^2),$$

where $\epsilon_{11} = n_1^2$ and $\epsilon_{33} = n_3^2$. The first expression follows from the first equation, and the second from the second. Hence,

$$D_2/D_3 = i(n^2 - n_3^2)/\gamma_{11} = iu.$$

With the known values for $n'$ or $n''$ (see Table 4.4) we obtain the following results for both amplitude ratios

$$(D_2/D_3)' \quad \text{or} \quad (D_2/D_3)'' = i\{(n_1^2 - n_3^2) \pm \sqrt{(n_1^2 - n_3^2)^2 + 4\gamma_{11}^2}\}/2\gamma_{11}$$
$$= iu' \quad \text{or} \quad iu'',$$

respectively. One recognizes immediately that $u' = -1/u''$, i.e., there exists two elliptically polarized waves with the same ellipticity, but opposite sense of rotation. We mention at this point that the general proof for an arbitrary direction of propagation and arbitrary symmetry proceeds in an entirely analogous manner. From $\operatorname{div} \boldsymbol{D} = 0$ it always follows that $\boldsymbol{g} \cdot \boldsymbol{D} = 0$, i.e., $\boldsymbol{D}$ has no components along the direction of propagation. The material equations are then to be considered only for both components in the plane perpendicular to $\boldsymbol{g}$ with corresponding results as above.

The determination of $\gamma_{11}$ is possible by analysing the elliptically polarized light emerging from a plane-parallel plate when a linear polarized wave enters the plate in perpendicular incidence. The plate normal runs parallel to $\boldsymbol{e}_1$.

Let the primary wave be represented by

$$\boldsymbol{D} = D_0 e^{2\pi i(k_1 x_1 - \nu t)} \boldsymbol{e}_2.$$

Thus the two waves

$$\boldsymbol{D}' = \frac{D_0}{1+u''^2} e^{2\pi i(k_1' x_1 - \nu t)} \boldsymbol{e}_2 + \frac{iu''D_0}{1+u''^2} e^{2\pi i(k_1' x_1 - \nu t)} \boldsymbol{e}_3,$$

$$\boldsymbol{D}'' = -\frac{iu''D_0}{1+u''^2} e^{2\pi i(k_1'' x_1 - \nu t)} \boldsymbol{e}_3 + \frac{u''^2 D_0}{1+u''^2} e^{2\pi i(k_1'' x_1 - \nu t)} \boldsymbol{e}_2$$

propagate within the crystal ($x_1 \geq 0$).

After traversing the thickness $L$, the two elliptically polarized waves superimpose to a wave whose ellipticity and position of the major semiaxis is to be measured according to the methods discussed in Section 4.3.6.5. These quantities contain the value $\gamma_{11}$ as well as the refractive indices $n'$ and $n''$.

The resulting elliptically polarized wave is composed of the real parts of the vibrating components in $\boldsymbol{e}_2$ and $\boldsymbol{e}_3$:

$$\operatorname{Re}(D_2) = \frac{D_0}{1+u''^2}(\cos 2\pi A + u''^2 \cos 2\pi(A+d))$$

$$\operatorname{Re}(D_3) = \frac{u''D_0}{1+u''^2}(\sin 2\pi(A+d) - \sin 2\pi A) \quad \text{with}$$

$$A = k_1(x_1 - L) + k_1' L - \nu t \quad \text{for} \quad x_1 > L \quad \text{and}$$

$$d = (k_1'' - k_1')L \;=\; (n'' - n')L/\lambda_0.$$

With the relation

$$\cos u + B\cos(u+v) = \sqrt{1+B^2+2B\cos v}\cos(u+\delta),$$

where

$$\tan\delta = \frac{B\sin v}{1+B\cos v}$$

and the relation used above for $(\sin u - \sin v)$ one finds

$$\mathrm{Re}(D_2) = \frac{D_0}{1+u''^2}\sqrt{1+u''^4+2u''^2\cos 2\pi d}\cos 2\pi(A+\delta)$$

$$\mathrm{Re}(D_3) = \frac{2u''D_0}{1+u''^2}\sin\pi d\cdot\cos 2\pi(A+d/2) \quad \text{with}$$

$$\tan 2\pi\delta = \frac{u''^2\sin 2\pi d}{1+u''^2\cos 2\pi d}.$$

With $u''=1$ these values change into the formula derived previously for the superposition of two circular polarized waves.

Finally we note that one can also have formally effects of *second-order optical activity* in all centrosymmetric PSG except 4/m3, which are to be described by a fourth rank tensor $\{g_{ijkl}\}$ given by

$$D_i = \epsilon_{ij}E_j + g_{ijk}\frac{\partial E_j}{\partial x_k} + g_{ijkl}\frac{\partial^2 E_j}{\partial x_k \partial x_l}$$

with $g_{ijkl} = -g_{jikl}$ (Haussühl, 1990).

#### 4.3.6.8 **Double refracting, optically active, and absorbing crystals**

Interference phenomena occurring, in general, in a plane-parallel plate can be calculated approximately with the aid of a model constructed of thin, only double refracting, only optically active, and only absorbing layers stacked alternately. When entering the next respective layer, both linearly polarized or both elliptically polarized waves must then be split according to the new directions of vibration. Using a computer, this process can be repeated in quasi-infinitesimal steps. In practice, it has been shown that in crystals with weak double refraction (e.g., $|n' - n''| < 0.05$) a few triple layers per mm of traversed thickness give sufficient agreement with experimental findings.

Other methods, as, e.g., the visually clear Poincaré representation or an elegant matrix method suggested by Jones (1948) are described in detail in an overview article by Ramachandran and Ramaseshan (1967).

#### 4.3.6.9 **Dispersion**

The dependence of the refractive indices, the absorption coefficients and the components of the gyration tensor on the frequency of the wave is called *dispersion*. In an extended sense, the dependence of inducing quantities, such as

temperature, mechanical stress, electric and magnetic fields, also fall in the domain of dispersion. We shall discuss these effects (electro-optics, piezo-optics, magneto-optics) partly in more detail in later sections. The phenomena of dispersion can only be described in a satisfactory manner using atomistic models of matter. In the classical picture, optical phenomena are attributed to the interaction of the electric field with the oscillators present in the matter. On the one hand, this concerns the states of the electrons responsible for the optical behavior close to the appropriate eigenfrequencies and on the other hand, the mutual oscillations of the lattice particles. The latter determine in many substances the optical properties in the infrared spectral region. As with all interactions in oscillating systems, the difference between the frequency $\nu$ of the exciting wave and the eigenfrequencies $\nu_k$ play a decisive role. From simple model calculations one can show that the interaction of the individual oscillators can be described to a good approximation by the following relation for the principal refractive indices:

$$n_j(\nu)^2 = 1 + \sum_k \frac{(e^2/m)A_{jk}}{\nu^2 - \nu_k^2},$$

where the coefficients $A_{jk}$ are proportional to the number of the $k$th oscillators with eigenfrequency $\nu_k$. $e$ is the electron charge, and $m$ the mass of the electron. In crystals with a simple structure, dispersion, in a not too broad spectral range, can often be well described by two dispersion oscillators. In many applications, dispersion formulae, as e.g., the *Sellmeier equation*

$$n^2 = B_1 + B_2/(\lambda_0^2 - B_3) - B_4\lambda_0^2$$

have proven useful. Their approximate validity confirms the relation mentioned above. $\lambda_0 = c/\nu$ is the vacuum wavelength. The functions $n_j(\nu)$ are obtained by a computer fit of the coefficients $B_i$ to the measured values.

The *Lorentz–Lorenz formula* gives excellent results for the estimation of a mean refractive index, especially in ionic crystals. The formula is obtained from the Clausius–Mosotti relation (see Section 4.3.3), when one replaces $\epsilon_{\text{rel}}$ by $n^2$:

$$\frac{n^2 - 1}{n^2 + 2} = \frac{\rho}{M}R.$$

$R$ is proportional to the mean effective polarizability for the respective frequency and is called molar refraction. Experimentally one finds that $R$ is composed of quasi-additive and quasi-invariant contributions of the lattice particles, the so-called ionic refractions.

### 4.3.7 Electrical Conductivity

The well-known statement of Ohm's law $U = IR$, where $U$ represents the electric voltage in a piece of conducting wire, $R$ the electric resistance and $I$ the current density, must be written in a generalized form when we want to apply it to crystals. We imagine a linear relationship between the vector of the electric current density $\boldsymbol{I}$ and the vector of the electric field strength given by

$$I_i = s_{ij} E_j.$$

The components $s_{ij}$ are material constants independent of the form of the crystal. They specify the *electrical conductivity tensor*, and are to be considered as reciprocal resistances. In experiments we measure the current density in units of charge per $\mathrm{mm}^2$ cross-section persecond. The Coulomb (Symbol C) is mainly used as the unit of charge. Thus the unit of current density is Ampére $\mathrm{mm}^{-2}$. The electric field strength is given in Volt $\mathrm{mm}^{-1}$. The components $s_{ij}$ then have the dimension Ampére $\mathrm{Volt}^{-1}\,\mathrm{mm}^{-1} = \mathrm{Ohm}^{-1}\,\mathrm{mm}^{-1}$. The scarce experimental findings so far on conducting crystals of low symmetry indicate that the electrical conductivity tensor is symmetric, hence $s_{ij} = s_{ji}$. This condition is also required by the *Onsager principle* that is based on the reversibility of processes at atomic scale. A short and secure explanation cannot be given here, so that in the following we will assume the correctness of Onsager's principle (see e.g., Landau-Lifschitz, 1968, p. 374). In crystals, normally no charge creation takes place so that $\mathrm{div}\,\boldsymbol{I} = 0$. The electric field strength is connected to the electrostatic potential by $E_j = -(\mathrm{grad}\,U)_j$.

Thus the general potential equation for conducting crystals is

$$s_{ij}\frac{\partial^2 U}{\partial x_i \partial x_j} = 0 \quad \text{(summed over } i, j = 1, 2, 3).$$

The measurement of electrical conductivity is naturally best achieved with the aid of longitudinal effects on thin crystal plates. One measures the electric voltage $U$ applied on the metallized surfaces of the plate and the current density $I$. The electric field is perpendicular to the surface of the plate. In the case of very low conductivity it is important to take care that the currents over the edges of the plates are kept small or do not enter into the results of the measurement. In order to prevent the interfering effects of heating up the probe during the measurement, it is recommended to work only with extremely small electric power. Since highly accurate commercial current- and voltage-measuring instruments are available also for extremely small currents up to an order of magnitude of $10^{-14}$ Ampére, such measurements do not cause any principal difficulties. It has been shown, however, that the values of conductivity exhibit strong scattering, even in crystals of very high purity and

good quality (low density of lattice defects). The reason is the special role of lattice imperfections for the conduction mechanisms. In metallic conducting crystals lattice imperfections lead to a scattering of the moving charge carriers and thus to a reduction in conductivity, while impurities and lattice imperfections in distinctly weak conductors as, e.g., in most ionic crystals usually result in a strong increase in conductivity. Insights on the type of lattice imperfections can be gained from measurements of the temperature dependence of electric conductivity. Such investigations are thus suitable, within a certain scope, for the characterization of lattice defects.

The anisotropy effects of electrical conductivity are usually extremely small. One observes, for example, in the trigonal crystals of bismuth a ratio $s_{11}/s_{33}$ of about 1.29 at 273 K. In the layer structure of graphite one finds a far better conductivity in the planes perpendicular to the sixfold axis than in those parallel to the sixfold axis. Aside from these layer structures, a distinct anisotropy also exists in structures with conductivity along certain lattice directions similar to a bundle of mutually isolated metal threads. Such a cable-type and uniaxial conductivity, as observed, for example, in certain platinum compounds such as $K_2Pt(CN)_4Br_{0.3} \cdot 3.2H_2O$ or in $LiIO_3$, where a $s_{33}/s_{11}$ of about 1000 appears, cannot always be adequately described with our picture of a second-rank tensor because practically only current threads exist parallel to the unique cable direction. This is represented for a probe of hexagonal $LiIO_3$ cut at 45° to the sixfold axis (Fig. 4.20). If the probe is long enough, the conductivity along the sixfold axis is no longer effective, because the current threads can no longer connect both electrodes. A further important phenomenon is the formation of layers of extremely reduced conductivity at the boundary of two different types of media. These so-called depletion layers play an important role in

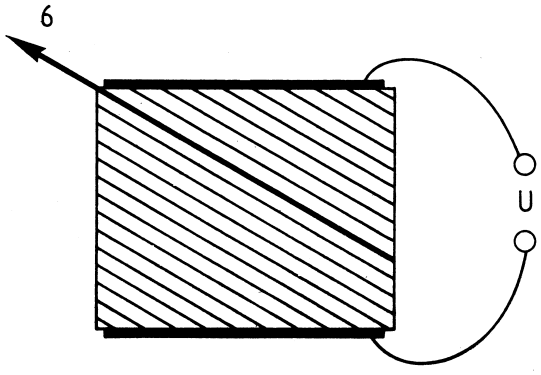


**Figure 4.20** Cable-conductivity in uniaxial conductors (example $LiIO_3$). The current threads cannot connect the electrodes in the case of a specimen cut sufficiently inclined toward the cable axis (in $LiIO_3$ the sixfold axis).

electronic devices, where they are created in a great variety of forms for specific functions (transistor properties). In crystals with polar symmetry, the formation of depletion layers in a unique preferential direction, as for example, in hexagonal $LiIO_3$, can generate highly differing values of the direct current conductivity along the unique direction and its counterdirection. Such effects can be explained by a change of the medium close to the electrodes during current passage. In ionic crystals such effects result often by the depletion of an ion type, for example, lithium ions in the region of the cathode. These phenomena of conductivity cannot be explained by our tensorial approach.

Further effects in connection with electrical conductivity, such as the deviation from Ohm's law, the influence of a magnetic field, or external mechanical strain will be discussed in later sections.

### 4.3.8 Thermal Conductivity

The transport of thermal energy obeys laws analogous to the transport of electric charge. The thermal current density appears instead of the electric current density and the electric field $\boldsymbol{E} = -\operatorname{grad} U$ is replaced by the temperature gradient $\operatorname{grad} T = (\partial T/\partial x_i)\boldsymbol{e}_i$, where we consider the temperature $T$ as a function of position.

The *thermal conductivity* is then represented by

$$Q_i = -\lambda_{ij}(\operatorname{grad} T)_j.$$

The vector $\boldsymbol{Q}$ specifies the flow of heat per second through a cross-section of $1\,\mathrm{mm}^2$ (units Joule $\mathrm{mm}^{-2}\,\mathrm{s}^{-1}$). Here we also assume the validity of Onsager's principle, which requires that the tensor $\{\lambda_{ij}\}$ is symmetric, hence $\lambda_{ij} = \lambda_{ji}$. The measurement should be carried out preferably on a heat plate conductometer, if high accuracy is required and moreover when strong anisotropy effects are expected. This equipment is constructed analogously to the case of electrical conductivity (Fig. 4.21). Again only longitudinal effects are measured. The probe, in the form of a plate, is placed between two metal plates of high thermal conductivity (e.g., copper), which because of their good conducting properties maintain an almost equal temperature over their complete volume. A small heater is mounted on one of the plates. The heat flows through the probe into the second metal plate, that is cooled either by the uniform flow of a coolant or by a Peltier element. If one succeeds in directing the heat loss in the heated plate almost exclusively over the probe, then the applied electrical energy is equal to the total amount of heat transported. After equilibrium, the temperatures $T_1$ and $T_2$ produce a temperature gradient $(T_1 - T_2)/D$ in the probe of thickness $D$. Hence the longitudinal effect along the plate normals is

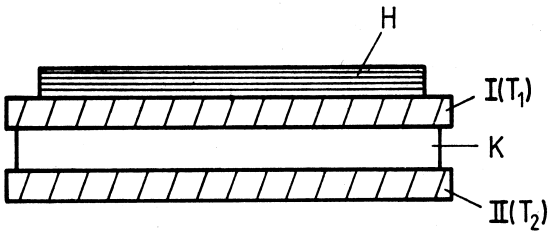


**Figure 4.21** Thermal conductometer. H heating plate, K crystal. The plates $I(T_1)$ and $II(T_2)$ are contacted by a thin film of a liquid with high thermal conductivity.

given by

$$Q_1' = -\lambda_{11}'(T_1 - T_2)/D = W_{el}/F,$$

where $W_{\mathrm{ep}}$ is the applied electrical power and $F$ is the cross-section of the probe.

Suitable measures must be taken to suppress heat losses. Furthermore, just as in the case of electrical conductivity one must ensure a quasi-loss-free transfer of heat from the plates to the probe and out of the probe. Thin films of oil as a contact material have proven suitable in this respect. If one performs measurements on plates of the same orientation but with different thicknesses and plots $Q_1'/(T_1 - T_2)$ as a function of $1/D$, the slope of the curve gives a reliable value for the longitudinal effect $\lambda_{11}'$.

Another method is based on the measurement of the propagation velocity of heat pulses along a cylindrical rod. For crystals this method is only useful in special cases due to the large lengths required.

The interpretation of thermal conductivity proceeds from the scattering of acoustic waves while propagating through a crystal. The heat content determines the number of thermally generated phonons. According to a simple theory of Debye, which should be familiar to the reader from basic courses in physics, the dependence of heat conductivity on the mean free wavelength $\Lambda$ of the phonons, the specific heat $C_p$, and the mean sound velocity $\bar{v}$ of the phonons in a given direction is described by the relationship:

$$\lambda' = \tfrac{1}{3} C_p \Lambda \bar{v}.$$

Here we recognize the important relation between thermal conductivity and acoustic properties. The latter will be discussed in Section 4.5.1.

### 4.3.9 Mass Conductivity

The phenomenon of *mass conductivity*, which appears for example, during filtration through a porous layer, the migration of oil through porous rocks, or

the passage of gas through a thin membrane is completely analogous to electrical and thermal conductivity. The driving force is the gradient of the hydrostatic pressure, in other words, the pressure difference $(p_1 - p_2)/D$ per unit length. The mass current density vector $S$, which describes the transported mass in units of time and surface area is connected to the pressure gradient through

$$S_i = -q_{ij}(\text{grad}\, p)_j.$$

The mass permeability tensor $\{q_{ij}\}$ depends not only on the material but also on the liquid or gas to be transported.

Mass conductivity measurements are made, in principle, under the same aspects discussed for the measurement of thermal conductivity, i.e., it is appropriate to measure the longitudinal effect of a flow running perpendicularly through a plane-parallel plate. In single crystals this property has not yet been quantitatively investigated so far. Crystals with very large lattice particles or with certain vacancies or channel structures, as for example, the zeolites or chelates, which are sometimes used as "molecular sieves," possess an anisotropic permeability. The diffusion of liquids or gases in crystals under the influence of a pressure gradient also belongs to the field of mass conductivity.

### 4.3.10 Deformation Tensor

The mechanical change of shape of a medium is called deformation. This is described by the deformation tensor, also called strain tensor, whereby the rigid displacements and rotations accompanying the deformation shall be left out of consideration. We measure the deformation through the displacement experienced by two neighboring points $P_1$ and $P_2$. Let both points have the coordinates $(x_1, x_2, x_3)$ and $(x_1 + \Delta x_1, x_2 + \Delta x_2, x_3 + \Delta x_3)$ in a fixed undeformed coordinate system. Deformation carries over both points to the points $P_1'$ and $P_2'$ with the coordinates

$$(x_1 + \xi_1, x_2 + \xi_2, x_3 + \xi_3) \quad \text{and}$$
$$(x_1 + \Delta x_1 + \xi_1 + \Delta\xi_1, x_2 + \Delta x_2 + \xi_2 + \Delta\xi_2, x_3 + \Delta x_3 + \xi_3 + \Delta\xi_3).$$

. Before deformation, the mutual position of both points is described by the vector $\Delta\boldsymbol{x}$ and after deformation by the vector $\Delta\boldsymbol{x} + \Delta\boldsymbol{\xi}$ (Fig. 4.22). The vector

$$\Delta\boldsymbol{\xi} = (\Delta\xi_1, \Delta\xi_2, \Delta\xi_3)$$

is called the displacement vector.

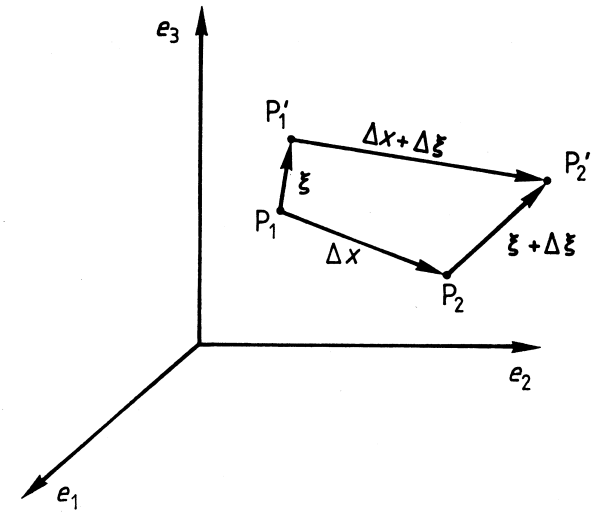


**Figure 4.22** Positions of points $P_1$ and $P_2$ before and after deformation ($P_1'$ and $P_2'$).

We now consider the components of the vector $\Delta\boldsymbol{\xi}$ expanded in a Taylor series in components of $\Delta\boldsymbol{x}$, thus

$$\xi_i(\Delta\boldsymbol{x}) - \xi_i(0) = \Delta\xi_i = \frac{\partial\xi_i}{\partial x_j}\Delta x_j + \frac{1}{2}\frac{\partial^2\xi_i}{\partial x_j \partial x_k}\Delta x_j \Delta x_k + \cdots$$

The first term of the expansion is sufficient for many purposes:

$$\Delta\xi_i = \frac{\partial\xi_i}{\partial x_j}\Delta x_j.$$

The quantities $\frac{\partial\xi_i}{\partial x_j}$ are the components of the *displacement tensor*—a second rank tensor. The tensor property is recognized from the interconnection of the vectors $\Delta\boldsymbol{\xi}$ and $\Delta\boldsymbol{x}$.

We now resolve the displacement tensor

$$\frac{\partial\xi_i}{\partial x_j} = \varepsilon_{ij} + r_{ij} \quad \text{with} \quad \varepsilon_{ij} = \frac{1}{2}\left(\frac{\partial\xi_i}{\partial x_j} + \frac{\partial\xi_j}{\partial x_i}\right) \quad \text{and} \quad r_{ij} = \frac{1}{2}\left(\frac{\partial\xi_i}{\partial x_j} - \frac{\partial\xi_j}{\partial x_i}\right).$$

The symmetric part $\{\varepsilon_{ij}\}$ is called the *deformation tensor*, and the antisymmetric part $\{r_{ij}\}$ the *rotation tensor*. The tensor $\{r_{ij}\}$ gives rise to a rigid rotation. If $\boldsymbol{u}$ is a rotation vector whose length is proportional to the angle of rotation and whose axis runs parallel to the rotation axis, whereby the rotation appears clockwise along the direction of $\boldsymbol{u}$, we have for sufficiently small angles to a reasonable approximation

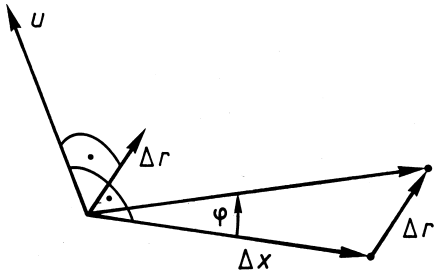


**Figure 4.23** Rotary part $\Delta r$ of the displacement vector.

$$\boldsymbol{u} \times \Delta \boldsymbol{x} = \begin{vmatrix} \boldsymbol{e}_1 & \boldsymbol{e}_2 & \boldsymbol{e}_3 \\ u_1 & u_2 & u_3 \\ \Delta x_1 & \Delta x_2 & \Delta x_3 \end{vmatrix} = \Delta \boldsymbol{r}.$$

Hence $\Delta \boldsymbol{r}$ is perpendicular to the axis of rotation and its length is proportional to the angle of rotation and to the distance of the end point of $\Delta \boldsymbol{x}$ from the axis of rotation (Fig. 4.23). This corresponds to a rigid rotation about the axis $\boldsymbol{u}$, where $\boldsymbol{u}$ is an axial vector (pseudo vector), because the vector product of $\boldsymbol{u}$ with a polar vector $\Delta \boldsymbol{x}$ generates a polar vector $\Delta \boldsymbol{r}$. Setting $\boldsymbol{u} = -(r_{23}, r_{31}, r_{12})$ gives $(\boldsymbol{u} \times \Delta \boldsymbol{x})_i = r_{ij} \Delta x_j = \Delta r_i$, thus the asserted property of $\{r_{ij}\}$ is proven. In the following, we will mainly be concerned with the deformation tensor $\{\varepsilon_{ij}\}$. For some applications it is useful to introduce the so-called Lagrangian deformation tensor instead of $\{\varepsilon_{ij}\}$. This is obtained when we consider the difference of the squares of the distance of $P_1$ and $P_2$ after and before the deformation.

We have

$$\begin{aligned}(\Delta \boldsymbol{x} + \Delta \boldsymbol{\xi})^2 - (\Delta \boldsymbol{x})^2 &= 2\Delta \boldsymbol{x} \cdot \Delta \boldsymbol{\xi} + (\Delta \boldsymbol{\xi})^2 \\ &= 2\Delta x_i \frac{\partial \xi_i}{\partial x_j} \Delta x_j + \frac{\partial \xi_k}{\partial x_i} \frac{\partial \xi_k}{\partial x_j} \Delta x_i \Delta x_j,\end{aligned}$$

when we again content ourselves with the first approximation. Thus

$$\begin{aligned}\frac{1}{2}((\Delta \boldsymbol{x} + \Delta \boldsymbol{\xi})^2 - (\Delta \boldsymbol{x})^2) &= \frac{1}{2} \left\{ \left( \frac{\partial \xi_i}{\partial x_j} + \frac{\partial \xi_j}{\partial x_i} \right) + \frac{\partial \xi_k}{\partial x_i} \frac{\partial \xi_k}{\partial x_j} \right\} \Delta x_i \Delta x_j \\ &= \eta_{ij} \Delta x_i \Delta x_j.\end{aligned}$$

$\{\eta_{ij}\}$ is the *Lagrangian deformation tensor*, which according to $\eta_{ij} = \varepsilon_{ij} + \zeta_{ij}$ contains, apart from the usual deformation tensor, the tensor formed from the product $\frac{\partial \xi_k}{\partial x_i} \frac{\partial \xi_k}{\partial x_j}$ and hence provides a next step in the approximation of finite deformations. We will return to this point in particular when discussing nonlinear elastic phenomena.

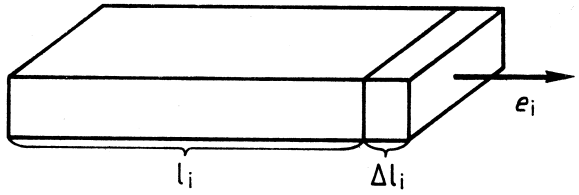


**Figure 4.24** Longitudinal effect of the strain tensor along $e_i$: $\Delta l_i / l_i = \varepsilon_{ii}$.

The components of the deformation tensor are easily accessible to a physical interpretation. The longitudinal components $\varepsilon_{ii}$ describe the relative change in length in the direction $\boldsymbol{e}_i$ occurring during the deformation. Since

$$\Delta\xi_i = \varepsilon_{ii}\Delta x_i + \frac{\partial \xi_i}{\partial x_j}\Delta x_j,$$

where $j \neq i$. The longitudinal effect is

$$\frac{\partial \xi_i}{\partial x_i} = \frac{\Delta l_i}{l_i} = \varepsilon_{ii},$$

when we specify the difference of the coordinates in direction $\boldsymbol{e}_i$ by $l_i$ and their change by $\Delta l_i$ (Fig. 4.24).

The components $\varepsilon_{ij}$ $(i \neq j)$ are called shear components because they directly indicate the shear of a volume element. Consider two points $P_1$ and $P_2$ lying on the coordinate axes belonging to $\boldsymbol{e}_1$ or $\boldsymbol{e}_2$, hence possessing the coordinates $(\Delta x_1, 0, 0)$ and $(0, \Delta x_2, 0)$ (Fig. 4.25). The deformation carries the

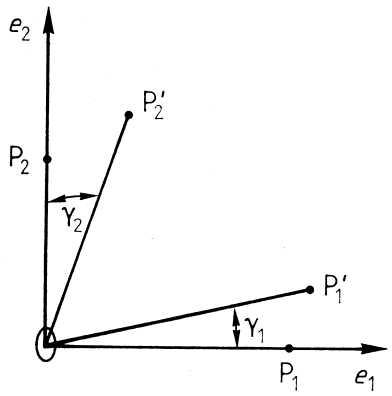


**Figure 4.25** Interpretation of the component $\varepsilon_{ij}$ $(i \neq j)$ as shear component.

points over into

$$P_1' : \left\{ \left(1 + \frac{\partial \xi_1}{\partial x_1}\right) \Delta x_1, \frac{\partial \xi_2}{\partial x_1} \Delta x_1, \frac{\partial \xi_3}{\partial x_1} \Delta x_1 \right\} \quad \text{and}$$
$$P_2' : \left\{ \frac{\partial \xi_1}{\partial x_2} \Delta x_2, \left(1 + \frac{\partial \xi_2}{\partial x_2}\right) \Delta x_2, \frac{\partial \xi_3}{\partial x_2} \Delta x_2 \right\}.$$

The angles $\gamma_1$ and $\gamma_2$ which are enclosed by the sections $0P_1'$ and $0P_2'$ and the coordinate axes $\boldsymbol{e}_1$ or $\boldsymbol{e}_2$ are approximately given by $\left(\frac{\partial \xi_i}{\partial x_j} \ll 1\right)$:

$$\tan \gamma_1 = \frac{\partial \xi_2}{\partial x_1} \Delta x_1 \Big/ \left(1 + \frac{\partial \xi_1}{\partial x_1}\right) \Delta x_1 \approx \frac{\partial \xi_2}{\partial x_1}$$
$$\tan \gamma_2 = \frac{\partial \xi_1}{\partial x_2} \Delta x_2 \Big/ \left(1 + \frac{\partial \xi_2}{\partial x_2}\right) \Delta x_2 \approx \frac{\partial \xi_1}{\partial x_2}.$$

The difference $\gamma_{12}$ of the angles $\sphericalangle(P_1\, 0\, P_2)$ and $\sphericalangle(P_1'\, 0\, P_2')$ is called the shear in the $x_1, x_2$ plane. If the angles are sufficiently small we can replace the tangent by the argument and obtain as an approximation

$$\gamma_{12} = \gamma_1 + \gamma_2 \approx \tan \gamma_1 + \tan \gamma_2 \approx \frac{\partial \xi_2}{\partial x_1} + \frac{\partial \xi_1}{\partial x_2} = 2\varepsilon_{12}.$$

The same is true in all other coordinate planes. In general $\gamma_{ij} \approx 2\varepsilon_{ij}$. Hence $\gamma_{ij}$ describes, to a first approximation, the change in the angle of a right angle formed by the sides parallel $\boldsymbol{e}_i$ and $\boldsymbol{e}_j$.

In total we have six independent tensor components, three longitudinal and three transversal ones. However, in the principal axes' representation only three longitudinal components appear, i.e., the general deformation can be described, in the framework of the approximation discussed, by three mutually perpendicular longitudinal deformations. In the directions of the principal axes $l_i + \Delta l_i = \Delta x_i' = \Delta x_i + \varepsilon_{ii} \Delta x_i = (1 + \varepsilon_{ii}) \Delta x_i$. A sphere $\sum_i (\Delta x_i)^2 = 1$ thus becomes the deformation ellipsoid

$$\sum_i \frac{(\Delta x_i')^2}{(1 + \varepsilon_{ii})^2} = 1.$$

The relative change in volume associated with the deformation, to a first approximation, is given by

$$\frac{V' - V}{V} = \frac{\Delta V}{V} \approx \varepsilon_{11} + \varepsilon_{22} + \varepsilon_{33} \quad \text{with}$$
$$V = \Delta x_1 \Delta x_2 \Delta x_3 \quad \text{and} \quad V' = \Delta x_1' \Delta x_2' \Delta x_3'.$$

Since the sum of the principal components is an invariant, this relationship is valid in any arbitrary reference system.

We will become more familiar with deformations induced by thermal, mechanical, electrical, or magnetic processes in the chapters to come.

### 4.3.11 Thermal Expansion

*Thermal expansion* belongs to the anharmonic effects. It is caused by the change of the mean center-of-mass position of the lattice particles resulting from an increase in the amplitude of thermal vibrations with increasing temperature. The phenomenological description is given by

$$\varepsilon_{ij} = \alpha_{ij}\Delta T + \beta_{ij}(\Delta T)^2 + \gamma_{ij}(\Delta T)^3 + \cdots$$

In a small temperature range of a few K the first term normally suffices when the deformation is to be represented with an accuracy of around 1%. Otherwise higher terms must be added.

The tensors of thermal expansion $\{\alpha_{ij}\}$, $\{\beta_{ij}\}$, $\{\gamma_{ij}\}$, and so on are all of second rank. With the aid of longitudinal effects they can be measured directly from the change of the linear dimensions within a small temperature interval. The following methods have proven suited for precision measurements of small changes in length:

*(a) Inductive dilatometer*(Fig. 4.26). The probe in the form of a parallelepiped or cylinder carries a rod of extremely low thermal expansion (quartz glass; invar), on the top of which a cylindrical permanent magnet (ferrite rod) is attached. The magnet immerses in a coil. The inductivity of the coil depends on the depth of immersion. Hence a change in length results in a change of inductance and thus a change in the resonant frequency of the oscillating

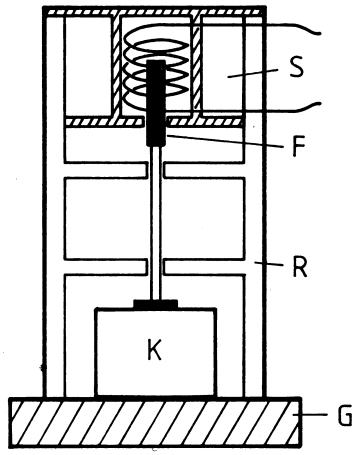


**Figure 4.26** Inductive dilatometer. G ground plate, K crystal, R distance holder ring, F ferrite rod, S HF coil.

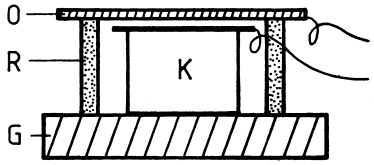


**Figure 4.27** Capacitive dilatometer. G ground plate, K crystal with electrode, R distance ring made from invar or quartz glass, O upper copper electrode.

circuit coupled to the coil. The unit is calibrated by measuring the change in frequency as a function of immersion depth. In commercial devices the change in frequency, over a wide range, is proportional to immersion depth. These dilatometers possess the advantage that the requirements in respect to quality and plane-parallelism of the probe are low.

*(b) Capacitive dilatometer* (Fig. 4.27). One side of the probe, machined plane-parallel, carries one plate of a plate capacitor. The other plate of the capacitor is mounted at a fixed distance from the probe plate by the aid of a quartz glass ring. A change in probe thickness leads to a change in capacitance, which is measured to high accuracy by the change in the resonant frequency of an oscillating circuit in a similar manner as with the inductive dilatometer.

*(c) Optical interference dilatometer*(Fizeau interferometer; Fig. 4.28). In this method, the change in length is measured directly from the change of the optical path between the surface of the probe and a reference plate.

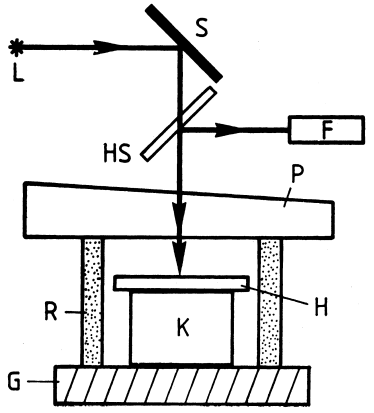


**Figure 4.28** Optical interference dilatometer (Fizeau interferometer). G ground plate, K crystal with one-sided polished auxiliary plate H, distance ring R, slightly wedge-shaped reference plate P, semipermeable mirror HS, metallic mirror M, light source L, telescope or photo-detector F. The waves reflected at the bottom-side of P and the top-side of H generate the interference pattern, which can be directly observed above P. The parts H, R and P are made of quartz glass.

The crystal K and the support for the reference plate are mounted on a flat metal plate. Polishing the probe, which must have plane-parallel faces perpendicular to the direction of measurement, is not required when one places a thin plate of quartz glass, plane-polished on one side, on the probe. The ring carrying the reference plate should preferably be made of quartz glass, too. The optical assembly is mounted in a temperature controlled cell.

The beam of light reflected on the top surface of the auxiliary plate and on the lower surface of the reference plate generates an interference pattern which can be observed with a telescope (adjusted approximately to the lower surface of the reference plate). The number $N$ of interference fringes passing an engraved mark on the reference plate within a small temperature range $\Delta T$ provides a direct measure of the change in length. A correction must be made for the change in the optical path resulting from the quartz support and from the change of refractive power in air in the small gap between both plates.

We then have

$$\alpha'_{11} = \frac{\varepsilon'_{11}}{\Delta T} = \frac{\Delta D}{D\Delta T} = \frac{N'\lambda_0}{2D\Delta T},$$

where $\lambda_0$ is the wavelength of light, $D$ is the thickness of the probe along $\boldsymbol{e}'_1$ and $N'$ is the corrected number of fringes. The correction is calculated with the help of the known expansion coefficients of air and quartz glass (see annex Table 12.10).

Visual observation with the simple interferometer enables a reading accuracy of about 1/20 of a fringe. Photometric methods enable a substantially increased accuracy. The reproducibility of such measurements is often affected by the plastic deformation of the probe due to the unavoidable inhomogenous temperature distribution in the probe during heating and cooling.

*(d) Strain gauge.* This method uses the change in electrical resistance of a wire as a function of mechanical strain to measure the deformation of rigid bodies. The strain gauge is cemented on a side face of the probe in the prescribed measurement direction. Normally strain gauges cannot be used for further measurements on other probes, because when removed from a probe, the resulting mechanical strain leads to a change in the specific resistance per unit strain as given by the manufacturer. Since this information only represents mean values of a production series, one can only have limited confidence in the measured values.

*(e) X-ray precision measurements of the temperature dependence of the lattice constants.* The methods of the precise determination of lattice constants are described in detail in the literature. For large crystals the Bragg method or the method of Bond (simple goniometer) is especially suitable. For small crystals, the multicircle diffractometer and for powder specimens, the Guinier method are suitable. One must pay particular attention to the exact temperature setting of the crystal. As an example for the evaluation, let us consider the gen-

eral case of a triclinic crystal, where the temperature dependence $\partial\theta/\partial T$ of the diffraction angle $\theta$ was measured for the following reflections: (100), (010), (001), (110), (101) and (011). Of course any reflections can be used additionally. From Bragg's condition $2d\sin\theta = \lambda$ ($\lambda$ is the wavelength of the x-rays) we obtain for the temperature dependence of the lattice constant $d$

$$\frac{1}{d}\frac{\partial d}{\partial T} = -\cot\theta\frac{\partial\theta}{\partial T}.$$

The $d$-value of a reflection $\boldsymbol{h} = h_i\boldsymbol{a}_i^* = (h_1h_2h_3)$ is given by $d = 1/|\boldsymbol{h}|$. $h_i$ are the Miller indices and $\boldsymbol{a}_i^*$ the vectors of the reciprocal system (Section 1.5.3). Hence with the temperature dependence of a $d$-value we also know the longitudinal deformation (longitudinal effect) along $\boldsymbol{h}$. To determine the tensors of thermal expansion in the crystal-physical system we only need to calculate the unit vectors in the direction of the $\boldsymbol{h}$ vectors in the crystal-physical system. For this purpose we use the formulae derived in Section 2.2.

For example

$$\frac{\boldsymbol{h}_{100}}{|\boldsymbol{h}_{100}|} = \frac{a_3}{a_1^*a_2^*V}\boldsymbol{e}_1 + \cos\alpha_3^*\boldsymbol{e}_2.$$

The measurement perpendicular to (010) gives us directly $\alpha_{22} = \partial d/d\partial T$. For the longitudinal effect in all other directions $\boldsymbol{e}_1' = u_{1j}\boldsymbol{e}_j$ we have

$$\frac{\partial d}{d\partial T} = \alpha_{11}' = u_{1i}u_{1j}\alpha_{ij}.$$

With our six selected reflections we still have available five further linear equations for the determination of the remaining $\alpha_{ij}$. It is appropriate to include additional measurements of the temperature dependence of other $d$-values and to apply a least-squares procedure to the overdetermined system.

As an example we consider triclinic lithium hydrogen oxalate hydrate. Table 4.5 presents the values measured with an optical interference dilatometer. The measurements were performed in the temperature interval from 20 to $-20°$C.

Using the formula for the longitudinal effect one gets $\alpha_{11}$, $\alpha_{22}$ and $\alpha_{33}$ directly from measurement nos. 1, 2, and 3. With these and from no. 4 we get $\alpha_{12}$ and from no. 6 $\alpha_{13}$. From no. 8 one calculates finally $\alpha_{23}$. The nos. 5 and 7 are used for control purposes. The tensor of thermal expansion is then, in units of $10^{-6}/\mathrm{K}$

$$\alpha_{11} = 23.7; \qquad \alpha_{22} = 19.2; \qquad \alpha_{33} = 60.9;$$
$$\alpha_{12} = -6.0; \qquad \alpha_{13} = -40.5; \qquad \alpha_{23} = 18.5.$$

The principal axes' transformation yields the principal values

$$\lambda_1 = 91.76, \qquad \lambda_2 = 15.60, \qquad \lambda_3 = -3.56$$

**Table 4.5** Measurement of the thermal expansion of triclinic $LiHC_2O_4 \cdot H_2O$ at 273 K.

| Nr. | $u_{11}$ | $u_{12}$ | $u_{13}$ | Direction of measurement | Longitudinal effect $\alpha'_{11}$ $[10^{-6}K^{-1}]$ |
|---|---|---|---|---|---|
| 1 | 1 | 0 | 0 | $[100]'$ | 23.7 |
| 2 | 0 | 1 | 0 | $[010]'$ | 19.2 |
| 3 | 0 | 0 | 1 | $[001]'$ | 60.9 |
| 4 | 0.714 | 0.700 | 0 | $\approx [110]'$ | 15.6 |
| 5 | −0.700 | 0.714 | 0 | $\approx [\bar{1}10]'$ | 27.5 |
| 6 | −0.465 | 0 | 0.885 | | 85.6 |
| 7 | 0.885 | 0 | 0.465 | $[101]$ | −2.1 |
| 8 | −0.329 | $\sqrt{2}/2$ | 0.626 | | 73.2 |

with the associated principal axes' directions (eigenvectors) (see Section 4.3.2)

$$\begin{aligned} \boldsymbol{e}'_1 &= 0.5112\boldsymbol{e}_1 - 0.2518\boldsymbol{e}_2 - 0.8218\boldsymbol{e}_3, \\ \boldsymbol{e}'_2 &= -0.3505\boldsymbol{e}_1 - 0.9341\boldsymbol{e}_2 + 0.0681\boldsymbol{e}_3, \\ \boldsymbol{e}'_3 &= 0.7849\boldsymbol{e}_1 - 0.2529\boldsymbol{e}_2 + 0.5657\boldsymbol{e}_3. \end{aligned}$$

Accordingly, the crystal possesses an unusually strong anisotropy. With increasing temperature the crystal contracts most strongly in a direction approximately parallel to $[101]$, hence it lies almost in the cleavage plane $(\bar{1}01)$. One observes the maximum thermal expansion nearly perpendicular to the cleavage plane. This property is essentially responsible for the unusually strong tendency for crack formation parallel to the cleavage plane. Consequently, when working with the crystal (grinding and polishing) one must pay special attention to ensure that no large temperature gradients are created in the probe.

In particular, it should be mentioned that the principal axes of the quadries of the dielectric constants and the thermal expansion almost coincide. The dielectric maximum or minimum corresponds to a minimum or maximum, respectively, of the thermal expansion. Here we observe a close correlation of two physical properties which otherwise do not exhibit a direct relationship.

The case of negative expansion is rather rarely observed. As examples for negative expansion we mention the orthorhombic crystal species calcium formate and ammonium hydrogen phthalate. In these crystals, the quadric has the form of a hyperboloid. These crystals can be used to prepare samples which show practically no thermal expansion in one direction within a certain temperature interval (see Exercise 15).

The tensors $\{\beta_{ij}\}$, $\{\gamma_{ij}\}$, and so on, introduced above, can be derived from the temperature dependence of the tensor components

$$\alpha_{ij}(\Delta T) = \alpha_{ij}(0) + \frac{\partial \alpha_{ij}}{\partial T}\Delta T + \frac{1}{2}\frac{\partial^2 \alpha_{ij}}{\partial T^2}(\Delta T)^2 + \cdots$$

(e.g., $\beta_{ij} = \partial \alpha_{ij}/\partial T$).

We will take up the relation between thermal expansion and elastic properties when discussing the Grüneisen tensor (see Exercise 29).

### 4.3.12 Linear Compressibility at Hydrostatic Pressure

By analogy to thermal expansion, one can describe a deformation produced by a change in the hydrostatic pressure $\Delta p$, by a second-rank tensor:

$$\varepsilon_{ij} = l_{ij}\Delta p,$$

where $\{l_{ij}\}$ is the *tensor of linear compressibility*. This tensor represents a second-rank tensor invariant of the elasticity tensor. We will return to this relationship later (see Section 4.5.3).

In principle, linear compressibility can be measured with methods similar to those employed for thermal expansion, where instead of a thermal measurement cell a pressure cell is used. If one works, for example, with an optical interferometer, then the change in the optical path resulting from a change in pressure in the empty cell must be carefully taken into account. If the required accuracy is not too high, the use of a strain gauge is recommended. A far more convenient and accurate method is the determination of the linear compressibility with the help of the measurement of sound velocities (see Section 4.5.6). X-ray methods for the determination of lattice constants have proven successful for the investigation of linear compressibility subjected to extreme pressures and temperatures.

### 4.3.13 Mechanical Stress Tensor

We consider the entirety of the external forces acting on a volume element of a body. Imagine the volume element to have the form of a parallelepiped with edges parallel to the basic vectors of a Cartesian reference system (Fig. 4.29). The external forces then act on the boundary faces of this parallelepiped. We resolve the forces in components acting perpendicular and tangential to the faces. If the forces are distributed homogenously over the faces, it is useful to introduce the so-called stresses, i.e., the forces per unit area. Hence stress = force/area. Positive stress means tensile force. The following nine mutually independent stresses can appear: three *normal stresses* $\sigma_{ii}$ and six *shear stresses* $\sigma_{ij}$ $(i \neq j)$, $(i, j = 1, 2, 3)$.

The first index gives the direction of the force (stress), the second the direction of the normal on the face on which the stress acts. For example $\sigma_{22}$ means the stress acting in the direction of the basic vector $\boldsymbol{e}_2$ and exerted across the face perpendicular to $\boldsymbol{e}_2$. The stress $\sigma_{32}$ points in the direction $\boldsymbol{e}_3$ and acts across the face perpendicular to $\boldsymbol{e}_2$. If one goes on to infinitesimal dimensions

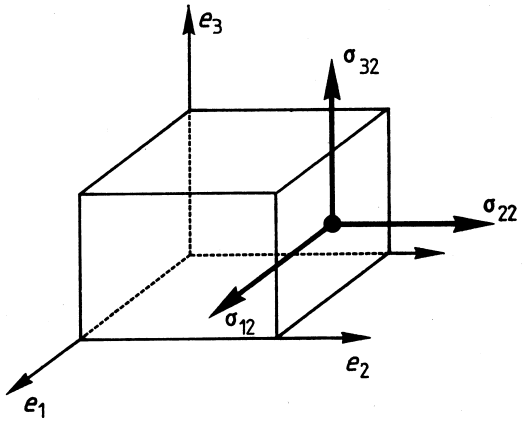


**Figure 4.29** Definition of the stress tensor.

of the volume element, one can describe the state of stress at each point of a body by specifying these nine stresses. The quantities $\sigma_{ij}$ are components of a second-rank tensor, which we will prove as follows:

Let the force acting on an arbitrary test triangle $A_1A_2A_3$ with the normals $\boldsymbol{f} = f_i\boldsymbol{e}_i$ and given state of stress be $\boldsymbol{P} = P_i\boldsymbol{e}_i$ (Fig. 4.30). We then have $P_i = \sigma_{ij}q_j$, where $q_j$ is the area of the triangle $0A_iA_k$ ( = projection of the triangle $A_1A_2A_3$ on the plane perpendicular to $\boldsymbol{e}_j$). Let the length of $\boldsymbol{f}$ be equal to the

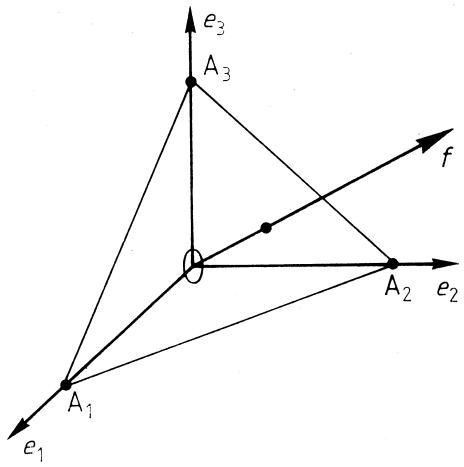


**Figure 4.30** The triangle $A_1A_2A_3$ for the proof of the tensor character of the stress tensor.

area of the triangle $A_1A_2A_3$. Then $f_i = q_i$. This results from

$$\begin{aligned} \boldsymbol{f} &= (d_2\boldsymbol{e}_2 - d_1\boldsymbol{e}_1) \times (d_3\boldsymbol{e}_3 - d_2\boldsymbol{e}_2)/2 \\ &= (d_2d_3\boldsymbol{e}_1 + d_3d_1\boldsymbol{e}_2 + d_1d_2\boldsymbol{e}_3)/2 \quad = \quad q_i\boldsymbol{e}_i, \end{aligned}$$

where we set $0A_i = d_i$ for the intercepts. The same result is obtained in a more elegant way with the help of Gauss's theorem

$$\int_V \operatorname{div} \boldsymbol{u} dV = \int_{\text{surface}} \boldsymbol{u} \cdot d\boldsymbol{f}.$$

If $\boldsymbol{u}$ is a constant vector, the left side vanishes, and hence

$$\int_{\text{surface}} \boldsymbol{u} \cdot d\boldsymbol{f} = 0.$$

Applying this to the tetrahedron $0A_1A_2A_3$ gives $f_i = q_i$, when all face normals point outward of the tetrahedron. Hence we have

$$P_i = \sigma_{ij} f_j.$$

Since $P_i$ and also $f_j$ are components of a vector, the quantities $\sigma_{ij}$, according to the theorem on tensor operations, form a second-rank tensor, the *stress tensor*.

We now examine the symmetry of the stress tensor. Consider the torque $\boldsymbol{M}$ exerted on the test parallelepiped of Fig. 4.29. A force $\boldsymbol{K}$ acting on a lever arm, represented by the vector $\boldsymbol{x}$, gives rise to the torque $\boldsymbol{M} = \boldsymbol{x} \times \boldsymbol{K}$. $\boldsymbol{M}$ is an axial vector, which as we have seen in Section 4.3.10, can be represented by an antisymmetric second-rank tensor analogous to the rotation vector. Let the parallelepiped have edge lengths $x_i$ along the basic vectors $\boldsymbol{e}_i$. We then get, for example,

$$M_1\boldsymbol{e}_1 = x_2\boldsymbol{e}_2 \times \boldsymbol{K}_3 + x_3\boldsymbol{e}_3 \times \boldsymbol{K}_2,$$

where $\boldsymbol{K}_2$ or $\boldsymbol{K}_3$ are the tangential forces acting along $\boldsymbol{e}_2$ or $\boldsymbol{e}_3$, respectively,

$$\boldsymbol{K}_3 = \sigma_{32}x_1x_3\boldsymbol{e}_3, \qquad \boldsymbol{K}_2 = \sigma_{23}x_1x_2\boldsymbol{e}_2.$$

Hence

$$M_1 = V(\sigma_{32} - \sigma_{23}).$$

$V = x_1x_2x_3$ is the volume of the parallelepiped. In general

$$M_i = -V(\sigma_{jk} - \sigma_{kj}), \quad i,j,k \text{ cyclic in } 1,2,3.$$

If the torque is represented as an antisymmetric tensor $\{M^*_{ij}\}$, then $M_i = M^*_{jk} = -M^*_{kj}$.

All torques must vanish, if the volume element is in equilibrium, i.e., $\sigma_{ij} = \sigma_{ji}$; the stress tensor is symmetric in this case. The antisymmetric part of the stress tensor establishes the torque. The question of whether, in a static experiment, a torque appears or not can be clearly decided. In dynamic processes, for example, the propagation of elastic waves, the existence of torques and corresponding rotational motions must be carefully checked. If nothing is explicitly said, we assume in the following that the stress tensor is always symmetric. Hence it normally possesses six independent components. In the principal axes' representation only the three principal stresses $\sigma'_{ii}$ appear. These are the longitudinal components in the directions of the principal axes (normal stresses). This means that each state of stress, that does not generate a torque, is to be represented by three mutually perpendicular normal stresses. Shear stresses do not appear in a parallelepiped cut parallel to the principal axes' directions of the stress tensor!

The most important examples of stress tensors in the principal axes' representation are:

a) Uniaxial tension parallel to $\boldsymbol{e}_1$. The stress tensor only contains the components $\sigma_{ii}$. We have $\sigma_{ii} = K_i/q_i$, where $K_i$ acts in the direction $\boldsymbol{e}_i$ on the face perpendicular to $\boldsymbol{e}_i$ with cross-section $q_i$.

b) Biaxial tension parallel to $\boldsymbol{e}_i$ and $\boldsymbol{e}_j$. Here we only have the two principal stresses $\sigma_{ii}$ and $\sigma_{jj}$. This state of stress appears when we apply a tension on two faces of a rectangular parallelepiped or put it in a biaxial clamping device.

c) Triaxial tension in three mutually perpendicular directions. This is realizable by clamping a rectangular parallelepiped in an assembly with three independent uniaxial pressure generators arranged perpendicular to one another, where only the components $\sigma_{11}$, $\sigma_{22}$, and $\sigma_{33}$ appear. An important special case is hydrostatic pressure $p$, where $\sigma_{11} = \sigma_{22} = \sigma_{33} = -p$.

d) Pure shear stress. We assume $\sigma_{12} = \sigma_{21} \neq 0$, all other $\sigma_{ij} = 0$. The associated principal axes' representation is obtained through a plane principal axes' transformation by rotating about $\boldsymbol{e}_3$. According to Section 4.3.2 we have for the angle $\varphi$ of rotation

$$\tan 2\varphi = \frac{2\sigma_{12}}{\sigma_{11} - \sigma_{22}}, \quad \text{hence} \quad 2\varphi = 90^\circ, \quad \varphi = 45^\circ.$$

Thus $\sigma'_{11} = \sigma_{12}$ and $\sigma'_{22} = -\sigma_{12}$, all remaining $\sigma'_{ij}$ vanish. That is, the state of a pure shear stress $\sigma_{12}$ is equivalent to a longitudinal stress (tension) of magnitude $\sigma'_{11} = \sigma_{12}$ along $(\boldsymbol{e}_1 + \boldsymbol{e}_2)$ and perpendicular to this a longitudinal stress of opposite sign (compressive stress) $\sigma'_{22} = -\sigma_{12}$

along $(\boldsymbol{e}_1 - \boldsymbol{e}_2)$. These directions run parallel to the diagonals of the face of the cube perpendicular to $\boldsymbol{e}_3$ (Fig. 4.29).

The stress tensor, as an inducing quantity, is easy to realize in static experiments.

## 4.4 Third-Rank Tensors

First of all we try to gain an overview of the form of the tensors in the 32 PSG. As already discussed in the general introduction, all polar tensors of uneven rank vanish with the existence of an inversion center. Hence we only need to consider the following PSG (non-Laue groups): 1, 2, m, 22, mm, 3, 32, 3m, 4, 42, 4m, $\bar{4}$, $\bar{4}2$, 6, 62, 6m, $\bar{6}$, $\bar{6}2$, 23, 43, and $\bar{4}3$. In the case of pseudo tensors, the Laue groups require a more detailed inspection.

At first we consider a two-fold symmetry axis parallel to $\boldsymbol{e}_i$ or a symmetry plane perpendicular to $\boldsymbol{e}_i$. These are represented by the following transformation matrices (see also Section 3.8.2):

$$
\begin{aligned}
2 \parallel \boldsymbol{e}_i: &\quad u_{ii} = 1, \quad u_{jj} = u_{kk} = -1, \quad u_{ij} = 0 \ \text{ for } \ i \neq j, \\
\bar{2} \parallel \boldsymbol{e}_i: &\quad u_{ii} = -1, \quad u_{jj} = u_{kk} = 1, \quad u_{ij} = 0 \ \text{ for } \ i \neq j.
\end{aligned}
$$

In both cases $t'_{ijk} = (-1)^q t_{ijk}$. In the first case, $q$ is equal to the number of indices $j$ and $k$ together and in the second, equal to the number of index $i$. With uneven $q$, the respective tensor component vanishes. Therefore, in the case of a two-fold axis parallel $\boldsymbol{e}_i$, only those components exist, in which the indices $j$ and $k$ together occur an even number of times, i.e., the index $i$ occurs an odd number of times. In the case of a symmetry plane perpendicular to $\boldsymbol{e}_i$ the complementary existence condition is valid: the index $i$ occurs an even number of times. Similar as with second-rank tensors, it is useful for an overview to write the components in the form of a matrix. This matrix looks like

$$
(t_{ijk}) = \begin{pmatrix}
t_{111} & \underline{t_{112}} & t_{113} & \underline{t_{121}} & t_{122} & \underline{t_{123}} & t_{131} & \underline{t_{132}} & t_{133} \\
\underline{t_{211}} & t_{212} & \underline{t_{213}} & t_{221} & \underline{t_{222}} & t_{223} & \underline{t_{231}} & t_{232} & \underline{t_{233}} \\
t_{311} & \underline{t_{312}} & t_{313} & \underline{t_{321}} & t_{322} & \underline{t_{323}} & t_{331} & \underline{t_{332}} & t_{333}
\end{pmatrix}.
$$

Even with tensors of higher rank, the overview is made easier, when the components are arranged in three rows, where the first index in the first row is 1, in the second row 2 and in the third row 3. The further indices in each row are to be selected in the sequence of the scheme for a tensor of the next lowest rank.

The 13 components existing in the case of a two-fold axis parallel to $\boldsymbol{e}_2$ are underlined; the remaining 14 components exist in the case of $\bar{2} \equiv$ m parallel

to $e_2$ (symmetry plane perpendicular to $e_2$!). A third-rank pseudo tensor with m $\parallel e_2$ is of the same type as a polar tensor with 2 $\parallel e_2$!

For all PSG with the subgroup 22 it is immediately recognizable that only those components exist in which each index occurs an odd number of times, hence $t_{123}$, $t_{132}$, $t_{231}$, $t_{213}$, $t_{312}$, and $t_{321}$. In the PSG mm in the standard setting ($e_3$ parallel to the intersection edge of the symmetry planes) only such components can appear, in which the indices 1 or 2 occur an even number of times, hence $t_{113}$, $t_{131}$, $t_{223}$, $t_{232}$, $t_{311}$, $t_{322}$, and $t_{333}$.

The effect of a three-fold axis parallel $e_3$ requires a more detailed inspection of the transformation behavior. At this point we present a complete derivation of the conditions in order to show how, in analogous cases of higher rank tensors, one proceeds in practice. The rotation about a three-fold axis is represented by

$$\boldsymbol{R}_{\pm 3 \parallel e_3} = \begin{pmatrix} -1/2 & \pm\sqrt{3}/2 & 0 \\ \mp\sqrt{3}/2 & -1/2 & 0 \\ 0 & 0 & 1 \end{pmatrix}$$

$+$ means clockwise rotation, $-$ anticlockwise rotation, when one looks in the direction $e_3$. The simultaneous calculation for both directions of rotation yields two conditions for each operation, because the sign-dependent parts must be considered separately.

We obtain

$$t'_{111} = t_{111} = -\frac{1}{8}t_{111} \pm \frac{\sqrt{3}}{8}(t_{112} + t_{121}) - \frac{3}{8}t_{122} \pm \frac{\sqrt{3}}{8}t_{211} - \frac{3}{8}(t_{212} + t_{221}) \pm \frac{3\sqrt{3}}{8}t_{222}.$$

The parts coupled with the change of sign must vanish, hence

$$t_{112} + t_{121} + t_{211} + 3t_{222} = 0. \tag{4.1}$$

The remainder gives

$$3t_{111} + t_{122} + t_{212} + t_{221} = 0. \tag{4.2}$$

Further conditions result from

$$t'_{122} = t_{122} = -\frac{3}{8}t_{111} \mp \frac{\sqrt{3}}{8}(t_{112} + t_{121}) - \frac{1}{8}t_{122} \pm \frac{3\sqrt{3}}{8}t_{211} + \frac{3}{8}(t_{212} + t_{221}) \pm \frac{\sqrt{3}}{8}t_{222}.$$

From which we obtain

$$-t_{112} - t_{121} + 3t_{211} + t_{222} = 0 \tag{4.3}$$

and

$$t_{111} + 3t_{122} - t_{212} - t_{221} = 0. \tag{4.4}$$

From (4.1) and (4.3) one finds

$$t_{211} = -t_{222} = \tfrac{1}{2}(t_{112} + t_{121}),$$

and from (4.2) and (4.4)

$$t_{122} = -t_{111} = \tfrac{1}{2}(t_{212} + t_{221}).$$

From

$$t'_{112} = t_{112} = \mp\frac{\sqrt{3}}{8}t_{111} - \frac{1}{8}t_{112} + \frac{3}{8}t_{121} \pm \frac{\sqrt{3}}{8}t_{122} + \frac{3}{8}t_{211} \pm \frac{\sqrt{3}}{8}t_{212} \mp \frac{3\sqrt{3}}{8}t_{221} - \frac{3}{8}t_{222}$$

we get the conditions

$$-t_{111} + t_{122} + t_{212} - 3t_{221} = 0 \tag{4.5}$$

and

$$-3t_{112} + t_{121} + t_{211} - t_{222} = 0. \tag{4.6}$$

Similarly from

$$t'_{212} = t_{212} = -\frac{3}{8}t_{111} \mp \frac{\sqrt{3}}{8}t_{112} \pm \frac{3\sqrt{3}}{8}t_{121} + \frac{3}{8}t_{122} \mp \frac{\sqrt{3}}{8}t_{211} - \frac{1}{8}t_{212} + \frac{3}{8}t_{221} \pm \frac{\sqrt{3}}{8}t_{222}$$

we get the conditions

$$-t_{112} + 3t_{121} - t_{211} + t_{222} = 0 \tag{4.7}$$

and

$$t_{111} - t_{122} + 3t_{212} - t_{221} = 0. \tag{4.8}$$

With (4.5) and (4.8) as well as (4.6) and (4.7) one finally finds

$$t_{212} = t_{221} = t_{122} = -t_{111}$$

and

$$t_{112} = t_{121} = t_{211} = -t_{222}.$$

We see that these relations are permutable in the indices 1 and 2, as we expect on the basis of the equivalence of $\boldsymbol{e}_1$ and $\boldsymbol{e}_2$ with respect to the three-fold axis. This relationship is also of great value for similar questions. Thus the transformation of $t_{121}$, $t_{211}$, $t_{221}$, and $t_{222}$ does not lead to new conditions.

We now turn our attention to those components carrying the index 3 once or twice.

$$t'_{113} = t_{113} = \frac{1}{4}t_{113} \mp \frac{\sqrt{3}}{4}t_{123} \mp \frac{\sqrt{3}}{4}t_{213} + \frac{3}{4}t_{223}.$$

Consequently $t_{113} = t_{223}$ and $t_{123} = -t_{213}$. The analogous transformation for $t_{131}$ and $t_{311}$ leads to $t_{131} = t_{232}$, $t_{132} = -t_{231}$, $t_{311} = t_{322}$, and $t_{312} = -t_{321}$.

$$t'_{133} = t_{133} = -\frac{1}{2}t_{333} \pm \frac{\sqrt{3}}{2}t_{233} \quad \text{gives} \quad t_{133} = t_{233} = 0;$$

likewise one finds $t_{313} = t_{323} = t_{331} = t_{322} = 0$.

Finally we have $t'_{333} = t_{333}$ (no condition!).

Therefore, in the PSG 3 there exist the following nine independent components of a third-rank polar tensor:

$$\begin{aligned}
&t_{111} = -t_{122} = -t_{212} = -t_{221}\\
&t_{222} = -t_{211} = -t_{121} = -t_{112}\\
&t_{113} = t_{223}, \quad t_{123} = -t_{213}, \quad t_{131} = t_{232},\\
&t_{132} = -t_{231}, \quad t_{311} = t_{322}, \quad t_{312} = -t_{321}, \quad t_{333}.
\end{aligned}$$

With these we can now immediately determine the form of the third-rank tensors in the remaining trigonal and hexagonal PSG by taking into account the additional symmetry elements (see Table 4.6).

Finally the effect of 4 and $\bar{4}$ has to be checked. Since 4 as well as $\bar{4}$ contain a two-fold axis, it suffices to consider only such tensor components containing the index 3 an odd number of times (4 or $\bar{4} \parallel \boldsymbol{e}_3$!).

With

$$\boldsymbol{R}_{\pm 4 \parallel e_3} = \begin{pmatrix} 0 & \pm 1 & 0 \\ \mp 1 & 0 & 0 \\ 0 & 0 & 1 \end{pmatrix} \quad \text{and} \quad \boldsymbol{R}_{\pm \bar{4} \parallel e_3} = \begin{pmatrix} 0 & \mp 1 & 0 \\ \pm 1 & 0 & 0 \\ 0 & 0 & -1 \end{pmatrix}$$

one obtains for PSG 4 the seven independent components $t_{113} = t_{223}$, $t_{131} = t_{232}$, $t_{311} = t_{322}$, $t_{123} = -t_{213}$, $t_{132} = -t_{231}$, $t_{312} = -t_{321}$, $t_{333}$ and for PSG $\bar{4}$ the six independent components $t_{113} = -t_{223}$, $t_{131} = -t_{232}$, $t_{311} = -t_{322}$, $t_{123} = t_{213}$, $t_{132} = t_{231}$, $t_{312} = t_{321}$.

Table 4.6 gives the form of the third-rank tensors in the remaining tetragonal and cubic PSG. The effect of the other symmetry elements results from the rules previously discussed. With the cubic PSG, the three-fold axis demands $t_{123} = t_{231} = t_{312}$ etc. (cyclic permutation!).

**Table 4.6** Independent components of polar tensors in acentric PSG of the trigonal, tetragonal, hexagonal, and cubic systems. All otherwise existing components result from the relations valid in PSG 3 and 4, respectively (see text). The PSG of lower symmetry are discussed in the text.

| PSG | Positions of the symmetry elements | Conditions for existence | Independent $t_{ijk}$ |
|---|---|---|---|
| 3 | $3 \parallel e_3$ | – | $t_{111}, t_{222}, t_{113}, t_{123}, t_{131}, t_{132}, t_{311}, t_{312}, t_{333}$ |
| 32 | $2 \parallel e_1$ | Index 1 odd-numbered | $t_{111}, t_{123}, t_{132}, t_{312}$ |
| 3m | $\mathrm{m} = \bar{2} \parallel e_1$ | Index 1 even-numbered | $t_{222}, t_{113}, t_{131}, t_{311}, t_{333}$ |
| 4 | $4 \parallel e_3, 2 \parallel e_3$ | Index 3 odd-numbered | $t_{113}, t_{131}, t_{311}, t_{123}, t_{132}, t_{312}, t_{333}$ |
| $\bar{4}$ | $\bar{4} \parallel e_3, 2 \parallel e_3$ | Index 3 once | $t_{113}, t_{131}, t_{311}, t_{123}, t_{132}, t_{312}$ |
| 6 | $6 \parallel e_3, 2 \parallel e_3$ | Index 3 odd-numbered | $t_{113}, t_{123}, t_{131}, t_{132}, t_{311}, t_{312}, t_{333}$ |
| 62 | $2 \parallel e_1$ | Indices 3 and 1 odd-numbered | $t_{123}, t_{132}, t_{312}$ |
| 6m | $\mathrm{m} = \bar{2} \parallel e_1$ | Index 3 odd-numbered, Index 1 even-numbered | $t_{113}, t_{131}, t_{311}, t_{333}$ |
| $\bar{6} \equiv 3/\mathrm{m}$ | $\mathrm{m} = \bar{2} \parallel e_3$ | Index 3 even-numbered | $t_{111}, t_{222}$ |
| $\bar{6}2 \equiv 3/\mathrm{m}2$ | $\mathrm{m} = \bar{2} \parallel e_3, 2 \parallel e_1$ | Index 3 even-numbered, Index 1 odd-numbered | $t_{111}$ |
| 42 | $2 \parallel e_1$ | Index 1 odd-numbered | $t_{123}, t_{231}, t_{312}$ |
| 4m | $\mathrm{m} = \bar{2} \parallel e_1$ | Index 1 even-numbered | $t_{113}, t_{131}, t_{311}, t_{333}$ |
| $\bar{4}2$ | $2 \parallel e_1$ | Index 1 odd-numbered | $t_{123}, t_{231}, t_{312}$ |
| 23 | $2 \parallel e_i$ | All indices odd-numbered and cyclic | $t_{123}, t_{132}$ |
| $\bar{4}3$ | $\bar{4} \parallel e_i$ | All indices odd-numbered and cyclic | $t_{123} = t_{213}$ |
| 43 | $4 \parallel e_i$ | All indices odd-numbered and cyclic | $t_{123} = -t_{213}$ |

Furthermore, symmetry reduction leads to the result that third-rank pseudo tensors can exist in all PSG.

The quadric $F = t_{ijk}x_ix_jx_k$ contains ten coefficients that can be conveniently determined with the help of longitudinal effects. Measurements in the directions $\boldsymbol{e}_i$ directly give the components $t_{111}$, $t_{222}$ and $t_{333}$. The longitudinal effect in the bisectors of the Cartesian basic vectors $\boldsymbol{e}'_1 = \sqrt{2}/2(\boldsymbol{e}_i \pm \boldsymbol{e}_j)$ is

$$t'_{111\pm} = \frac{\sqrt{2}}{4}t_{iii} \pm \frac{\sqrt{2}}{4}t_{jjj} \pm \frac{\sqrt{2}}{4}(t_{iij} + t_{iji} + t_{jii}) + \frac{\sqrt{2}}{4}(t_{jji} + t_{jij} + t_{ijj}).$$

From $(t'_{111+} + t'_{111-})$ and $(t'_{111+} - t'_{111-})$ one gets the six coefficients $(t_{iij} + t_{iji} + t_{jii})$ with $i, j = 1, 2, 3$. From a further measurement, e.g., in the direction of one of the space diagonals $\boldsymbol{e}'_1 = \frac{\sqrt{3}}{3}(\boldsymbol{e}_1 \pm \boldsymbol{e}_2 \pm \boldsymbol{e}_3)$, one can also determine the tenth coefficient $(t_{123} + t_{132} + t_{231} + t_{213} + t_{312} + t_{321})$ taking into account the already known coefficients. To improve accuracy, it is often advisable to perform measurements in other directions, too.

In any case, we can acquire only a part of the tensor components with the help of longitudinal effects. We need the measurement of transversal effects to completely determine the tensor.

We will address the problem of extreme values when discussing concrete examples of these tensors. A principal axes' transformation, whereby all components with mixed indices vanish, as is the case with second-rank tensors, does not exist here.

### 4.4.1
### Piezoelectric Tensor

In the pyroelectric effect we observe an electric polarization $\boldsymbol{P}$, proportional to the temperature difference within a small temperature range. The application of mechanical stress, expressed by the stress tensor $\{\sigma_{ij}\}$, can also give rise to an electric polarization. This phenomenon is known as the *piezoelectric effect*. For a sufficiently small, homogenous test volume, one has

$$\Delta P_i = d_{ijk}\sigma_{jk} + d_{ijklm}\sigma_{jk}\sigma_{lm} + \cdots$$

The tensor $\{d_{ijk}\}$ represents the *linear piezoelectric effect* and $\{d_{ijklm}\}$ the *quadratic piezoelectric effect* and so on. Normally the linear effect is sufficient for the description of an experiment. Because the stress tensor is symmetric, there is no possibility to distinguish between the components $d_{ijk}$ and $d_{ikj}$. Therefore, we must assume that the tensor $\{d_{ijk}\}$ is symmetric in the second and third index positions, hence $d_{ijk} = d_{ikj}$. This condition reduces the number of independent components of the third-rank tensor from 27 to 18. In the light of the overview gained in the previous section, the form of the piezoelectric tensor can be immediately read. Table 4.7 presents the results for all

**Table 4.7** Independent components of third-rank tensors in the acentric PSG under interchangeability of the second and third order index position (example piezoelectric tensor). $Z$ is the number of independent components.

| PSG | $Z$ | Independent components |
|---|---|---|
| 1 | 18 | $d_{ijk} = d_{ikj}$ $(i,j,k = 1,2,3)$ |
| $2 \parallel e_2$ | 8 | $d_{112}, d_{123}, d_{211}, d_{213}, d_{222}, d_{233}, d_{312}, d_{323}$ |
| $\bar{2} \parallel e_2$ | 10 | $d_{111}, d_{113}, d_{122}, d_{133}, d_{212}, d_{223}, d_{311}, d_{313}, d_{322}, d_{333}$ |
| 22 | 3 | $d_{123}, d_{231}, d_{312}$ |
| mm2, $2 \parallel e_3$ | 5 | $d_{113}, d_{223}, d_{311}, d_{322}, d_{333}$ |
| $3 \parallel e_3$ | 6 | $d_{111} = -d_{122} = -d_{212}, d_{222} = -d_{211} = -d_{121}, d_{113} = d_{223}, d_{123} = -d_{213}, d_{311} = d_{322}, d_{333}$ |
| 32, $2 \parallel e_1$ | 2 | $d_{111} = -d_{122} = -d_{212}, d_{123} = -d_{213}$ |
| 3m, $\bar{2} \parallel e_1$ | 4 | $d_{113} = d_{223}, d_{222} = -d_{211} = -d_{121}, d_{311} = d_{322}, d_{333}$ |
| $4 \parallel e_3$ | 4 | $d_{113} = d_{223}, d_{123} = -d_{213}, d_{311} = d_{322}, d_{333}$ |
| 42, $2 \parallel e_1$ | 1 | $d_{123} = -d_{213}$ |
| 4m, $\bar{2} \parallel e_1$ | 3 | $d_{113} = d_{223}, d_{311} = d_{322}, d_{333}$ |
| $\bar{4}$ | 4 | $d_{113} = -d_{223}, d_{123} = d_{213}, d_{311} = -d_{322}, d_{312}$ |
| $\bar{4}2$, $2 \parallel e_1$ | 2 | $d_{123} = d_{213}, d_{312}$ |
| $6 \parallel e_3$ | 4 | $d_{113} = d_{223}, d_{123} = -d_{213}, d_{311} = d_{322}, d_{333}$ |
| 62, $2 \parallel e_1$ | 1 | $d_{123} = -d_{213}$ |
| 6m, $\bar{2} \parallel e_1$ | 3 | $d_{113} = d_{223}, d_{311} = d_{322}, d_{333}$ |
| $\bar{6}$ | 2 | $d_{111} = -d_{122} = -d_{212}, d_{222} = -d_{211} = -d_{121}$ |
| $\bar{6}2$, $2 \parallel e_1$ | 1 | $d_{111} = -d_{122} = -d_{212}$ |
| 23 | 1 | $d_{123} = d_{231} = d_{312} = d_{213} = d_{132} = d_{321}$ |
| 43 | 0 | – |
| $\bar{4}3$ | 1 | $d_{123} = d_{231} = d_{312} = d_{213} = d_{132} = d_{321}$ |
| $\infty \parallel e_3$ | 4 | $d_{113} = d_{223}, d_{123} = -d_{213}, d_{311} = d_{322}, d_{333}$ |
| $\infty 2$ | 1 | $d_{123} = -d_{213}$ |
| $\infty$m | 3 | $d_{113} = d_{223}, d_{311} = d_{322}, d_{333}$ |
| $\overline{\infty}, \overline{\infty}2$ | 0 | – |

piezoelectric PSG. Of special interest is the fact that PSG 43 shows no piezoelectric effect, because the conditions $d_{123} = -d_{213}$ and $d_{123} = d_{231} = d_{213}$ can only be fulfilled with $d_{ijk} = 0$. The two other cubic piezoelectric PSG to be considered, namely 23 and $\bar{4}3$, possess only one independent component $d_{123} = d_{231} = d_{312} = d_{132} = d_{213} = d_{321}$.

#### 4.4.1.1 Static and Quasistatic Methods of Measurement

Piezoelectric effects can best be observed and measured as longitudinal and transversal effects under the application of uniaxial pressure. In the quantitative determination of the piezoelectric tensor one must pay attention that mechanical stresses are homogenously transferred over the test object so that the influence of boundary effects can be neglected and also that a simple relationship can be assumed between inducing stress and charge generation. The easiest accessible method is the longitudinal effect (Fig. 4.31). At first we will study a probe in the form of a rectangular parallelepiped. If we apply a uniaxial pressure $\sigma'_{11}$ in the direction $e'_1$, one observes a change in charge $\Delta Q$ on the

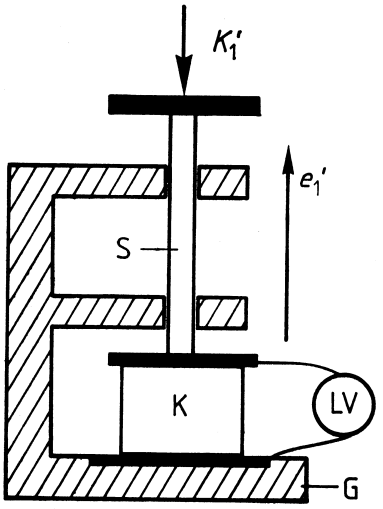


**Figure 4.31** Measurement of the longitudinal piezoelectric effect. G ground plate, K crystal, S pressure bar, and LV charge amplifier.

faces cut perpendicular to $e_1'$. The latter must be made electrically conducting by vapor deposition of a metal or with conducting paste. We then have

$$\Delta P_1' = K\frac{\Delta Q}{x_2' x_3'} = d_{111}'\frac{KK_1'}{x_2' x_3'}, \quad \text{hence} \quad \Delta Q = d_{111}' K_1',$$

where $\Delta Q$ means the charge difference appearing on the face in question, which can be measured with a commercial charge amplifier, and $K_1'$ is the uniaxial acting force. $K$ is the constant of the system of measurement used. Most important is that the dimensions of the probe do not come into play. As long as the state of stress distributes itself to a certain extent homogenously over the cross-section, one observes only minor deviations from the theoretical value, even when the cross-section of the probe along the direction of pressure varies considerably. The measurement of the longitudinal effect can be miniaturized, without special precautions, down to probe dimensions 0.1 mm thick (plates) and 0.5 mm long (thin needle), where one can still obtain reliable values for the constant $d_{111}'$. Thus according to the evaluation of longitudinal effects described in the previous section, the quadric $F = t_{ijk}x_i x_j x_k$ with its ten coefficients can be completely determined.

Including transversal effects it is now possible to completely determine the piezoelectric tensor also in the case of triclinic crystals. We use the same pressure cell as with the longitudinal effect and also apply a uniaxial stress $\sigma_{11}'$ parallel $e_1'$. The metallized pair of faces, however, are now arranged parallel to the direction of pressure, that is, perpendicular to $e_2'$ or $e_3'$ (Fig. 4.32). Thus

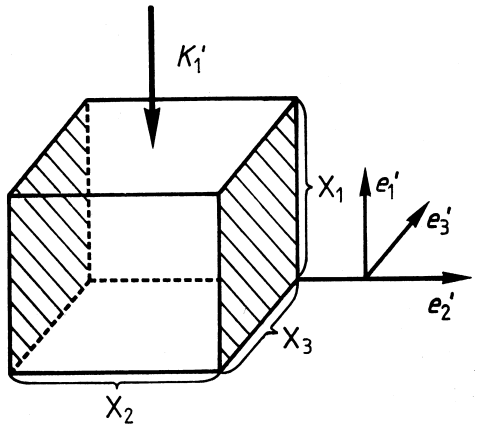


**Figure 4.32** Parallelepipedic specimen for the measurement of the piezoelectric transversal effect $d'_{211}$ (uniaxial stress parallel $e'_1$, surfaces of the electrodes perpendicular to $e'_2$).

for the generation of charge on the face perpendicular to $e'_2$ we have

$$\Delta P'_2 = K\frac{\Delta Q}{x'_1 x'_3} = d'_{211}\frac{KK'_1}{x'_2 x'_3}, \quad \text{hence} \quad \Delta Q = d'_{211}K'_1\frac{x'_1}{x'_2}.$$

Accordingly, with constant force $K'_1$, the observed change in charge depends on the ratio of the length $x'_1$ of the specimen to the separation of the electrodes $x'_2$. The dimension $x'_3$ does not matter. For a high accuracy of the measurement as well as for the practical generation of electric charges with the help of the transversal effect the specimen should be prepared as long as possible in the direction of pressure and as thin as possible in the direction of the normals on the surface of the electrodes. The measurements require that the specimens possess nearly the form of a rectangular parallelepiped. Moreover, geometrically similar specimens produce the same change in charge $\Delta Q$ under identical load conditions.

If we conduct such measurements with uniaxial stress direction parallel to $e_i$ and electrode normals parallel to $e_j$, we directly obtain the six components $d_{jii}$ $(i, j = 1, 2, 3)$. Thus we can now determine the components $d_{iij}$ using the coefficients $(d_{jii} + d_{iij} + d_{iji}) = (d_{jii} + 2d_{iij})$ available from the quadric. The three missing components $d_{123}$, $d_{231}$, and $d_{312}$ are obtained from measurements of transversal effects on 45° cuts, in other words, parallelepipeds bounded by a pair of faces perpendicular to $e'_1 = e_i$ and two pair of faces with the normals $e'_2 = \sqrt{2}/2(e_j + e_k)$ and $e'_3 = \sqrt{2}/2(-e_j + e_k)$, $(i, j, k$ cyclic in $1, 2, 3)$. For this orientation and with uniaxial stress parallel to $e'_2$ or $e'_3$ we have

$$d'_{122} = \tfrac{1}{2}d_{ijj} + \tfrac{1}{2}d_{ikk} + d_{ijk} \quad \text{or} \quad d'_{133} = \tfrac{1}{2}d_{ijj} + \tfrac{1}{2}d_{ikk} - d_{ijk}.$$

Thus

$$d_{ijk} = (d'_{122} - d'_{133})/2.$$

The procedure outlined above now provides a measurement scheme for the complete determination of the piezoelectric tensor.

To check the measurements and to increase accuracy, it is also useful to determine the transversal effects $d'_{311}$, $d'_{322}$, $d'_{233}$, and $d'_{211}$ on the 45° cuts for which the following relations, to be proved by transformation, are valid:

$$d'_{211} = \frac{\sqrt{2}}{2} d_{jii} + \frac{\sqrt{2}}{2} d_{kii},$$
$$d'_{311} = -\frac{\sqrt{2}}{2} d_{jii} + \frac{\sqrt{2}}{2} d_{kii},$$
$$d'_{233} = \frac{\sqrt{2}}{4}(d_{jjj} + d_{kkk} - 2d_{jkj} + d_{jkk} - 2d_{kjk} + d_{kjj}), \quad \text{and}$$
$$d'_{322} = \frac{\sqrt{2}}{4}(-d_{jjj} + d_{kkk} - 2d_{jkj} - d_{jkk} + 2d_{kjk} + d_{kjj}).$$

Of interest are the relations

$$d'_{211} + d'_{311} = \sqrt{2} d_{kii},$$
$$d'_{211} - d'_{311} = \sqrt{2} d_{jii},$$
$$d'_{233} + d'_{322} = \frac{\sqrt{2}}{2}(d_{kkk} + d_{kjj} - 2d_{jkj}), \quad \text{and}$$
$$d'_{233} - d'_{322} = \frac{\sqrt{2}}{2}(d_{jjj} + d_{jkk} - 2d_{kjk}).$$

From the principal cut (edges parallel to $\boldsymbol{e}_i$) and the three 45° cuts we obtain 36 (=4×9) measurement results, which allow a reliable determination of the piezoelectric tensor.

One can achieve a higher measurement accuracy by employing a dynamic pressure generator, as for example, a spring connected to a harmonically vibrating loud speaker membrane or connected to a motor-driven eccentric. With the help of a phase-sensitive amplification of the piezoelectric signal it is possible to attain a hundred-fold increase in the sensitivity of the method. In any case, one must pay particular attention to the fact that just as with the pyroelectric effect, the surface conductivity remains small or does not cause a reduction in the true piezoelectric signal. For the measurement of electrical charges, compensation methods have proven to be of great advantage. In these methods, the charge appearing is immediately compensated by an opposing charge generated by the compensator so that only very small charge differences and hence small electric voltages are present at the crystal. The

complete compensation charge is then measured. Also in the case of a certain volume conductivity of the specimen it is important to eliminate and measure the charge as promptly as possible.

In crystals of higher symmetry, such as $\alpha$-quartz, lithium niobate, potassium bromate, lithium iodate, $KH_2PO_4$ or in cubic crystals like the isotype group of zinc blende-type, just to mention a few examples, the determination of the tensor is comparably unproblematic. These examples are briefly explained below. The experimental values are presented in Table 12.14 (annex).

**(a) $\alpha$-Quartz (32)**

The following components are present: $d_{111} = -d_{122} = -d_{212} = -d_{221}$ and $d_{123} = d_{132} = -d_{231} = -d_{213}$. Measuring the longitudinal effect along the direction of the two-fold axis ($\boldsymbol{e}_1$) gives us immediately $d_{111}$. As a control, a transversal measurement with uniaxial stress in the direction $\boldsymbol{e}_2$ (perpendicular to $\boldsymbol{e}_1$ and $\boldsymbol{e}_3$) and charge generation on the pair of faces perpendicular to $\boldsymbol{e}_1$ is useful. In doing so, the constant to be measured $d_{122}$ is identical to $-d_{111}$. For the determination of $d_{123}$ we appropriately employ the transversal effect on a 45° cut with the edges parallel to $\boldsymbol{e}'_1 = \boldsymbol{e}_1$, $\boldsymbol{e}'_2 = \frac{\sqrt{2}}{2}(\boldsymbol{e}_2 + \boldsymbol{e}_3)$ and $\boldsymbol{e}'_3 = \frac{\sqrt{2}}{2}(-\boldsymbol{e}_2 + \boldsymbol{e}_3)$. With uniaxial stress along $\boldsymbol{e}'_2$ or $\boldsymbol{e}'_3$ we obtain

$$d'_{122} = \tfrac{1}{2}d_{122} + d_{123}$$

or

$$d'_{133} = \tfrac{1}{2}d_{122} - d_{123}$$

and hence two independent values for $d_{123}$.

At present, $\alpha$-quartz is used more than all other crystals together in the application of the piezoelectric effect. We will discuss the construction of sound generators, frequency stabilizers, frequency filters etc. later. Because of their good mechanical stability, quartz crystals are also employed preferably in devices for the measurement of mechanical stress and deformation as well as for electrically controlled precision feeds.

**b) Lithium niobate ($LiNbO_3$) and $KBrO_3$ (3m)**

Here, the following components exist: $d_{222} = -d_{112} = -d_{121} = -d_{211}$, $d_{113} = d_{223} = d_{131} = d_{232}$, $d_{311} = d_{322}$, $d_{333}$.

$d_{222}$ and $d_{333}$ are found directly from the longitudinal effects along $\boldsymbol{e}_2$ and $\boldsymbol{e}_3$, respectively, whereby $\boldsymbol{e}_1$ runs perpendicular to the mirror plane. From the transversal effect with uniaxial stress in the direction $\boldsymbol{e}_1$ and charge generation on the pair of faces perpendicular to the three-fold axis ($\boldsymbol{e}_3$) one obtains $d_{311}$. The still missing component $d_{113}$ results from the longitudinal effect with

uniaxial stress parallel to

$$e_1' = \frac{\sqrt{2}}{2}(\mp e_1 + e_3).$$

Owing to their relatively large coefficients $d_{333}$, both crystals are especially suitable for the production of piezoelectric stress sensors and sound generators. Why, in spite of their superiority with respect to piezoelectric effects, the preferential application of $\alpha$-quartz is not in danger will be discussed later.

**c) Lithium iodate (6)**

The following components exist: $d_{113} = d_{223} = d_{131} = d_{232}$, $d_{311} = d_{322}$, $d_{123} = d_{132} = -d_{213} = -d_{231}$, and $d_{333}$. From the longitudinal effect along the six-fold axis one directly obtains $d_{333}$. The component $d_{311}$ is directly measurable from the transversal effect with uniaxial stress along $e_1$ (this direction can be chosen arbitrarily perpendicular to the six-fold axis, since the piezoelectric tensor possesses cylindrical symmetry in all hexagonal PSG!) and charge generation on a pair of faces perpendicular to the six-fold axis. $d_{113}$ and $d_{123}$, as described under (a) or (b), are to be determined on 45° cuts.

Lithium iodate possesses unusually large longitudinal- and transversal effects, which can be used to generate sound waves. We will discuss the influence of the extreme anisotropic electric conductivity in Section 4.5.5.

**d) Sphalerite type ($\bar{4}3$)**

Only one independent constant exists $d_{123} = d_{231} = d_{312} = d_{132} = d_{213} = d_{321}$. Its most reliable determination is via the longitudinal effect along the space diagonals of the Cartesian reference system, hence along

$$e_1' = \frac{\sqrt{3}}{3}(\pm e_1 \pm e_2 \pm e_3).$$

Here we have

$$d_{111}' = \pm\left(\frac{\sqrt{3}}{3}\right)^3 6d_{123} = \pm\frac{2}{3}\sqrt{3}d_{123}.$$

The sign is equal to the product of the signs of the components of $e_1'$. In addition, one has the transversal effects $d_{122}'$ and $d_{133}'$ on a 45° cut with the edges $e_1' = e_1$, $e_2' = \frac{\sqrt{2}}{2}(e_2 + e_3)$, $e_3' = \frac{\sqrt{2}}{2}(-e_2 + e_3)$, which yields $d_{122}' = d_{123}$ and $d_{133}' = -d_{123}$ directly, whereby $e_2'$ or $e_3'$ specify the direction of the uniaxial stress and $e_1$ denotes the normal on the charge generating pair of faces.

If these crystals form tetrahedra $\{111\}$, corresponding to the associated point symmetry group, then one can measure the constant $d_{123}$ without further preparation.

#### 4.4.1.2 **Extreme Values**

For many applications it is important to know the directions of the maximum or minimum effects. As an example, we consider the extreme values of the longitudinal effect in the point symmetry groups containing the symmetry group 22 as a subgroup (22, 42, 62, $\bar{4}2$, 23, $\bar{4}3$). The longitudinal effect along the direction $\boldsymbol{e}'_1 = u_{1i}\boldsymbol{e}_i$ is

$$d'_{111} = u_{1i}u_{1j}u_{1k}d_{ijk} = u_{11}u_{12}u_{13} \cdot 2(d_{123} + d_{231} + d_{312}) = u_{11}u_{12}u_{13} \cdot 2d.$$

In the PSG 42 and 62 $d = 0$ because $d_{123} = -d_{231}$ and $d_{312} = 0$. We proceed according to the well-known prescription and form the auxiliary function $H = d'_{111} - \lambda \sum_i u_{1i}^2$, which under the constraint $\sum_i u_{1i}^2 = 1$ allows the calculation of the extreme value of $d'_{111}$. $\lambda$ is a factor still to be determined. An extreme value of $H$ and hence of $d'_{111}$ is present, when

$$\frac{\partial H}{\partial u_{1i}} = 2u_{1j}u_{1k}d - 2\lambda u_{1i} = 0.$$

If we divide $u_{1j}u_{1k}d = \lambda u_{1i}$ by the corresponding equation $u_{1i}u_{1k}d = \lambda u_{1j}$, we obtain

$$\frac{u_{1j}}{u_{1i}} = \frac{u_{1i}}{u_{1j}} \quad \text{or} \quad u_{1i}^2 = u_{1j}^2 = u_{1k}^2 = \frac{1}{3} \quad \text{because} \quad \sum_i u_{1i}^2 = 1.$$

Hence extreme values appear in the directions of the space diagonals of the Cartesian reference system

$$\boldsymbol{e}'_1 = \frac{\sqrt{3}}{3}(\pm\boldsymbol{e}_1 \pm \boldsymbol{e}_2 \pm \boldsymbol{e}_3).$$

The extreme values are

$$\frac{\pm 2\sqrt{3}}{9}d.$$

In the cubic PSG $d'_{111} = \pm\frac{2}{\sqrt{3}}d_{123}$.

For certain applications of the piezoelectric effect it is desirable that pure longitudinal effects appear, i.e., that the associated transversal effects completely vanish. We consider this question for crystals of the minimum symmetry 22. The conditions are

$$d'_{211} = d'_{311} = 0.$$

We have

$$\begin{aligned} d'_{k11} &= 2u_{k1}u_{12}u_{13}d_{123} + 2u_{k2}u_{13}u_{11}d_{231} + 2u_{k3}u_{11}u_{12}d_{312} \\ &= 2\boldsymbol{e}'_k \cdot (u_{12}u_{13}d_{123}\boldsymbol{e}_1 + u_{13}u_{11}d_{231}\boldsymbol{e}_2 + u_{11}u_{12}d_{312}\boldsymbol{e}_3) \;=\; 0 \end{aligned}$$

for $k = 2$ or 3. Since $\boldsymbol{e}'_k \cdot \boldsymbol{e}'_1 = 0$ we find from the above equation that the components $u_{1i}$ of $\boldsymbol{e}'_1 = u_{1i}\boldsymbol{e}_i$ have the following form:

$$u_{11} = qu_{12}u_{13}d_{123}, \quad u_{12} = qu_{13}u_{11}d_{231}, \quad \text{and} \quad u_{13} = qu_{11}u_{12}d_{312}$$

with an arbitrary factor $q$. If we multiply these expressions one after the other with $u_{11}$ or $u_{12}$ and $u_{13}$ we obtain

$$\begin{aligned} u_{11}^2 &= qu_{11}u_{12}u_{13}d_{123}, \\ u_{12}^2 &= qu_{11}u_{12}u_{13}d_{231}, \\ u_{13}^2 &= qu_{11}u_{12}u_{13}d_{321}. \end{aligned}$$

Hence the ratio

$$u_{11}^2 : u_{12}^2 : u_{13}^2 = d_{123} : d_{231} : d_{312} \quad \text{must be satisfied.}$$

From this we see that all $d_{ijk}$ must have the same sign. For cubic crystals, we obtain the result that pure longitudinal effects appear in the directions of the space diagonals of the Cartesian (and crystallographic) reference system.

Finally we take a look at the situation of the PSG 32, in which also $\alpha$-quartz crystallizes. For the longitudinal effect we obtain

$$d'_{111} = u_{11}^3 d_{111} + u_{11}u_{12}^2 d_{122} + u_{11}u_{12}^2 \cdot 2d_{212} + u_{11}u_{12}u_{13} \cdot 2(d_{123} + d_{231}).$$

The last term vanishes because $d_{123} = -d_{231}$. With $d_{122} = d_{212} = -d_{111}$ we get $d'_{111} = d_{111}(u_{11}^3 - 3u_{11}u_{12}^2)$. From

$$H = d'_{111} - \lambda \sum_i u_{1i}^2 \quad \text{and} \quad \frac{\partial H}{\partial u_{1i}} = 0$$

we find $u_{13} = 0$. Accordingly, the extreme values lie in the plane perpendicular to the three-fold axis. With $u_{11}^2 + u_{12}^2 = 1$ and $u_{11} = \cos\varphi$ we obtain

$$d'_{111} = d_{111}(4u_{11}^3 - 3u_{11}) = d_{111}(4\cos^3\varphi - 3\cos\varphi) = d_{111}\cos 3\varphi.$$

It is now sufficient to study the behavior of

$$\frac{\partial d'_{111}}{\partial \varphi} = -3d_{111}\sin 3\varphi = 0.$$

We obtain $\varphi = m\pi/3$ with integer $m$. An extreme value appears in the direction $\boldsymbol{e}_1$ ($m = 0$), which is repeated with alternating sign after each $\pi/3$ rotation. This rapid change of the extreme values is the reason why $d_{111}$ in crystals of the PSG 32 are relatively small. The variation of $d'_{111}$ in the plane perpendicular to the three-fold axis is shown in Fig. 4.33.

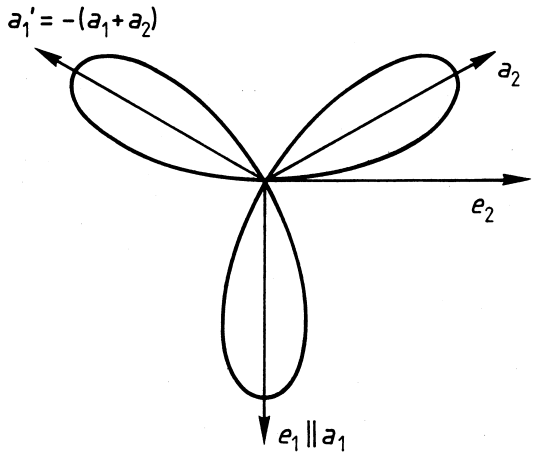


**Figure 4.33** Variation of the longitudinal effect $d'_{111}$ in crystals belonging to PSG 32 along directions perpendicular to the threefold axis (e.g., $\alpha$-quartz).

#### 4.4.1.3 **Converse Piezoelectric Effect (First-Order Electrostriction)**

A type of reversal of the usual piezoelectric effects appears when a crystal in an external electric field experiences a deformation. For a small homogenous volume element, the relation is written as

$$\varepsilon_{ij} = \hat{d}_{ijk} E_k.$$

$\{\varepsilon_{ij}\}$ is the deformation tensor and $\{\hat{d}_{ijk}\}$ the *first-order electrostriction tensor*. Because of the symmetry of the deformation tensor we must also assume the interchangeability of the first two index positions, hence $\hat{d}_{ijk} = \hat{d}_{jik}$. Otherwise all the aspects discussed for the piezoelectric tensor are valid when one takes into consideration that the interchangeability of the indices is different. As we shall see in Section 5, thermodynamical relations demand that the components of the piezoelectric and electrostrictive tensors take on the same numerical value. That is, $\hat{d}_{ijk} = d_{kij}$, where, however, certain boundary conditions are to be observed. Thus one can measure the piezoelectric tensor also with the help of electrostriction. In particular, the measurement of both effects on the same specimen provides very good control potential. The measurement of the deformations appearing in the converse piezoelectric effect is preferably performed using optical interferometry methods of high resolution. Figure 4.34 shows the scheme of such an arrangement (*Michelson interferometer*). Again, the specimen has preferably the form of a rectangular parallelepiped. It is furnished on one side with an optical mirror. A laser beam strikes a semitransparent optical plate at 45° incidence so that the beam is split. Let one beam, e.g., that passing straight through, strike the specimen in vertical inci-

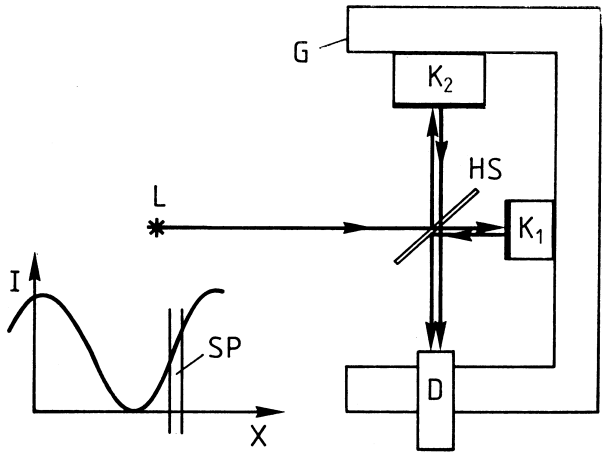


**Figure 4.34** Scheme of a Michelson interferometer. G ground plate, L light source, HS semitransparent mirror, $K_1$ and $K_2$ crystal and auxiliary crystal, respectively, with electrodes (and polishing), D detector. Maximum resolution is realized, if the detector slit SP is placed at the position of the steepest intensity variation in the interference pattern (between maximum and minimum of intensity).

dence. This beam is reflected and deflected by 90° at the beam splitter. The second beam strikes the auxiliary crystal of the known piezoelectric effect, also furnished with a mirror, where it is reflected. The beam passing straight through the splitter interferes with the other beam to build a pattern of interference fringes. By carefully adjusting one of the crystals one can set the interfringe distance to the desired width. With the help of a narrow slit in front of the detector (photomultiplier or photodiode) one can find a position of the strongest increase in intensity. This is located between a maximum and an adjacent minimum of the fringes. This is the setting of the highest sensitivity for the detection of fringe pattern displacement. If in one of the two crystals a homogenous mechanical deformation is produced along the direction of the wave normal of the beam, one observes a displacement of the fringes corresponding to twice the deformation path. An especially high accuracy is realizable, when the fringe displacement is compensated with the help of the second crystal by producing an equally large deformation, for example by means of the converse piezoelectric effect. If one works with an electric alternating field, where the amplitude can be set independently at each crystal, one can achieve, with the help of a lock-in amplifier, an accuracy an order of magnitude higher than required for the measurement of the normal converse first-order piezoelectric effect. The lock-in technique largely suppresses a substantial part of disturbing phenomena (vibration, inhomogeneous heating, and detector intrinsic noise). For this reason such an arrangement is also

suitable to measure second- and higher order effects. We will return to this in Section 4.5.3.

Here we again measure longitudinal effects with the electric field in the direction of the beam and transversal effects with the electric field perpendicular to the beam direction. The complete determination of the first-order electrostriction tensor can be carried out using a strategy similar to that outlined above.

Of course, other types of interferometers can be used for purposes of this kind. Somewhat more versatile than the interferometer described here is a device where the light beam is transmitted through the specimen. Changes in the optical path are measured. These, however, contain a fraction arising from a change in the refractive index under the influence of the electric field (electrooptical effect, Section 4.4.2).

This method requires a substantially higher optical quality of the crystal and also a rather perfect preparation (plane-parallelism of the surfaces through which the light passes, surface finish).

The measurement of electrostriction with the help of strain gauges, comfortable as it is, hardly achieves the desired accuracy except in the case of very large effects. In contrast, the highly precise determination of lattice constants offers a competitive alternative to the optical interference methods (see Section 4.3.11).

We will become acquainted with other methods to measure piezoelectric effects in connection with the propagation of sound waves in piezoelectric crystals, where a coupling appears between the elastic and piezoelectric constants. This electromechanical coupling is the basis for the construction of sound generators and resonators.

A method to qualitatively test whether a substance possesses piezoelectric properties was reported by Giebe and Scheibe. The method works on powder samples and allows certain conclusions concerning the order of magnitude of the effects. The powder is immersed in a high-frequency electric field. Individual grains, excited to acoustic resonances at a certain frequency depending on their dimensions, give weak interfering signals which are amplified and detected.

### 4.4.2
### First-Order Electro-Optical Tensor

In Section 4.3.6 we became familiar with the indicatrix $a_{ij}x_ix_j = 1$ which we employed to describe the propagation of electromagnetic waves in non-absorbing and optically non-active crystals. The refractive indices $n_{ij}$ are related to the "polarization constants" $a_{ij}$ according to $a_{ij} = n_{ij}^{-2}$ (see Section 4.3.6). An external electric field $\boldsymbol{E}$ can give rise to a change in the polarisation

constants

$$a_{ij} - a_{ij}^0 = \Delta a_{ij} = r_{ijk}E_k + r_{ijkl}E_kE_l + \ldots$$

The tensor $\{r_{ijk}\}$ is called the ***first-order electro-optical tensor***. It is of the same form as the converse piezoelectric tensor $\{\hat{d}_{ijk}\}$ because of the interchangeability of the first two index positions. Hence, we can directly take over the set of independent tensor components.

The concept of the measurement of longitudinal- and transversal effects with respect to the optical properties of crystals cannot be directly realized, because the laws of light propagation do not allow arbitrary directions of vibration in the propagation directions. In a simple measurement arrangement let us assume that a light wave strikes the surface of a rectangular parallelepiped at vertical incidence. The possible directions of vibration in the crystal, without external field, are deduced from the sectional ellipse of the original indicatrix. With the electric field applied either parallel or perpendicular to the ray direction (Fig. 4.35), we expect a change in the indicatrix, which will be expressed in two phenomena; firstly, a new sectional ellipse is created with altered principal axes directions and secondly, the lengths of the principal axes are altered, i.e., a change results in the refractive indices, hence in the velocity of light. In the orthorhombic system, the directions of the principal axes remain unchanged, to a first approximation, due to symmetry. The same is valid for the distinct principal axis parallel to the twofold axis or perpendicular to the symmetry plane in monoclinic crystals and for the principal axis parallel

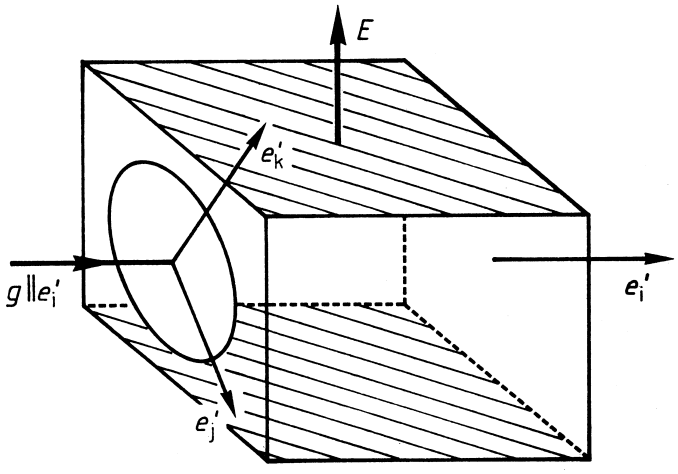


**Figure 4.35** Arrangement for electrooptic measurements. Electric field $\boldsymbol{E}$ perpendicular to the propagation direction $\boldsymbol{g}$ (transversal arrangement). In the longitudinal arrangement $\boldsymbol{E}$ and $\boldsymbol{g}$ are parallel.

to the principal symmetry axis in trigonal, tetragonal and hexagonal crystals. In cubic and in optically uniaxial crystals—except in certain singular directions of the electric field—the degeneracy of the indicatrix is canceled, i.e., the indicatrix takes on the form of a triaxial ellipsoid. We will now examine to what extent we can actually expect a measurable rotation of the indicatrix compared with the initial situation.

In the following, we designate the transmission direction (vertical incidence) with $\boldsymbol{e}'_i$ and the two directions of vibration with $\boldsymbol{e}'_j$ and $\boldsymbol{e}'_k$ (directions of the semiaxes of the sectional ellipse). The sectional ellipse in the plane perpendicular to $\boldsymbol{e}'_i$ is

$$a'_{jj}x'^2_j + a'_{kk}x'^2_k = 1.$$

After the change $\{\Delta a_{ij}\}$ (calculated in the dotted system!) we have

$$(a'_{jj} + \Delta a'_{jj})x'^2_j + (a'_{kk} + \Delta a'_{kk})x'^2_k + 2\Delta a'_{jk}x'_jx'_k = 1$$

(no summation here).

We now perform a rotation in the new principal axes system of the sectional ellipse and obtain for the angle of rotation (see Section 4.3.2)

$$\tan 2\varphi = \frac{2\Delta a'_{jk}}{a'_{jj} + \Delta a'_{jj} - a'_{kk} - \Delta a'_{kk}}.$$

By tensor transformation we can calculate the quantities $\Delta a'_{jk}$ from the tensor components in the crystal–physical reference system according to $\Delta a'_{jk} = r'_{jkl}E'_l$.

The quantities $a'_{jj}$ and $a'_{kk}$ are known ($a'_{jj} = n'^{-2}_{jj}$, $a'_{kk} = n'^{-2}_{kk}$); furthermore,

$$\Delta a'_{jj} = -2\Delta n'_{jj}/n'^3_{jj} \quad \text{and} \quad \Delta a'_{kk} = -2\Delta n'_{kk}/n'^3_{kk} \quad (\text{because } a_{ij} = n^{-2}_{ij}).$$

Hence, the magnitude of the angle of rotation depends decisively on the difference of refractive indices and naturally, on the quantity $\Delta a'_{jk}$. Experience shows that the angle of rotation remains virtually unobservable by a double refraction $(n'_{jj} - n'_{kk}) > 0.03$, i.e., the position of the principal axes of the sectional ellipse is virtually unchanged. If, however, the sectional ellipse has the form of a quasicircle ($n'_{jj} \approx n'_{kk}$) or a circle, then the rotation or the position of the sectional ellipse due to the field must be taken into account.

In all other cases, the approximation of the vanishing angle of rotation leads to a substantial simplification of the measurement procedure. Let the optical path difference of the two light waves passing through a crystal of thickness $L$ and the refractive indices $n'_{jj}$ and $n'_{kk}$ in the direction $\boldsymbol{e}'_i$ be given by $G = L(n'_{jj} - n'_{kk})$. For a change, we have

$$\Delta G = L\Delta(n'_{jj} - n'_{kk}) + (n'_{jj} - n'_{kk})\Delta L.$$

If we write for $\Delta n'$ the values $-n'^3\Delta a'/2$ and for $\Delta L$ the induced quantity from the converse piezoelectric effect

$$\Delta L = L\varepsilon'_{ii} = L\hat{d}'_{iil}E'_l,$$

we get

$$\Delta G = -\frac{L}{2}(n'^3_{jj}r'_{jjl}E'_l - n'^3_{kk}r'_{kkl}E'_l) + (n'_{jj} - n'_{kk})L\hat{d}'_{iil}E'_l.$$

(with fixed $j$ and $k$; summation over $l$). Accordingly, to determine the components $r_{ijk}$ the knowledge of the piezoelectric tensor is also required, because the electric field causes a change of the geometric path length $L$. When the effects are sufficiently large, the measurements can be made with the help of a Sénarmont compensator (see Section 4.3.6.5). Higher accuracy is achieved when one works with an alternating electric field that induces an oscillation of the direction of vibration of the linear polarized light behind the Sénarmont compensator. A Faraday cell placed in the ray path behind the Sénarmont compensator can be used to compensate this oscillation by producing an opposing magnetooptical Faraday effect (see Section 4.4.5). The current in the coil of the calibrated Faraday cell required for this purpose is a measure of the rotation and thus for the path difference originating in the crystal.

With the aid of these so-called relative measurements, performed in different directions, the components $r_{ijk}$ in many PSG, in particular in those of higher symmetry, can be completely determined. In triclinic and monoclinic crystals it is, however, also necessary to add so-called absolute measurements, where only the change in the optical path of one of the waves propagating in the direction $\boldsymbol{e}'_i$ is measured separately. High measurement accuracy is not only achieved with a *Jamin interferometer* (Fig. 4.36), where light is transmitted

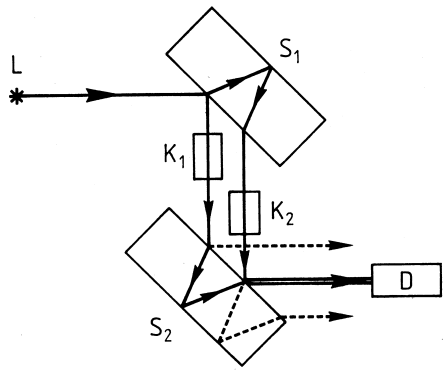


**Figure 4.36** Scheme of a Jamin interferometer. L light source, $S_1$ and $S_2$ are glass plates with metallized reverse side, $K_1$ and $K_2$ are specimen and auxiliary crystal, respectively, D detector.

through the crystal only once, but also with the previously described Michelson interferometer. One now places a crystal with known electrooptical effect in the second beam to enable a compensation measurement. The above formula for $\Delta G$ is also true for the absolute measurement when instead of $n'_{kk}$ or $n'_{jj}$ for the refractive index of air ($n \approx 1$) the value 0 is written for the second beam and for $r'_{kkl}$ or $r'_{jjl}$. The accuracy is increased by orders of magnitude, when one works with an electric alternating field employing a lock-in amplifier, whereby the detector, as described in Section 4.4.1.3, adjusted in a region of largest changes in intensity (between a maximum and an adjacent mimimum of the interference pattern). The difference of the absolute measurements for both directions of vibration $\boldsymbol{e}'_j$ and $\boldsymbol{e}'_k$ must naturally agree with relative measurement in the respective direction. Thus one also has a complete control of the measurements. Except on lithium hydrogen oxalate-hydrate (Ramadan, 1982) no measurements of the complete electrooptical tensor of a triclinc crystal have been reported. The strategy for such a task is not essentially more complicated as with the piezoelectric effect. For a better overview it is appropriate to leave the crystal–physical reference system and select the Cartesian reference system of the semi-axes of the indicatrix instead. In this system, where we specify its basic vectors with $\boldsymbol{e}^0_i$, the above formula derived for the path difference takes on an essentially simpler form, when we also note the electrooptical tensor in the optical reference system. In particular, one can, if the rotation of the indicatrix is negligible, directly determine longitudinal effects and transversal effects with the help of absolute measurements, at least for the optical principal directions. In this way, one can immediately acquire the following nine components: $r^0_{iii}$, $r^0_{iij}$ $(i, j = 1, 2, 3)$. If, for example, we apply the electric field in the direction $\boldsymbol{e}^0_2$ and irradiate also in the direction $\boldsymbol{e}^0_2$, we obtain the transversal effects $r^0_{112}$ or $r^0_{332}$ for the directions of vibration $\boldsymbol{e}^0_1$ or $\boldsymbol{e}^0_3$. If we transmit in the direction $\boldsymbol{e}^0_1$, we obtain the longitudinal effect $r^0_{222}$ and again the transversal effect $r^0_{332}$ for the directions of vibration $\boldsymbol{e}^0_2$ or $\boldsymbol{e}^0_3$. Transmission in the direction $\boldsymbol{e}^0_3$ again yields $r^0_{112}$ and $r^0_{222}$. Further measurements on 45°-cuts give the possibility of measuring the remaining nine components. With the help of the transformation $\boldsymbol{e}_i = u_{ij}\boldsymbol{e}^0_j$, which presents the basic vectors of the crystal–physical system in the crystal–optical system, we obtain the components $r_{ijk}$ from the components $r^0_{ijk}$ according to

$$r_{ijk} = u_{ii^*} u_{jj^*} u_{kk^*} r^0_{i^*j^*k^*}.$$

In any case it is necessary to correct for the converse piezoelectrical effect beforehand.

If the sectional ellipse rotates when an electric field is applied, then the formula for the path difference given above must be modified. The new position of the semiaxes of the sectional ellipse, expressed through the angle of rotation $\varphi$, results in an additional equation containing the components $r_{ijk}$. While the

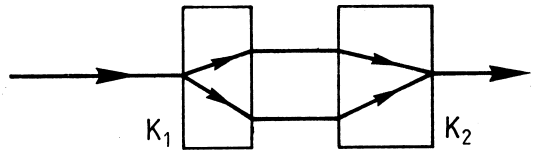


**Figure 4.37** Compensation of the ray double refraction of plane-parallel plates. $K_1$ crystal (specimen), $K_2$ auxiliary crystal with known ray double refraction.

piezoelectric correction remains, one must enter into the first term the calculated change of the refractive indices for the new directions of vibration. We will return to this type of special cases later.

At this point it is appropriate to make a few comments on the performance of the measurements. Often the crystals possess such a strong double refraction that when making relative measurements the waves are separated in space and cannot interfere. In such a situation one places a second specimen in the ray path to compensate for the double refraction. For the routine measurements of such effects it is useful to prepare a set of plates of known double refraction (ray separation at vertical incidence). For this purpose, it is best to use crystals of high optical quality and good stability of the surface finish, for example, orthorhombic calcium formate. A suitable compensation plate is then selected for each measurement and placed with the correct orientation in the ray path (Fig. 4.37).

A certain problem appears when measuring the effect, if ray direction and electric field are parallel to each other. The specimen must then be equipped with transparent electrodes. Here, optical glass plates with a thin conducting film of $SnO_2$ have proven good. The plates are prepared, for example, by spraying them with a solution of $SnCl_4$ in HCl and methanol. At about 450°C a conducting transparent film of $SnO_2$ is formed by oxidation, which is also mechanically very stable. The glass plates are attached with paraffin oil or some other immersion liquid to the finely ground faces of the specimen. In this manner one can almost always avoid polishing the specimen.

In most PSG the electrooptical effects are also superimposed by effects of optical activity. This, however, is only noticeable when a sectional ellipse in the form of a circle or quasi-circle is present, as for example, in cubic crystals of the PSG 23.

We now discuss a few typical examples. First we consider crystals with the subgroup 22 (PSG 22, 42, $\bar{4}2$, 62, 23 and $\bar{4}3$). No more than three independent components exist $r_{123}$, $r_{231}$ and $r_{312}$. We have $\Delta a_{12} = r_{123}E_3$, $\Delta a_{23} = r_{231}E_1$ and $\Delta a_{31} = r_{312}E_2$ and $\Delta a_{ii} = 0$. Hence, the sum of the principal refractive indices remains constant because $\sum_i \Delta a_{ii} = 0$. Furthermore, no measurable effect occurs in the direction of the semiaxes of the indicatrix. We must therefore

employ 45°-cuts. We apply the electric field parallel to $\boldsymbol{e}_1'$ at the 45°-cut with the edges parallel $\boldsymbol{e}_1' = \boldsymbol{e}_i$, $\boldsymbol{e}_2' = \frac{\sqrt{2}}{2}(\boldsymbol{e}_j + \boldsymbol{e}_k)$, $\boldsymbol{e}_3' = \frac{\sqrt{2}}{2}(-\boldsymbol{e}_j + \boldsymbol{e}_k)$. Using the transformation matrix

$$\begin{pmatrix} 1 & 0 & 0 \\ 0 & \frac{\sqrt{2}}{2} & \frac{\sqrt{2}}{2} \\ 0 & -\frac{\sqrt{2}}{2} & \frac{\sqrt{2}}{2} \end{pmatrix}$$

one finds for $i = 1$, with transmission along $\boldsymbol{e}_3'$, $\Delta a_{11}' = 0$ and $\Delta a_{22}' = \Delta a_{23} = r_{231}E_1$. Moreover, $\hat{d}_{331}' = -\hat{d}_{231}$ and

$$n_{22}'^2 = \frac{2n_{22}^2 n_{33}^2}{n_{22}^2 + n_{33}^2}.$$

One obtains analogous values for $i = 2$ or 3. Hence, for arbitrary $i$, the change in the path difference is given by

$$\Delta G = \frac{L}{2}(n_{22}')^3 r_{jki}E_i - (n_{ii} - n_{22}')L\hat{d}_{jki}E_i$$

(do not sum over $i$!).

Thus we directly obtain the components $r_{jki}$ ($i \neq j \neq k \neq i$).

The peculiar situation of a circular sectional ellipse may be explained on crystals of the PSG $\bar{4}2$ as an example. Let the electric field and the ray direction be parallel to the fourfold axis, therefore parallel to $\boldsymbol{e}_3$. Then $\Delta a_{12} = \Delta a_{21} = r_{123}E_3$. After the field is applied, the sectional ellipse takes the form

$$a_{11}x_1^2 + a_{11}x_2^2 + 2\Delta a_{12}x_1x_2 = 1.$$

The principal axes transformation gives $\tan 2\varphi = \infty$, hence $\varphi = 45°$. The new directions of vibration are

$$\boldsymbol{e}_1' = \frac{\sqrt{2}}{2}(\boldsymbol{e}_1 + \boldsymbol{e}_2) \quad \text{and} \quad \boldsymbol{e}_2' = \frac{\sqrt{2}}{2}(-\boldsymbol{e}_1 + \boldsymbol{e}_2).$$

Consequently $a_{11}' = a_{11} + \Delta a_{12}$ and $a_{22}' = a_{11} - \Delta a_{12}$. The path difference is then

$$\Delta G = -Ln_{11}^3 r_{123}E_3 = n_{11}^3 r_{123}U.$$

The electrostrictive part vanishes since $\hat{d}_{333} = 0$. In this case, with fixed electrical voltage $U$, $\Delta G$ does not depend on the length $L$ of the transmission path because $E_3 = -U/L$. If the light passes through the same specimen in the direction $\boldsymbol{e}_1'$ and the electric field persists parallel $\boldsymbol{e}_3$, a change

$$\Delta G = -\frac{L}{2}n_{11}^3 r_{123}E_3 + (n_{11} - n_{33})L\hat{d}_{123}E_3$$

in the path difference occurs, whereby the electrooptical part, at the same field strength, is only half as large as in the case of transmission in the direction of the electric field.

We now want to get an overview of the obtainable electrooptical effects in different transmission and field directions in cubic crystals. We search for the directions of extreme changes of refractive indices in a given field direction. We proceed in the same manner as discussed in Section 4.3.2 (principal axes transformation). The auxiliary function

$$H=(a_{11}(x_1^2+x_2^2+x_3^2)+2r_{123}x_1x_2E_3+2r_{231}x_2x_3E_1+2r_{312}x_3x_1E_2-1)-\lambda\sum_i x_i^2$$

also attains an extreme value, when the length of the radius vector of the indicatrix, which is equal to the associated refractive index, becomes extreme. For $\Delta a_{ij}$ we write the quantity $r_{ijk}E_k$, respectively. Extreme values appear, when $\partial H/\partial x_i = 0$ for $i = 1, 2, 3$, thus, for example,

$$\begin{aligned}\frac{\partial H}{\partial x_1} &= (a_{11}-\lambda)2x_1+2rx_2E_3+2rx_3E_2 \;=\; 0\\ \frac{\partial H}{\partial x_2} &= (a_{11}-\lambda)2x_2+2rx_1E_3+2rx_3E_1 \;=\; 0\end{aligned}$$

with $r_{123} = r_{231} = r_{312} = r$. Multiplying the first equation by $x_2$, the second by $x_1$, and subtracting gives $E_3(x_2^2 - x_1^2) = x_3(x_1E_1 - x_2E_2)$. The corresponding expressions are obtained by forming the difference

$$\left(x_i\frac{\partial H}{\partial x_j}-x_j\frac{\partial H}{\partial x_i}\right)=0.$$

In general, it is true that $E_k(x_i^2 - x_j^2) = -x_k(x_iE_i - x_jE_j)$, where $i, j, k$ are cyclic in $1, 2, 3$.

We now consider some concrete examples. First let $\boldsymbol{E}$ be parallel to [110], thus

$$\boldsymbol{E}=\frac{\sqrt{2}|\boldsymbol{E}|}{2}(\boldsymbol{e}_1+\boldsymbol{e}_2).$$

This results from the above equation with $E_3 = 0$: $x_3 = 0$ or $x_1 = x_2$ (because $E_1 = E_2$). With $x_3 = 0$ one gets $x_1^2 = -x_1x_2$ and $x_2^2 = -x_1x_2$, hence $x_2 = -x_1$ and $x_1 = 0$ or $x_2 = 0$.

Therefore, we have found three extreme directions

$$\boldsymbol{e}_1'=\frac{\sqrt{2}}{2}(\boldsymbol{e}_1-\boldsymbol{e}_2)\parallel[1\bar{1}0],\quad \boldsymbol{e}_1''=\boldsymbol{e}_2\quad\text{and}\quad \boldsymbol{e}_1'''=\boldsymbol{e}_1.$$

The refractive indices do not change in these directions ($\Delta a_{11} = \Delta a_{22} = \Delta a_{12} = 0$ for $E_1 = E_2$ and $E_3 = 0$!).

The other condition $x_1 = x_2$ gives $E_1(x_1^2 - x_3^2) = -x_1^2 E_1$ with $E_1 = E_2$, hence $x_3 = \pm\sqrt{2}x_1$, and thus

$$\boldsymbol{e}_2' = \frac{1}{2}(\boldsymbol{e}_1 + \boldsymbol{e}_2 - \sqrt{2}\boldsymbol{e}_3),$$
$$\boldsymbol{e}_3' = \frac{1}{2}(\boldsymbol{e}_1 + \boldsymbol{e}_2 + \sqrt{2}\boldsymbol{e}_3).$$

Both these directions are perpendicular to $\boldsymbol{e}_1'$. The associated principal refractive indices are calculated from the corresponding eigenvalues $\lambda_i$. These results, for example, from $\partial H/\partial x_i = 0$

$$\begin{aligned} \lambda_1 &= a_{11} \rightarrow \Delta a_{11}' = 0; \\ \lambda_2 &= a_{11} - r_{123}\sqrt{2}E_1 \rightarrow \Delta a_{22}' = -r_{123}\sqrt{2}E_1; \\ \lambda_3 &= a_{11} + r_{123}\sqrt{2}E_1 \rightarrow \Delta a_{33}' = r_{123}\sqrt{2}E_1. \end{aligned}$$

Transmitting light perpendicular to the electric field in the direction $\boldsymbol{e}_1' \parallel [1\bar{1}0]$ produces a path difference $\Delta G = Ln^3 r_{123}\sqrt{2}E_1 = Ln^3 r_{123}|\boldsymbol{E}|$ sign $\boldsymbol{E}$. The electrostrictive part vanishes because $n_{11} = n_{22} = n_{33}$.

In cubic crystals the direction of the maximal longitudinal effect coincides with a principal axis direction of the indicatrix modified by the electric field. By analogy with the method discussed pveviously for the piezoelectric effect (see Section 4.4.1.2), we form the auxiliary function $H = r_{111}' - \lambda \sum_i x_i^2$ for the effect $\Delta a_{11}' = r_{111}' E_1'$ and calculate its extreme values. As before, for $\boldsymbol{e}_1' = u_{1i}\boldsymbol{e}_i$ we obtain the directions of the space diagonals of the cube, hence

$$u_{1i} = \pm\frac{1}{\sqrt{3}}.$$

With this we find

$$\Delta a_{11}' = r_{111}' E_1' = 6r_{123}\left(\frac{1}{\sqrt{3}}\right)^3 |\boldsymbol{E}| \text{ sign } \boldsymbol{E}.$$

In the plane perpendicular to $\boldsymbol{e}_1'$, thus perpendicular to a threefold axis, the indicatrix forms a circular section. We have $\Delta a_{22}' = \Delta a_{33}' = -\Delta a_{11}'/2$ because $\sum_i \Delta a_{ii} = 0$. Hence, a transmission in all directions perpendicular to the electric field ($\boldsymbol{E}$ along the threefold axis) produces a path difference

$$\Delta G = -\frac{\sqrt{3}Ln^3}{2} r_{123}|\boldsymbol{E}| \text{ sign } \boldsymbol{E} \quad \text{with} \quad \Delta a_{11}' - \Delta a_{22}' = \frac{3}{2}\Delta a_{11}'.$$

Table 4.8 presents the most important arrangements of field and transmission directions for cubic crystals of the PSG $\bar{4}3$.

Crystals of the PSG 23 usually exhibit such a strong optical activity that the formulae derived in Section 4.3.6.7 for the interplay of optical activity and

**Table 4.8** Electro-optical effect in distinct directions of cubic crystals; $g$ propagation vector, $e_2'$ and $e_3'$ directions of vibration, $L$ length of transmission.

| $\boldsymbol{E} \parallel$ | $g \parallel e_1' \parallel$ | $e_2' \parallel$ | $e_3' \parallel$ | $\Delta G$ |
|---|---|---|---|---|
| [001] | [001] | [110] | $[\bar{1}10]$ | $-Ln^3 r_{123}\lvert\boldsymbol{E}\rvert \operatorname{sign} \boldsymbol{E}$ |
| [001] | $[\bar{1}10]$ | [001] | [110] | $\frac{L}{2} n^3 r_{123}\lvert\boldsymbol{E}\rvert \operatorname{sign} \boldsymbol{E}$ |
| [110] | $[1\bar{1}0]$ | $[11-\sqrt{2}]$ | $[11\sqrt{2}]$ | $Ln^3 r_{123}\lvert\boldsymbol{E}\rvert \operatorname{sign} \boldsymbol{E}$ |
| [111] | $[1\bar{1}0]$ | [111] | $[11\bar{2}]$ | $-\frac{\sqrt{3}L}{2} n^3 r_{123}\lvert\boldsymbol{E}\rvert \operatorname{sign} \boldsymbol{E}$ |

double refraction (here induced double refraction) must be used. For a first approximation one assumes that the dependence of the optical activity on the electric field strength is negligible. Under this presupposition the tensor components $r_{123}$ of optically active crystals can be measured with methods similar to those outlined above.

The practical application of the electrooptical effect is limited mainly to the modulation of light. All other modulation methods cannot compete with the almost inertia-less control of the electrooptical modulator. This is especially true for cubic crystals because the electrostrictive part is missing. In this context, it is very convenient that the modulation, to a sufficient approximation, follows the frequency of the applied electric field. The specimen is located in diagonal position between crossed polarizers (see Section 4.3.6.3; $\varphi = 45°$). If one neglects reflection and absorption losses, the transmitted intensity is given by

$$I' = I_0 \sin^2 \pi d = I_0(1 - \cos 2\pi d)/2,$$

where $d = L(n'' - n')/\lambda_0 = G/\lambda_0$ is the measured path difference in units of the vacuum wavelength. Changing the path difference, for example, via the electrooptical effect, gives

$$I'' = I_0 \sin^2\{\pi(G + \Delta G)/\lambda_0\} = I_0(1 - \cos\{2\pi(G + \Delta G)/\lambda_0\})/2.$$

Thus we observe a modulated part

$$I'' - \frac{I_0}{2} = \Delta I = \frac{1}{2} I_0 \left\{ \sin \frac{2\pi}{\lambda_0} G \sin \frac{2\pi}{\lambda_0} \Delta G - \cos \frac{2\pi}{\lambda_0} G \cos \frac{2\pi}{\lambda_0} \Delta G \right\}.$$

If $L$ is adjusted so that $L(n'' - n')$ is an odd multiple of a quarter of the vacuum wavelength, hence $G = (2m + 1)\lambda_0/4$, for $m$ integer, we obtain

$$\Delta I = \pm \frac{I_0}{2} \sin \frac{2\pi}{\lambda_0} \Delta G.$$

For sufficiently small $\Delta G$ a quasi-sinusoidal modulation arises, when the electric field varies sinusoidally. This is approximately correct for very small $\Delta G$

even with an arbitrary primary path difference $G$. In cubic crystals, because $G = 0$, the following is true:

$$\Delta I = -\frac{I_0}{2} \cos 2\pi \frac{\Delta G}{\lambda_0}.$$

A measure for the efficiency of the electrooptical effect is the half-wave voltage $U_0$ required to produce a path difference change of $\lambda_0/2$ and thus a maximum of the intensity $I''$ for the case $G = m\lambda_0$, $m$ integer. The dimensions of the specimen must be given, for example, transmission length and thickness in the field direction both 10 mm. In the devices, half-wave voltages as small as possible are preferred. At present, only a few crystals are known exhibiting a half-wave voltage less than 100 V as, for example, $K(Nb, Ta)O_3$.

### 4.4.3
### First-Order Nonlinear Electrical Conductivity (Deviation from Ohm's Law)

The dependence of current density on the electric field is for most substances linear up to very high field strengths. The possible deviations are described by a Taylor series of the type

$$I_i = s_{ij}E_j + s_{ijk}E_jE_k + s_{ijkl}E_jE_kE_l + \cdots .$$

The tensor $\{s_{ijk}\}$ contains the *first-order nonlinear conductivity*. Its behavior is completely analogous to the piezoelectric tensor $\{d_{ijk}\}$. The measurement is performed with the help of the longitudinal effect as with the measurement of Ohmic conductivity. If one applies an alternating electric field $E_1' = E_0 \sin \omega t$ to a plane-parallel plate with the normal $\boldsymbol{e}_1'$, one observes a current density

$$I_1' = s_{11}'E_1' + s_{111}'E_1'^2 = s_{11}'E_0 \sin \omega t + s_{111}'E_0^2(1 - \cos 2\omega t)/2$$

(with $\sin^2 \omega t = (1 - \cos 2\omega t)/2$). Hence there appears a direct current component $s_{111}'E_0^2/2$ and a frequency-doubled component $s_{111}'E_0^2(\cos 2\omega t)/2$, both of which can be measured with sensitive instruments. The frequency-doubled component can best be detected using a lock-in amplifier with compensation. Consequently, the heat produced in the specimen by the high field and current strengths and therefore the associated change in Ohmic conductivity have no influence on the measurement. The quadratic dependence of the effect on the field strength allows a reliable control of the measurement.

Centrosymmetrc crystals (almost all metals) and crystals of the PSG 43 do not possess a first-order nonlinear effect. Therefore, one can test, with the help of nonpiezoelectric cubic crystals, whether the primary voltage is free of components of the first harmonic. Here, the deviation from Ohm's law begins with the second-order effect (third power of the field strength), whereby,

in the case of an alternating field, components with the triple frequency appear in the current density. In semiconductors, conduction to a large extent is mainly caused by defects. The symmetry properties of these defects do not always coincide with the space group symmetry or the site symmetry in the undisturbed lattice. In such cases, first-order effects can also be observed in centrosymmetric crystals.

### 4.4.4 Nonlinear Dielectric Susceptibilty

The dielectrical and optical properties discussed in Sections 4.3.3 and 4.3.6 are based on a linear relation between the electric displacement $\boldsymbol{D}$ and the electric field strength $\boldsymbol{E}$ according to $D_i = \epsilon_{ij} E_j$. When discussing higher order effects, this relationship must be supplemented by adding higher order terms, hence

$$\begin{aligned} D_i = {} & \epsilon_{ij} E_j + \epsilon_{ijk} E_j E_k + \epsilon_{ijkl} E_j E_k E_l + \cdots \\ & + g_{ijk} \frac{\partial E_j}{\partial x_k} + g_{ijkl} \frac{\partial^2 E_j}{\partial x_k \partial x_l} + \cdots \\ & + f_{ijkl} E_j \frac{\partial E_k}{\partial x_l} + \cdots . \end{aligned}$$

The top row corresponds to the normal Taylor series. With the first term in the second row we were able to describe in Section 4.3.6.7 the optical activity. Until recently, the prevailing opinion was that higher order dielectric effects were practically undetectable. In the meantime we know quite a number of higher order phenomena which are simple to realize experimentally. With the developement of coherent light sources (laser) it became possible to produce effects of frequency multiplication and frequency mixing in the field of optics. At low frequencies, hence in the usual dielectric range, one still requires special experimental techniques to detect higher order effects. In this section we will address the optical effects. Instead of the hitherto employed material equation $D_i = \epsilon_{ij} E_j$ we must use the equation above. Here we will consider only one more step in the series expansion in each case, for example, $\epsilon_{ijk} E_j E_k$ or $\epsilon_{ijkl} E_j E_k E_l$. The simplest and for most problems adequate model for nonlinear effects consists in allowing the existence of one or more plane waves propagating in a crystal according to the usual laws of crystal optics, hence without loss of energy. The directions of vibration of the $\boldsymbol{D}$-vector associated with each direction of propagation are fixed as well as the associated electric fields. If a nonlinear interaction of the components of the electric fields produces additional electric displacements, i.e., polarizations, then these generate secondary waves when migrating through the crystal, which differ in direction of vibration, direction of propagation, and frequency from the primary waves. If we let a linear polarized wave strike a crystal plate, two linear polarized waves

$\boldsymbol{D}'$ and $\boldsymbol{D}''$ propagate in the crystal with their propagation vectors running parallel only in the case of perpendicular incidence or optical isotropy. The associated $\boldsymbol{E}$-vectors $\boldsymbol{E}' = \boldsymbol{E}'_0 e^{2\pi i(\boldsymbol{k}'\cdot\boldsymbol{x}-\nu t)}$ and $\boldsymbol{E}'' = \boldsymbol{E}''_0 e^{2\pi i(\boldsymbol{k}''\cdot\boldsymbol{x}-\nu t)}$, cause in the volume elements, through which they pass, a nonlinear polarization $\boldsymbol{D}^{\mathrm{NL}}$:

$$\begin{aligned} D_i^{\mathrm{NL}} = {} & \epsilon_{ijk}(E'_j E'_k + E'_j E''_k + E''_j E'_k + E''_j E''_k) \\ & + \epsilon_{ijkl}(E'_j E'_k E'_l + E'_j E'_k E''_l + \cdots E''_j E''_k E''_l). \end{aligned}$$

The quadratic part of the first term consists of the partial waves

$$\begin{aligned} D_i^{\mathrm{NL}}(2\nu) = {} & \epsilon_{ijk} E'_{j0} E'_{k0} e^{2\pi i(2\boldsymbol{k}'_0\cdot\boldsymbol{x}-2\nu t)} \\ & + \epsilon_{ijk}(E'_{j0} E''_{k0} + E''_{j0} E'_{k0}) e^{2\pi i((\boldsymbol{k}'_0+\boldsymbol{k}''_0)\cdot\boldsymbol{x}-2\nu t)} \\ & + \epsilon_{ijk} E''_{j0} E''_{k0} e^{2\pi i(2\boldsymbol{k}''_0\cdot\boldsymbol{x}-2\nu t)}. \end{aligned}$$

Here we assume that $\{\epsilon_{ijk}\}$ is virtually independent of frequency.

These three waves are firmly coupled with the fundamental wave. We call them bound waves. They possess twice the frequency of the fundamental wave. We therefore speak of the *frequency doubling* effect (or SHG: *second harmonic generation*). The generation of the first and third partial wave, each of them emanating from only one fundamental wave, is refered to as a *type-I-process*, the generation of the "mixed wave" as a *type-II-process*. Only those components of $\boldsymbol{D}^{\mathrm{NL}}(2\nu)$ compatible with the indicatrix for the double frequency and compatible with the associated directions of vibration allow the propagation of the so-called free waves. The intensity of these frequency-doubled waves is calculated from the Maxwell equations taking into consideration the previously discussed boundary conditions in Section 4.3.6.1. An important situation for the frequency doubling of laser radiation is realized, when the fundamental wave and the frequency-doubled free wave (harmonic) possess the same propagation velocity with respect to direction and magnitude. In this case the fundamental waves, on passing through the crystal, feed their frequency-doubled components in-phase to the harmonic. The intensity of the harmonic, as opposed to an arbitrary situation, increases by many orders of magnitude due to constructive interference and is thus made easily accessible to visual observation. This special situation is called *phase matching*. The conditions for type-I-processes are $n'(\nu) = n(2\nu)$ or $n''(\nu) = n(2\nu)$ and for type-II-processes $n'(\nu) + n''(\nu) = 2n(2\nu)$. Possible directions of phase matching are obtained from the intercept of the index surfaces for both frequencies $\nu$ and $2\nu$. A vector leading from the center of the index surfaces to an intercept point shows a possible phase matching direction. Under normal dispersion ($\partial n/\partial\nu > 0$), the associated directions of vibration are different. Only a specific anisotropy of refractive indices allows an intercept of the index surfaces at all. In cubic crystals no normal phase matching occurs due to

the missing anisotropy. Nevertheless, phase matching in a very restricted frequency range is conceivable in the case of anomalous dispersion ($\partial n/\partial \nu < 0$). In optical uniaxial crystals, the directions of vibration of the fundamental and of the free second harmonic waves are mutually perpendicular in the case of phase matching. Biaxial crystals offer a higher probability for the existence of phase matching directions due to the wider variation of anisotropy. According to Hobden (1967) one can distinguish between a total of 13 different types of phase matching (Hobden classes).

Since the anisotropy as well as the dispersion of the refractive indices are very small, a very good knowledge of the refractive indices or vacuum wavelengths is required to determine the directions of phase matching. We will return to the calculation of phase matching directions at the end of this section.

The effects of frequency doubling, as far as they are based on the existence of the tensor $\{\epsilon_{ijk}\}$, only appear in piezoelectric crystals, because the tensors $\{\epsilon_{ijk}\}$ and $\{d_{ijk}\}$ belong to the same symmetry type (see Table 4.7). Similarly with the piezoelectric effect, there also exists a powder test, with which one can determine to a high degree of probability, whether a crystal species possesses an inversion center or not (here an exception is also the PSG 43 with vanishing third-rank tensors). This so-called SHG test is carried out as follows: the specimen in the form of a powder is applied as a thin layer on a polished glass plate. If the preparation is irradiated with a strong laser beam, one can expect that several crystal grains always are oriented in a favorable position for frequency doubling. The light emerging from the preparation, from which the primary radiation was removed by suitable filters, is analyzed with the help of photon counting techniques, if necessary, using energy-discrimination methods. Decisive is, whether the number of measured photons with twice the energy (frequency) surmounts the background value. On comparing with specimens, which show no effect, for example corundum powder, this statement is in almost all cases investigated so far unambiguously answered. The method can be made substantially more sensitive than required for routine investigations by employing pulse techniques coupled with a synchronously running counter.

A number of methods are available to measure the tensor $\{\epsilon_{ijk}\}$ of which in particular the *wedge method* (Jerphagnon, 1968) and the method of *Maker interferences* deserve special attention (Maker et al., 1962). In the wedge method, the intensity of the second harmonic wave at perpendicular incidence is measured on a slightly wedge-shaped crystal (Fig. 4.38). If one neglects the effect of double refraction and absorption losses, one expects an intensity of the second harmonic varying periodically with the transmission length through the crystal. Up to the first maximum, only the constructive components add to

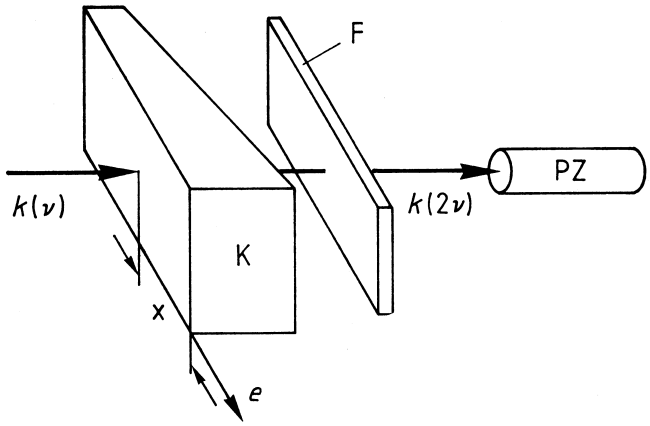


**Figure 4.38** Wedge method. K crystal (specimen), F filter for suppressing the primary radiation, PZ photon counter. The intensity of the frequency-doubled radiation (second harmonic) varies periodically with the shift $x$ of the wedge-shaped specimen along the direction $e$.

the harmonic. The associated transmission thickness

$$L_c = \frac{\lambda_0}{4(n(2\nu) - n(\nu))}$$

is termed the coherence length for the given direction of propagation, whereby $\lambda_0$ refers to the vacuum wavelength of the fundamental wave. With increasing thickness further contributions of the generating wave become more and more out of phase with the harmonic and finally effect complete destruction of the harmonic. After this minimum a maximum of the second harmonic again builds up and so on. Thus if one shifts the specimen perpendicular to the finely bundled fundamental wave, one observes a periodic change in the intensity. The intensity of the maxima is proportional to the square of the product of coherence length, effective nonlinear coefficient $\epsilon_{\text{eff}}$ and intensity of the fundamental wave. $\epsilon_{\text{eff}}$ is calculated as a function of the components $\epsilon_{ijk}$ for the given direction of vibration of the fundamental wave by means of tensor transformation. The calibration of the intensity of the harmonic can be performed with the aid of a standard specimen, for example made of $KH_2PO_4$. By varying the transmission direction and the direction of vibration of the fundamental wave, it is possible, in principle, to determine all tensor components. The problem of the relative sign of tensor components is solvable by measuring those effective nonlinear coefficients, which contain sums or differences of the components $\epsilon_{ijk}$.

In the Maker interference method, the intensity of the harmonic is investigated on a thin plane-parallel plate as a function of the angle of incidence

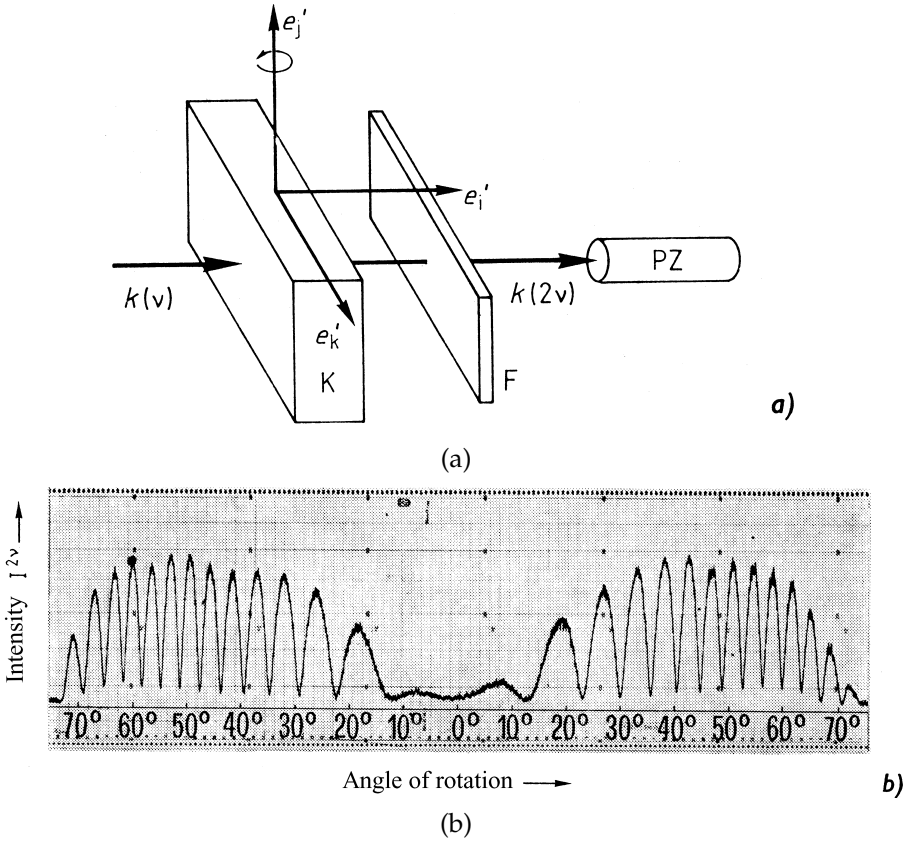


**Figure 4.39** (a) Method of Maker interferences. K plane-parallel specimen, rotatable around the axis $e_j'$, F filter for suppressing the primary radiation, PZ photon counter. (b) Maker interferences obtained on a thin (010)-plate of $LiHC_2O_4 \cdot H_2O$. Axis of rotation and direction of vibration of the fundamental wave parallel to the shortest semi-axis of the indicatrix, direction of vibration of the frequency-doubled wave (second harmonic) perpendicular to the axis of rotation.

and the direction of vibration of the fundamental wave (Fig. 4.39). Maxima appear also here, when an odd multiple of the coherence length is realized in the given direction. In contrast to the wedge method, the effective nonlinear coefficient changes from maximum to maximum. Furthermore, differences in reflection losses appear as a function of the angle of incidence, which must be taken into consideration. As before, a standard specimen is used for the calibration of the intensity. From the envelope of the maxima, which can even be determined with good accuracy on specimens of moderate optical quality, one can extract the effective nonlinear coefficient for the direction of perpendicular incidence. Important is that in the case of negligible double refraction the envelope is independent of the specimen thickness. An evaluation of the

**Table 4.9** Arrangement for the measurement of non-linear optical effects on thin plates.

| No. | Plate normal and vector $\boldsymbol{g}$ | $\boldsymbol{D}(\nu)$ (fundamental wave) | $\boldsymbol{D}(2\nu)$ (2nd harmonic) | Eff. coeff. for perp. incidence | Type |
|---|---|---|---|---|---|
| 1 | $\boldsymbol{e}_i^0$ | $\boldsymbol{e}_j^0$ | $\boldsymbol{e}_j^0$ | $\epsilon_{jjj}$ | I |
| 2 | $\boldsymbol{e}_i^0$ | $\boldsymbol{e}_j^0$ | $\boldsymbol{e}_k^0$ | $\epsilon_{kjj}$ | I |
| 3 | $\boldsymbol{e}_i^0$ | $\frac{\sqrt{2}}{2}(\boldsymbol{e}_j^0 \pm \boldsymbol{e}_k^0)^*$ | $\boldsymbol{e}_j^0$ | $\epsilon_{jjj}, \epsilon_{jkk}, \epsilon_{jjk}$ | II** |
| 4 | $\frac{\sqrt{2}}{2}(\boldsymbol{e}_i^0 + \boldsymbol{e}_j^0)$ | $\frac{\sqrt{2}}{2}(-\boldsymbol{e}_i^0 + \boldsymbol{e}_j^0)$ | $\boldsymbol{e}_k^0$ | $\frac{1}{2}(\epsilon_{kii} - 2\epsilon_{kij} + \epsilon_{kjj})$ | I |

* before entering the specimen

**) the effective coefficient is a function of $\epsilon_{jjj}$, $\epsilon_{jkk}$, $\epsilon_{jjk}$, $n_{jj}$ and $n_{kk}$.

complete range of the envelope curve and also of the whole interference curve with the help of computer-supported matching of the intensity to the observations can lead to a substantial improvement in accuracy. The progression of the intensity is calculated by variation of the components $\epsilon_{ijk}$.

A derivation of formulae for the evaluation of Maker interferences on optically uniaxial crystals was given by Jerphagon & Kurtz (1970). The corresponding formulae for biaxial crystals were derived by Bechthold (1977). In the meantime, the latter have also been used for the determination of the complete tensor $\{\epsilon_{ijk}\}$ on triclinic lithium hydrogen oxalate-monohydrate.

A substantial simplification of the measurements results, when one assumes the validity of the so-called *Kleinman rule* (1962). This rule states that nonabsorbing dispersion-free crystals possess a totally symmetric tensor $\{\epsilon_{ijk}\}$. Experimental observations confirm, in fact, that only small deviations from total symmetry appear. For crystals of the PSG 42 and 62, the Kleinman rule would have the consequence that absolutely no frequency doubling effect would be observed. On the few examples of these PSG investigated so far, weak effects of frequency doubling could be observed, so that one cannot assume a severe validity of the Kleinman rule.

Measurements with the wedge method and with the method of Maker interferences are preferentially carried out on plates cut parallel to the principal planes of the indicatrix.

The following arrangements have proven useful and are also suitable for the complete determination of the tensor of triclinic crystals (see Table 4.9). Let the principal axes of the indicatrix be specified by $\boldsymbol{e}_i^0$. Except in triclinic and monoclinic systems, the optical principal axes coincide anyway with the basic vectors $\boldsymbol{e}_i$ of the crystal–physical system. The indices $i, j, k$ should be different.

Variation of the indices results in a total of 21 different arrangements already at perpendicular incidence. To record Maker interferences one turns the plate, during transmision, about the direction of $\boldsymbol{D}(\nu)$ or $\boldsymbol{D}(2\nu)$ taken as the axis of rotation. From the progression of the envelope of the Maker interferences one can obtain information on the relative sign of the components $\epsilon_{ijk}$.

In order not to jeopardize the validity of the simple model, the plate thickness should not be too large so that a noticeable spacial separation of the volume, through which the fundamental and the harmonic pass, does not occur as a consequence of ray double refraction.

From the above table we recognize immediately that all crystals with 22 as a subgroup, hence also those of PSG $\bar{4}2$ and the cubic crystals of PSG 23 and $\bar{4}3$, show no effect in the arrangements 1 to 3. In these cases we work with arrangement 4, whereby the orientation of the 45°-cuts, in the case of the cubic crystals, is referred to the crystal–physical system.

There exists another way of determining the sign, which, however, yet has not been used routinely. Namely, one obtains, apart from the frequency-doubled radiation via nonlinear processes, also a contribution of constant polarization. Let us consider, for example, a type-I-process of the kind $D_1 = \epsilon_{12}E_2 + \epsilon_{122}E_2^2$ with $\boldsymbol{E} = E_2\boldsymbol{e}_2 = E_{20}\cos(2\pi(\boldsymbol{k}\cdot\boldsymbol{x} - \nu t))\boldsymbol{e}_2$. Because $\cos^2 u = (1 + \cos 2u)/2$ we obtain a constant contribution $D_{10} = E_{20}^2\epsilon_{122}/2$, which is measurable in the case of sufficiently high field strength. In the example discussed the specimen has to be equipped with a conducting pair of faces perpendicular to $\boldsymbol{e}_1$, on which one observes a charge density similar to that detected in pyroelectric or piezoelectric effects. The sign of $\epsilon_{122}$ corresponds directly to the sign of the measured polarization.

Apart from collinear processes discussed here, where the fundamental and the harmonic show approximately the same propagation direction, the possibility exists of generating a new radiation, when two laser beams meet at a finite angle. In the volume covered by both waves, nonlinear frequency mixing effects occur, where waves appear with sum and difference frequencies of both fundamental waves. Even with collinear superposition of two parallel laser beams of different frequencies, such sum and difference frequencies are observable, as one can immediately derive the general relationship between $\boldsymbol{D}$ and $\boldsymbol{E}$.

Furthermore, under certain conditions, the so-called threshold processes can produce rays with half frequencies and arbitrary frequencies within a certain frequency range. These first appear, just as with starting a laser, from a definite energy density onwards. The frequency of the generated rays depends on the direction of the fundamental in the crystal and can be varied, to an extent, by rotating the crystal (parametric oscillator; see Bloembergen, 1965).

Finally, we discuss some questions concerning the practical application of frequency doubling under phase matching conditions. In optical uniaxial crystals the phase matching angle can be easily calculated from the index surfaces, because they are rotationally symmetric for both frequencies. The

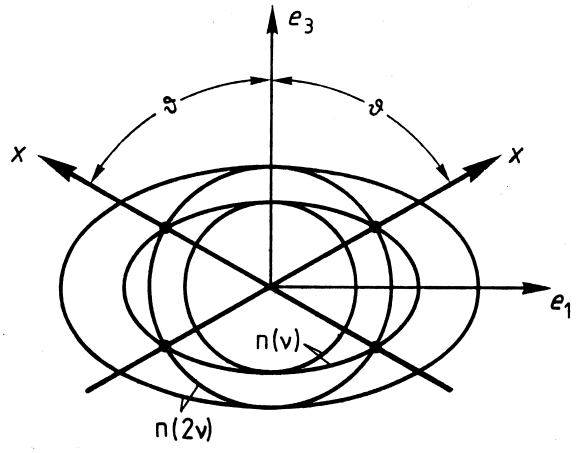


**Figure 4.40** Construction of the direction of phase matching of fundamental wave with frequency $\nu$ and second harmonic with frequency $2\nu$ for the case of an optically positive uniaxial crystal ($n_1 = n_2 < n_3$). The ordinary wave of the doubled frequency (harmonic), which is represented in the index-surface by a sphere with radius $n(2\nu)$ takes on the same propagation velocity as the extraordinary fundamental wave along all directions within a cone around the optical axis parallel $e_3$.

equation of the index surface is (see Section 4.3.6.1)

$$\sum_i x_i^2 = n_1^2 \quad \text{and} \quad (x_1^2 + x_2^2)/n_3^2 + x_3^2/n_1^2 = 1.$$

Due to rotational symmetry it suffices to consider a principal cut with $x_2 = 0$. In the case of normal dispersion ($n(2\nu) > n(\nu)$) in optical positive crystals ($n_3 > n_1$), the refractive index of ordinary waves for the double frequency ($n_1(2\nu)$) can coincide with the extraordinary wave of the fundamental frequency $n_e(\nu)$ (Section 4.40). For optically negative crystals ($n_3 < n_1$) the reverse is true.

In the case of $n_3 > n_1$, $x_1^2 + x_3^2 = n_1^2(2\nu)$ and $x_1^2/n_3^2(\nu) + x_3^2/n_1^2(\nu) = 1$ intersect. $\vartheta$ is the angle between the phase matching direction and the optic axis. With $x_1 = n_1(2\nu)\sin\vartheta$ and $x_3 = n_1(2\nu)\cos\vartheta$ one finds

$$\sin^2\vartheta = \frac{1/n_1^2(\nu) - 1/n_1^2(2\nu)}{1/n_1^2(\nu) - 1/n_3^2(\nu)}.$$

Correspondingly, for $n_3 < n_1$ we get

$$\sin^2\vartheta = \frac{1/n_1^2(\nu) - 1/n_1^2(2\nu)}{1/n_3^2(2\nu) - 1/n_1^2(2\nu)}.$$

Normally, the range of the angle $\Delta\vartheta$ of the cone about the optic axis, in which phase matching is observable, is extremely small, namely of the order of a few

arc minutes. In rare cases, the index surfaces intersect just about tangentially, i.e., the refractive indices differ very little over a large angular range. Such a situation is called noncritical phase matching, where $\vartheta \approx 90°$. This means that for all partial waves of a divergent laser beam, there exists large coherence lengths and thus a high rate of conversion of the energy of the fundamental into the frequency-doubled harmonic.

The phase matching directions for type-II-processes are calculated in an analogous way.

To judge whether a crystal is suitable as a technical frequency doubler, the following criteria should be considered:

1. good transparency in the frequency range between $\nu$ and $2\nu$,
2. existence of quasinoncritical phase matching directions,
3. large effective nonlinear coefficients,
4. high irradiation strength (since the efficiency of frequency conversion grows in proportion to the square of the intensity of the fundamental wave, it is advantageous to work with very high laser power!) and
5. capability to manufacture crystals of sufficient size and optical quality.

At present, irradiation strength and manufacturing capability can hardly be predicted. Crystals with high mechanical strength as, for example, $LiNbO_3$ tend to form optical defects under weak irradiation. Others, like lithium formate-hydrate are mechanically weak in comparison, however, show a good irradiation strength. A certain role is surely played by the regeneration capability of the crystal and the existence of certain primary defects, in particular chemical impurities and micro-inclusions in the crystal.

Further effects of nonlinear optical properties as, for example, the effects of frequency tripling and frequency quadrupling, brought about by the tensors $\{\epsilon_{ijkl}\}$ and $\{\epsilon_{ijklm}\}$ will only be mentioned here. Since $\{\epsilon_{ijkl}\}$ is a fourth-rank tensor, it exists in all materials. Therefore, with sufficiently high intensity of the coherent fundamental wave, one can observe in all materials a radiation of triple frequency arising from the product $E_j E_k E_l$. While frequency doubling effects are observable in phase matching directions of crystals already at very weak laser powers of the fundamental wave in an amount of a fraction of a milliwatt, one requires for the generation of frequency tripling and higher effects far higher powers, even with phase matching. In other words, the search for crystals with high irradiation strength as well as strong effects of this kind is still in progress. Fields of application are, for example, laser systems based on the generation of stimulated Raman scattering (see e.g., Kaminskii et al., 2000).

### 4.4.5 Faraday Effect

If a cubic crystal (electrically nonconducting) or some other optically isotropic medium is placed in a magnetic field, one observes a rotation of the direction of vibration of a linear polarized wave similar as in optical activity. However, while in optical activity the rotation per mm optical path is the same in all directions, one finds here a change in the sense of rotation, when the propagation direction is reversed. This magnetooptical effect, named after its discoverer *Faraday effect*, is proportional to the magnetic field strength. It emerges that the influence of the magnetic field on the propagation of light also appears in anisotropic crystals. To describe the phenomena, we demand, just as with optical activity, that no additional energy terms arise, i.e., we attach an additional term to the electric displacement that is proportional to the magnetic field $\boldsymbol{H}$ and satisfies the condition $q''_{ij} = -q''_{ji}$

$$D_i = \epsilon_{ij}E_j + z_{ijk}E_jH_k = (\epsilon_{ij} + z_{ijk}H_k)E_j.$$

The analogous relationship in optical activity is

$$D_i = \epsilon_{ij}E_j + g_{ijk}\frac{\partial E_j}{\partial x_k} = \epsilon_{ij}E_j + 2\pi i g_{ijk}k_kE_j,$$

for the case that $\boldsymbol{E}$ represents a plane wave $\boldsymbol{E} = \boldsymbol{E}_0 e^{2\pi i(\boldsymbol{k}\cdot\boldsymbol{x}-\nu t}$ (see Section 4.3.6.7).

Corresponding to the condition $g_{ijk} = -g_{jik}$ for optical activity, here we must also demand that $z_{ijk}$ are antisymmetric in the first two indices and furthermore, are purely imaginary. If we substitute $z_{ijk}$ by $i\zeta_{lk}$ or $-i\zeta_{lk}$ with $l \neq i, j$ and $i, j, l$ cyclic or anticyclic in 1,2,3 and introduce the vector $\boldsymbol{Z}$ with the components $Z_l = \zeta_{lk}H_k$, we obtain

$$D_i = \epsilon_{ij}E_j - i(\boldsymbol{Z} \times \boldsymbol{E})_i.$$

This form corresponds to the description of optical activity. Now, with respect to tensor properties, $\{z_{ijk}\}$ behaves as a third-rank axial tensor in crystals with rotation–inversion axes. This is different to the polar tensor $\{g_{ijk}\}$ which we used in the description of optical activity. The tensor $\{z_{ijk}\}$ makes no distinction between rotation axes and rotation–inversion axes. It exists in all point symmetry groups. The experimentally found difference to optical activity also comes to light. If we substitute $\boldsymbol{k}$ by $-\boldsymbol{k}$, hence reverse the direction of propagation, the vector $\boldsymbol{G}$ changes its sign in optical activity, while the vector $\boldsymbol{Z}$ remains unchanged. In optical activity, if we look in the propagation direction, the direction of $\boldsymbol{G}$ reverses when the viewing direction is reversed, so that the sense of rotation of the $\boldsymbol{D}$-vector of an elliptically polarized wave

is conserved, in contrast to the Faraday effect. We can describe the modification of light propagation by the Faraday effect directly by adopting the corresponding relationships for optical activity (see Section 4.3.6.7). In particular it is true that linear polarized waves in a crystal without magnetic field become elliptically polarized waves, as soon as a magnetic field acts. We expect pure circular polarized waves, if the magnetic field lies in the direction of the optic axis in optically uniaxial crystals.

An application of the Faraday effect is realized in the Faraday modulator, a cylindrical specimen made from an isotropic material inserted in a current-carrying cylindrical magnetic coil. If an alternating current flowing through the coil generates a magnetic field of the same frequency, then the direction of vibration of a linear polarized wave propagating along the coil axis in the material oscillates at the same cycle about the position without magnetic field. The Faraday cell is thus a useful aid in optical precision measurements with modulation techniques (see Section 4.4.2).

In conducting materials the magnetic field gives rise to far higher additional effects due to the direct interaction with the charge carriers, which we can only refer to here (Voigt effect, magnetoband absorption).

In ferromagnetic and other magnetically ordered materials, the associated magnetic point symmetry groups are to be applied to derive the independent components of the tensor $\{z_{ijk}\}$.

Meanwhile the Faraday effect has been investigated on numerous crystals. A measurement arrangement has proven successful, where the specimen (a thin crystal plate) placed in a magnetic field, is continuously rotated about an axis perpendicular to the magnetic field and the change in the light emerging from the plate is continuously analyzed (Kaminsky, Haussühl, 1993). An important result of the investigations on ionic crystals is the quasiadditivity of the specific Faraday rotation (Verdet's constant) of the lattice particles (Haussühl, Effgen, 1988).

### 4.4.6
### Hall Effect

As an example for a more complex relationship we discuss here one of the many interesting magnetic effects. The *Hall effect* is observed in electric conductors including semiconductors. Let a plate, through which an electric current density $\boldsymbol{I}$ is flowing, be simultaneously immersed in a magnetic field $\boldsymbol{H}$ with a component transverse to the current. The charge carriers experience a force deflecting them perpendicular to $\boldsymbol{I}$ and $\boldsymbol{H}$ (Lorentz force). Thus in the surface elements perpendicular to $\boldsymbol{I}$ and $\boldsymbol{H}$ an electric polarization develops and builds up an electric field. Figure 4.41 shows a schematic arrangement for the measurement of the effect. To a first approximation the field strength is

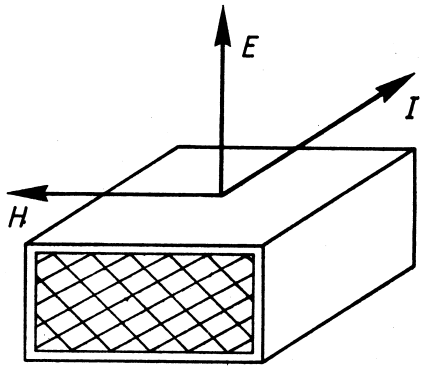


**Figure 4.41** Scheme for the measurement of the Hall effect on a rectangular parallelepipedron. The surfaces perpendicular to the current density vector $\boldsymbol{I}$ and the electric field $\boldsymbol{E}$, respectively, are metallized. Between these surfaces a sufficiently wide isolating gap has to be installed.

proportional to current density and magnetic field strength

$$E_i = k_{ijk} I_j H_k.$$

Thus we are dealing with a third-rank axial tensor, which as we have seen, can exist in all PSGs. Since $\boldsymbol{I}$ as well as $\boldsymbol{H}$ change their sign with time reversal, the Hall tensor $\{k_{ijk}\}$ just as $\boldsymbol{E}$ is not affected by time reversal. In crystals with magnetic order the respective magnetic symmetry group must be considered for symmetry reduction. Furthermore, it should be noted that the Onsager relation for transport processes with time reversal is valid, which here takes of the form $k_{ijk} = -k_{jik}$. Hence, the transformation properties are completely analogous to those of the Faraday effect $\{z_{ijk}\}$ (see Section 4.4.5). For example, cubic crystals possess only one component, namely $k_{123}$

$$k_{123} = k_{231} = k_{312} = -k_{213} = -k_{321} = -k_{132}.$$

In crystals with 22 as a subgroup only three independent components appear, namely, $k_{123}$, $k_{231}$ and $k_{312}$.

Introducing a vector $\boldsymbol{R}$ with the components $R_l = r_{lk} H_k$ and the condition $r_{lk} = k_{ijk}$ ($l \neq i, j$ and $i, j, l$ cyclic in 1, 2, 3), the Hall effect can also be described by a vector product $E_i = (\boldsymbol{I} \times \boldsymbol{R})_i$, where $\boldsymbol{R}$ is an axial vector and $\{r_{lk}\}$ a polar tensor.

The measurement of the Hall effect is most simple, even in the case of triclinic crystals. Maximally nine independent components $k_{ijk}$ exist. If we select the principal axes system of the tensor of electrical conductivity as the reference system, we can preset the direction of the electric current vector $\boldsymbol{I} \parallel \boldsymbol{e}'_2$ on a thin plate cut according to the Cartesian axes of this system. Similarly,

we can set the external magnetic field parallel to the plate normal $\boldsymbol{e}'_3$. We then directly measure the coefficients $k'_{123}$ perpendicular to $\boldsymbol{I}$ and $\boldsymbol{H}$ according to

$$E'_1 = k'_{123} I'_2 H'_3.$$

All coefficients can be determined by interchanging the directions of $\boldsymbol{I}$, $\boldsymbol{H}$, and $\boldsymbol{E}$. Hence, we require three such plates.

The Hall effect allows important statements concerning charge carriers in conductors. From its sign one can directly deduce the sign of the charge (positive Hall coefficient means positive charge carriers). Moreover, the absolute magnitude of the Hall coefficient provides a measure for the mobility of the charge carriers.

We mention here a qualitative interpretation of the Hall effect for an isotropic medium sufficient for many applications. The field strength $\boldsymbol{E}$ generated by the Hall effect perpendicular to $\boldsymbol{I}$ and $\boldsymbol{H}$ must compensate the Lorentz force $\boldsymbol{K}$ acting on the charge carriers, which move with the mean velocity $\boldsymbol{v}$ in the direction $\boldsymbol{I}$. Hence, $\boldsymbol{K} = e\boldsymbol{v} \times \boldsymbol{H} = e\boldsymbol{E}$ and consequently $\boldsymbol{E} = \boldsymbol{v} \times \boldsymbol{H}$, where $e$ is the charge of a carrier. The total current is then $\boldsymbol{I}_{\text{tot}} = Qenv$. $Q = db$ is the cross-section, $d$ is the thickness of the plate parallel to the field and $b$ is the width of the plate = separation of the electrodes, where the electric voltage $U = b|\boldsymbol{E}|\text{sign}\boldsymbol{E}$ is measured. $n$ means the number of charge carriers per volume element. Hence,

$$\boldsymbol{E} = \frac{\boldsymbol{I}_{\text{tot}} \times \boldsymbol{H}}{Qen} \quad \text{or with} \quad \boldsymbol{I} = \boldsymbol{I}_{\text{tot}}/Q$$
$$\boldsymbol{E} = \frac{\boldsymbol{I} \times \boldsymbol{H}}{en}.$$

Thus the Hall coefficient corresponds to the quantity $1/en$.

A specimen exhibiting a large Hall effect, the so-called Hall generator (e.g., made from InAs or InSb) can be used to directly measure the magnetic field strength.

## 4.5 Fourth-Rank Tensors

The symmetry reduction for the general fourth-rank tensor with its $3^4 = 81$ components would take up too much space here. Thus we limit ourselves to the two important types, namely those tensors with permutability of the first and second as well as the third and fourth position (type A) and those tensors with the additional permutability of both first positions with both last

positions (type B). We are thus dealing with the conditions

$$\text{Type A}: \; t_{ijkl} = t_{jikl} = t_{ijlk} = t_{jilk},$$
$$\text{Type B}: \; t_{ijkl} = t_{klij} \quad \text{(in addition to the conditions of type A)}.$$

The most important representatives for type A are: the piezooptical tensor, the second-order electrooptical effect (Kerr effect), electrostriction and second-order magnetostriction. The following relationships are valid:

$$\begin{aligned} \Delta a_{ij} &= q_{ijkl}\sigma_{kl}, & \Delta a_{ij} &= r_{ijkl}E_kE_l, \\ \varepsilon_{ij} &= \hat{d}_{ijkl}E_kE_l, & \varepsilon_{ij} &= f_{ijkl}H_kH_l. \end{aligned}$$

The permutability is a consequence of the interconnection of two second-rank symmetric tensors ($\Delta a_{ij}$, $\sigma_{ij}$, $E_iE_j$, $H_iH_j$). The most significant representative of type B is the elasticity tensor, which links the deformation tensor and the mechanical stress tensor according to $\sigma_{ij} = c_{ijkl}\varepsilon_{kl}$ or $\varepsilon_{ij} = s_{ijkl}\sigma_{kl}$. Here, the pairwise permutability is based on the reversibility of mechanical deformation work, which we will consider in detail.

In any case a careful check is required to determine the influence of symmetry and physical aspects. Since a symmetric second-rank tensor possesses at most six independent components, the maximum number of independent components in type A reduces to $6 \times 6 = 36$ and in type B to $(6 \cdot 5)/2 + 6 = 21$. Because the intrinsic symmetry of all the even-rank tensors possesses an inversion center, the number of distinguishable tensors based on crystallographic symmetry are at most equal to the number of the Laue groups, hence 11 ($\bar{1}$, 2/m, 2/mm, $\bar{3}$, $\bar{3}2$, 4/m, 4/mm, 6/m, 6/mm, m3, 4/m3). Only these 11 cases are to be investigated for polar tensors.

If a twofold axis parallel to $\boldsymbol{e}_2$ exists, then

$$t_{ijkl} = (-1)^q t_{ijkl},$$

where $q$ is equal to the number of indices 2, i.e., the index 2 only is allowed to occur an even number of times. It is appropriate to arrange the fourth-rank tensors of type A and B in the form of $6 \times 6$-matrices according to the following scheme (for monoclinic crystals $2 \parallel \boldsymbol{e}_2$):

| | 11 | 22 | 33 | 23 | 31 | 12 |
|---|---|---|---|---|---|---|
| 11 | 1111 | 1122 | 1133 | – | 1131 | – |
| 22 | 2211 | 2222 | 2233 | – | 2231 | – |
| 33 | 3311 | 3322 | 3333 | – | 3331 | – |
| 23 | – | – | – | 2323 | – | 2312 |
| 31 | 3111 | 3122 | 3133 | – | 3131 | – |
| 12 | – | – | – | 1223 | – | 1212 |

Hence, in type A there exists 20 independent components and 13 independent components in type B.

In the PSG 22 each index is allowed to appear only an even number of times. Thus for orthorhombic crystals only the following scheme persists with 12 independent components for type A and 9 for type B:

$$\begin{pmatrix} 1111 & 1122 & 1133 & & & \\ 2211 & 2222 & 2233 & & 0 & \\ 3311 & 3322 & 3333 & & & \\ & & & 2323 & & \\ & 0 & & & 3131 & \\ & & & & & 1212 \end{pmatrix}.$$

As with second- and third-rank tensors, the operation of the threefold axis requires the most effort also here. Again we have

$$3 \parallel \boldsymbol{e}_3, \quad \text{hence} \quad \boldsymbol{R}_{\pm 3 \parallel \boldsymbol{e}_3} = \begin{pmatrix} -\frac{1}{2} & \pm\frac{\sqrt{3}}{2} & 0 \\ \mp\frac{\sqrt{3}}{2} & -\frac{1}{2} & 0 \\ 0 & 0 & 1 \end{pmatrix}.$$

In order to arrange the symmetry reduction clearly one must proceed systematically. In a symmetry operation the respective tensor components transform in certain subsets among themselves. We will again return to this aspect latter. For the moment, let us consider the special case of index 3 which is directly assigned to the direction of the axis of rotation. There exist five subsets of tensor components, arranged according to the number of index 3

- missing (9 components of type $t_{1111}$, $t_{1112}$, $t_{1122}$ etc.),
- once (12 components of type $t_{1113}$, $t_{1123}$, $t_{1223}$ etc.),
- twice (10 components of type $t_{1133}$, $t_{1313}$, $t_{1323}$ etc.),
- three times (4 components $t_{1333}$, $t_{2333}$, $t_{3313}$, $t_{3323}$),
- four times (1 component $t_{3333}$).

We begin with the first subset and find for type A:

$$t'_{1111} = t_{1111} = \frac{1}{16}(t_{1111} + 9t_{2222} + 3t_{1122} + 3t_{2211} + 12t_{1212}) \mp \frac{\sqrt{3}}{8}(t_{1112} + t_{1211} + 3t_{2212} + 3t_{1222}), \tag{4.9}$$

$$t'_{2222} = t_{2222} = \frac{1}{16}(9t_{1111} + t_{2222} + 3t_{1122} + 3t_{2211} + 12t_{1212}) \pm \frac{\sqrt{3}}{8}(3t_{1112} + 3t_{1211} + t_{2212} + t_{1222}), \tag{4.10}$$

$$t'_{1122} = t_{1122} = \frac{1}{16}(3t_{1111} + 3t_{2222} + t_{1122} + 9t_{2211} - 12t_{1212}) \pm \frac{\sqrt{3}}{8}(t_{1112} - 3t_{1211} + 3t_{2212} - t_{1222}), \tag{4.11}$$

$$t'_{2211} = t_{2211} = \frac{1}{16}(3t_{1111} + 3t_{2222} + 9t_{1122} + t_{2211} - 12t_{1212}) \pm \frac{\sqrt{3}}{8}(-3t_{1112} + t_{1211} - t_{2212} + 3t_{1222}). \tag{4.12}$$

Correspondingly, there exist further equations for $t'_{1112}$, $t'_{1211}$, $t'_{2212}$, $t'_{1222}$ and $t'_{1212}$, which, however, do not result in new conditions. From these four double equations we obtain eight conditions. The terms with alternating signs must vanish. Hence, from (4.9) or (4.10) we have

$$t_{1112} + t_{1211} + 3t_{2212} + 3t_{1222} = 0$$

and

$$3t_{1112} + 3t_{1211} + t_{2212} + t_{1222} = 0$$

and thus

$$t_{1211} = -t_{1112} \quad \text{and} \quad t_{2212} = -t_{1222}.$$

Similarly (4.11) and (4.12) yield

$$t_{1112} - 3t_{1211} + 3t_{2212} - t_{1222} = 0 \quad \text{and}$$
$$-3t_{1112} + t_{1211} - t_{2212} + 3t_{1222} = 0,$$

hence together with the above result

$$t_{1112} = -t_{2212} = -t_{1211} = t_{1222}.$$

From (4.9) or (4.10) we find

$$5t_{1111} = 3t_{2222} + t_{1122} + t_{2211} + 4t_{1212} \quad \text{and}$$
$$5t_{2222} = 3t_{1111} + t_{1122} - t_{2211} + 4t_{1212}.$$

From the difference and the sum of these conditions we get $t_{1111} = t_{2222}$ or $t_{1212} = (t_{1111} - t_{1122}/2 - t_{2211}/2)/2$. From (4.11) and (4.9) we get $t_{1122} = t_{2211}$ as well as the important relation $t_{1212} = (t_{1111} - t_{1122})/2$.

The remaining conditions give us nothing new. In total, the subset with missing index 3 furnishes the following three independent components $t_{1111}$, $t_{1122}$ and $t_{1112}$.

In the subset with one index 3, symmetry transformation gives the following result:

$$t'_{1113} = t_{1113} = -\frac{1}{8}(t_{1113} + 6t_{1223} + 3t_{2213}) \pm \frac{\sqrt{3}}{8}(3t_{2223} + 2t_{1213} + t_{1123}), \tag{4.13}$$

$$t'_{2223} = t_{2223} = -\frac{1}{8}(t_{2223} + 6t_{1213} + 3t_{1123}) \mp \frac{\sqrt{3}}{8}(3t_{1113} + 2t_{1223} + t_{2213}), \tag{4.14}$$

$$t'_{1123} = t_{1123} = \frac{1}{8}(-3t_{2223} + 6t_{1213} - t_{1123}) \pm \frac{\sqrt{3}}{8}(-t_{1113} + 2t_{1223} - t_{2213}), \tag{4.15}$$

$$t'_{1213} = t_{1213} = \frac{1}{8}(-3t_{2223} + 2t_{1213} + 3t_{1123}) \pm \frac{\sqrt{3}}{8}(-t_{1113} - 2t_{1223} + t_{2213}). \tag{4.16}$$

The conditions for the components with interchanged first and second index pairs have the same coefficients. Further conditions, for example, for $t'_{2123}$ bring nothing new.

From (4.13) we have:

$$3t_{2223} + 2t_{1213} + t_{1123} = 0 \quad \text{and} \tag{4.17}$$

$$3t_{1113} + 2t_{1223} + t_{2213} = 0; \tag{4.18}$$

from (4.15)

$$-3t_{2213} + 2t_{1223} - t_{1113} = 0 \quad \text{and} \tag{4.19}$$

$$3t_{1123} + t_{2223} - 2t_{1213} = 0; \tag{4.20}$$

from (4.16)

$$-t_{1113} - 2t_{1223} + t_{2213} = 0 \quad \text{and} \tag{4.21}$$

$$2t_{1213} + t_{2223} - t_{1123} = 0. \tag{4.22}$$

From (4.17) and (4.20) respectively from (4.18) and (4.19) one obtains $t_{2223} = -t_{1123}$ and $t_{1123} = t_{1213}$, respectively, $t_{1113} = -t_{2213}$ and $t_{1113} = -t_{1223}$.

The pairwise interchange of the indices (1. pair against 2. pair) yields analogous equations with the same coefficients. Hence, in this subset we have the following four independent components with one index 3:

$$t_{1113} = -t_{2213} = -t_{1223}, \quad t_{2223} = -t_{1123} = -t_{1213},$$
$$t_{1311} = -t_{1322} = -t_{2312}, \quad t_{2322} = -t_{2311} = -t_{1312}.$$

For the subset with twice index 3 we have

$$t'_{1133} = t_{1133} = \frac{1}{4}(t_{1133} + 3t_{2233} \pm \sqrt{3}2t_{1233}),$$
$$t'_{1313} = t_{1313} = \frac{1}{4}(t_{1313} + 3t_{2323} \pm \sqrt{3}t_{2313} \pm \sqrt{3}t_{1323}).$$

This gives

$$t_{1133} = t_{2233}, \quad t_{1313} = t_{2323}, \quad t_{1233} = 0 \quad \text{and} \quad t_{2313} = -t_{1323}.$$

Furthermore, after interchanging the index pairs we get $t_{3311} = t_{3322}$ and $t_{3312} = 0$. In total there also exist four independent components.

The components with index 3 three times all vanish because $t'_{1333} = -\frac{1}{2}t_{1333} \pm \frac{\sqrt{3}}{2}t_{2333}$ and so on. Finally, only $t'_{3333} = t_{3333}$ remains. Accordingly, a PSG with threefold rotation axis or rotation–inversion axis (PSG 3 and $\bar{3}$) possesses the following type A tensor with a total of 12 independent components:

| | 11 | 22 | 33 | 23 | 31 | 12 |
|---|---|---|---|---|---|---|
| 11 | 1111 | 1122 | 1133 | 1123 | 1131 | 1112 |
| 22 | 1122 | 1111 | 1133 | −1123 | −1131 | −1112 |
| 33 | 3311 | 3311 | 3333 | – | – | – |
| 23 | 2311 | −2311 | – | 3131 | 2313 | −1311 |
| 31 | 3111 | −3111 | – | −2313 | 3131 | 2311 |
| 12 | −1112 | 1112 | – | −1131 | 1123 | 1212*) |

*) $t_{1212} = \frac{1}{2}(t_{1111} - t_{1122})$

In the Laue class $\bar{3}$m we place the twofold axis parallel $\boldsymbol{e}_1$ and note the condition "index 1 even number of times." Starting from the above table, we obtain in the PSG 32, 3m and $\bar{3}$m the following eight independent components for type A: $t_{1111}$, $t_{1122}$, $t_{1133}$, $t_{1123}$, $t_{3311}$, $t_{3333}$, $t_{2311}$ and $t_{1313}$. Which components appear at all is read directly from the above scheme.

For the symmetry reduction resulting from a fourfold axis parallel $\boldsymbol{e}_3$ we only need to consider those components where the index 3 appears an even

number of times because a fourfold axis simultaneously represents a twofold axis (2 is a subgroup of 4!). With

$$\boldsymbol{R}_{\pm 4\parallel e_3} = \begin{pmatrix} 0 & \pm 1 & 0 \\ \mp 1 & 0 & 0 \\ 0 & 0 & 1 \end{pmatrix}$$

we obtain the following conditions:

$$t_{1111} = t_{2222}, \quad t_{1122} = t_{2211}, \quad t_{1212} = t_{2121}, \quad t_{1121} = -t_{2212}, \quad t_{1211} = -t_{2122},$$
$$t_{1133} = t_{2233}, \quad t_{3311} = t_{3322}, \quad t_{1313} = t_{2323}, \quad t_{1323} = -t_{2313}, \quad t_{1233} = -t_{2133} = 0,$$
$$t_{3312} = -t_{3321} = 0, \quad t_{3333} = t_{3333}.$$

Hence a type A tensor has the following form (10 independent components) for the Laue class 4/m (PSG 4, $\bar{4}$ and 4/m):

| | 11 | 22 | 33 | 23 | 31 | 12 |
|---|---|---|---|---|---|---|
| 11 | 1111 | 1122 | 1133 | – | – | 1112 |
| 22 | 1122 | 1111 | 1133 | – | – | −1112 |
| 33 | 3311 | 3311 | 3333 | – | – | – |
| 23 | – | – | – | 3131 | 2331 | – |
| 31 | – | – | – | −2331 | 3131 | – |
| 12 | 1211 | −1211 | – | – | – | 1212 |

In the Laue class 4/mm the twofold axis parallel $\boldsymbol{e}_i$ ($i = 1, 2, 3$) requires that all indices are present an even number of times. Thus from the above scheme $t_{1112}$, $t_{1211}$ and $t_{2331}$ vanish, so that only seven independent components remain.

We calculate the effect of a sixfold rotation axis or rotation–inversion axis by adding to the result of the threefold axis the condition of a twofold axis parallel $\boldsymbol{e}_3$ (index 3 only an even number of times). For the Laue class 6/m (PSG 6, $\bar{6}$ and 6/m) this leads to the following eight independent tensor components: $t_{1111}$, $t_{1122}$, $t_{1133}$, $t_{1112}$, $t_{3311}$, $t_{3333}$, $t_{3131}$, $t_{2313}$. Otherwise, the scheme for the threefold axis is valid. The Laue class 6/mm (PSG 62, 6m, $\bar{6}$m and 6/mm) includes the condition "index 1 an even number of times" because of the twofold axis parallel $\boldsymbol{e}_1$, so that only the following six independent components exist:

$$t_{1111}, t_{1122}, t_{1133}, t_{3311}, t_{3333}, t_{3131}.$$

We achieve the symmetry reduction in both cubic Laue classes in the shortest way by applying the operation of the threefold axis in the direction of the space diagonals of the Cartesian reference system to the result of orthorhombic or tetragonal crystals. We have

$$\boldsymbol{R}_{3\parallel e_1+e_2+e_3} = \begin{pmatrix} 0 & 1 & 0 \\ 0 & 0 & 1 \\ 1 & 0 & 0, \end{pmatrix}$$

i.e. the transformation interchanges the indices cyclically. Hence, in the Laue class m3 (PSG 23 and m3) there exists the following four independent components:

$$t_{1111} = t_{2222} = t_{3333}, \quad t_{1122} = t_{2233} = t_{3311},$$
$$t_{2211} = t_{3322} = t_{1133}, \quad \text{and} \quad t_{1212} = t_{2323} = t_{3131}.$$

In the Laue class 4/m3 (PSG 43, $\bar{4}3$ and 4/m3) $t_{1122}$ equals $t_{2211}$, so that only three independent components exist.

In the case of the cylindrical symmetries $\infty$/m and $\infty$/mm we have the situation of the Laue class 6/m and 6/mm, respectively. The isotropy, derived from the conditions of the Laue class 4/m3 under the inclusion of cylindrical symmetry, demands that

$$t_{1212} = (t_{1111} - t_{1122})/2,$$

so that only two independent components exist.

The corresponding type B tensors can be immediately derived from the complete formulae for type A tensors given above by allowing the permutation of the index pairs (see Table 4.10).

Tensors with other intrinsic symmetries, for example, the permutability of three index positions, as in the case of nonlinear dielectric susceptibility or the permutability of indices of only one pair, as with the electrically induced piezoelectric effect, can be easily reduced by employing an analogous method as above.

### 4.5.1 Elasticity Tensor

Mechanical stresses and deformations are, within the limits of *Hooke's law*, proportional to one another. For sufficiently small stresses and deformations we can describe the relationship of these quantities, when we neglect infinitesimal torques or rotations, by:

$$\varepsilon_{ij} = s_{ijkl}\sigma_{kl} \quad \text{or} \quad \sigma_{ij} = c_{ijkl}\varepsilon_{kl}.$$

In the first case we assume that the mechanical stresses are inducing quantities, which represent the normal situation in elastostatics. We will see later that the reverse is an even more favorable representation in dynamic processes. Furthermore, we assume that the stresses and deformations are of such a nature that no plastic, i.e., permanent deformations appear. We call this limit for the deformations or stresses the critical limit with the corresponding critical deformation or critical stress. We will return to this point in Section 6.1.1. Moreover, we assume that the deformations are small enough to guarantee

**Table 4.10** Fourth-rank tensors of type B (permutability of indices within the first and second pair and pairwise; example elasticity tensor).

$\bar{1}$ ($Z = 21$):

| | | | | | |
|---|---|---|---|---|---|
| 1111 | 1122 | 1133 | 1123 | 1131 | 1112 |
| 1122 | 2222 | 2233 | 2223 | 2231 | 2212 |
| 1133 | 2233 | 3333 | 3323 | 3331 | 3312 |
| 1123 | 2223 | 3323 | 2323 | 2331 | 1223 |
| 1131 | 2231 | 3331 | 2331 | 3131 | 1231 |
| 1112 | 2212 | 3312 | 1223 | 1231 | 1212 |

2/m ($Z = 13$):

| | | | | | |
|---|---|---|---|---|---|
| 1111 | 1122 | 1133 | 0 | 1131 | 0 |
| 1122 | 2222 | 2233 | 0 | 2231 | 0 |
| 1133 | 2233 | 3333 | 0 | 3331 | 0 |
| 0 | 0 | 0 | 2323 | 0 | 1223 |
| 1131 | 2231 | 3331 | 0 | 3131 | 0 |
| 0 | 0 | 0 | 1223 | 0 | 1212 |

2/mm ($Z = 9$):

| | | | | | |
|---|---|---|---|---|---|
| 1111 | 1122 | 1133 | 0 | 0 | 0 |
| 1122 | 2222 | 2233 | 0 | 0 | 0 |
| 1133 | 2233 | 3333 | 0 | 0 | 0 |
| 0 | 0 | 0 | 2323 | 0 | 0 |
| 0 | 0 | 0 | 0 | 3131 | 0 |
| 0 | 0 | 0 | 0 | 0 | 1212 |

$\bar{3}$ ($Z = 7$)

| | | | | | |
|---|---|---|---|---|---|
| 1111 | 1122 | 1133 | 1123 | 1131 | 0 |
| 1122 | 1111 | 1133 | −1123 | −1131 | 0 |
| 1133 | 1133 | 3333 | 0 | 0 | 0 |
| 1123 | −1123 | 0 | 3131 | 0 | −1131 |
| 1131 | −1131 | 0 | 0 | 3131 | 1123 |
| 0 | 0 | 0 | −1131 | 1123 | 1212* |

$\bar{3}$m ($Z = 6$):

| | | | | | |
|---|---|---|---|---|---|
| 1111 | 1122 | 1133 | 1123 | 0 | 0 |
| 1122 | 1111 | 1133 | −1123 | 0 | 0 |
| 1133 | 1133 | 3333 | 0 | 0 | 0 |
| 1123 | −1123 | 0 | 3131 | 0 | 0 |
| 0 | 0 | 0 | 0 | 3131 | 1123 |
| 0 | 0 | 0 | 0 | 1123 | 1212* |

4/m ($Z = 7$):

| | | | | | |
|---|---|---|---|---|---|
| 1111 | 1122 | 1133 | 0 | 0 | 1112 |
| 1122 | 1111 | 1133 | 0 | 0 | −1112 |
| 1133 | 1133 | 3333 | 0 | 0 | 0 |
| 0 | 0 | 0 | 3131 | 0 | 0 |
| 0 | 0 | 0 | 0 | 3131 | 0 |
| 1112 | −1112 | 0 | 0 | 0 | 1212 |

4/mm ($Z = 6$):

| | | | | | |
|---|---|---|---|---|---|
| 1111 | 1122 | 1133 | 0 | 0 | 0 |
| 1122 | 1111 | 1133 | 0 | 0 | 0 |
| 1133 | 1133 | 3333 | 0 | 0 | 0 |
| 0 | 0 | 0 | 3131 | 0 | 0 |
| 0 | 0 | 0 | 0 | 3131 | 0 |
| 0 | 0 | 0 | 0 | 0 | 1212 |

6/m, 6/mm, ∞/m, ∞/mm ($Z = 5$):

| | | | | | |
|---|---|---|---|---|---|
| 1111 | 1122 | 1133 | 0 | 0 | 0 |
| 1122 | 1111 | 1133 | 0 | 0 | 0 |
| 1133 | 1133 | 3333 | 0 | 0 | 0 |
| 0 | 0 | 0 | 3131 | 0 | 0 |
| 0 | 0 | 0 | 0 | 3131 | 0 |
| 0 | 0 | 0 | 0 | 0 | 1212* |

m3, 4/m3 ($Z = 3$):

| | | | | | |
|---|---|---|---|---|---|
| 1111 | 1122 | 1122 | 0 | 0 | 0 |
| 1122 | 1111 | 1122 | 0 | 0 | 0 |
| 1122 | 1122 | 1111 | 0 | 0 | 0 |
| 0 | 0 | 0 | 1212 | 0 | 0 |
| 0 | 0 | 0 | 0 | 1212 | 0 |
| 0 | 0 | 0 | 0 | 0 | 1212 |

∞/m∞ (Isotropy, $Z = 2$):

| | | | | | |
|---|---|---|---|---|---|
| 1111 | 1122 | 1122 | 0 | 0 | 0 |
| 1122 | 1111 | 1122 | 0 | 0 | 0 |
| 1122 | 1122 | 1111 | 0 | 0 | 0 |
| 0 | 0 | 0 | 1212* | 0 | 0 |
| 0 | 0 | 0 | 0 | 1212* | 0 |
| 0 | 0 | 0 | 0 | 0 | 1212* |

* $t_{1212} = \frac{1}{2}(t_{1111} - t_{1122})$

the validity of Hooke's law. We will discuss the nonlinear elastic properties observed far before the limit to plastic deformation is reached in Section 4.6.3. While we can still work, in this section, with the ordinary deformation tensor, we will employ the Lagrangian deformation tensor $\{\eta_{ij}\}$ for the relationship between stress and deformation in the case of nonlinear elastic properties.

An important simplification arises from the permutability of the first with the second index pair. The proof is analogous to that of the symmetry of the dielectric tensor, namely from the reversibility of the deformation work. This

is per unit volume

$$\Delta W = \sigma_{ij}\Delta\varepsilon_{ij}, \quad \frac{\partial W}{\partial \varepsilon_{ij}} = \sigma_{ij}c_{ijkl}\varepsilon_{kl}.$$

Reversibility demands that $\Delta W$ forms a complete differential, hence

$$\frac{\partial^2 W}{\partial\varepsilon_{ij}\partial\varepsilon_{kl}} = \frac{\partial^2 W}{\partial\varepsilon_{kl}\partial\varepsilon_{ij}}$$

and thus $c_{ijkl} = c_{klij}$ is true.

The permutability of the indices within the first and second pair is a consequence of the symmetry of the stress tensor and the deformation tensor. The same is true for the $s$-tensor $s_{ijkl} = s_{klij}$ and so on, as one recognizes from the calculation of $\varepsilon_{ij} = s_{ijkl}\sigma_{kl}$ from $\sigma_{ij} = c_{ijkl}\varepsilon_{kl}$.

Voigt already introduced an abbreviation, which we also use here, with two indices instead of the four, according to the following scheme: $ii \to i$, $ij \to 9 - i - j$ for $i \neq j$ (thus, for example, $c_{1122} \to c_{12}$ or $c_{1232} \to c_{64}$). One must never forget that this abbreviation does not lead to a second-rank tensor. In all operations involving tensor transformations, one must, in any case, return to the four indices representation. We call the quantities $c_{ij}$, following common usage, the elastic constants and $s_{ij}$ the elastic coefficients. Many authors prefer the terms stiffnesses for $c_{ij}$ and compliances for $s_{ij}$.

If the $s$-tensor or the $c$-tensor is known, then one can be calculated from the other by matix inversion. Because

$$\varepsilon_{ij} = s_{ijkl}\sigma_{kl} = s_{ijkl}c_{klmn}\varepsilon_{mn}, \quad \text{i.e.,} \quad s_{ijkl}c_{klmn} = \delta_{im}\delta_{jn}.$$

In Voigt notation, one has

$$s_{qp} = \frac{(-1)^{p+q}A_{pq}}{D},$$

where $A_{pq}$ is the subdeterminant of the matrix $(c_{pq})$ after eliminating the $p$th row and the $q$th column and $D$ is the determinant of $(c_{pq})$. When converting from $s_{pq}$ to $s_{ijkl}$ it is absolutely essential to note the following multiplicity rule resulting from the permutability of the indices:

$$s_{ij} \to s_{iijj}, \quad s_{i,9-k-l} \to 2s_{iikl}, \quad s_{9-i-j,9-k-l} \to 4s_{ijkl}.$$

As an example, we consider the relations for cubic crystals. We have:

$$s_{1111} = s_{11} = \frac{c_{11} + c_{12}}{(c_{11} - c_{12})(c_{11} + 2c_{12})},$$
$$s_{1122} = s_{12} = \frac{-c_{12}}{(c_{11} - c_{12})(c_{11} + 2c_{12})}, \quad 4s_{1212} = s_{66} = 1/c_{66}.$$

With the first attempts to describe anisotropic elasticity in the eighteenth century a discussion began concerning the question, whether the elasticity tensor is totally symmetric or not (rari-constant or multiconstant theory). We can express the deviation from total symmetry by the six relationships $c_{iijk} - c_{ijik} = g_{mn}(-1)^{mn(m-n)/2}$, where $m \neq i, j$ and $n \neq i, k$. We are dealing with a second-rank tensor invariant with the components $g_{mn}$, as one can immediately recognize from the representation $g_{mn} = \frac{1}{2} e_{mik} e_{njl} c_{ijkl}$, where $\{e_{mik}\}$ is the Levi-Civitá tensor (see Section 3.7).

The relations $c_{iijk} - c_{ijik} = 0$ are called *Cauchy relations*. The tensor $\{g_{mn}\}$ is a second-rank tensor invariant of the elasticity tensor. It describes the deviations from the Cauchy relations. The prerequisites for the validity of the Cauchy relations are given as (see Leibfried, 1955):

1. pure central forces exist between the lattice particles,
2. each particle possesses a central symmetry and thus is located in a symmetry center of the lattice,
3. no anharmonicity (pure Hooke's law),
4. no thermal energy content,
5. no initial stress.

There does not exist one single substance for which the Cauchy relations are fulfilled, although some crystals, as for example, NaCl, exhibit only a small deviation. From the experimental data one can recognize that the deviations from the Cauchy relations allow statements concerning bonding properties of the particles. Crystals with predominantly ionic bonds show, to a large extent, positive components $g_{mn}$, those with directional bonding, in particular, with strongly covalent bonds, negative $g_{mn}$ (Haussühl, 1967). Interestingly, an asphericity of the electron distribution of the ions gives rise to positive $g_{mn}$. That is, the deviation from the Cauchy relations may give hints on atomistic bonding details. We will become acquainted with other physically interesting invariants of the elasticity tensor in the following.

The tensor $\{g_{mn}\}$ represents the deviation of the elasticity tensor from its totally symmetric part. Accordingly, Hehl and Itin (2002) were able to show rather elegantly that$\{g_{mn}\}$ constitutes, in a group-theoretical sense, an irreducible piece of the elasticity tensor.

### 4.5.2 Elastostatics

Here we consider the deformations appearing in equilibrium with external forces or the required mechanical stresses in equilibrium with a given deformation. The time-dependent processes until equilibrium is achieved will be

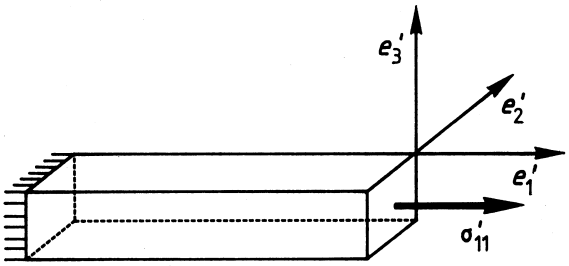


**Figure 4.42** Measurement of Young's modulus on a thin bar by application of uniaxial stress $\sigma'_{11}$.

neglected. We then have

$$\frac{\partial \sigma_{ij}}{\partial t} = 0 \quad \text{and} \quad \frac{\partial \varepsilon_{ij}}{\partial t} = 0 \quad (t \text{ time}).$$

All quantities before and after the deformation are described in the same fixed reference system. Furthermore, we assume the validity of Hooke's law.

Whereas the solution of general problems of elastostatics often requires considerable mathematical efforts, as, for example, the problem of the bending of a curved bar with variable cross-section or the torsion of a thin rod of nonuniform cross-section, we will treat here only problems that are relevant for practical measurments in crystals. A decisive role is played by the boundary conditions to which the specimen is exposed. These must be formulated as simply as possible in order to directly apply the fundamental elastostatic equation $\varepsilon_{ij} = s_{ijkl}\sigma_{kl}$. In particular, arrangements are preferred that lead to a homogoneous deformation of the complete crystal, that is, where

$$\frac{\partial \varepsilon_{ij}}{\partial x_k} = 0.$$

As a very important and experimentally easily accessibile example we first investigate the longitudinal deformation of a bar with fixed cross-section (according to form and size) under uniaxial stress along the bar axis $\boldsymbol{e}'_1$ (Fig. 4.42). We have

$$\varepsilon'_{11} = \left(\frac{\Delta l_1}{l_1}\right)' = s'_{1111}\sigma'_{11}.$$

$(\Delta l_1/l_1)'$ is the relative change in length along $\boldsymbol{e}'_1$. The boundary conditions are $\sigma'_{11} \neq 0$, otherwise $\sigma'_{ij} = 0$. The material property $1/s'_{1111}$ is called *Young's modulus*. For an arbitrary direction $\boldsymbol{e}'_1 = u_{1i}\boldsymbol{e}_i$ one has

$$s'_{1111} = u_{1i}u_{1j}u_{1k}u_{1l}s_{ijkl}.$$

The right-hand side contains the following 15 coefficients:

$$s_{iiii}\ (3), \quad 4s_{iiij}\ (6), \quad 2(s_{iijj} + 2s_{ijij})\ (3) \quad \text{and} \quad 4(s_{iijk} + 2s_{ijik})\ (3) \quad \text{with} \quad i = 1,2,3.$$

Accordingly, from such longitudinal measurements, even when we select many different directions $\boldsymbol{e}'_1$, we obtain only the coefficients of the quadric $F = s_{ijkl}x_ix_jx_kx_l$.

If we also include measurements of the longitudinal deformation occurring perpendicular to the bar axis, the so-called *lateral contraction*

$$\varepsilon'_{22} = \left(\frac{\Delta l_2}{l_2}\right)' = s'_{2211}\sigma'_{11} \quad \text{and} \quad \varepsilon'_{33} = \left(\frac{\Delta l_3}{l_3}\right)' = s'_{3311}\sigma'_{11}$$

we can, in principle, determine all 21 independent tensor component $s_{ijkl}$ of a triclinic crystal.

The measurements are performed as in the case of thermal expansion with optical methods employing inductive or capacitive path sensors as well as with the help of strain gauges. The uniaxial stress is transferred to the crystal, for example, by applying weights, or by springs tightened by a motor-driven feed. An increase in measurement accuracy of the signal is achieved using a lock-in amplifier, when one works with a periodic load. One can also employ X-ray methods to determine the change in the lattice constants under uniaxial stress resulting from the deformation as with measurements of thermal expansion (see Section 4.3.11). The complete determination of the elasticity tensor, using these methods, has only been successful for a few highly symmetric crystals. For isotropic substances (building materials, ceramics, glasses, plastics), where sufficiently large specimens can be prepared, the static method is of major importance, in particular in understanding the elastic behavior beyond Hooke's law up to plastic deformation and fracture.

Since the qualitative measurement, even on small crystals with dimensions of a few mm, delivers at least the order of magnitude of the deformation and in particular its sign, such tests, for example, with the help of strain gauges, can serve to supplement and check other methods.

A variant of the measurement of Young's modulus is the bending test of thin rods with homogeneous cross-section (*beam bending*), where Young's modulus is the effective material constant for the beam axis (longitudinal dilatation or compression with bending on the convex or concave side of the rod, respectively). For practical measurements, this method, used by Voigt and coworkers (1884) in thousands of measurements to determine the elasiticity tensor of NaCl and KCl, is today rarely taken into consideration because of the low accuracy. This also applies to variants such as bending of thin plates, as employed, for example, by Coromilas for the measurement of some elastic coefficients of gypsum and mica (1877).

The ratio of longitudinal transverse contraction and dilatation, in our example $\varepsilon'_{22}/\varepsilon'_{11}$, for arbitrary beam directions $\boldsymbol{e}'_1$ and directions $\boldsymbol{e}'_2$ perpendicular to these, is called *Poisson's ratio*. It plays, among other things, an important role in the evaluation of the stiffness of composite materials.

### 4.5.3 Linear Compressibility Under Hydrostatic Pressure

If we expose an arbitrarily shaped specimen to a hydrostatic pressure $p$ ($\sigma_{ij} = -p\delta_{ij}$), we observe a change in the dimensions, described by the longitudinal effect

$$\varepsilon'_{11} = \sum_k s'_{11kk}\sigma_{kk}$$

($\sigma'_{kk} = \sigma_{kk}$). With $\boldsymbol{e}'_1 = u_{1i}\boldsymbol{e}_i$ we have

$$\varepsilon'_{11} = \sum_k u_{1i}u_{1j}s_{ijkk}(-p) = -pu_{1i}u_{1j}S_{ij}.$$

The quantities $S_{ij} = s_{ijkl}\delta_{kl}$ form a second-rank tensor invariant (contraction of the $s$-tensor). This experimentally easily accessible tensor property, provides, for many applications, sufficient information concerning the elastic behavior of materials. The measurement is performed conveniently by attaching strain gauges to the side faces of a parallelepipedic specimen. However, one must make a correction for the pressure dependence of the electrical resistance of the strain gauges.

From the sum $\sum \varepsilon'_{ii}$ of the principal deformations we obtain the *volume compressibility*

$$K = -\frac{d\log V}{dp} \approx \sum_i \varepsilon'_{ii}/p = -\frac{\Delta V}{Vp},$$

where $p$ is sufficiently small and $V$ is an arbitrary volume of the specimen. A precise measurement of the volume compressibility is even possible with small crystal grains suspended in a nonsolving liquid in a pressure cell to measure the change in volume $\Delta V$ after pressure loading. The measured total compressibility of the suspension arises from the fractional volumina $V_i/V$ and the compressibilities $K_i$ of the $i$th components of the suspension

$$K = \sum_i K_i V_i/V,$$

as one can easily verify. In the case of two components, when the compressibility of one of them is known as well as the fractional volumina, one can determine the compressibility of the other component. At higher hydrostatic

pressures the X-ray determination of the lattice constants has been proven to be very successful for the determination of the compressibility. (see Section 4.3.11).

For $K$ we obtain from above

$$K = \sum_{i,k} s_{iikk}.$$

For cubic crystals one has

$$K = 3(s_{11} + 2s_{12}) = \frac{3}{c_{11} + 2c_{12}};$$

and for trigonal, tetragonal, and hexagonal crystals

$$K = (s_{11} + s_{22} + s_{33} + 2s_{12} + 2s_{23} + 2s_{31}) = \frac{c_{11} + c_{12} + 2c_{33} - 4c_{31}}{c_{33}(c_{11} + c_{12}) - 2c_{31}^2}$$

(matrix inversion of the $c$-tensor, see above).

$K$ is a scalar invariant of the elasticity tensor, thus independent of the reference system. For crude considerations concerning stiffness behavior, the reciprocal compressibility is often a very useful measure. Moreover, just this elastic quantity is easily accessible to calculation from simple lattice models.

The tensor of the linear compressibility $\{S_{ij}\}$ is also involved in experiments, where crystals are exposed to a general stress described by the stress tensor $\{\sigma_{ij}\}$. According to Hooke's law we expect deformations $\varepsilon_{kl} = s_{klij}\sigma_{ij}$, which lead to a variation of the metric of the crystal (Lattice constants $a_i$ and angles $\alpha_i$). From these variations, which are accessible by high-resolution X-ray or neutron diffraction techniques, the resulting relative change of the unit cell volume $\varepsilon = \Delta V/V = \varepsilon_{11} + \varepsilon_{22} + \varepsilon_{33}$ can be derived. From Hooke's law we obtain $\varepsilon = \varepsilon_{11} + \varepsilon_{22} + \varepsilon_{33} = \sum s_{kkij}\sigma_{ij} = S_{ij}\sigma_{ij}$ (summation over $k, i, j = 1, 2, 3$). We recognize that the tensor connecting the components $\varepsilon_{ij}$ of the deformation tensor with the hydrostatic pressure $p$ ($\sigma_{ij} = -p$ for $i = j$ and 0 otherwise) and the tensor connecting the relative variation of the volume $\varepsilon = \Delta V/V$ with the components $\sigma_{ij}$ of the stress tensor are identical. This is due to the interchangeability of the first and second pair of indices ($s_{ijkl} = s_{klij}$). In the field of X-ray studies $S_{ij}$ are called X-ray elasticity factors and bear the symbol $F_{ij}$.

### 4.5.4
### Torsion Modulus

If one succeeds in producing thin crystal rods, fibers or films, then one can apply the known methods to measure the *torsion modulus* of metal fibers also to crystals. The requirement is a constant cross-section of the fiber or rod and a certain minimum length of a few mm. The specimen can be statically twisted

and the restoring force measured with a torsion balance. Low-frequency dynamic measurements, where the specimen is furnished with a large external mass to reduce the frequency of oscillation, can enable a substantial increase in measuring accuracy. Since in the meantime one can manufacture thin hairlike crystals (so-called "whiskers") from many materials, this method is of certain significance, when larger crystals are not available. The same applies to the torsion of strips or thin plates.

Concerning the mathematical treatment of problems with complex boundary conditions, we refer to numerous literature on this subject (for example, Love, 1926, 1944; Voigt, 1928).

### 4.5.5 Elastodynamic

With the development of ultrasound techniques the dynamic methods, in particular, for precision measurements on crystals, have largely superseded the static methods. The dynamic processes are characterized by the fact that at least for one component $\sigma_{ij}$ the following is true:

$$\frac{\partial \sigma_{ij}}{\partial x_k} \neq 0 \quad \text{and} \quad \frac{\partial \sigma_{ij}}{\partial t} \neq 0;$$

hence for at least one $\varepsilon_{ij}$

$$\frac{\partial \varepsilon_{ij}}{\partial x_k} \neq 0 \quad \text{and} \quad \frac{\partial \varepsilon_{ij}}{\partial t} \neq 0$$

is fulfilled.

To begin with, let us study the forces acting on a volume of a parallelepipedic specimen of dimensions $\Delta x_i$ in the directions $\boldsymbol{e}_i$ ($i = 1, 2, 3$) (Fig. 4.43).

$$\{\sigma_{ii}(\boldsymbol{x}) - \sigma_{ii}(\boldsymbol{x}_0)\}\Delta x_j \Delta x_k + \{\sigma_{ij}(\boldsymbol{x}) - \sigma_{ij}(\boldsymbol{x}_0)\}\Delta x_i \Delta x_k + \{\sigma_{ik}(\boldsymbol{x}) - \sigma_{ik}(\boldsymbol{x}_0)\}\Delta x_i \Delta x_j \quad \text{with} \quad i \neq j \neq k \neq i.$$

Here $\boldsymbol{x} - \boldsymbol{x}_0 = \Delta x_i \boldsymbol{e}_i$. These forces are equal to the product of the mass of the specimen volume

$$\Delta m = \rho \Delta x_1 \Delta x_2 \Delta x_3$$

and the $i$th component of the acceleration $\partial^2 \xi_i / \partial t^2$, where $\boldsymbol{\xi}$ is the displacement vector and $\rho$ is the density. If one expands

$$\sigma_{ij}(\boldsymbol{x}) = \sigma_{ij}(\boldsymbol{x}_0) + \frac{\partial \sigma_{ij}}{\partial x_q} \Delta x_q + \cdots \qquad \text{(here one must sum over } q\text{)}$$

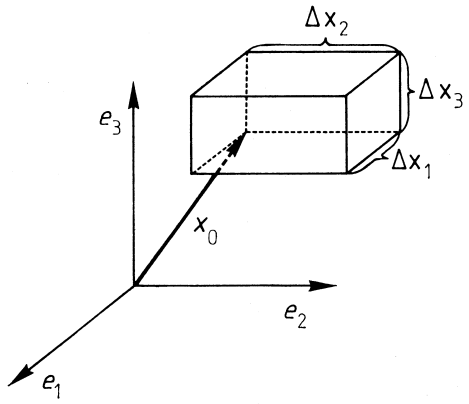


**Figure 4.43** Parallelepipedic specimen.

and contends oneself with the first differential quotient, one gets

$$\frac{\partial \sigma_{ii}}{\partial x_q}\Delta x_j \Delta x_k \Delta x_q + \frac{\partial \sigma_{ij}}{\partial x_q}\Delta x_i \Delta x_k \Delta x_q + \frac{\partial \sigma_{ik}}{\partial x_q}\Delta x_i \Delta x_j \Delta x_q = \rho \Delta x_1 \Delta x_2 \Delta x_3 \frac{\partial^2 \xi_i}{\partial t^2}.$$

After dividing by $\Delta x_1 \Delta x_2 \Delta x_3$, one has for $i = 1, 2, 3$

$$\frac{\partial \sigma_{ii}}{\partial x_q}\frac{\Delta x_q}{\Delta x_i} + \frac{\partial \sigma_{ij}}{\partial x_q}\frac{\Delta x_q}{\Delta x_j} + \frac{\partial \sigma_{ik}}{\partial x_q}\frac{\Delta x_q}{\Delta x_k} = \rho \frac{\partial^2 \xi_i}{\partial t^2}.$$

Since $\Delta x_i$ shall be freely selectable, independent of one another, we must demand that $\partial \sigma_{ij}/\partial x_q = 0$ for $q \neq j$.

This results in the elastodynamic basic equations

$$\frac{\partial \sigma_{ij}}{\partial x_j} = \rho \frac{\partial^2 \xi_i}{\partial t^2} \quad \text{(summing over } j = 1, 2, 3 \text{ at fixed } i\text{, respectively)},$$

which we can also write as $\mathrm{Div}\, \sigma_{ij} = \rho \partial^2 \xi_i / \partial t^2 \boldsymbol{e}_i$. The operation Div is the so-called vector divergence which, by differentiation and summation, generates the vector $\frac{\partial \sigma_{ij}}{\partial x_j}\boldsymbol{e}_i$ from the tensor $\{\sigma_{ij}\}$.

If we now introduce the linear relationship of Hooke's law $\sigma_{ij} = c_{ijkl}\varepsilon_{kl}$ with

$$\varepsilon_{kl} = \frac{1}{2}\left(\frac{\partial \xi_k}{\partial x_l} + \frac{\partial \xi_l}{\partial x_k}\right), \quad \text{we obtain}$$

$$\frac{\partial \sigma_{ij}}{\partial x_j} = \frac{1}{2} c_{ijkl}\left(\frac{\partial^2 \xi_k}{\partial x_l \partial x_j} + \frac{\partial^2 \xi_l}{\partial x_k \partial x_j}\right).$$

Because $c_{ijkl} = c_{ijlk}$, the following elastodynamic basic equations result for deformations within the limits of Hooke's law:

$$\frac{\partial \sigma_{ij}}{\partial x_j} = c_{ijkl}\frac{\partial^2 \xi_k}{\partial x_j \partial x_l} = \rho \frac{\partial^2 \xi_i}{\partial t^2}.$$

Now we will consider the propagation of plane waves, where especially simple laws exist just as in optics. Hence we write $\boldsymbol{\xi} = \boldsymbol{\xi}_0 e^{2\pi i(\boldsymbol{k}\cdot\boldsymbol{x}-\nu t)}$. $\boldsymbol{k}$ is the propagation vector with magnitude $|\boldsymbol{k}| = 1/\lambda$ as before; $\lambda$ is the wavelength of the plane wave and $\nu$ the frequency. With $\boldsymbol{k}\cdot\boldsymbol{x} = k_i x_i$ and

$$\frac{\partial^2 \xi_i}{\partial t^2} = -4\pi^2\nu^2\xi_i \quad \text{and} \quad \frac{\partial^2 \xi_k}{\partial x_j \partial x_l} = -4\pi^2 k_j k_l \xi_k$$

we obtain $\rho\nu^2\xi_i - c_{ijkl}k_j k_l \xi_k = 0$.

Setting $\boldsymbol{k} = |\boldsymbol{k}|\boldsymbol{g}$ with $\boldsymbol{g} = g_i \boldsymbol{e}_i$ and noting that $\nu/|\boldsymbol{k}| = \nu\lambda = v$ signifies the propagation velocity, the elastodynamic basic equations for plane waves, assuming the validity of Hooke's law, take the form

$$(-\rho v^2 \delta_{ik} + c_{ijkl} g_j g_l)\xi_k = A_{ik}\xi_k = 0$$

for $i = 1, 2, 3$ ($\delta_{ik} = 1$ for $i = k$, otherwise 0). Here $\xi_k$ denote the components of the displacement vector, whose position with respect to the propagation vector is to be calculated from the system of equations, when the components $c_{ijkl}$ are known and the propagation direction $\boldsymbol{g}$ is given. The system only yields a solutions for $\boldsymbol{\xi} \neq 0$ when its determinant vanishes, hence

$$|A_{ik}| = |-\rho v^2 \delta_{ik} + c_{ijkl} g_j g_l| = 0.$$

Since we will use these determinants, the so-called *Christoffel determinants*, repeatedly, let us write them out

$$\begin{vmatrix} -\rho v^2 + c_{1j1l}g_j g_l & c_{1j2l}g_j g_l & c_{1j3l}g_j g_l \\ c_{2j1l}g_j g_l & -\rho v^2 + c_{2j2l}g_j g_l & c_{2j3l}g_j g_l \\ c_{3j1l}g_j g_l & c_{3j2l}g_j g_l & -\rho v^2 + c_{3j3l}g_j g_l \end{vmatrix} = 0.$$

Thus we obtain a third-order equation in $v^2$ for each given propagation direction $\boldsymbol{g}$, i.e., in general, three different values for $v^2$. The propagation velocity of the associated wave is the same in a direction and in its opposite direction. We now show that the velocities $v'$, $v''$, and $v'''$ belonging to the displacement vectors $\boldsymbol{\xi}'$, $\boldsymbol{\xi}''$, and $\boldsymbol{\xi}'''$ are mutually perpendicular, i.e., $\boldsymbol{\xi}' \cdot \boldsymbol{\xi}'' = 0$, where $\boldsymbol{\xi}'$ and $\boldsymbol{\xi}''$ are two of the three displacement vectors.

The following basic equations are valid for both velocities $v'$ and $v''$,

$$\begin{aligned} -\rho v'^2 \xi_i' + c_{ijkl} g_j g_l \xi_k' &= 0 \\ -\rho v''^2 \xi_i'' + c_{ijkl} g_j g_l \xi_k'' &= 0. \end{aligned}$$

Multiplying the first equation by $\xi_i''$, the second by $\xi_i'$, forming the difference and summing over $i$ gives us

$$-\rho(v'^2 - v''^2)\xi_i'\xi_i'' + c_{ijkl} g_j g_l (\xi_k'\xi_i'' - \xi_i'\xi_k'') = 0.$$

The second term vanishes because $c_{ijkl} = c_{klij}$. Therefore,

$$(v'^2 - v''^2)\xi'_i\xi''_i = 0, \quad \text{hence} \quad \boldsymbol{\xi}' \cdot \boldsymbol{\xi}'' = 0, \quad \text{in the case} \quad v' \neq v''.$$

Accordingly, the three displacement vectors are mutually perpendicular, as stated, and form a Cartesian reference system, which also in the case of triclinic crystals is produced by nature for each arbitrary propagation direction. The special case $v' = v''$ (degeneracy) appears in crystals only in distinct singular directions. Here, we can only ascertain that the displacement vectors for $v'$ and $v''$ are perpendicular to the displacement vector $\boldsymbol{\xi}'''$ belonging to $v'''$. The case $v' = v'' = v'''$ does not exist. We can easily calculate the position of the displacement vectors, when we write the basic equations in the form $A_{ik}\xi_k = 0$ with

$$A_{ik} = -\rho v^2 \delta_{ik} + c_{ijkl} g_j g_l,$$

where $A_{ik}$, for fixed $i = 1, 2, 3$, form the components of a vector perpendicular to the associated $\boldsymbol{\xi}$ (for each fixed $v$, which first must be calculated from the determinant). Thus, $\boldsymbol{\xi}$ runs parallel to the vector product of any two arbitrary vectors of the three vectors $\boldsymbol{A}_i = A_{ik}\boldsymbol{e}_k$, hence $\boldsymbol{\xi} = q\boldsymbol{A}_i \times \boldsymbol{A}_j$, where $q$ is an arbitrary constant.

In general, the propagation direction $\boldsymbol{g}$ and the displacement vector $\boldsymbol{\xi}$, according to the above, form an angle $\zeta$ given by

$$\cos\zeta = \frac{[\boldsymbol{g}, \boldsymbol{A}_i, \boldsymbol{A}_j]}{|\boldsymbol{A}_i \times \boldsymbol{A}_j|}.$$

If $\zeta = 0$, we speak of a pure *longitudinal wave*, as also appearing, for example, in liquids and gases; for the case $\zeta = 90^\circ$ we have a pure *transverse wave* analogous to the $\boldsymbol{D}$-wave in optics. Here, we are also dealing with singular cases. In an arbitrary direction, we expect a *combination wave* composed of a longitudinal and a transversal component. Both propagate simultaneously in the same direction with the same velocity.

An interesting relationship exists between the extreme values of the longitudinal effect $c'_{1111}$ in a direction $\boldsymbol{e}'_1 = u_{1j}\boldsymbol{e}_j$ and the character of the wave. We consider the auxiliary function $H = c'_{1111} + \lambda \sum_i u_{1i}^2$, where $\sum_i u_{1i}^2 = 1$. Extreme values of $H$ appear, when $\partial H/\partial u_{1i} = 0$, hence,

$$4c_{ijkl}u_{1j}u_{1k}u_{1l} + 2\lambda u_{1i} = 0 \quad \text{with} \quad c'_{1111} = u_{1i}u_{1j}u_{1k}u_{1l}c_{ijkl}.$$

The factor 4 in the first term stems from the permutability of the indices. If we multiply this equation with $u_{1i}$ and sum over $i$, we find $\lambda = -2c'_{1111}$. Thus

$$-c'_{1111}u_{1i} + c_{ijkl}u_{1j}u_{1k}u_{1l} = 0.$$

The elastodynamic basic equation is completely analogous to

$$-\rho v^2 \xi_i + c_{ijkl} g_j g_l \xi_k = 0.$$

Multiplying the first equation by $\xi_i$, the second by $u_{1i}$, summing over $i$ and forming the difference gives

$$(-c'_{1111} + \rho v^2) u_{1i} \xi_i + c_{ijkl} (u_{1j} u_{1k} u_{1l} \xi_i - g_j g_l u_{1i} \xi_k) = 0.$$

The second term vanishes, when we make $\boldsymbol{e}'_1 = \boldsymbol{g}$, i.e., the propagation direction lies in the direction of an extreme value of the longitudinal effect. If $\boldsymbol{e}'_1 \cdot \boldsymbol{\xi} \neq 0$, we have $\rho v^2 = c'_{1111}$. If we now compare the initial equations and note that $g_i = u_{1i}$, we recognize immediately that $\xi_i$ must equal $q g_i$; $q$ is again an arbitrary constant. This means that a pure longitudinal wave runs in the direction of an extreme value of the longitudinal effect. Because of the orthogonality of the three displacement vectors, both waves perpendicular to the propagation direction are polarized and thus represent pure transverse waves. As a supplementary comment, let us note that according to Neumann's principle, an extreme value for $c'_{1111}$ must be present along rotation axes or rotation–inversion axes with $n \geq 2$. Accordingly, pure longitudinal waves exist in these directions. Even in triclinic crystals there exists at least three different directions with pure longitudinal waves.

As just discussed, the condition of the solvability of the elastodynamic basic equations leads to a third-order equation in $\rho v^2$. The coefficients of the powers of $\rho v^2$ depend on $c_{ijkl}$ as well as on the propagation direction $\boldsymbol{g}$. The coefficient for the term $(\rho v^2)^2$ possesses a special significance in so far as, according to the fundamental theorem of algebra, it is equal to the sum of the roots, hence, equal to

$$\rho(v'^2 + v''^2 + v'''^2).$$

From the determinant $|A_{ik}|$, one obtains, for these coefficients, the value $c_{ijkl} g_j g_l \delta_{ik} = \sum_{i=1,2,3} c_{ijil} g_j g_l$. The quantities $E_{jl} = c_{ijkl} \delta_{ik}$ represent the components of a second-rank tensor (contraction of the tensor $\{c_{ijkl}\}$). The sum of the squares of the propagation velocities, multiplied by the density, is accordingly, for each arbitrary direction $\boldsymbol{e}'_1 = g_{1i} \boldsymbol{e}_i$ (with $g_{1i} = g_i$) equal to the longitudinal effect of the tensor $\{E_{jl}\}$. We call the tensor $\{E_{jl}\}$ the *dynamic elasticity*. It represents the directional dependence of the averaged squares of the sound velocity and is thus a useful measure for the elastic anisotropy. This relation plays a helpful role as a control in the practical determination of the elastic constants.

At a first glance, the impression exists that the basic equations derived here adequately describe the elastic behavior for all materials. This is, however,

incorrect. Of great practical importance are the additional interactions occurring in piezoelectric and piezomagnetic crystals (crystals with ordered magnetic structure). The piezoelectric effect causes, via the stress components $\sigma_{ij}$, an electric displacement. The elastic waves are thus accompanied by electric waves. The simultaneous elastic, piezoelectric, and dielectric interactions are described to a first approximation, under negligibly small pyroelectric effect, by the following equations:

$$\varepsilon_{ij} = s^E_{ijkl}\sigma_{kl} + \hat{d}_{ijm}E_m = s^E_{ijkl}\sigma_{kl} + d_{mij}E_m,$$
$$D_i = d_{ikl}\sigma_{kl} + \epsilon^{\sigma}_{im}E_m \quad (\hat{d}_{ijm} = d_{mij}, \quad \text{see Section 4.4.1.3}).$$

In the case of a elastomagnetic interaction, a corresponding term of the magnetostriction and the associated relation for the magnetization would be added. As we have seen in the derivation of the elastodynamic basic equations, it may be easy to use the deformation as an inducing quantity. Instead of the above equations we then have with $\hat{e}_{ijm} = -e_{mij} = c_{ijkl}\hat{d}_{klm}$

$$\sigma_{ij} = c^E_{ijkl}\varepsilon_{kl} + \hat{e}_{ijm}E_m = c^E_{ijkl}\varepsilon_{kl} - e_{mij}E_m$$
$$D_i = e_{ikl}\varepsilon_{kl} + \epsilon^{\varepsilon}_{im}E_m.$$

The upper indices $E$ and $\varepsilon$ mean: at constant electric field and constant deformation state, respectively. The reason for replacing the quantities $-e_{mij}$ by the coefficients $\hat{e}_{ijm}$ in the same manner as $\hat{d}_{ijm} = d_{mij}$ (apart from the sign), will be explained in Section 5. Moreover, the Maxwell equations must be fulfilled.

As before $\operatorname{Div}\sigma_{ij} = \rho\partial^2\xi_i/\partial t^2\boldsymbol{e}_i$. Further, in nonconducting crystals we have $\operatorname{div}\boldsymbol{D} = 0$. We can describe the electric field coupled to the elastic wave, to sufficient approximation, by $\boldsymbol{E} = -\operatorname{grad}\phi$, where the potential $\phi$ possesses the form $\phi = \phi_0 e^{2\pi i(\boldsymbol{k}\cdot\boldsymbol{x}-\nu t)}$ analogous to the elastic wave $\boldsymbol{\xi} = \boldsymbol{\xi}_0 e^{2\pi i(\boldsymbol{k}\cdot\boldsymbol{x}-\nu t)}$.

This means $\boldsymbol{E} \parallel \boldsymbol{g}$ and $\operatorname{rot}\boldsymbol{E} = 0$ and hence $\boldsymbol{B} = \text{const.}$ and $\boldsymbol{D} = \text{const.}$ The justification for this statement was given by Hutson & White (1962) on the basis of the exact relationship derived by Kyame (1949). These authors showed that the relative deviations from the exact solutions for $v^2$ are proportional to the square of the ratio of sound- to light velocity in the crystal, hence in the order of magnitude of at most $10^{-8}$.

Thus,

$$\operatorname{Div}\sigma_{ij} = \{c^E_{ijkl}g_jg_l\xi_k + e_{mij}g_mg_j\phi\}(-4\pi^2\boldsymbol{k}^2)\boldsymbol{e}_i.$$

$\operatorname{div}\boldsymbol{D} = 0$ gives $\boldsymbol{g}\cdot\boldsymbol{D} = 0$, if $\boldsymbol{D} = \boldsymbol{D}_0 e^{2\pi i(\boldsymbol{k}\cdot\boldsymbol{x}-\nu t)}$, hence $e_{nkl}g_ng_l\xi_k - \epsilon^{\varepsilon}_{rs}g_rg_s\phi = 0$ or

$$\phi = \frac{e_{nkl}g_ng_l\xi_k}{\epsilon^{\varepsilon}_{rs}g_rg_s}.$$

The denominator $\epsilon^{\varepsilon}_{rs} g_r g_s$ represents the longitudinal effect of the dielectric tensor in the propagation direction $\boldsymbol{g}$. Thus, for piezoelectric crystals, we obtain the following basic equations ($i = 1, 2, 3$)

$$\left\{ -\rho v^2 \delta_{ik} + \left( c^{E}_{ijkl} + \frac{e_{mij} e_{nkl} g_m g_n}{\epsilon^{\varepsilon}_{rs} g_r g_s} \right) g_j g_l \right\} \xi_k = 0.$$

New indices were used in some positions, when this was required for the independence of the summation.

The difference compared to the basic equations for nonpiezoelectric materials is that instead of $c^{E}_{ijkl}$ the quantities

$$c^{D}_{ijkl}(\boldsymbol{g}) = c^{E}_{ijkl} + \frac{e_{mij} e_{nkl}}{\epsilon^{\varepsilon}_{rs} g_r g_s} g_m g_n$$

appear. That $c^{D}_{ijkl}$ actually takes this form in the case $\boldsymbol{D} = 0$, results from the relation $D_i = e_{ikl} \varepsilon_{kl} + \epsilon^{\varepsilon}_{im} E_m = 0$, after multiplying the $i$th equation by $g_i$, summing over $i$ and introducing the resulting expression for $\phi$ in the equation for $\sigma_{ij}$.

This is consistent with the condition $\boldsymbol{D} = \text{const.}$, which follows from the Maxwell equations owing to $\operatorname{rot} \boldsymbol{H} = 0$. Hence, for piezoelectric and nonpiezoelectric crystals we can write the basic equation in the general form $(-\rho v^2 \delta_{ik} + c^{D}_{ijkl} g_j g_l) \xi_k = 0$. Since $c^{D}_{ijkl} = c^{D}_{klij}$, all relations derived from the ordinary elastodynamic basic equations are equally valid. In particular, even in piezoelectric crystals, the displacement vectors $\boldsymbol{\xi}'$, $\boldsymbol{\xi}''$ and $\boldsymbol{\xi}'''$ associated with a propagation direction $\boldsymbol{g}$ are mutually orthogonal. If one succeeds to measure the components $c^{D}_{ijkl}$ and $c^{E}_{ijkl}$ or their difference, one obtains statements on piezoelectric quantities important not only for the determination of the piezoelectric tensor but also for the technical application of such crystals. The quantity $(c^{D}_{ijkl} - c^{E}_{ijkl}) / c^{D}_{ijkl}$ is a measure of the fraction of electrical energy to the total energy of the elastic wave. This and similarly defined quantities are called *coupling factors*. We will return to these later.

In piezoelectric crystals possessing a certain electrical conductivity, as for example, $LiO_3$ or semiconductors of the GaAs-type or CdS-type, an attenuation of elastic waves occurs because the accompanying electric field breaks down due to the conductivity (Hutson & White, 1962). The elastic wave experiences thereby continuously a loss of energy. In the relationships just derived, this phenomenon can be taken into account by introducing complex dielectric constants. In pyroelectric crystals, the relationships derived above must be modified by adding pyroelectric terms (see Section 5).

Before we turn to the procedures for the measurement of propagation velocities of elastic waves, a few remarks are necessary on the validity of the derived relationships. From our approach it is clear that only small deformations are allowed in order to remain within the limits of Hooke's law (linear

elasticity). We will discuss higher order effects in Section 4.6.3. Moreover, we have neglected all types of mechanical damping (scattering and excitation processes) by assuming real components $c_{ijkl}$, without, however, giving extra emphasis to this aspect. We have also not considered that similar effects as found in optical activity, may exist between the components of the stress and the deformation tensor. Such effects have actually been observed in certain crystals (*acoustic activity*). We will also return to this point. The greatest problem in all these measurements is, however, the approach of plane waves, in which we have assumed that they propagate completely independently in all directions. This strictly applies only to infinitely extended bodies. One must therefore carefully consider under which circumstances the relationships gained above may be taken as a sufficient approximation.

To what extent one can regard a crystal as approximately infinite depends on the ratio $B$ of the specimen dimensions perpendicular to the wave normals and the wavelength $\lambda$. Experimentally it has been found that from $B/\lambda > 20$ on, the specimen dimensions have no influence on the observed propagation velocities exceeding 0.5% of the value for an infinite crystal. This is also confirmed by simple model calculations. For the practical measurements of propagation velocities it is therefore appropriate to adjust the wavelength by selecting the frequency to fulfil the above condition. In contrast to crystal optics in the visible spectrum, one observes over a wide frequency range, no substantial dependence of the propagation velocity of elastic waves on frequency. In most materials a weak dispersion begins first above 1000 MHz. The energy of quanta with a frequency of 1000 MHz is usually by far too small to excite states of elastic oscillations in lattice particles.

In some measurement methods the specimen is externally irradiated with sound waves (for example, pulse-echo; forced oscillations). It should then be noted that just as in optics, the sound wave and the associated elastic energy flux density, represented by the ray vector $\boldsymbol{s}$, can encompass a finite angle, leading to a sideways drift of the sound ray. We obtain the energy flux density vector from the total elastic energy $W$ per unit volume as follows: We have

$$W = \frac{1}{2}\int_V \left(\rho \frac{\partial \xi_i}{\partial t}\frac{\partial \xi_i}{\partial t} + \sigma_{ij}\varepsilon_{ij}\right) dV;$$

the first terms correspond to the kinetic energy constant and the second to the familiar elastic deformation work. The time change of this total energy is

$$\frac{\partial W}{\partial t} = \int_V \left(\rho \frac{\partial \xi_i}{\partial t}\frac{\partial^2 \xi_i}{\partial t^2} + \frac{\partial}{2\partial t}(\sigma_{ij}\varepsilon_{ij})\right) dV.$$

With $\sigma_{ij} = c_{ijkl}\varepsilon_{kl}$ we get

$$\frac{\partial}{\partial t}(\sigma_{ij}\varepsilon_{ij}) = 2\sigma_{ij}\frac{\partial \varepsilon_{ij}}{\partial t}.$$

Inserting the dynamic basic equation

$$\frac{\partial \sigma_{ij}}{\partial x_j} = \rho \frac{\partial^2 \xi_i}{\partial t^2}$$

in the first term results in

$$\frac{\partial W}{\partial t} = \int_V \left( \frac{\partial \xi_i}{\partial t} \frac{\partial \sigma_{ij}}{\partial x_j} + \sigma_{ij} \frac{\partial \varepsilon_{ij}}{\partial t} \right) dV = \int_V \frac{\partial}{\partial x_j} \left( \sigma_{ij} \frac{\partial \xi_i}{\partial t} \right) dV.$$

From Gauss's theorem, the volume integral is equal to a surface integral given by $\int_V \operatorname{div} \boldsymbol{Q} dV = \int_O \boldsymbol{Q} \cdot d\boldsymbol{o} = \int_O Q_j n_j df$, where $d\boldsymbol{o}$ specifies a surface element of size $df$ with the surface normal (unit vector) $\boldsymbol{n} = n_j \boldsymbol{e}_j$. Thus

$$\frac{\partial W}{\partial t} = \int_O \sigma_{ij} \frac{\partial \xi_i}{\partial t} n_j df.$$

If we now imagine the specimen volume as a rectangular parallelepiped with edges parallel to the Cartesian basic vectors, we recognize that $\sigma_{ij} \partial \xi_i / \partial t$ represents the $j$th component of the energy flux density vector. Hence, we have $s_j = \sigma_{ij} \partial \xi_i / \partial t$, whereby the sign is selected such that the components parallel to the propagation direction become positive. In the case of an elastic wave $\boldsymbol{\xi} = \boldsymbol{\xi_0} e^{2\pi i(\boldsymbol{k}\cdot\boldsymbol{x} - \nu t)}$, $s_j = \frac{\omega^2}{v} c_{ijkl} \xi_i \xi_k g_l$, as one can easily confirm ($\omega = 2\pi\nu$).

For the time average we obtain

$$\bar{s_j} = \frac{\omega^2}{2v} c_{ijkl} \xi_{0i} \xi_{0k} g_l.$$

We can now calculate the angle between the ray vector $\boldsymbol{s}$ and propagation direction $\boldsymbol{g}$ with the help of $\boldsymbol{s} \cdot \boldsymbol{g}$. The important cases are those in which both vectors lie parallel to each other. This always applies to pure longitudinal waves. As proof let $\boldsymbol{e}'_1$ be parallel to the propagation direction. Then $g'_1 = 1$, $g'_2 = g'_3 = \xi'_2 = \xi'_3 = 0$ and $\boldsymbol{\xi} = \xi'_1 \boldsymbol{e}'_1$ parallel to the propagation direction. Thus $\bar{s'_1} = \frac{\omega^2}{2v} \xi_0^2 c'_{1111}$ and $\bar{s'_j} = \frac{\omega^2}{2v} \xi_0^2 c'_{1j11}$ for $j = 2$ and 3. From the basic equation $(-\rho v^2 \delta_{ik} + c_{ijkl} g_j g_l) \xi_k = 0$ one obtaines in the primed system for pure longitudinal waves

$$-\rho v^2 g'_i + c'_{ijkl} g'_j g'_k g'_l = 0$$

and especially for $g'_1 = 1$, $g'_2 = g'_3 = 0$

$$g'_1 = \frac{c'_{1111}}{\rho v^2} = 1, \quad g'_2 = \frac{c'_{2111}}{\rho v^2} = 0 \quad \text{and} \quad g'_3 = \frac{c'_{3111}}{\rho v^2} = 0.$$

Therefore, $c'_{2111} = c'_{3111} = 0$ and hence $\bar{s'_2} = \bar{s'_3} = 0$.

If transverse waves with $\boldsymbol{\xi} \parallel \boldsymbol{e}_1$ run along an $n$-fold rotation- or rotation-inversion axis parallel to $\boldsymbol{e}_3$, hence $g_3 = 1$, $g_1 = g_2 = \xi_2 = \xi_3 = 0$, one finds $\bar{s_j} = c_{1j13}\xi_0^2\frac{\omega^2}{2v}$. If $n$ or $\bar{n}$ is even, the index 3 may only occur an even number of times (2 or $\bar{2}$ is contained in $n$ or $\bar{n}$, respectively!). This means $\bar{s_1} = \bar{s_2} = 0$ and $\bar{s_3} = c_{1313}\xi_0^2\frac{\omega^2}{2v}$.

In general, with a threefold axis, the energy flow runs askew to the propagation direction. This causes the so-called internal conic refraction, an analogous phenomenon known in optics, which here, however, can also appear in cubic crystals (see Exercise 28).

### 4.5.6 Dynamic Measurement Methods

Dynamic methods to measure elastic properties have achieved a special significance in solid-state research with the development of ultrasound technology and precision frequency measurements. In the following, we discuss the most important methods.

These are

1. Pulse-echo methods,
2. Schaefer–Bergmann method,
3. Resonances of plates and rods,
4. Brillouin scattering,
5. Neutron scattering,
6. X-ray scattering (thermal scattering).

#### 1. Pulse-Echo Methods and Related Methods

The specimen in the form of a plane-parallel plate of thickness $L$ in the direction of the face normals is irradiated with short ultrasonic pulses of a few microseconds duration (about 20 wave trains at 10 MHz). The ultrasonic generator, usually a thin quartz plate excited to mechanical oscillations by a high-frequency electric field, is fixed to one side of the specimen by a thin film of an appropriate resin, for example (Fig. 4.44). The ultrasonic pulse is reflected at the boundary and returns to the generator, which in the meantime is electronically switched to act as a receiver. It transforms, via the piezoelectric effect, a part of the elastic energy of the incoming echo into a voltage pulse, which can be observed on an oscilloscope with time-proportional $x$-deflection. Repeated reflections of the same pulse generate a sequence of quasiequidistant echos in time, when the propagation direction remains unchanged. The time difference of $m$ consecutive echos corresponds to the delay time of the sound wave

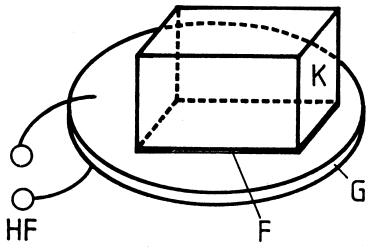


**Figure 4.44** Pulse-echo method. The crystal K (a plane-parallel plate) is pasted on the ultrasonic generator G by an oil film F or a highly viscous material (necessary in the case of transverse waves). In the intervals between the pulses the generator works as a piezoelectric ultrasound probe.

through the $2m$-fold specimen length and a certain path length covered by the sound wave in the generator or receiver until reaching the maximum of the electric pulse. The required correction can be experimentally determined, for example, by measurements on specimens of the same orientation but different thicknesses. Let $\Delta t$ be the corrected delay time. The velocity of the elastic wave is then $v = 2mL/\Delta t$. The delay time $\Delta t$ can be directly read from the scale of the oscilloscope after calibration using standards with known sound velocity or determined by the aid of electronic measuring equipment. One repeats the pulses after a few milliseconds to hold the oscillogram still.

To generate longitudinal waves or waves with large longitudinal components we work with a so-called thickness resonator, for example, a quartz plate cut perpendicular to the direction $\boldsymbol{e}_1$ of the longitudinal piezoelectric effect (perpendicular to a twofold axis; X-cut). Paraffin oil and at lower temperatures, a mixture of low boiling hydrocarbons have proven suitable as a cementing liquid. Transverse waves, for example, can be generated with quartz plates, whose normals are perpendicular to $\boldsymbol{e}_1$ (general Y-cut). The displacement vector of these waves then lies parallel to $\boldsymbol{e}_1$ (in the face of the plate) when an electric field with a component $E_2$ is applied. The transfer of the transverse waves to the specimen can only be achieved, with good efficiency, with the help of high-strength adhesives or cementing with a highly viscous liquid. Standard cementing materials are beeswax with paraffin oil additive for lower temperatures, benzophenone for temperatures around 20° and high-strength dental cement for higher temperatures. We will discuss below, in more detail, the quantitative treatment of the oscillating piezoelectric plate.

With commercial equipment, primarily conceived to test materials for cracks and other inhomogeneities, sound velocities can be measured to an accuracy of about 0.5%, when the dimensions of the specimens are at least ten times the wavelength and the propagation direction remains sufficiently

sharp for all echos. In this regard, it is essential that the surface of the generator emitting the ultrasonic pulse is sufficiently large.

For precision measurements, the simple pulse-echo method is less suitable, in particular with crystals of low symmetry, because pure wave types are only possible in a few distinct directions. Hence two or all three combination waves are simultaneously excited. The selection of echos is easy in principle, but inaccuracies creep in when trying to determine the position of the maxima of the voltage pulses triggered by the echos.

We illustrate a special advantage, in comparison to most other methods, in more detail. This is the measurement of the attenuation of the sound waves which one can read directly from the decay of the maxima of the voltage pulses of consecutive echos. To describe the attenuation it is convenient to introduce an individual attenuation coefficient $\alpha$ for each wave.

Then

$$\boldsymbol{\xi} = \boldsymbol{\xi}_0 e^{2\pi i(\boldsymbol{k}\cdot\boldsymbol{x}-\nu t)} e^{-\alpha(\boldsymbol{g}\cdot\boldsymbol{x})}.$$

This behavior can also be formally described with a complex propagation vector $\boldsymbol{k} = \boldsymbol{k}' + i\boldsymbol{k}''$, where $\boldsymbol{k}'' \parallel \boldsymbol{k}$ and $v = \nu/|\boldsymbol{k}'|$.

Hence

$$\alpha = 2\pi|\boldsymbol{k}''| \qquad (\text{because} \quad \alpha\boldsymbol{g} = 2\pi\boldsymbol{k}'').$$

The attenuation coefficients with respect to elastic constants are by no means to be represented as components of a tensor. Similar to optics, there also exists a formal description for elastic absorption with the aid of complex components of the elasticity tensor. Since, however, the major part of the attenuation is usually generated by inhomogeneities, such an approach is of limited use. One can gain certain insights concerning the perfection of crystals from attenuation phenomena.

The value $\alpha$ results from the amplitude ratio of two consecutive echos according to

$$\frac{|\boldsymbol{\xi}_{0,n+1}|}{|\boldsymbol{\xi}_{0,n}|} = e^{-Q} e^{-\alpha 2L}.$$

The factor $e^{-Q}$ takes into account the losses due to reflection at the generator and on the other side of the specimen. $e^{-Q}$ can be eliminated by measurements on two specimens of different lengths $L$ and $L'$.

The exponential decay of the amplitudes of the echos is directly read from the envelope of the voltage maxima on the screen of the oscilloscope (Fig. 4.45). Deviations from plane-parallelism as well as a divergence of the sound beam lead to oscillations of the envelope, which can impair the accuracy of the measurement.

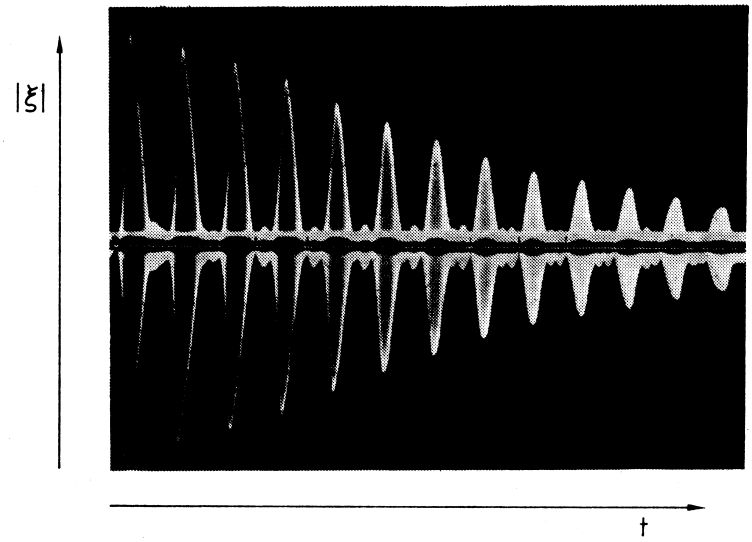


**Figure 4.45** A sequence of pulse-echos of longitudinal waves in NaF. Propagation direction [100], frequency 5 MHz, length of specimen about 30 mm.

One can also directly record the sound pulse on the surface opposite to the generator-side with the help of a piezoelectric receiver (transmission).

Electronic processing of the time displacement of primary pulse and echo or transmission pulse enables a substantial improvement in the accuracy of measurement of small relative changes in sound velocity. Forgacs (1960) achieved an improvement using the time difference between start and arrival of the signal as a frequency-determining element for the repetition of the start pulse (sing-around-method). A second interesting method is the superposition of the echo or the transmission signal with the primary pulse. In this method one obtains, dependent on the frequency of the carrier wave of the pulse, sharply adjustable superposition profiles, which respond sensitively to small changes in the sound velocity (McSkimin, 1961). With these and related methods, one can, under suitable conditions, measure changes in sound velocity of the order of $10^{-8}$. These methods are particularly suited for the measurement of changes in elastic properties under the influence of external parameters, as for example, hydrostatic or unidirectional pressure, temperature, electric and magnetic fields. The accuracy of the measurement of the absolute sound velocity cannot, however, be substantially increased by these methods, because the influence of the adhesive film and the generator or receiver cannot be directly eliminated.

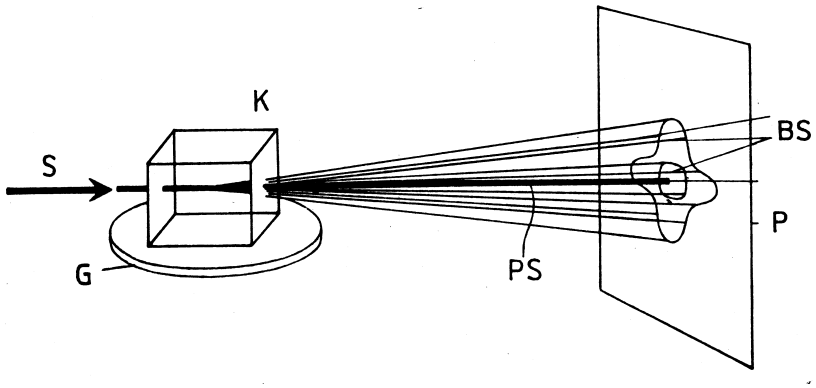


**Figure 4.46** Schaefer–Bergmann method (diffraction of light by ultrasonic waves; S light beam, K crystal with ultrasound generator G, P photoplate or ground glass screen, PS primary beam, BS diffracted rays).

**2. Schaefer–Bergmann Method**

The periodic distortions accompanying a sound wave can cause a change in refractive indices due to the elastooptical effect $\Delta a_{ij} = p_{ijkl}\varepsilon_{kl}$. This results in the creation of a sine-shaped variation of the refractive index, that is, an optical grating, on which light can be diffracted. Now, if one irradiates a crystal, of no particular shape, with a sound wave of fixed frequency, a broad spectrum of sound waves of different propagation directions and displacement vectors are generated due to multiple reflections at the boundaries. A detailed analysis shows that in the case of small diffraction angles, only those sound waves can contribute to a noticeable diffraction of light, whose propagation vector is oriented approximately perpendicular to the propagation vector of the monochromatic light beam (Fig. 4.46). Hence, one furnishes the specimen with an optically transparent pair of faces approximately perpendicular to the face of the sound generator.

A monochromatic light beam entering the crystal approximately perpendicular to the pair of transparent faces, finds sound wave fields in nearly all propagation directions within these faces and is thus diffracted just about uniformly in all directions. The diffraction angle is taken from the formula for the optical ruled grating, as long as the diffraction angles are small enough and the optical path through the crystal is so short that the depth of the sound grating can be neglected. For optically quasiisotropic materials, a sufficient approximation is $2d \sin \vartheta = m\lambda$ analogous to the Bragg condition. $2\vartheta$ is the diffraction angle, i.e., the angle of deflection of the diffracted wave from the direction of incidence, $d$ is the acoustic wave length, $\lambda$ the optical wavelength and $m$ the order of the diffraction. Since, to a first approximation, only pure sinusoidal displacements occur, the higher orders cannot be interpreted by

corresponding Fourier coefficients, as for example, in the case of X-ray diffraction. Rather, effects of multiple diffraction are present, that is, each strongly diffracted wave acts as a new primary wave. Since, in general, for each propagation direction, three different wave types exist with different propagation velocities, one obtains, outgoing from the crystal, three cones of diffracted rays which generate three curves on a photographic plate or screen behind the crystal. From these, the diffraction angles for the propagation directions perpendicular to the light beam and hence the propagation velocity of the ultrasonic waves can be determined. In the case of strong anisotropy, one obtains separate diffraction patterns for both directions of vibration of the incident light wave. These patterns show nearly the same diffraction angle in the case of weak ray double refraction. However, easily measurable deviations of around one percent occur in cases of strong double refraction, even if the diffraction angles are small (Küppers, 1971). The cause for the splitting is different refraction when the light wave enters and emerges as well as momentum conservation in the scattering process. Corresponding corrections are necessary, if a higher measurement accuracy is required. If $R$ is the effective distance between the crystal and the photographic plate and $2r$ is the distance between the diffraction spots on the photographic plate belonging to the propagation vectors $\boldsymbol{g}$ and $-\boldsymbol{g}$, one obtains the angle of diffraction $2\vartheta$ from

$$\tan 2\vartheta = r/R.$$

Assuming that the source of the diffracted ray lies in the geometrical center of the crystal, which is the case, when the specimen is uniformly irradiated by the primary ultrasonic wave. This takes into account the refraction of the diffracted ray at the rear of the crystal, one obtains for the effective distance $R = R_0 - L(1 - 1/n)/2$, where $R_0$ is the geometric distance crystal center-photographic plate, $L$ the length of the crystal in the direction of the light wave and $n$ the refractive index. Hence, one obtains for the velocity of the ultrasonic wave deflecting the light ray by the diffraction angle $2\vartheta$

$$v = \nu d = \nu \frac{\lambda}{2 \sin \vartheta} \qquad (m = 1),$$

where $\nu$ denotes the frequency of the ultrasonic wave. To achieve higher accuracy, it is recommended to make $R_0$, as well as the frequency $\nu$ of the ultrasonic wave as large as possible, for example, $R_0 = 5\,\mathrm{m}$, $\nu$ around 20 MHz. Good sharpness of the diffraction spots is obtained, when the intense primary light beam travels through a pinhole (opening about 30 $\mu$m) and with the help of a field lens, through the vibrating crystal to the photographic plate to form there an image of the pinhole, enlarged by a factor of about five (Fig. 4.47). The third Laue condition is effective in long specimens and with large diffraction angles. That is, the intensity of the diffracted wave takes on its maximum under the

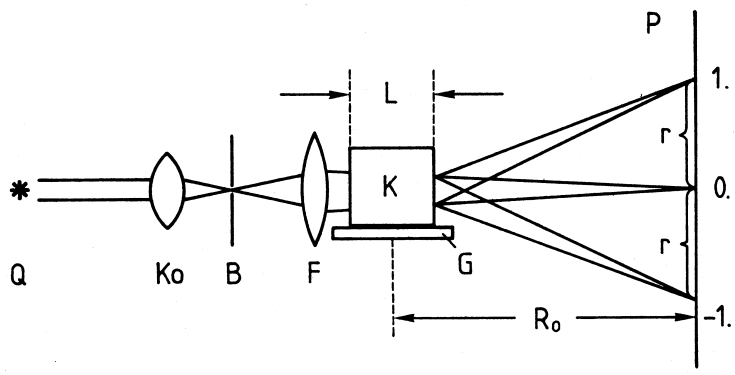


**Figure 4.47** Arrangement of the Schaefer–Bergmann method. Q light source, Ko condenser, B fine pinhole, F field lens for imaging the pinhole through the crystal K on the photo plate or screen, respectively, G ultrasound generator, L length of the crystal, $R_0$ distance crystal—photo plate, r distance of the diffraction spots of first and minus first order from the primary spots 0.

Bragg condition (angle of incidence = angle of emergence, measured against the normals of the elastic wavefront). This means that one can only observe reflections with large diffraction angles (above about 30°) the Bragg condition is realized. Accordingly, with light waves of arbitrary incidence, one obtains, in such cases, only very few and weak reflections, if any at all. In order to obtain a diffraction spectrum of all propagation vectors perpendicular to the light ray it is thus necessary to keep the diffraction angles sufficiently small ($\vartheta < 3°$), i.e., the frequency of the ultrasound waves must be correspondingly low, in contrast to the above requirement for large diffraction angles in favor of higher accuracy. In specimens with arbitrary boundaries, a high proportion of reflected waves is created from the primary ultrasound wave, whose wave normals run outside the plane perpendicular to the light ray, and hence, do not contribute to diffraction. If one furnishes the crystal with a "gothic arch" type boundary as in Fig. 4.48, a major portion of the acoustic primary wave is transferred, via reflection, into partial waves with propagation directions within the plane. This results, in particular, in a more uniform distribution of the excited waves and to a substantial increase in the intensity of the diffracted light waves. The exposure times for making a diffraction photograph can thus be reduced to a fraction of a second. Furthermore, the intensity of the primary ultrasound wave can be minimized to largely avoid the interfering effects of crystal heating.

For the evaluation of Schaefer–Bergmann elastograms it is advantageous, when the plane of each effective propagation vector is chosen by taking into consideration the symmetry properties of the crystal, for example, in or-

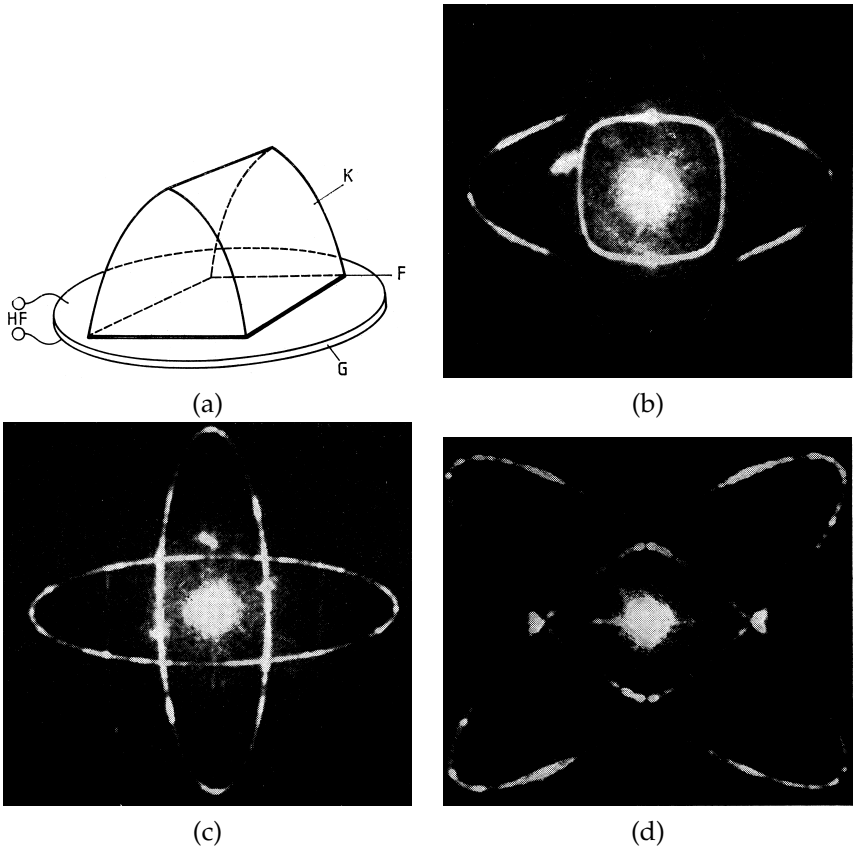


**Figure 4.48** (a) "Gothic arch" type shape of the specimen for the generation of a wide spectrum of propagation vectors within the plane perpendicular to the light beam by reflection of the primary ultrasound wave (for symbols see Fig. 4.44). (b) Elastogram of KCl (PSG 4/m3), light beam along $[100]$, primary ultrasound wave along $[001]$. (c) Elastogram of $KH_2PO_4$ (PSG $\bar{4}$m), light beam along $[001]$, primary ultrasound wave along $[100]$. (d) Elastogram of calcium formate (PSG mmm), light beam along $[001]$, primary ultrasound wave along $[010]$. The anisotropy of the diffraction angles allows to recognize the Laue symmetry in the direction of the optical transmission.

thorhombic crystals the planes (100), (010), and (001). In triclinic crystals the evaluation is simplified, when the light wave is incident in the direction of the Cartesian basic vectors $\boldsymbol{e}_i$. Then namely, one $g_i$ vanishes in each of the elastodynamic basic equations, so that only a fraction of the components $c_{ijkl}$ is involved. From only three Schaefer–Bergmann elastograms of specimens with a 'gothic arch' shape one obtains the sound velocities for hundreds of independent directions, from which the complete elasticity tensor can be determined with the help of a suitable computer program.

This advantage is in confrontation with the disadvantage of low measurement accuracy. In the case of first-order diffraction, one normally achieves an accuracy of around 0.2% in determining the velocity of sound. The reason lies in a mutual coupling of the elastic waves, which, similar to coupled pendula, can influence the effective restoring forces (these correspond to the elastic constants). If one works with plane-parallel plates instead of the "gothic arch" shape, standing waves form between these plates at certain frequencies (resonances), generating a strongly pronounced optical grating in a single propagation direction. This produces multiple reflections of very high order, so that the diffraction angle can be measured to a relative accuracy of up to $10^{-5}$ thanks to the larger values for $2mr$. Moreover, by specifying the direction of vibration of the generator, one can excite quite definite wave types. Furthermore, with this boundary, an elastic primary wave of substantially lower power will suffice. By adding such precision measurements for some distinct directions, one can determine the elasticity tensor, even of triclinic crystals, to good accuracy. Indeed, the elasticity tensor of a triclinic crystal, namely $CuSO_4 \cdot 5H_2O$, was completely determined by this procedure (Haussühl & Siegert, 1969).

The Schaefer–Bergmann method is of course not suited for strongly absorbing crystals. Since the intensity of the diffracted rays depends on the elastooptical constants, the method of light diffraction on ultrasound waves can also be used to measure elastooptical properties (see Section 4.5.9.2).

#### 3a. Resonances of Plates and Rods

We observe the simplest vibrating forms on plane-parallel plates and parallelepipedic rods thanks to the clear boundary conditions. Firstly, we consider a plane-parallel plate of thickness $L$ with unlimited sides, suspended free of external stress. The possible forms of vibration must satisfy the differential equation

$$\frac{\partial \sigma_{ij}}{\partial x_j} = \frac{1}{2} c_{ijkl} \left( \frac{\partial^2 \xi_k}{\partial x_j \partial x_l} + \frac{\partial^2 \xi_l}{\partial x_j \partial x_k} \right) = \rho \frac{\partial^2 \xi_i}{\partial t^2}$$

as well as the boundary conditions "no external stresses." We select $\boldsymbol{e}_3$ parallel to the plate normal, and the origin in the center of the plate. Thus $\sigma_{3i}(L/2) = \sigma_{3i}(-L/2) = 0$ for $i = 1, 2, 3$. We need not consider the other boundary conditions, because we are only searching for solutions independent of the position coordinates $x_1$ and $x_2$, i.e., those that are homogeneous within each cross-section perpendicular to $\boldsymbol{e}_3$.

Assuming an antisymmetric solution for a standing wave

$$\begin{aligned} \boldsymbol{\xi} &= \boldsymbol{\xi_0} \sin(2\pi \boldsymbol{k} \cdot \boldsymbol{x}) \cos \omega t \\ &= \xi_0 \sin(2\pi k_3 x_3) \cos \omega t \end{aligned}$$

in the above equation, gives

$$(-\rho v^2 \delta_{ik} + c_{i3k3})\xi_k = 0,$$

where $\omega/2\pi k_3 = v$ is the vave velocity.

From the condition for the solution (Det. $= 0$), we obtain the three velocities $v'$, $v''$ and $v'''$, as for an infinite crystal where the wave propagates in the direction $\boldsymbol{e}_3$. The associated displacement vectors are calculated according to the rules discussed in Section 4.5.12. A general solution for the freely vibrating plate can be obtained by a linear combination of the three special solutions according to

$$\boldsymbol{\xi} = (\boldsymbol{\xi}'_0 \sin(2\pi k'_3 x_3) + \boldsymbol{\xi}''_0 \sin(2\pi k''_3 x_3) + \boldsymbol{\xi}'''_0 \cdots) \cos \omega t.$$

The boundary conditions $\sigma_{3i}(\pm L/2) = 0$ lead to

$$c_{i3k3}\xi'_{0k} 2\pi k'_3 \cos(2\pi k'_3 L/2) + c_{i3k3}\xi''_{0k} 2\pi k''_3 \cos(2\pi k''_3 L/2) + \xi'''_{0k} \ldots) = 0$$

with $i = 1, 2, 3$. This system of equations has only solutions with $\boldsymbol{\xi} \neq 0$, when its determinant vanishes. We must have $\cos(\pi k_3 L) = 0$ for one of the three values $k_3 = k'_3$, $k''_3$ or $k'''_3$. This means $k_3 L = (2n-1)/2$, where $n$ is integer. If, for example, the solution with $v''$ is excited, we must have $k''_3 = 1/\lambda'' = (2n-1)/2L$, i.e., an odd multiple of half the wavelength must equal the plate thickness.

We obtain a similar result for a symmetric solution of a standing wave $\boldsymbol{\xi} = \boldsymbol{\xi}_0 \cos(2\pi k_3 x_3) \cos \omega t$, however, with the condition, that now an integer multiple of the wavelength is equal to the plate thickness. Both results, the antisymmetric and the symmetric, together lead to the result that the characteristic vibrations of the infinite plane plate always appear, when an integer multiple of half the wavelength of the associated wave of the infinite crystal is equal to the plate thickness. The associated resonance frequencies are integer multiples of the fundamental frequency $\nu_1 = v/2L$, when no dispersion is present, which, as previously discussed, virtually always applies approximately below 1000 MHz. If one succeeds to excite the plate to its characteristic vibrations and measures the associated resonance frequencies, one has the possibility to determine the wave velocity $v$ from the difference of these frequencies and the plate thickness according to $v = 2L(\nu_n - \nu_m)/(n-m)$, as one can directly read from the resonance condition ($v = \nu\lambda$). $\nu_n$ or $\nu_m$ specify the $n$th or $m$th resonance frequency.

An advantageous property of the resonances of thick plates consists in the fact, that the three states of vibration can be measured independent of one another, in other words, without coupling. For freely vibrating plane-parallel plates of piezoelectric crystals, the resonance condition $L = m\lambda/2$ ($m$ integer) is also valid. Instead of $c_{ijkl}$, however, the components $c^D_{ijkl}$ derived above

must employed. The proof is carried out analogously, whereby

$$\sigma_{ij} = c^E_{ijkl}\varepsilon_{kl} - e_{mij}E_m, \qquad D_i = e_{ikl}\varepsilon_{kl} + \epsilon^{\varepsilon}_{im}E_m$$

with $E_m = -(\text{grad}\,\phi)_m$ and $\boldsymbol{D}\cdot\boldsymbol{g} = 0$. Corresponding conditions apply to magnetostrictive crystals.

A change in the boundary conditions, as for example, in the case of forced vibrations, leads to a modified resonance condition, to which we will come later. The simplest way to excite resonances is by using a sound generator, which in order to transfer the vibrations must be brought in contact with one of the faces of the crystal. The vibrations can be transferred via an air gap, a thin wire, a rigid connection between generator and crystal, or directly by cementing the generator on the specimen. In particular, the latter is necessary, when exciting sound waves with strong transverse components. In excitation via air or wire contact, one observes hardly any interfering coupling between generator and specimen, i.e., the resonance frequencies of the crystal plate are nearly not influenced by the generator. This does not apply when the generator is firmly attached to the crystal. Rather, one observes resonances of the combined system. The resonance condition can be easily calculated, when the generator possesses also the form of a plane-parallel plate and generator and specimen posses a similar sound wave resistance $\rho v$, i.e., when the sound wave can travel through the boundary surface between generator and specimen without strong reflection losses.[2] If, on the other hand, the sound wave resistance of both media is considerably different, one observes a strong coupling only close to the resonances of the generator. This arrangement has especially proven advantageous for the practical routine measurement of elastic properties. In a preferred version for investigations at very high frequencies (over 100 MHz) a thin piezoelectric generator, for example, made of hexagonal CdS is vapor-deposited on the crystal.

Electrostrictive crystals can be directly excited to vibrate by applying a high-frequency electric field to the metallized faces of the plate. Analogously magnetostrictive crystals can be excited by external magnetic fields. We will return to this in more detail in the next section. The resonances can also be excited in a wide frequency range with the help of the quadratic electrostrictive effect (see Section 4.5.10) or by the forces emanating from a high-frequency electric field of a plate capacitor, one plate of which is the metallized face of the

**2**) The intensity of the sound wave reflected at the boundary surface of two isotropic media $I$ and $II$ is given by (see, for example, Lord Raleigh, 1945)

$$\frac{I_{\text{re}}}{I_0} = \frac{\left(1 - \frac{\rho_{\text{I}} v_{\text{I}} \cos\alpha_{\text{II}}}{\rho_{\text{II}} v_{\text{II}} \cos\alpha_{\text{I}}}\right)^2}{\left(1 + \frac{\rho_{\text{I}} v_{\text{I}} \cos\alpha_{\text{II}}}{\rho_{\text{II}} v_{\text{II}} \cos\alpha_{\text{I}}}\right)^2}.$$

specimen. Here, however, one only achieves small sound amplitudes, so that special measures are needed to detect the resonances.

In the state of resonance, the free faces of the plate vibrate with maximum amplitude, when the amplitude of the exciting wave remains quasiconstant over a broad frequency range. The most important resonance-detection methods are based on this property. In order not to affect the character of the free vibration, only a small part of the vibrational energy may be tapped for the detection. This, for example, can be accomplished with capacitive or piezoelectric transfer. We then talk of a capacitive or piezoelectric sensor. Another possibility consists in measuring the electric power of the generator as a function of the frequency of the field. In this case, one observes a weak feedback of the vibration state on the generator. Hence, one can determine the resonance frequencies very accurately with simple electronic measures.

A further possibility, which has proven preeminently useful in practice, is based on the diffraction of monochromatic light by standing acoustic waves in the resonance state, as with the Schaefer–Bergmann method. In the resonance state, only one strong wave exists, which is easy to observe via the diffraction effect, even when the acoustic power of the generator is weak. This simple method offers the special advantage, that from the angle of diffraction one obtains an independent statement on the velocity of sound and on the directly excited wave type. If one works with polarized light, whose direction of vibration is adjustable, one can observe the resonances at substantially lower acoustic powers. For this purpose, one places a second polarizer in the ray path, which eliminates a large part of the disturbing background radiation on the screen. Crystals with weak elasto-optical effects or insufficient optical transparency can also be investigated with this method. In this case one cements an auxiliary crystal, made of a material with an extremely large elasto-optical effect, as for example, RbI, on the face of the specimen plate opposite the generator. The auxiliary crystal is furnished with a plane parallel pair of faces for the transmission of the light beam. Furthermore, the auxiliary crystal should possess optical quality in order to produce sharp diffraction spots. Finally, one must ensure that the auxiliary crystal does not have a disturbing influence on the resonances of the crystal plate. This occurs through two measures: firstly, the auxiliary crystal is furnished with an irregular boundary on the face opposite to that where the sound enters (for example, "gothic arch" form as in the normal Schaefer–Bergmann method), and secondly, one selects an auxiliary crystal with a sound wave resistance $\rho v$, sufficiently different from that of the specimen. The resonances are somewhat attenuated by the auxiliary crystal. The crucial thing, however, is that the resonance frequencies are not substantially influenced by the generator nor by the auxiliary crystal, when one remains outside the resonance area of the generators. One works with a set of generators covering a large frequency range from, for example,

**Table 4.11** Resonance frequencies $f$ in MHz of a plane-parallel plate of $LiHSeO_3$. Plate normal and propagation direction $[001]$, thickness 7.353 mm, temperature 292 K. Only resonances of the order $(2m + 1)$ were recorded. The measurement between the orders (80+1) and (104+1) are omitted.

| $m$ | $f$ | $m$ | $f$ | $m$ | $f$ | $m$ | $f$ | $m$ | $f$ | $m$ | $f$ |
|---|---|---|---|---|---|---|---|---|---|---|---|
| 1 | 10.534 | 19 | 15.140 | 37 | 19.760 | 55 | 24.381 | 73 | 28.990 | 115 | 39.767 |
| 3 | 11.047 | 21 | 15.665 | 39 | 20.272 | 57 | 24.888 | 75 | 29.500 | 117 | 40.282 |
| 5 | 11.560 | 23 | 16.180 | 41 | 20.786 | 59 | 25.400 | 77 | 30.013 | 119 | 40.790 |
| 7 | 12.070 | 25 | 16.693 | 43 | 21.300 | 61 | 25.915 | 79 | 30.525 | 121 | 41.305 |
| 9 | 12.582 | 27 | 17.209 | 45 | 21.810 | 63 | 26.430 | (80–106) | | 123 | 41.815 |
| 11 | 13.095 | 29 | 17.720 | 47 | 22.320 | 65 | 26.942 | 107 | 37.713 | 125 | 42.331 |
| 13 | 13.607 | 31 | 18.223 | 49 | 22.830 | 67 | 27.452 | 109 | 38.226 | 127 | 42.841 |
| 15 | 14.120 | 33 | 18.735 | 51 | 23.344 | 69 | 27.962 | 111 | 38.735 | 129 | 43.358 |
| 17 | 14.630 | 35 | 19.248 | 53 | 23.870 | 71 | 28.475 | 113 | 39.250 | 131 | 43.872 |

10 to 30 MHz. One observes a strong coupling only close to the fundamental frequency of a generator, i.e., a frequency shift of the resonance compared to the free vibration. One recognizes this by comparison with the frequency of the resonances, recorded by another generator with another fundamental frequency. Investigations using piezoelectric crystals, whose resonances can be directly excited, confirm this important finding. One observes very weak coupling with transverse waves. If one utilizes only resonances lying outside the frequency range of the coupling with the generator, one obtains, with great accuracy, an equidistant frequency spectrum of the unbounded plan-parallel plate. As an example, we present the measurements on a crystal of $LiHSeO_3$ (PSG 222). Table 4.11 lists the measured fundamental frequencies (generator fundamental frequencies 8.24 and 40 MHz). The plate had a thichness of $L = 7.353\,\text{mm}$. Hence, for the velocity of sound of the longitudinal wave along $[001]$ we get the value

$$v = 2L\frac{\nu_n - \nu_m}{m - n} = 3.7713\,\text{kms}^{-1}$$

with $m = 1$ and $n = 131$.

This value is in excellent agreement with the values obtained using the pulse-echo method or with the Schaefer–Bergmann method. Since both frequencies $\nu_m$ and $\nu_n$ were measured with an absolute error below 2 kHz, the value determined for $v$ is at most subjected to an error of 0.05%, whereby $|\Delta L/L| < 0.03\%$ was assumed. This accuracy is sufficient for all normal requirements. The accuracy of the absolute determination of the velocity of sound is limited by the measurement of the thickness $L$. Only with special effort it is possible to determine the thickness with an error substantially below 0.01%. This also presupposes that the specimens are prepared plane-parallel with the corresponding accuracy. In the acquisition of relative changes of sound velocities, as, for example, occurring under the influence of temper-

ature, hydrostatic or uniaxial pressure and electric or magnetic fields, one also achieves a substantially higher accuracy with this method, when one records the diffraction signals with a photomultiplier and employs the possibilities made available by electronic signal processing based on pulse controlled sound excitation and detection. A substantial improvement is also achieved using phase-sensitive lock-in techniques to amplify the signal during frequency-modulated sound excitation. Thus the accuracy of frequency measurements of resonances using well-prepared plates can be increased to give relative errors below $10^{-7}$ to $10^{-8}$ with comparatively little effort. This procedure requires, by far the least effort, and hence, must be given preference over other methods.

Finally, precision measurements of frequencies of fundamentals and low-order harmonics on rods, cylinders and plates must be mentioned, which similar to a tuning fork are mechanically excited. The specimens have to be arranged and excited in the way that those vibrational states occur, which are favored mainly by the respective boundary condition, and that damping by the arrangement is largely suppressed. This means that the specimen shall only lie with the nodes of vibration on the support and excitation shall occur on the expected antinodes. With the help of sensitive piezoelectric sensors, the vibrations of the specimen can be recorded by sound emission in air and the associated resonance frequencies determined with high accuracy. Naturally, optical interferometric methods can also be used to detect the vibrations. From longitudinal and flexural vibrations of rods one can very accurately determine dynamic Young's moduli and from transverse and torsional vibrations certain shear moduli, even on specimens with dimensions of a few mm.

### 3b. Forced Vibrations of Piezoelectric Crystals

We now consider two important examples of special specimen shapes, namely, the plane-parallel unbounded plate and the thin rod. Both can be experimentally realized to a good approximation. The thin plate plays an important role in the application of piezoelectric crystals for acoustic generators and detectors as well as in the manufacture of high-frequency generators and related devices such as frequency stabilizers and frequency selectors in communication technology. In both cases, a comparatively simple relation exists between the observed resonance frequencies and the material constants.

We first consider the plane-parallel plate. The basic equations are (see Section 4.5.12):

$$\sigma_{ij} = c^{E}_{ijkl}\varepsilon_{kl} - e_{mij}E_m, \qquad D_i = e_{ikl}\varepsilon_{kl} + \epsilon^{\varepsilon}_{im}E_m.$$

Moreover, we set $E_m = -(\operatorname{grad}\phi)_m$ and only allow plane waves

$$\boldsymbol{\xi} = \boldsymbol{\xi}_0 e^{2\pi i(\boldsymbol{k}\cdot\boldsymbol{x}-\nu t)} \quad \text{and} \quad \phi = \phi_0 e^{2\pi i(\boldsymbol{k}\cdot\boldsymbol{x}-\nu t)}.$$

As previously, for dynamic processes we have

$$\frac{\partial \sigma_{ij}}{\partial x_j} = \rho \frac{\partial^2 \xi_i}{\partial t^2}.$$

Hence, the general basic equation for the propagation of plane waves in the form derived above is valid

$$(-\rho v^2 \delta_{ik} + c^D_{ijkl} g_j g_l)\xi_k = 0$$

with

$$c^D_{ijkl} = c^E_{ijkl} + \frac{e_{mij} e_{nkl}}{\epsilon_{rs} g_r g_s} g_m g_n,$$

where $\boldsymbol{g}$ is the unit vector in the direction of the wave normals. We only consider vibrational states, which are homogeneous over the complete cross-section parallel to the faces of the plate; i.e., all derivatives $\partial/\partial x_1$ and $\partial/\partial x_2$ vanish, when $\boldsymbol{g} = \boldsymbol{e}_3$ is perpendicular to the faces of the plate. Let the plate be suspended force free, i.e., we have $\sigma_{3i}(x_3) = 0$ for $x_3 = \pm L/2$, hence,

$$\sigma_{31}(\pm L/2) = c^E_{31k3} \frac{\partial \xi_k}{\partial x_3} - e_{331} E_3 = 0$$
$$\sigma_{32}(\pm L/2) = c^E_{32k3} \frac{\partial \xi_k}{\partial x_3} - e_{332} E_3 = 0$$
$$\sigma_{33}(\pm L/2) = c^E_{33k3} \frac{\partial \xi_k}{\partial x_3} - e_{333} E_3 = 0.$$

Because $\boldsymbol{E} = -\operatorname{grad} \phi$ we have $\boldsymbol{E} \parallel \boldsymbol{g}$. These conditions fully correspond to the situation discussed above for free vibrations. Now, as a further decisive parameter we add the electric boundary condition. We imagine electrodes attached to the faces of the plate (for example, by deposition of a thin metallized film), to which we apply a voltage $\phi = \phi_0 \cos \omega t$, so that on both faces the boundary conditions

$$\phi(\pm L/2) = \pm \phi_0 \cos \omega t$$

are to be fulfilled.

To solve the problem, we must determine the three, in the direction $\boldsymbol{g} = \boldsymbol{e}_3$, possible sound velocities and the associated displacement vectors $\boldsymbol{\xi}^{(1)}$, $\boldsymbol{\xi}^{(2)}$ and $\boldsymbol{\xi}^{(3)}$ (previously specified by $\boldsymbol{\xi}'$, $\boldsymbol{\xi}''$, $\boldsymbol{\xi}'''$) from the dynamic basic equations. Each solution is coupled to an electric potential $\phi$, obtained from the relation

$$D_3 = e_{3k3} \frac{\partial \xi_k}{\partial x_3} + \epsilon^{\varepsilon}_{33} E_3 = \text{const.}$$

by integrating with respect to $x_3$ ($\boldsymbol{D}$ = const. was already derived as a secondary condition in Section 4.5.12). From $E_3 = -\partial\phi/\partial x_3$, one obtains by integration

$$e_{3k3}\xi_k - \epsilon^{\varepsilon}_{33}\phi = qx_3 + q_0,$$

hence,

$$\phi = \frac{e_{3k3}}{\epsilon^{\varepsilon}_{33}}\xi_k - q'x_3 - q'_0,$$

where $q$, $q_0$, $q'$ and $q'_0$ are constants of integration possessing the same time dependence as $\xi_k$.

The electric boundary conditions then take on the form

$$\phi(\pm L/2) = \frac{e_{3k3}}{\epsilon^{\varepsilon}_{33}}\xi_k(\pm L/2) \mp q'L/2 - q'_0 = \pm\phi_0 \cos\omega t.$$

The general solution consists of a superposition of the three waves in the form $\boldsymbol{\xi} = \sum_\mu C^{(\mu)}\boldsymbol{\xi}^{(\mu)}$, whereby the complex coefficients $C^{(\mu)}$ are so adjusted, that the boundary conditions are fulfilled. We now imagine $\boldsymbol{\xi}$ to be resolved in a symmetric and an antisymmetric part according to $\boldsymbol{\xi} = \boldsymbol{\xi}_s + \boldsymbol{\xi}_a$ with $\boldsymbol{\xi}_s(x_3) = \boldsymbol{\xi}_s(-x_3)$ and $\boldsymbol{\xi}_a(x_3) = -\boldsymbol{\xi}_a(-x_3)$. In the general approach for a plane wave, this means that $\boldsymbol{\xi}_s$ only contains terms of the form $\cos(2\pi k_3 x_3)$ and $\boldsymbol{\xi}_a$ only terms of the form $\sin(2\pi k_3 x_3)$.

Hence, by subtraction or addition of both boundary conditions, we obtain

$$q' = -\frac{2\phi_0}{L}\cos\omega t + \frac{2e_{3k3}}{L\epsilon^{\varepsilon}_{33}}\xi_{a,k}(L/2)$$

and

$$q'_0 = 0.$$

This means, the electric boundary conditions are only fulfilled by the antisymmetric part of the solution. Conversely, the applied voltage can only excite antisymmetric forms of vibration. Symmetric vibrations can be excited through the quadratic electrostrictive effect (see Section 4.5.10), however, with by far lower amplitudes.

If we now eliminate $E_3$ in the mechanical boundary conditions $\sigma_{3i}(\pm L/2) = 0$ with the help of the above result for $q'$ and consider only the antisymmetric solution

$$\boldsymbol{\xi}_a = \sum_\mu \boldsymbol{\xi}_0^{(\mu)} \sin(2\pi k_3^{(\mu)} x_3)\cos\omega t,$$

we obtain

$$\sum_{\mu}\left(c^{E}_{3ik3}+\frac{e_{33i}e_{3k3}}{\epsilon^{\varepsilon}_{33}}\right)2\pi k_3^{(\mu)}\xi_{0k}^{(\mu)}\cos(\pi k_3^{(\mu)}L)\cos\omega t+\frac{2e_{33i}}{L}\phi_0\cos\omega t$$
$$-\sum_{\mu}\frac{2e_{33i}e_{3k3}}{L\epsilon^{\varepsilon}_{33}}\xi_{0k}^{(\mu)}\sin(\pi k_3^{(\mu)}L)\cos\omega t=0,$$

hence,

$$\sum_{\mu}\left(c^{D}_{3ik3}\cdot\pi k_3^{(\mu)}\cos(\pi k_3^{(\mu)}L)-\frac{e_{33i}e_{3k3}}{L\epsilon^{\varepsilon}_{33}}\sin(\pi k_3^{(\mu)}L)\right)\xi_{0k}^{(\mu)}\;=\;-\frac{e_{33i}}{L}\phi_0$$
$$\text{for}\quad i=1,2,3.$$

This system of equations yields the contributions of the wave type $\boldsymbol{\xi}^{(\mu)}$ to the solution $\boldsymbol{\xi}_a$. The ratio $\xi_{01}^{(\mu)}:\xi_{02}^{(\mu)}:\xi_{03}^{(\mu)}$ is assumed to be known from the solution of the basic equations. Plate resonances appear, when at least one of the amplitudes $\xi^{(\mu)}$ becomes unlimited, i.e., when the determinant

$$\left|c^{D}_{3ik3}\pi k_3^{(\mu)}\cos(\pi k_3^{(\mu)}L)-\frac{e_{33i}e_{3k3}}{L\epsilon^{\varepsilon}_{33}}\sin(\pi k_3^{(\mu)}L)\right|$$

vanishes.

The practical utilization of this condition for the determination of material constants is only worthwhile in the case of pure longitudinal- or transverse waves.

For a pure longitudinal wave along $\boldsymbol{e}_3$ ($\xi_1=\xi_2=0$, $\xi_3\neq 0$), the boundary condition for $i=3$ is

$$\left(c^{D}_{3333}\cdot\pi k_3\cos(\pi k_3L)-\frac{e^2_{333}}{L\epsilon^{\varepsilon}_{33}}\sin(\pi k_3L)\right)\xi_{03}=-\frac{e_{333}}{L}\phi_0.$$

Hence, a resonance occurs when

$$\tan(\pi k_3L)=(\pi k_3L)\frac{\epsilon^{\varepsilon}_{33}c^{D}_{3333}}{e^2_{333}}=(\pi k_3L)/k_t^2,$$

where $k_t^2$ is the coupling factor $(c^{D}_{3333}-c^{E}_{3333})/c^{D}_{3333}=e^2_{333}/\epsilon^{\varepsilon}_{33}c^{D}_{3333}$, which we were previously already acquainted with. A pure transverse wave with displacement vector parallel $\boldsymbol{e}_1$ ($\xi_1\neq 0$, $\xi_2=\xi_3=0$) gives, for $i=1$, the boundary condition

$$\left(c^{D}_{3113}\cdot\pi k_3\cos(\pi k_3L)-\frac{e^2_{331}}{L\epsilon^{\varepsilon}_{33}}\sin(\pi k_3L)\right)\xi_{01}=-\frac{e_{331}}{L}\phi.$$

The analogous condition

$$\tan(\pi k_3 L) = (\pi k_3 L)/k_{35}^2$$

with the coupling factor $k_{35}^2 = e_{331}^2/\epsilon_{33}^{\varepsilon} c_{3131}^D$ applies for diverging of $\xi_{01}$.

We obtain similar conditions for the case of other propagation and displacement directions of pure wave types.

The equation $\tan X = X/k^2$ with $X = \pi k_3 L$ represents a frequency condition. We can use the approximate condition $\tan X \to \infty$ for solutions with very high values of $X/k^2$. Here, $X = (2m-1)\pi/2$, hence, $L = (2m-1)\lambda/2$ or

$$\nu = \frac{(2m-1)}{2}\frac{v}{L} \quad \text{with} \quad k_3 = 1/\lambda$$

and $m$ integer. This condition is identical with the resonance condition for the freely vibrating plate, where, however, only the odd multiples of half the wavelength (antisymmetric states of vibration) are allowed. Thus, from the higher order resonance frequencies we can determine, with sufficient accuracy, the propagation velocity of the associated wave. In the region of small and medium values of $X/k^2$ characteristic deviations of free resonances appear: The resonance frequencies are not multiples of the fundamental frequency. The situation is best seen by means of a graphical representation (Fig. 4.49). The line $Y = X/k^2$ intersects the tangent curves $Y = \tan X$ once in each interval between $(m-1)\pi < X \leq m\pi$. Since $k^2$ is smaller than one in each case, there exists for $m = 1$ also one solution. For practical utilization, the method proposed by Onoe, Thiersten & Meitzler (1963) has proven to be optimal. The solutions $X_m$ of the equation $\tan X_m = X_m/k^2$ are calculated as a function of $k^2$ in the range $0 \leq k^2 < 1$, which can be carried out with a simple iteration method of the type

$$X_m^{(s+1)} = m\pi + \arctan(X_m^{(s)}/k^2).$$

The resulting ratios

$$\frac{X_n}{X_m} = \frac{\pi L/\lambda_n}{\pi L/\lambda_m} = \frac{\nu_n}{\nu_m}$$

are directly accessible to experiment. They depend monotonically on $k^2$, not, however, on the plate thickness $L$ and the velocity of sound $v$. Therefore, from the measured ratios of resonance frequencies, one can determine the associated coupling factors by a comparison with the tabled values. A sufficiently large deviation from the ratio $(2n-1)/(2m-1)$ is only obtained with $k$-values above approximately 0.1 as well as for $m$ and $n = 1, 2$ and 3. An extract of values sufficient for practical applications is presented in Table 4.12. With the

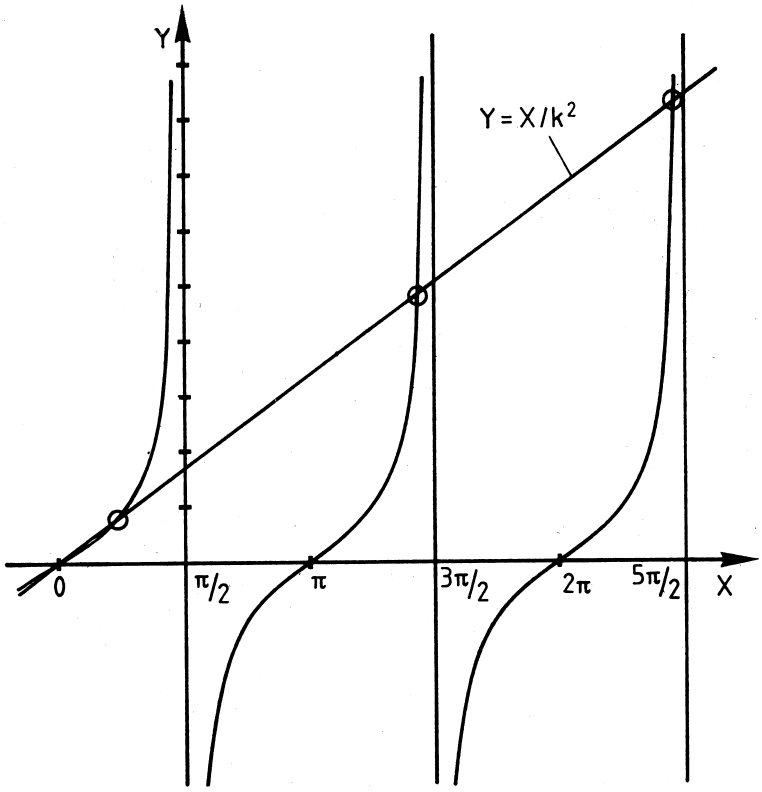


**Figure 4.49** Intersection of $Y = \tan X$ with $Y = X/k^2$ ($k^2 < 1$). In each interval $(m-1)\pi < X \leq m\pi$ the line $Y = X/k^2$ intersects the curves $Y = \tan X$ just once.

help of these $k^2$-values and the sound velocities obtained from higher order resonance frequencies, one can determine the square of the piezoelectric coefficients $e_{33i}$ according to

$$e_{33i}^2 = k_{3j}^2 \epsilon_{33}^{\varepsilon} c_{3i3i}^{D}$$

($j = 6 - i$), when the associated dielectric constant $\epsilon_{33}^{\varepsilon}$ is known, too. We can, to a sufficient approximation, insert a value for $\epsilon_{33}^{\varepsilon}$ measured in the range of higher frequencies, for example around 10 MHz. Of course, the relationships discussed here also apply approximately to the case of combination waves with strong longitudinal- or transverse components. The method of piezoelectric resonances of plane-parallel plates fails in the case of very small coupling coefficients, which, for the application, are usually of little interest. The resonance frequencies can be simply and very accurately identified by the minima of the ac resistance of the plate connected in series with an auxiliary resistor, when sweeping through a broad frequency range during electrical excitation.

**Table 4.12** Ratio of resonance frequencies of quasi-unlimited plane plates as a function of the coupling coefficient $k$. Excitation of vibrations in an ac electric field parallel to the normals of the plate.

| $k$ | $\nu_2/\nu_1$ | $\nu_3/\nu_1$ | $k$ | $\nu_2/\nu_1$ | $\nu_3/\nu_1$ | $k$ | $\nu_2/\nu_1$ | $\nu_3/\nu_1$ |
|---|---|---|---|---|---|---|---|---|
| 0 | 3 | 5 | 0.35 | 3.148 | 5.265 | 0.70 | 3.917 | 6.625 |
| 0.05 | 3.003 | 5.005 | 0.40 | 3.201 | 5.359 | 0.75 | 4.185 | 7.094 |
| 0.10 | 3.011 | 5.020 | 0.45 | 3.265 | 5.474 | 0.80 | 4.561 | 7.751 |
| 0.15 | 3.025 | 5.045 | 0.50 | 3.344 | 5.614 | 0.85 | 5.132 | 8.744 |
| 0.20 | 3.045 | 5.080 | 0.55 | 3.441 | 5.787 | 0.90 | 6.123 | 10.461 |
| 0.25 | 3.071 | 5.128 | 0.60 | 3.563 | 6.002 | 0.95 | 8.430 | 14.447 |
| 0.30 | 3.105 | 5.189 | 0.65 | 3.717 | 6.274 | | | |

If one is able to transmit light through the plate parallel to the plate surfaces, resonance frequencies can be observed by the diffraction of light as discussed above. With this method, resonances have been detected up to very high orders, in individual cases exceeding 1000.

The thin plane-parallel rod, which we now consider, is treated similarly to the plane-parallel plate. Let the length, width, and thickness extend in the directions $\boldsymbol{e}_1$, $\boldsymbol{e}_2$ and $\boldsymbol{e}_3$. Let $L_1 \gg L_2 > L_3$ specify the respective dimensions. If one applies an electric alternating field to the plane faces perpendicular to $\boldsymbol{e}_3$, one can excite vibrations in the rod, whose frequencies are fixed by the length $L_1$. Since the crystal is not exposed to any external forces

$$\sigma_{ij} = 0 \qquad (i,j = 1,2,3)$$

is true for all points on the surface. Inside the crystal, all $\sigma_{2i}$ and $\sigma_{3i}$ vanish to a good approximation, because the dimensions $L_2$ and $L_3$ are so small that no significant mechanical stresses can form between the side faces. This means, however, that only the stress component $\sigma_{11}$ exists. It depends solely on $x_1$ because

$$\frac{\partial \sigma_{11}}{\partial x_2} \quad \text{and} \quad \frac{\partial \sigma_{11}}{\partial x_3}$$

are also approximately zero as a consequence of the small dimensions. The equation of motion for the rod is then

$$\frac{\partial \sigma_{11}}{\partial x_1} = \rho \frac{\partial^2 \xi_1}{\partial t^2}.$$

The mechanical deformation $\varepsilon_{11}$ connected with $\sigma_{11}$ is expressed by $\varepsilon_{11} = s^E_{1111}\sigma_{11} + d_{311}E_3$ hence,

$$\sigma_{11} = \frac{\varepsilon_{11}}{s^E_{1111}} - \frac{d_{311}}{s^E_{1111}} E_3.$$

We have, as a further material equation, to take notice of the relationship $D_3 = \epsilon_{33}^{\sigma} E_3 + d_{311}\sigma_{11}$, when ensuring that $E_1 = E_2 = 0$. The equation of motion then takes the form

$$\frac{1}{s_{1111}^E}\frac{\partial^2 \xi_1}{\partial x_1^2} = \rho \frac{\partial^2 \xi_1}{\partial t^2}$$

because

$$\frac{\partial E_3}{\partial x_1} = 0$$

(the broadsides perpendicular to $e_3$ are completely metallized!). Using the plane-wave approach $\xi_1 = \xi_{01} e^{2\pi i(k_1 x_1 - \nu t)}$ we get

$$\left(\rho\omega^2 - \frac{4\pi^2 k_1^2}{s_{1111}^E}\right)\xi_1 = 0, \quad \text{thus} \quad \rho v^2 = \frac{1}{s_{1111}^E}.$$

In contrast to the unlimited plate, the longitudinal component $c_{1111}^D$ is not effective in the rod but rather Young's modulus $(1/s_{1111}^E)$. This result also applies to nonpiezoelectric crystals. We obtain the resonance condition, as before, from the boundary conditions. Again, we imagine the general solution as composed of a symmetric and an antisymmetric part given by

$$\xi_1 = \xi_s \cos(2\pi k_1 x_1)\cos\omega t + \xi_a \sin(2\pi k_1 x_1)\cos\omega t.$$

Inserting the boundary conditions $\sigma_{11}(\pm L/2) = 0$ in the relation

$$\varepsilon_{11} = s_{1111}^E \sigma_{11} + d_{311} E_3$$

gives

$$-\xi_{0s}\sin(\pm\pi k_1 L_1) + \xi_{0a}\cos(\pm\pi k_1 L_1) = d_{311}E_{03}/2\pi k_1,$$

hence,

$$\xi_{0s} = 0 \quad \text{and} \quad \xi_{0a} = d_{311}E_{03}/(2\pi k_1 \cos(\pi k_1 L_1)).$$

Accordingly, only the antisymmetric states of vibration are excited. Our solution is then

$$\xi_1 = \frac{d_{311}E_{03}}{2\pi k_1 \cos(\pi k_1 L_1)}\sin(2\pi k_1 x_1)\cos\omega t.$$

Resonances appear, when $\cos(\pi k_1 L_1) = 0$, hence when $\pi k_1 L_1 = (2m-1)\pi/2$ or

$$\nu_m = \frac{(2m-1)v}{2L_1}$$

just as with the unlimited plate.

The portion of alternating current flowing over the metallized surfaces is

$$I_3 = \int \frac{dD_3}{dt} dF,$$

where integration is carried out over the surface perpendicular to $\boldsymbol{e}_3$. With $D_3 = D_{03} \cos \omega t$ one obtains

$$\frac{dD_3}{dt} = -\omega D_{03} \sin \omega t$$

and hence,

$$\begin{aligned} I_3 &= -\omega L_2 \int_{-L_1/2}^{+L_1/2} D_{03} \sin \omega t dx_1 \\ &= -\omega L_2 \int_{-L_1/2}^{+L_1/2} \left( \epsilon_{33}^{\varepsilon} E_{03} + \frac{d_{311}}{s_{1111}^E} \frac{\partial \xi_{01}}{\partial x_1} \right) \sin \omega t dx_1 \end{aligned}$$

using $\epsilon_{33}^{\sigma} = \epsilon_{33}^{\varepsilon} + d_{311}^2 / s_{1111}^E$. This relation is obtained by inserting the expression derived above for $\sigma_{11}$ in $D_3 = \epsilon_{33}^{\sigma} E_3 + d_{311} \sigma_{11}$. The result is with $\xi_1$ as given above

$$I_3 = -\omega L_1 L_2 \left( \epsilon_{33}^{\varepsilon} + \frac{d_{311}^2}{s_{1111}^E} \frac{\tan(\pi k_1 L_1)}{\pi k_1 L_1} \right) E_{03} \sin \omega t.$$

In the resonance state, the resistance is minimal because $\tan(\pi k_1 L_1) \to \infty$. However, there exists the possibility of an unlimited resistance when, namely, the expression in the brackets vanishes. For the respective frequency, the term "antiresonance frequency" has come into common usage. It must be

$$\tan X = -\frac{\epsilon_{33}^{\varepsilon} s_{1111}^E}{d_{311}^2} X \quad \text{with} \quad X = \pi k_1 L_1.$$

This relation, apart from the sign, is analogous to the resonance condition of the unlimited plate. If one now introduces the effective coupling coefficient

$$\frac{\epsilon_{33}^{\sigma} s_{1111}^E}{d_{311}^2} = 1/k^2$$

one obtains, with

$$\epsilon_{33}^{\varepsilon} = \epsilon_{33}^{\sigma} - \frac{d_{311}^2}{s_{1111}^E}$$

the antiresonance condition in the form

$$\tan X = X(k^2 - 1)/k^2 = -X/k'^2.$$

**Table 4.13** Ratio of the first antiresonance frequency and the first resonance frequency of thin and slender rods as function of the coefficient $k'^2 = k^2/(1-k^2)$ at an excitation in an ac electric field along the rod axis.

| $k'^2$ | $\nu_{A1}/\nu_1$ | $k'^2$ | $\nu_{A1}/\nu_1$ | $k'^2$ | $\nu_{A1}/\nu_1$ | $k'^2$ | $\nu_{A1}/\nu_1$ |
|---|---|---|---|---|---|---|---|
| 0 | 1 | 0.50 | 1.0921 | 1.00 | 1.2916 | 1.50 | 1.4879 |
| 0.05 | 1.0010 | 0.55 | 1.1094 | 1.05 | 1.3126 | 1.55 | 1.5051 |
| 0.10 | 1.0040 | 0.60 | 1.1276 | 1.10 | 1.3335 | 1.60 | 1.5218 |
| 0.15 | 1.0094 | 0.65 | 1.1467 | 1.15 | 1.3541 | 1.70 | 1.5535 |
| 0.20 | 1.0160 | 0.70 | 1.1664 | 1.20 | 1.3745 | 1.80 | 1.5832 |
| 0.25 | 1.0247 | 0.75 | 1.1866 | 1.25 | 1.3945 | 1.90 | 1.6108 |
| 0.30 | 1.0352 | 0.80 | 1.2072 | 1.30 | 1.4141 | 2.00 | 1.6364 |
| 0.35 | 1.0473 | 0.85 | 1.2281 | 1.35 | 1.4332 | | |
| 0.40 | 1.0609 | 0.90 | 1.2492 | 1.40 | 1.4520 | | |
| 0.45 | 1.0760 | 0.95 | 1.2704 | 1.45 | 1.4702 | | |

From a graphical representation, one sees that the antiresonance frequency $\nu_{Am}$ of $m$th order always lies higher than the resonance frequency $\nu_m$. The impedance behavior as a function of the frequency of the electric field enables two sets of data to be gained, namely, the resonance frequencies $\nu_1$, obtained with high accuracy from a higher resonance frequency according to $\nu_1 = \nu_m/(2m-1)$, and the associated antiresonance frequency, leading to a value for $k'^2$ or $k^2$. The ratio $\nu_{Am}/\nu_m$ is largest for $m = 1$. Therefore, one confines oneself to the measurement of the first antiresonance frequency. Then, $\nu_{A1}/\nu_1 = X_{A1}/X_1 = X_{A1}/(\pi/2)$ because $X_1 = \pi/2$. This ratio only depends on $k^2$ and not on $v$ and $L_1$. From a table of values $X_{A1}(k'^2)/X_1$, easily calculated by an iteration method of the type $X^{(s+1)} = \arctan(-X^{(s)}/k'^2)$, one can then extract $k'^2$ or $k^2$ and hence the piezoelectric coefficient $d^2_{311}$, when the dielectric constant $\epsilon^{\varepsilon}_{33}$ is known. Table 4.13 presents the values $X_{A1}/X_1 = \nu_{A1}/\nu_1$ as a function of $k'^2$, which suffice for practical use. By conducting measurements on rods of different orientations, one can thus determine certain components of the piezoelectric and elastic tensors. In any case, for the complete measurement of the elasticity tensor other measurements must be included, because the vibrations discussed here are only coupled with the longitudinal effects $s^{E\,\prime}_{1111}$.

Other wave types can also be excited in the thin rod under discussion. Again let $L_1 \gg L_2 > L_3$. Whilst previously the length $L_1$ was the frequency determining factor, let it now be the width $L_2$.

It is convenient to intentionally arrange the dimension along $\boldsymbol{e}_1$ irregularly in order to prevent the formation of the resonances discussed above. The electric field is again applied in the direction $\boldsymbol{e}_3$. The boundary conditions are now: $\partial\sigma_{ij}/\partial x_1 = 0$, because the crystal is quasiunlimited in the direction $\boldsymbol{e}_1$, $\sigma_{3i} = 0$ and $\partial\sigma_{ij}/\partial x_3 = 0$ in the whole crystal, because $L_3$ is very small, and $\sigma_{2i}(\pm L_2/2) = 0$.

We only consider states of vibration with propagation vector parallel $e_2$. Employing $\xi_i = \xi_{0i} e^{2\pi i(k_2 x_2 - \nu t)}$, we obtain from the elastodynamic basic equations, taking into consideration the above conditions

$$\rho \frac{\partial^2 \xi_1}{\partial t^2} = \frac{\partial \sigma_{12}}{\partial x_2} = c^E_{1212} \frac{\partial^2 \xi_1}{\partial x_2^2} + c^E_{1222} \frac{\partial^2 \xi_2}{\partial x_2^2}$$

and

$$\rho \frac{\partial^2 \xi_2}{\partial t^2} = \frac{\partial \sigma_{22}}{\partial x_2} = c^E_{2222} \frac{\partial^2 \xi_2}{\partial x_2^2} + c^E_{2212} \frac{\partial^2 \xi_1}{\partial x_2^2},$$

and hence,

$$(-\rho v^2 + c^E_{1212})\xi_1 + c^E_{1222}\xi_2 = 0,$$
$$c^E_{2212}\xi_1 + (-\rho v^2 + c^E_{2222})\xi_2 = 0.$$

This system has only solutions, when its determinant vanishes. We get the two solutions

$$\rho v^2 = \frac{c^E_{22} + c^E_{66}}{2} \pm \frac{1}{2}\sqrt{(c^E_{22} - c^E_{66})^2 + 4c^{E2}_{26}}$$

with

$$c_{2222} = c_{22}, \quad c_{1212} = c_{66}, \quad c_{2212} = c_{26}.$$

The boundary conditions

$$\sigma_{12}(\pm L_2/2) = c^E_{26} \frac{\partial \xi_2}{\partial x_2} + c^E_{66} \frac{\partial \xi_1}{\partial x_2} - e_{312} E_3 = 0,$$
$$\sigma_{22}(\pm L_2/2) = c^E_{22} \frac{\partial \xi_2}{\partial x_2} + c^E_{26} \frac{\partial \xi_1}{\partial x_2} - e_{322} E_3 = 0,$$
$$D_3 = \epsilon^\sigma_{33} E_3 + 2d_{312}\sigma_{12} + d_{322}\sigma_{22}$$

(all variables at the positions $+$ or $-L_2/2$) demonstrate that the electric field must, in general, simultaneously excite both solutions, because for each solution the amplitude ratio $\xi_{01}/\xi_{02}$ is fixed by the dynamic equations. Considerations similar to the previous situation lead to the conclusion that the resonance condition $\tan X = 0$ with $X = \pi \nu L_2/v$ also applies, hence

$$\nu_m = \frac{(2m-1)}{2L_2} v$$
$$= \frac{(2m-1)}{2L_2} \sqrt{\frac{1}{2\rho}\left((c^E_{22} + c^E_{66}) \pm \sqrt{(c^E_{22} - c^E_{66})^2 + 4c^{E2}_{26}}\right)}.$$

Thus, further elastic data can be extracted, which together with the other results allow a complete determination of the elasticity tensor. Antiresonance frequencies appear, too, from which one can derive additional data for the determination of piezoelectric coefficients. Since the boundary conditions cannot be exactly realized, one must expect certain deviations of the thus obtained values from $c_{ij}^{E}$ of the unlimited crystal.

Examples for the application of this method for the determination of elastic, dielectric and piezoelectric properties of the technologically important crystals are $\alpha$-quartz, $KH_2PO_4$ and Rochelle salt, which were described in detail by Mason (1954). The special advantages of the investigation of quadratic plates were explained by Bechmann (1951).

#### 3c. Resonant Ultrasound Spectroscopy (RUS)

We now come to a particularly effective method for the future experimental investigation of elastic properties, developed in the last decades. It presents the generalization of the determination of elastic properties from acoustic resonance frequencies of geometrically clearly defined test specimens, as discussed above for plane-parallel plates or rods. The problem of the calculation of acoustic resonances of homogeneous bodies, even in the case of anisotropic media, was solved by Demarest in 1969 for spheres and rectangular parallelepipeds. It turned out that the resonance frequencies of rectangular parallelepipeds, the so-called RPR spectrum ("rectangular parallelepiped resonances"), could be calculated with high accuracy from the density, orientation and dimensions of the parallelepiped and its elasticity tensor, however, with the aid of a powerful computer. The converse, namely the determination of the elasticity tensor from a sufficiently large region of the resonance spectrum of a rectangular parallelepipedic specimen with known density, orientation and dimensions could only be solved up to now with a least-squares-method. With this method one attempts to arrive at a data set of the elasticity tensor in iterative steps, whose calculated resonance spectrum agrees with the experimental data set. Before the calculations initial values for the components of the elasticity tensor must be selected most carefully. The first successful experiments were reported by Ohno (1976).

Rectangular parallelepipeds, whose edges run parallel to the basic vectors of a Cartesian reference system, in particular, that of the crystal-physical basic system, have proven best suited for the practical application of the method. In favorable cases, the dimensions of the specimens can be relatively small (under 1 mm). One must ensure that only minimal deviations from plane-parallelism (in the range of less than 0.5 per mille in the dimensions) and from orientation with respect to the Cartesian system (angular deviation less than 0.3°) occur. The larger the elastic anisotropy the more exact the orientation must be realized.

Commercial network analyzers are suitable for the measurement of the resonance frequencies. The specimens are fixed along a space diagonal, between a sound generator and a detector, such that one corner of the specimen lies on the generator and the opposite corner contacts the detector. The mechanical force on the specimen must be kept as low as possible to approximate the condition of a freely vibrating body. If one sweeps through a frequency interval with the generator, one expects in the case of a resonance deformation, which are communicated to the detector on the opposite corner (Fig. 4.50a). The inverse piezoelectric effect produces an electric signal at the detector, which can be recorded by a lock-in amplifier. Normally, i.e., at low acoustic damping, one obtains exceptionally sharp signals. For a comparatively unproblematic evaluation, it is advantageous, when the spectrum is recorded beginning with the lowest resonance frequency up to a specified maximum frequency without any gap. The number of the required resonances depends on the point symmetry group of the specimen and the desired accuracy. For example, with cubic crystals, about 30 resonances are sufficient, with triclinic crystals about six times more are needed to obtain confident results. If the experimental spectrum is incomplete, an evaluation with simple programs fails, since the computer-calculated resonance frequencies, continuously ordered according to rising frequency, do not agree with the sequence of the corresponding experimental frequencies. If, in the experimental sequence, one or the other resonance is missing, because, for example, the associated deformation only exhibited a small effective component at the detector, special computer programs must be employed to process the gaps in the spectrum. Such programs have been developed in the meanwhile. Anyway, additional efforts should be made to extract, by repeated measurements on the specimen in different settings, a complete spectrum within the specified frequency range. An example of such as spectrum is presented in Fig. 4.50b.

A short discussion of the fundamental principles of the method is appropriate. Naturally, the familiar basic equations previously discussed for the other methods apply. These we note here, however, for the case of piezoelectric crystals

$$\sigma_{ij} = c^E_{ijkl}\varepsilon_{kl} - e_{ijk}E_k \qquad \text{and} \qquad D_i = \epsilon^\varepsilon_{ij}E_j + e_{ijk}\varepsilon_{kl}.$$

As previously, $\{\sigma_{ij}\}$ designates the stress tensor, $\{\varepsilon_{kl}\}$ the deformation tensor, $\{e_{ijk}\}$ the piezoelectric $e$-tensor, $\{\epsilon^\varepsilon_{ij}\}$ the dielectric tensor at constant mechanical deformation, $\{D_i\}$ and $\{E_i\}$ the vectors of the electric displacement and the electric field strength (see Section 4.5.5). For each small specimen volume (Newton's axiom) we have

$$\frac{\partial\sigma_{ij}}{\partial x_j} = \rho\frac{\partial^2\xi_i}{\partial t^2},$$

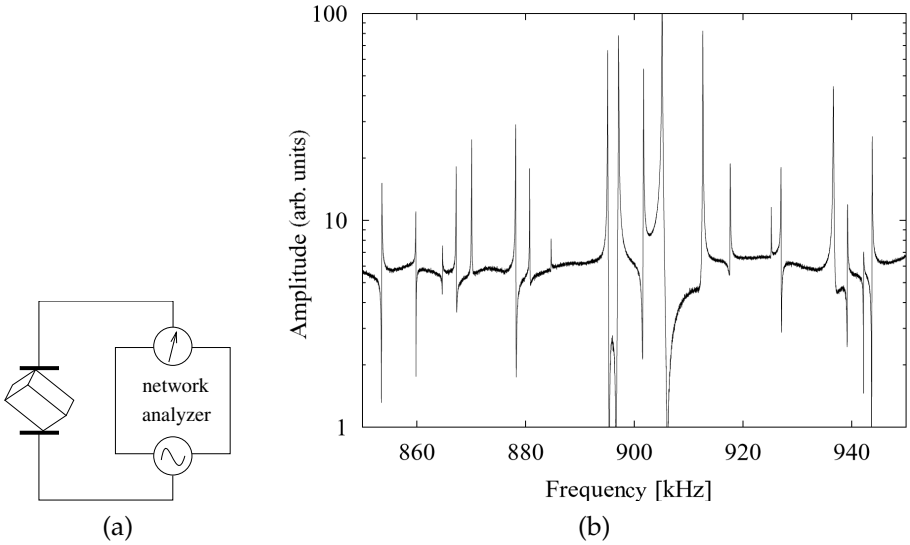


**Figure 4.50** (a) Scheme of the RUS method. (b) Part of the RUS spectrum of a rectangular parallelepipedron of $La_3Ga_5SiO_{14}$ having edge lengths of about 6 mm.

where $\boldsymbol{\xi} = \xi_i \boldsymbol{e}_i$ is the displacement vector, $\rho$ the density and $t$ the time. For the freely vibrating parallelepiped, the mechanical stress at the edges must vanish. The calculation of the possible characteristic vibrations of the probe under these boundary conditions is performed with the Lagrange formalism

$$L = \int (\text{kinetic energy density} - \text{potential energy density}) dV.$$

Integration is extended over the volume of the specimen. The first term follows from the product of the square of the sound velocity components with the density ($\sum_i \rho v_i^2/2$), the second, from the product of the components of the stress tensor with the components of the deformation tensor ($\sigma_{ij}\varepsilon_{ij}/2 = c^E_{ijkl}\varepsilon_{ij}\varepsilon_{kl}/2$ for nonpiezoelectric crystals). A harmonic time-dependence is assumed for the displacement vector, hence, $\xi = \xi_0 \cos(2\pi\nu t)$. According to the rules of variational calculus, the Lagrange function takes on extreme values in the case of stationary solutions, i.e., in the states of resonance. The method of Ritz, in which the components of the displacement vector and of the electric field strength are expanded with respect to suitable basic functions $\Phi(\boldsymbol{x})_s$ or $\Psi(\boldsymbol{x})_s$ in the configuration space $(x_1, x_2, x_3)$, has proven a practical procedure. The expansion has the form

$$\xi_i(\boldsymbol{x}) = a_{is}\Phi_s(\boldsymbol{x}) \qquad \text{as well as} \qquad E_i = -b_s(\text{grad}\,\Psi_s)_i.$$

In particular, such functions are preferably selected in the RPR-method, with which the boundary conditions can be adhered to without difficulty, for exam-

ple, with Legendre polynomials. In the last years, however, it turned out that power functions of the type $\Phi(\boldsymbol{x})_s = x_1^\lambda x_2^\mu x_3^\nu$, after suitable normalization, are also capable to realize the boundary conditions in a straightforward way. The advantage of these power functions lies in the fact that they can be employed, in contrast to Legendre polynomials, with a multitude of simple specimen forms (spheres, ellipsoids, cylinders, cones etc.). If one selects certain limits for the positive exponents $\lambda$, $\mu$, $\nu$ in the form $\lambda + \mu + \nu \leq Q$ with $Q \approx 14$, one obtains a correspondingly large number of coefficients $a_{is}$ and $b_s$. For $L$ to take on an extreme value, all derivatives of $L$ with respect to these coefficients must vanish. This condition is equivalent to an eigenvalue problem, in which the eigenvalues correspond to the squares of resonance frequencies. Ultimately, we are dealing with the solution of an eigenvalue problem for which standard programs are available (for example, in the freely available LAPACK program library). If resonance frequencies are known, one can then determine the associated resonance states. Detailed presentations of these interrelationships are found in, for example, Leisure & Willis (1997) and Migliori & Sarrao (1997).

Fortunately, in the meantime, extended programs have been developed, which are also applicable to piezoelectric crystals. However, various supplements and improvements are still required, which we will, in part, comment more precisely below. Recently, Schreuer could show that the general approach, introduced above for the basic equations of piezoelectric crystals, is suitable for the quantitative description of the RUS spectrum. Conversely, from the resonance spectrum of a piezoelectric crystal, the components of its elasticity tensor as well as those of its piezoelectric tensor can be determined with high internal consistency (Schreuer, 2002). Only the dielectric constants are required as additional input. Thus a further important field of application arises from this new method.

Finally, let us point out certain advantages and disadvantages of the RUS method.

Advantages:

- Even in the case of triclinic crystals, one only needs a single specimen to completely determine the elasticity tensor. Its dimensions can be smaller than 1 mm provided that the required plane-parallelism is achieved, the dimensions are determined to sufficient accuracy and errors in orientation are minimized. This opens the possibility to investigate elastic properties of materials in abundance, which for lack of adequate crystal size could not be treated up till now with conventional methods.

- The influence of external conditions, for example, electric field, magnetic field, mechanical stress (including hydrostatic pressure) and temperature, can be directly investigated on such specimens. The associated effects arise from the shift of the resonance frequencies.

- Finally, phase transitions can be detected, especially second-order ones, from anomalies of the shift of resonance frequencies accompanied by a change in external parameters, above all, the temperature. Acoustic attenuation phenomena connected with these phase transitions can also be identified.
- Apart from the elasticity tensor, the piezoelectric tensor can be simultaneously determined without much additional effort, when the dielectric tensor is known.
- Already in the current state of development, data acquisition in the RUS method is largely automated, likewise the evaluation in the case of highly symmetric crystals and the selection of appropriate starting values for a least-squares method.

Disadvantages:

- The specimen must possess a very high quality, since even small inhomogeneities, especially surface defects, can sensitively interfere with the spectrum. Conversely, this circumstance can be used to investigate defects and their effects on elastic or piezoelectric quantities.
- With a parallelepiped, the high requirements with respect to plane-parallelism and the accuracy of orientation is only achieved with considerable effort in contrast, for example, with a plane-parallel plate with arbitrary side boundaries.
- With specimens of small dimensions, the danger exists that the boundary areas affected by the preparation falsify the spectrum as a consequence of mechanically induced inhomogeneities. Thus, especially with relatively soft crystals, the RUS method on very small specimens can be problematic.
- Experience in the evaluation of spectra of crystals of low symmetry has taught us that the starting data set for a least-squares method may only deviate a little from the true elasticity tensor (less than about 10%), in order to achieve convergence of the iteration. Hence, computing cycles with a wide variation of initial values are required to obtain a reliable solution. One must endeavor to make use of restrictions based on crystal-chemical, physical and mathematical reasoning to reduce computing time to an acceptable level.
- A barrier also arises from the necessity of a gap-free data set in the hitherto used programs. This problem is easily solved by modifying the programs used currently, however, at the cost of considerably higher computing time.

- Since the acoustic resonances extend over a large frequency interval, one must be prepared for certain dispersion effects leading to a limitation in the attainable accuracy. However, it is known that the maximum dispersion in the crystals investigated so far in the range between 0.1 and 2 MHz amounts to not much more than two percent.

- The individual components of the elasticity tensor cannot be directly determined. Rather, they appear first after the complete determination of the elasticity tensor. The same applies to the dependence of individual components on external parameters.

From these remarks it follows that after elimination of the mentioned difficulties, the RUS method will, in many areas, be superior to the other established methods for the investigation of elastic properties. Certain problems, for example, the change of elastic properties under uniaxial pressure, from which one can derive nonlinear elastic effects, presumably remain not suited for the RUS method.

#### 4. Brillouin Scattering

In the Schaefer–Bergmann method, the diffraction of light on elastic waves entering the crystal is observed. In contrast, Brillouin scattering is caused by the thermally excited elastic waves of the lattice. These waves (phonons) represent a substantial part of the thermal energy of a crystal lattice. They propagate in all directions. Their frequency spectrum depends on the temperature and the bonding properties of the lattice. The highest frequencies, or the shortest wavelengths of these waves are bounded by two factors. Each photon possesses an energy quantum with the energy content $E = h\nu$, where $h$ is Planck's constant and $\nu$ is the frequency of the photon. According to the equipartition theorem, each degree of freedom of the vibrating system will contribute, on average, the energy $kT/2$, where $k$ is Boltzmann's constant and $T$ temperature. This means that waves with frequencies higher than $kT/2h$ are comparatively weakly excited according to the requirements of a Boltzmann distribution $e^{-h\nu/kT}$. Furthermore, wavelengths of the thermally excited elastic waves are limited. They cannot be smaller than twice the interplanar spacing $d$ of the lattice in the respective propagation direction ($\lambda \geq 2d$ or $1/\lambda = |\boldsymbol{k}| \leq |\boldsymbol{h}|/2$ with $|\boldsymbol{h}| = 1/d$, where $\boldsymbol{h}$ is the normal of the lattice plane concerned).

This condition corresponds to the highest resonance frequency of a thin plate bounded by parallel lattice planes. The $\boldsymbol{k}$-vectors originating from the origin of the reference system are accordingly bounded by a surface derived from the metric of the associated elementary cell (first Brillouin zone).

Naturally, light quanta can be diffracted by the thermally excited waves just as on artificially generated sound waves as in the case of the Schaefer–Bergmann method. However, the thermally excited waves are by no means

monochromatic, so that only a few photons are found in a small frequency interval $\Delta\nu$. From the conservation of energy and momentum in an interaction between a phonon and a photon of the light wave, the possibility arises of measuring the frequency and wavelength of the phonon and thus the velocity of the elastic wave. The momentum of the incoming photons $h\boldsymbol{k}_0$ and the quasimomentum of the phonons $h\boldsymbol{k}_p$ sum to give the momentum of the scattered photon $h\boldsymbol{k}_e$: $\boldsymbol{k}_0 \pm \boldsymbol{k}_p = \boldsymbol{k}_e$ (momentum conservation). The energy is given by $E_0 \pm E_p = E_e$, hence, $\nu_0 \pm \nu_p = \nu_e$ and because $\nu_0\lambda_0 = c/n_0$ ($n$ refractive index, $c$ light velocity in vacuum) and $\nu_p\lambda_p = v$

$$\left|\frac{\nu_e - \nu_0}{\nu_0}\right| = \frac{v n_0 \lambda_0}{c\lambda_p} \qquad \text{(energy conservation).}$$

If one selects a suitable experimental arrangement so that $\lambda_0 \approx \lambda_p$, a crude estimation shows that

$$\left|\frac{\nu_e - \nu_0}{\nu_0}\right| \approx \frac{10^6 \cdot 1.5}{3 \cdot 10^{10}} = 10^{-4}/2,$$

i.e., the energy and hence, the magnitude of the momentum of incoming and scattered photons hardly differ. When $n_0 = n_e$, we can set $|\boldsymbol{k}_0| = |\boldsymbol{k}_e|$, thus giving Bragg's condition $2d \sin\vartheta = \lambda_0$ with $d = \lambda_p$. In the case of optical anisotropy, the following condition applies:

$$\frac{1}{\lambda_0^2} + \frac{1}{\lambda_e^2} - \frac{2}{\lambda_0'\lambda_e}\cos 2\vartheta = \frac{1}{\lambda_p^2},$$

obtained by taking the square of $\boldsymbol{k}_0 - \boldsymbol{k}_e = \boldsymbol{k}_p$. $n_0$ and $n_e$ are the refractive indices belonging to $\boldsymbol{k}_0$ and $\boldsymbol{k}_e$, respectively, and not the refractive indices of the ordinary or extraordinary wave!

The experimental determination of the propagation velocity of elastic waves is best done, in particular, by selecting a fixed angle between the primary direction of photons of an intensive laser beam and the direction of observation of the scattered photons, preferably $2\vartheta = 90°$ (so called 90°-geometry, to suppress effects of refraction, Fig. 4.51). Then $\lambda_p = \lambda_0/\sqrt{2}$, in case $\lambda_0 = \lambda_e$. The associated frequencies are obtained from high-resolution spectroscopic measurements of the scattered light. Aside from photons of frequency $\nu_0$ (Rayleigh scattering), one finds two lines with frequency $\nu_0 \pm \nu_p$, which can be measured, with not too much effort, to an accuracy of around 0.1%. Hence, one has $v = \nu_p\lambda_p$, the propagation velocity of the elastic wave in the given direction. According to past experimental findings, a noticeable dispersion of the propagation velocity of elastic waves first sets in at a wavelength smaller than about twenty times the lattice spacings, hence, roughly below about 50 nm. Since the wavelength of visible light, for example, in the green spectral region is about 500 nm one can assume that the measured $v$-values hardly deviate

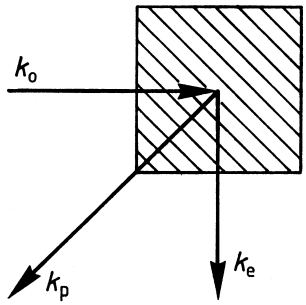


**Figure 4.51** Brillouin scattering under 90°-geometry. The photons incoming along $k_0$ appear to be reflected into the photons $k_e$ by the phonons propagating along $k_p$ (conservation of momentum and energy).

from the velocities observed with ultrasound methods at substantially lower frequencies. If one works with polarized laser light and takes into consideration the elastooptical effects of the elastic waves involved, one can, in favorable cases of higher symmetry, separately record the three possible wave types in each direction. Up to now, this method has been mainly applied to cubic crystals, in isolated cases also to orthorhombic and even to monoclinic crystals. Although the method does not achieve the precision of ultrasound measurements, it has gained particular importance because of the possibility of investigating relatively small crystals, most notably for the investigation of elastic properties under extreme pressure.

Related to the Brillouin scattering experiment just sketched are the so-called *stimulated Brillouin scattering* and its variants. If one fires an intensive laser beam (pulsed and focused) at a crystal that can withstand such a strong radiation exposure, the quadratic electrostrictive effect according to $\varepsilon_{ij} = d_{ijkl} E_k E_l$ produces a deformation, repeating itself periodically at a spacing of half the wavelength of the light wave, where $\boldsymbol{E}$ is the electric field of the light wave. Hence, the light wave generates phonons. These phonons can diffract the primary laser beam or even another laser beam entering at the correct scattering angle. We talk of stimulated Brillouin scattering in the case of back scattering of the primary laser light wave by these phonons. We then have $2\vartheta = 180°$, hence, $2\lambda_p = \lambda_0$. The difference in frequency of the scattered photons gives $\nu_p$ and thus the propagation velocity of the elastic waves. Whereas only a small fraction of the crystals tested so far could withstand the required high radiation exposure, more favorable conditions exist for the observation of diffraction, under oblique incidence, of a second laser beam on the phonons generated by the primary laser beam. In particular, this is also true when both pulsed light waves, time delayed, enter the crystal. In this way it is possible to derive the lifetime of the phonons concerned from the decay time of the scattered radiation (Eichler, 1977).

**5. Neutron Scattering**

With the development of intensive neutron sources, the scattering of neutrons has become one of the most attractive tools for the investigation of lattice dynamics. The scattering of neutrons on phonons also takes place under the conditions of momentum- or quasimomentum conservation and energy conservation. Consequently, the formal relationships are completely analogous to the Brillouin scattering just discussed. The experimental arrangement for the observation of neutron scattering is basically the same, albeit different in detail.

The first important problem is the generation of monochromatic neutrons. This occurs, for example, with the aid of time-of-flight spectrometers in the range of very slow neutrons or crystal monochromators, which reflect neutrons of discrete wavelengths through a fixed diffraction angle, similar to X-ray diffraction by constructive interference. Both methods are capable of continuously tuning the wavelength of the neutron wave over a wide range. The detection and frequency determination of the neutrons scattered by the crystal specimen is performed with time-of-flight spectrometers, crystal monochromators or scintillation detectors and related instruments. The effective $\boldsymbol{k}$-vectors of the phonons causing the scattering are fixed by adherence to a certain geometry for the primary and scattered neutron waves. The experimental evaluation, however, requires special efforts, since the wavelengths of the neutrons can change considerably in the scattering process. From the knowledge of $\lambda_0$, $\lambda_e$ and from the angle $2\vartheta$, one obtains the wavelength $\lambda_p$ of the phonons and from the change in energy of the neutrons, the frequency $\nu_p$ of the phonons and hence, the propagation velocity. Therefore, it is possible to measure the wave velocity and thus the dispersion of the phonons in a broad frequency- or wavelength range by rotating the crystal, varying the diffraction angle and the wavelength of the primary neutron wave. If one selects sufficiently short neutron wavelengths, then after a regular Bragg reflection at the lattice plane $\boldsymbol{h}$, a scattering by a phonon can follow. Then we have $\boldsymbol{k}_e = \boldsymbol{k}_0 + \boldsymbol{h} + \boldsymbol{k}_p$. The propagation vector $\boldsymbol{k}_e$ deviates from the Bragg direction. In this connection, one must not overlook the fact that multiple scattering processes can be superimposed on the neutron scattering discussed here, because each scattered neutron wave can act as a new primary wave. The low-frequency values obtained from the dispersion curves $\nu_p(\boldsymbol{k}_p)$ according to $v = \partial\nu_p/\partial|\boldsymbol{k}_p|$ at $|\boldsymbol{k}_p| = 0$ correspond to the acoustic sound velocities.

Figure 4.52 shows a phonon dispersion curve $\nu_p(\boldsymbol{k}_p)$. Since the length of the possible $\boldsymbol{k}$-vectors are limited by the lattice interplanar spacing ($\lambda/2 \geq d$), it is convenient to represent $\boldsymbol{k}_p$-vectors in the reciprocal lattice. The aforementioned first Brillouin zone mirrors this limitation of the $\boldsymbol{k}$-vectors. Specific symbols have been introduced for the notation of phonons of different propagation directions and lengths. An example is given in Fig. 4.53 for the cubic

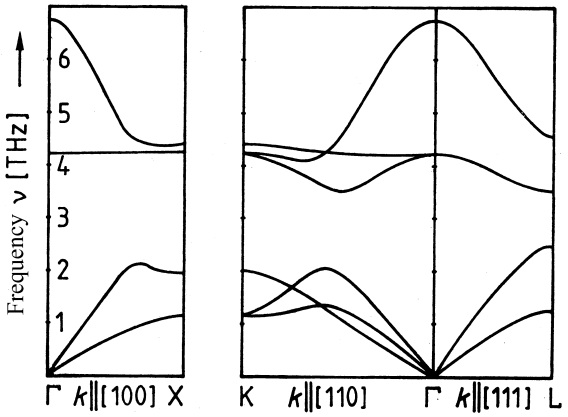


**Figure 4.52** Phonon dispersion curves of cubic RbCN at 300 K (Ehrhardt et al., 1980). The frequency ($\sim$ energy) of the phonons is recorded as a function of the length of the propagation vector $\boldsymbol{k}$. The curves starting from the Γ point represent the so-called acoustic branches. The linear region near Γ corresponds to the quasidispersion-free sound velocity. The other curves are called optical branches (see Fig. 4.53).

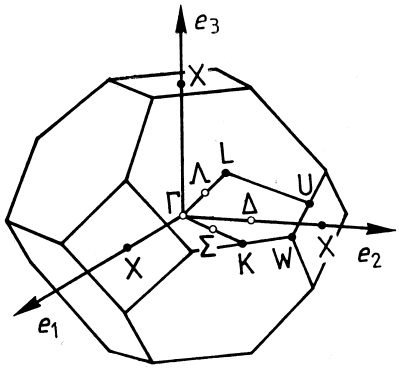


**Figure 4.53** Notation of phonons of a cubic face-centered lattice (first Brillouin zone). The inside points are designated by an empty circle, those at the border of the zone by a full circle.

face-centered lattice. Accordingly, a phonon at the Γ-point is equivalent to an infinite wavelength, i.e., it has the propagation velocity for the frequency 0 (acoustic part). The points at the boundary of the first Brillouin zone belong to the highest resonance frequencies of the lattice in the propagation direction leading from the Γ-point to the boundary point. The behavior of these characteristic vibrations of the lattice, subject to external parameters such as, pressure, temperature, electric and magnetic fields, plays an important role in the interpretation of the stability of the crystal lattice with respect to phase transitions.

**6. X-ray Scattering**

X-ray photons can, just like light photons in Brillouin scattering, interact with the thermally excited phonons of the crystal lattice. Since, in the case of X-rays, the relative change in frequency between the primary and scattered photons is even smaller than in Brillouin scattering and thus hardly measurable, and furthermore, the anisotropy of the refractive indices for X-rays can be fully ignored, $\boldsymbol{k}_0$ and $\boldsymbol{k}_e$ have, to a sufficient approximation, the same magnitude. Hence, the possibility of directly determining the frequency of the phonons involved in the scattering does not exist. One can gain information on the number of thermally excited phonons in certain frequency ranges from the intensity of the diffracted X-rays close to the Bragg reflections (thermally diffuse scattering). These phonons propagate approximately perpendicular to the Bragg direction. Hence, in the case of simply structured crystals, the application of a model for the frequency spectrum $Z_i(\boldsymbol{g}, \nu)$ of the phonons can help to obtain useful estimations of the propagation velocities dependent on the propagation direction $\boldsymbol{g}$ and the frequency. $Z_i(\boldsymbol{g}, \nu)d\nu$ is the number of phonons of the $i$th vibrational type ($i = 1, 2, 3$) in a frequency interval $d\nu$. The high expectations to receive precise data on elastic properties by such investigations (Wooster, 1962), even on very small crystals, were largely abandoned, because it turned out, that multiple processes make a reliable analysis nearly impossible. This became clear after a comparison of certain elastic constants of two orthorhombic crystals, namely, benzalazine and 1,3,5-triphenyl benzol, determined from thermal diffusion scattering and using ultrasound techniques (Joshi & Kashyap, 1964; Haussühl, 1965; Suresh Chandra & Hemkar, 1973; Haussühl, 1974). Conversely, one can calculate the intensity of thermal diffusion scattering from known elastic constants, neglecting multiple scattering processes. By comparing with experiment one can often draw interesting conclusions concerning anomalies of the phonon spectrum as well as on the existence of certain lattice defects.

The thermal motion of the lattice particles also has a strong influence on the effective scattering power of the atoms, described approximately with the help of the individual temperature factors (Debye–Waller factors). This thermal motion must be taken into account to obtain a firm determination of crystal structure. The evaluation of a large number of measured intensities $I(\boldsymbol{h})$ of reflections $\boldsymbol{h}$ allows, in many cases, statements on temperature factors. These data can contribute to the estimation of elastic properties and to the identification of anomalous dynamic processes, as, for example, observed in connection with phase transitions.

### 4.5.7 Strategy for the Measurement of Elastic Constants

To complete this section some advices are given for the strategy of determining elastic constants. Whereas simple measurement prescriptions can be provided for an efficient precise determination for crystals with high symmetry, hence, for example, for all crystals containing the PSG 2 or 22 as a subgroup, more extensive measurements are required for triclinic crystals. In any case, it is recommended to firstly concentrate the investigation of elastic waves propagating along the principal directions of the Cartesian reference system and their bisectors. If one succeeds in measuring all three wave types in each of these directions, that is, in a total of nine directions, one obtains for triclinic crystals 27 independent measurements, which should be sufficient for the determination of the 21 components of the elasticity tensor in centrosymmetric crystals. Further measurements in the direction of the four space diagonals of the Cartesian reference system contribute additional 12 independent data. With triclinic crystals, evaluation is conveniently performed using a computer program based on the least-squares method, which calculates a set of elastic constants from the elastodynamic basic equations giving the best agreement with the measured sound velocities.

The dynamic elasticity $\{E_{ij}\}$, a second-rank tensor invariant of the elasticity tensor discussed in Section 4.5 has proven useful for a control of the experimental values. The longitudinal effect $E'_{11}$ represents the sum of squares of the three wave velocities along $\boldsymbol{e}'_1 = u_{1i}\boldsymbol{e}_i$, multiplied by the density, hence, $E'_{11} = u_{1i}u_{1j}E_{ij} = \rho\sum_{s=1}^{3} v_s^2(\boldsymbol{e}'_1)$. Pairs of mutually perpendicular propagation directions $\boldsymbol{e}'_1$ and $\boldsymbol{e}'_2$ then obey

$$\sum_{s=1}^{3} v_s^2(\boldsymbol{e}'_1) + \sum_{s=1}^{3} v_s^2(\boldsymbol{e}'_2) = \sum_{s=1}^{3} v_s^2(\alpha\boldsymbol{e}'_1 + \beta\boldsymbol{e}'_2) + \sum_{s=1}^{3} v_s^2(\beta\boldsymbol{e}'_1 - \alpha\boldsymbol{e}'_2).$$

This relationship is taken directly from the plane principal axes transformation (see Section 4.3.2; $t_{ii} + t_{ij} = t'_{ii} + t'_{jj}$!). Thus, the sum of squares of all such pairs is constant as long as the associated propagation vectors lie in the plane spanned by $\boldsymbol{e}'_1$ and $\boldsymbol{e}'_2$. Accordingly, each of these equations enables a sensitive control for all such wave velocities.

With noncentric crystals, instead of $c^E_{ijkl}$, one must use the quantities $c^D_{ijkl}$, which, as we saw in Section 4.5.5, depend on the propagation direction. Here it is appropriate to separately measure the piezoelectric and dielectric tensors, and then with the help of approximate values for the components $c^E_{ijkl}$ arrive at an estimation of the differences $c^D_{ijkl} - c^E_{ijkl} = e_{mij}e_{nkl}g_m g_n / \epsilon^{\varepsilon}_{rs} g_r g_s$, where $e_{mij} = c^E_{ijst}d_{mst}$. $d_{mst}$ are the components of the piezoelectric tensor. Measurements of the coupling coefficients may also be useful. Approximate values for $c^E_{ijkl}$ are obtained from a first evaluation of the measurements of the prop-

agation velocities as in the case of centrosymmetric crystals, i.e., neglecting piezoelectric interactions. Even with large coupling coefficients of about 0.5 one achieves, after taking into account the piezoelectric correction, values of sufficient accuracy after only a few iteration steps (relative error for the principal constants $c_{iiii}$, $c_{iijj}$ and $c_{ijij}$ below 1%). As an example, we again cite the triclinic crystal lithium hydrogen oxalate-monohydrate. With the aid of the dielectric constants given in Section 4.3.3 and the piezoelectric constants determined by the methods discussed in Section 4.4.1, as well as the data of the measurements of a total of 34 propagation velocities in different directions and with different displacement vectors, the elasticity tensor could be completely determined (Haussühl, 1983). In doing so, however, measurements in other directions were included, which differed from those proposed, because the separate observation of the three possible wave types in each direction did not always succeed due to the strong coupling of the waves.

At this juncture, the necessity of an additional correction in crystals with strong pyroelectric effects must be pointed out (see Section 5).

Table 4.14 presents favorable measurement arrangements for an efficient determination of the components of the elasticity tensor and the associated solutions of the elastodynamic basic equations for nonpiezoelectric crystals. With the exception of triclinic crystals, the respective strategy allows an effortless determination of $c_{ijkl}$ without employing a computer. Of course, other data in nondistinct directions can be used. It is especially important to take care, that the position of the reference system in the crystal is unequivocally fixed. In many cases, as, for example, in the PSG 4/m or $\bar{3}$m it is not sufficient to alone obey the rule, introduced in Section 2.2 for the position of $\boldsymbol{e}_i$ with respect to the crystallographic basic vectors $\boldsymbol{a}_i$; rather an indication is required for which of the possible alternatives one has decided selecting a right-handed system (see exercise 8).

#### 4.5.7.1 **General Elastic Properties; Stability**

From the knowledge of the complete elasticity tensor one can derive all elastic material properties for arbitrary-shaped samples under any boundary conditions. This includes, for example, the propagation of surface waves or the calculation of elastic properties of pressed powders (see exercise 25) as well as the phenomena of refraction and reflection of sound waves. As mentioned in the introduction to this section, certain invariants, which are more easily accessible to discussion, as, for example, dynamic elasticity, linear compressibility under hydrostatic pressure, volume compressibility or the Debye temperature, deserve special interest. Even more complex properties, as, for example, the transversal contraction coefficient under uniaxial pressure or tension (Poisson's ratio), can be derived from these invariants with an accuracy hardly

**Table 4.14** Propagation directions $g$, displacement vectors $\xi$ and $\rho v^2$-values of distinct wave types in the Laue classes. $l$ pure longitudinal, $t$ pure transvere wave, $lt$ combination wave. For most other propagation directions the possible $\rho v^2$-values and $\xi$-vectors can only be calculated from the elastodynamic basic equations $(-\rho v^2 \delta_{ik} + c_{ijkl} g_j g_l)\xi_k = 0$ after part of the elastic constants are known.

| $g \parallel$ | $\xi \parallel$ | type | $\rho v^2$ |
|---|---|---|---|
| monoclinic (2/m; $e_2 \parallel 2$) | | | |
| $e_1$ | $e_2$ | t | $c_{66}$ |
| $e_1$ | $\xi \cdot e_2 = 0$ | lt | $\frac{1}{2}(c_{11}+c_{55}) \pm \frac{1}{2}\sqrt{(c_{11}-c_{55})^2+4c_{15}^2}$ |
| $e_2$ | $e_2$ | l | $c_{22}$ |
| $e_2$ | $\xi \cdot e_2 = 0$ | t | $\frac{1}{2}(c_{44}+c_{66}) \pm \frac{1}{2}\sqrt{(c_{44}-c_{66})^2+4c_{46}^2}$ |
| $e_3$ | $e_2$ | t | $c_{44}$ |
| $e_3$ | $\xi \cdot e_2 = 0$ | lt | $\frac{1}{2}(c_{33}+c_{55}) \pm \frac{1}{2}\sqrt{(c_{33}-c_{55})^2+4c_{35}^2}$ |
| $e_1 \pm e_3$ | $e_2$ | t | $\frac{1}{2}(c_{44}+c_{66} \pm 2c_{46})$ |
| $e_1 \pm e_3$ | $\xi \cdot e_2 = 0$ | lt | $\frac{1}{4}(c_{11}+c_{33}+2c_{55} \pm 2c_{15} \pm 2c_{35})$ $\pm\frac{1}{2}\sqrt{\frac{1}{4}(c_{11}-c_{33}\pm 2c_{15}\mp 2c_{35})^2+(c_{13}+c_{55}\pm c_{15}\pm c_{35})^2}$ |
| orthorhombic (2/mm) | | | |
| $e_i$ | $e_i$ | l | $c_{ii}$ |
| $e_i$ | $e_j$ $(i \neq j)$ | t | $c_{9-i-j,9-i-j}$ |
| $e_i \pm e_j$ | $e_k$ $(k \neq i,j)$ | t | $\frac{1}{2}(c_{9-i-k,9-i-k} + c_{9-j-k,9-j-k})$ |
| $e_i \pm e_j$ | $\xi \cdot e_k = 0$ $(k \neq i,j)$ | lt | $\frac{1}{4}(c_{ii}+c_{jj}+2c_{9-i-j,9-i-j})$ $\pm\frac{1}{2}\sqrt{\frac{1}{4}(c_{ii}-c_{jj})^2+(c_{ij}+c_{9-i-j,9-i-j})^2}$ |
| trigonal ($\bar{3}$) | | | |
| $e_3$ | $e_3$ | l | $c_{33}$ |
| $e_3$ | $\xi \cdot e_3 = 0$ | t | $c_{44} = c_{55}$ |
| trigonal ($\bar{3}2$/m; $e_1 \parallel 2$) | | | |
| $e_1$ | $e_1$ | l | $c_{11}$ |
| $e_1$ | $\xi \cdot e_1 = 0$ | t | $\frac{1}{2}(c_{44}+c_{66}) \pm \frac{1}{2}\sqrt{(c_{44}-c_{66})^2+4c_{14}^2}$ |
| $e_2$ | $e_1$ | t | $c_{66} = \frac{1}{2}(c_{11}-c_{12})$ |
| $e_2$ | $\xi \cdot e_1 = 0$ | lt | $\frac{1}{2}(c_{11}+c_{44}) \pm \frac{1}{2}\sqrt{(c_{11}-c_{44})^2+4c_{14}^2}$ |
| $e_3$ | $e_3$ | l | $c_{33}$ |
| $e_3$ | $\xi \cdot e_3 = 0$ | t | $c_{44} = c_{55}$ |
| $e_2 \pm e_3$ | $e_1$ | t | $\frac{1}{2}(c_{44}+c_{66} \pm 2c_{14})$ |
| $e_2 \pm e_3$ | $\xi \cdot e_1 = 0$ | lt | $\frac{1}{4}(c_{11}+c_{33}+2c_{44} \mp 2c_{14})$ $\pm\frac{1}{2}\sqrt{\frac{1}{4}(c_{11}-c_{33}\mp 2c_{14})^2+(c_{13}+c_{44}\mp c_{14})^2}$ |
| tetragonal (4/m) | | | |
| $e_1$ | $e_3$ | t | $c_{44} = c_{55}$ |
| $e_1$ | $\xi \cdot e_3 = 0$ | lt | $\frac{1}{2}(c_{11}+c_{66}) \pm \frac{1}{2}\sqrt{(c_{11}-c_{66})^2+4c_{16}^2}$ |
| $e_3$ | $e_3$ | l | $c_{33}$ |
| $e_3$ | $\xi \cdot e_3 = 0$ | t | $c_{44}$ |
| $e_1 \pm e_2$ | $e_3$ | t | $c_{44}$ |
| $e_1 \pm e_2$ | $\xi \cdot e_3 = 0$ | lt | $\frac{1}{2}(c_{11}+c_{66}) \pm \frac{1}{2}\sqrt{(c_{12}+c_{66})^2+4c_{16}^2}$ |

| $g \parallel$ | $\xi \parallel$ | type | $\rho v^2$ |
|---|---|---|---|
| tetragonal (4/mm), like 4/m with $c_{16} = 0$ | | | |
| $e_1 \pm e_3$ | $e_2$ | t | $\frac{1}{2}(c_{44} + c_{66})$ |
| $e_1 \pm e_3$ | $\xi \cdot e_2 = 0$ | lt | $\frac{1}{4}(c_{11} + c_{33} + 2c_{44})$ $\pm\frac{1}{2}\sqrt{\frac{1}{4}(c_{11} - c_{33})^2 + (c_{13} + c_{44})^2}$ |
| hexagonal (6/m und 6/mm) further $\infty$/m and $\infty$/mm | | | |
| $e_1$ | $e_1$ | l | $c_{11}$ |
| $e_1$ | $e_2$ | t | $c_{66} = \frac{1}{2}(c_{11} - c_{12})$ |
| $e_1$ | $e_3$ | t | $c_{44} = c_{55}$ |
| $e_3$ | $e_3$ | l | $c_{33}$ |
| $e_3$ | $\xi \cdot e_3 = 0$ | t | $c_{44} = c_{55}$ |
| $e_1 \pm e_3$ | $e_2$ | t | $\frac{1}{2}(c_{44} + c_{66})$ |
| $e_1 \pm e_3$ | $\xi \cdot e_2 = 0$ | lt | $\frac{1}{4}(c_{11} + c_{33} + 2c_{44})$ $\pm\frac{1}{2}\sqrt{\frac{1}{4}(c_{11} - c_{33})^2 + (c_{13} + c_{44})^2}$ |
| cubic (m3, 4/m3 | | | |
| $e_1$ | $e_1$ | l | $c_{11} = c_{22} = c_{33}$ |
| $e_1$ | $\xi \cdot e_1 = 0$ | t | $c_{44} = c_{55} = c_{66}$ |
| $e_1 \pm e_2$ | $e_3$ | t | $c_{44}$ |
| $e_1 \pm e_2$ | $e_1 \mp e_2$ | t | $\frac{1}{2}(c_{11} - c_{12})$ |
| $e_1 \pm e_2$ | $e_1 \pm e_2$ | l | $\frac{1}{2}(c_{11} + c_{12} + 2c_{44})$ |
| $e_1 \pm e_2 \pm e_3$ | $e_1 \pm e_2 \pm e_3$ | l | $\frac{1}{3}(c_{11} + 2c_{12} + 4c_{44})$ |
| $e_1 \pm e_2 \pm e_3$ | $\xi \cdot (e_1 \pm e_2 \pm e_3) = 0$ | t | $\frac{1}{3}(c_{11} - c_{12} + c_{44})$ |

achievable using straightforward static methods. Here, we shall merely discuss the mechanical stability criteria, giving a definite answer to the question, which ratios, at all, can the elastic constants take on in a stable crystal lattice. Firstly, we must demand that all quantities, which can be considered as elastic resistances, take on positive values, while otherwise, for example, even the smallest stress (tension) would suffice to contract or, under pressure, expand the crystal and thus violate the second law of thermodynamics. This means, for example, that the volume compressibility must always take on positive values, thus, for example, with cubic crystals, it must always be true $K = 3/(c_{11} + 2c_{12}) > 0$, i.e., $c_{11} > -2c_{12}$. Furthermore, all longitudinal effects must be positive, i.e., $c'_{11} > 0$ for arbitrary directions $e'_1 = u_{1i}e_i$. The same is true for Young's modulus in each direction $1/s'_{11}$. Moreover, all expressions derived for $\rho v^2$ from the elastodynamic basic equations must be positive. A number of these conditions for distinct directions is found in Table 4.14. For cubic crystals, we have, for example, $c_{11}$, $c_{44}$, $c_{11} - c_{12} > 0$, and hence $c_{11} > c_{12}$. Further, the determinant of $6 \times 6$ matrix of the elastic constants as well as their main adjuncts must take on positive values. This follows from the requirement that each change of a deformation component must be followed by a change of the corresponding stress component with the same sign. From the trend of the elastic constants as a function of temperature and uniaxial or

hydrostatic pressure, one can, with certain phase transition, in particular those of strongly second-order character, often observe a tendency to instability long before the transition is reached.

For example, certain wave velocities, on approaching a phase boundary, can continually decrease, causing the associated elastic resistances to become smaller, and in some cases nearly approach zero (elastic "soft modes"). Hence, to judge the stability, a knowledge of the temperature and pressure behavior of the elastic properties is of major importance. By virtue of the known rules concerning the $T$ and $P$ dependence of elastic constants in stable crystals, one can, in individual cases, recognize hints at possible phase transitions and characteristic changes in bonding coupled to elastic anomalies.

### 4.5.8 The Dependence of Elastic Properties on Scalar Parameters (Temperature, Pressure)

The quantities $dc_{ijkl}/dX$ can be determined from the measurement of the shift of resonance frequencies under the influence of an external parameter $X$ (temperature $T$ or pressure $P$) or by employing one of the other highly sensitive methods previously discussed.

If the relationship $\rho v^2 = f(c_{ijkl})$ is valid, the measured frequency shift, on account of $v = 2L\nu_m/m$, yields the following relation:

$$\frac{1}{f(c_{ijkl})}\frac{df(c_{ijkl})}{dX} = \frac{d\rho}{\rho dX} + \frac{2d\nu_m}{\nu_m dX} + \frac{2dL}{LdX}.$$

Instead of the differential quotients, one can also write the difference quotients, as occurring in the measurement. If $X$ is the temperature $T$, the first term represents the negative thermal volume expansion, and the last, the twofold linear thermal expansion. Similarly, in the case of pressure dependence, the first term represents the negative volume compressibility, and the last, the twofold linear compressibility. If one now carries out the measurements in the arrangements proposed in Table 4.14, one can determine the complete tensors $dc_{ijkl}/dX$. For the interpretation of these quantities it was found convenient to describe the temperature dependence by the *thermoelastic constants*

$$T_{ij} = \frac{dc_{ij}}{c_{ij}dT} = \frac{d\log c_{ij}}{dT}$$

and the pressure dependence by the *piezoelastic constants*

$$P_{ij} = \frac{dc_{ij}}{dp}.$$

$T_{ij}$ have the dimension (Grad Kelvin$^{-1}$), $P_{ij}$ are dimensionless. One observes only small variations of these quantities in groups of isotypic crystals with the same particle charge. The coefficients take on characteristic values for different structural types. If one considers other derivatives, this important fact for the crystal-chemical interpretation would not appear. As an example let us mention the temperature dependence of the reciprocal compressibility $dK^{-1}/dp$, a dimensionless quantity which takes on the value of around 5 in all stable crystals. This universal property deserves a more detailed discussion.

The temperature dependence of the given resonance frequency often plays a decisive role in the application of piezoelectric crystals for frequency generators and stabilizers in electrical engineering and electronics. From the relation given above we obtain the following conditions for a so-called *zero-cut* of the temperature $T$:

$$\frac{d\nu}{\nu dT} = \frac{df(c_{ijkl})}{2f(c_{ijkl})dT} - \frac{d\rho}{2\rho dT} - \frac{dL}{LdT} = 0.$$

This means, the temperature dependence of the given effective elastic constants $f(c_{ijkl})$ must be compensated for by the effects of thermal expansion contained in the second and third terms. This is satisfied by very few of the presently known crystal types, and only in certain distinct directions. For example, in $\alpha$-quartz perpendicular to the twofold axis, there exists a direction of a zero-cut of a transverse wave. By combining plates with opposite temperature behavior, it is possible to construct piezoelectric oscillators of $\alpha$-quartz possessing a frequency stability of $d\nu/\nu dT < 10^{-8}/\mathrm{K}$ over a wide temperature range. This property together with the excellent mechanical properties is the reason for the undisputed unique position of quartz for use in such devices.

In other applications, the temperature dependence of the resonance frequency of an oscillator is used to measure temperature. These devices (e.g., quartz thermometers) are not only highly sensitive, but also exhibit excellent stability in calibration. If the heat capacity of the oscillator is kept sufficiently small by miniaturization of the construction, one can employ these devices as radiation detectors and radiation measuring instruments.

### 4.5.9
### Piezooptical and Elastooptical Tensors

The change in refractive indices, i.e., the velocity of light, under the influence of an external mechanical stress or a deformation is described by *piezooptical* or *elastooptical tensors*. For the tensor representation of the optical properties, one selects, as with the electrooptical effect, the polarization tensor (see Section 4.4.2), whose components are interlinked with the refractive indices according

to $a_{ij} = (n_{ij})^{-2}$. To a first and mostly sufficient approximation, both effects are represented by

$$\Delta a_{ij} = q_{ijkl}\sigma_{kl} \quad (\{q_{ijkl}\} \text{ piezooptical tensor})$$
$$\Delta a_{ij} = p_{ijkl}\varepsilon_{kl} \quad (\{p_{ijkl}\} \text{ elastooptical tensor})$$

$\sigma_{kl}$ and $\varepsilon_{kl}$ are the components of the stress- and deformation tensor, respectively. From the symmetry of the stress- and deformation tensor it is found that $q_{ijkl} = q_{jikl} = q_{ijlk} = q_{jilk}$ and correspondingly $p_{ijkl} = p_{jikl} = p_{ijlk} = p_{jilk}$. At the end of this section we will return to a deviation from this symmetry. The number and type of independent components in the individual Laue classes was discussed in Section 4.5. The pair-wise permutation of the index positions is now not allowed. Thus the number of independent components compared to the elastic constants is substantially increased, for example, to 36 in triclinic crystals as against 21 in the elasticity tensor. Both tensors are not independent of one another, rather they carry over into each other according to $p_{ijkl} = q_{ijmn}c_{mnkl}$, as is easily seen by setting $\sigma_{mn} = c_{mnkl}\varepsilon_{kl}$.

#### 4.5.9.1 **Piezooptical Measurements**

The measurement of piezooptical effects can be performed according to the methods discussed in Section 4.4.2 (Electrooptics). The electrical field is now replaced by uniaxial or hydrostatic pressure. With perpendicular incidence, one obtains for the change in path difference of a plane parallel plate of thickness $L$

$$\Delta G = -\frac{L}{2}(n'^3_{jj}q'_{jjlm}\sigma'_{lm} - n'^3_{kk}q'_{kklm}\sigma'_{lm}) + (n'_{jj} - n'_{kk})Ls'_{iilm}\sigma'_{lm}$$

(summation is only over $l$ and $m$!).

The direction of radiation runs parallel $\boldsymbol{e}'_i$, and the direction of vibration of both waves parallel $\boldsymbol{e}'_j$ and $\boldsymbol{e}'_k$. To specify this relationship, we proceed in the same manner as with the electrooptical effect, i.e., under conditions of strong double refraction $(n'_{jj} - n'_{kk})$ we can neglect the rotation of the sectional ellipse by the piezooptical effect. We then describe the piezooptical effect in the Cartesian coordinate system $\{\boldsymbol{e}'_i, \boldsymbol{e}'_j, \boldsymbol{e}'_k\}$. In the case of degeneracy $n'_{jj} = n'_{kk}$, as, for example, in cubic crystals, the position of the sectional ellipse must be calculated taking into consideration the piezooptical effect. In the case of so called absolute measurements, the value for air (for example, $n'_{kk} \approx 1$, $q'_{kklm} = 0$) must be written for one of both waves. Knowledge of the elasticity coefficients $s'_{ijkl}$ is necessary for the evaluation of the measurements. These are calculated from the elastic constants by matrix inversion of the system $\sigma'_{ij} = c'_{ijkl}\varepsilon'_{kl}$. Furthermore, the aspects set forth in Section 4.4.2 (Electrooptics) are to be noted.

As with all optical measurements, one must set high demands on the optical quality of the specimens. Whereas with hydrostatic loads one can go to

very high pressure values, in the case of uniaxial stress one is usually limited to small loads of a few kp/cm$^2$ to prevent damaging the crystal due to inhomogeneous stress and plastic deformation. Reliable measurements of the change in the path difference can usually be achieved under these conditions, however, absolute measurements, made with the help of interferometers often cause quite a few problems because of the small effects involved. The sensitivity can be substantially improved by employing phase-lock techniques together with dynamic methods in which laud speaker membranes or a motor driven eccenter are used to transfer alternating pressure to the crystal. If one works with purely static or quasistatic methods, then the complete determination of the piezooptical tensor requires a certain number of absolute measurements. However, if elastooptical measurements are included then under favorable circumstances one can forgo absolute measurements and still achieve high accuracy. Because $p_{ijmn} = q_{ijkl}c_{klmn}$ one can feed the measured elastooptical values into the system of equations of $q_{ijkl}$ in order to obtain sufficient overdetermination for the solution. It is advantageous to use those elastooptical measurements combining minimal effort with high accuracy. We will return to this shortly.

For example, with the help of purely static methods employing uniaxial stress, the complete piezooptical tensor of monoclinic aminoethanesulfonic acid (Taurine) with its 20 independent components was determined (Haussühl & Uhl, 1969). Such measurements are more easily performed on optically inactive cubic crystals because of the low number of independent components (4 in PSG m3, 3 in PSG 4/m3) and because $n'_{jj} = n'_{kk} = n$. Table 4.15 presents the relationships for some important arrangements of cubic crystals.

If an optically active crystal type is present, then the interplay of induced double refraction and natural optical activity must be analyzed according to the aspects discussed in Section 4.3.6.8, whereby, to a first approximation it is assumed that the optical activity remains unchanged under the influence of mechanical stress. To what extent this assumption is correct is as yet not clearly resolved. No reliable measurements concerning the tensor $\Delta g_{ijk} = q_{ijklm}\sigma_{lm}$ are available which describe the change of optical activity under the influence of mechanical stress.

#### 4.5.9.2 **Elastooptical Measurements**

The *elastooptical* tensor is amenable to measurements via diffraction experiments as we have come to know from the Schaefer–Bergmann method or from Brillouin scattering. The elastic waves generate a periodic distortion in the crystal. The relation $a_{ij} = n_{ij}^{-2}$ leads to a measurable change in the refractive

**Table 4.15** Piezooptical and second-order electrooptical effects for some special directions in cubic crystals upon uniaxial stress along $e_1'(\sigma_{11}')$ or under the influence of an electric field along $e_1'(E_1')$. The light wave impinges perpendicularly onto the crystal surface, sample thickness in the direction $g \parallel e_i'$ of the incident light wave is $L$. $g$, $D'(\parallel e_j')$ and $D''(\parallel e_k')$ form a right coordinate system. In the case of the electrooptical effect, the coefficients $r_{ij}$ are assumed inplace of constants $q_{ij}$ (in Voigt notation).

| $\sigma_{11}'$ resp. $E' \parallel e_1'$ | $g \parallel e_i'$ | $D' \parallel e_j'$ | $D'' \parallel e_k'$ | $\left\{ \begin{array}{l} \Delta a_{jj}'/\sigma_{11}' \quad \text{resp.} \quad \Delta a_{jj}'/E_1' \\ \Delta a_{kk}'/\sigma_{11}' \quad \text{resp.} \quad \Delta a_{kk}'/E_1' \\ \Delta G/\sigma_{11}' \quad \text{resp.} \quad \Delta G/E_1' \end{array} \right.$ |
|---|---|---|---|---|
| [100] | [010] | [001] | [100] | $\left\{ \begin{array}{l} q_{31} = q_{12} \\ q_{11} \\ -Ln^3(q_{31} - q_{11})/2 \end{array} \right.$ |
| [100] | [001] | [100] | [010] | $\left\{ \begin{array}{l} q_{11} \\ q_{21} \\ -Ln^3(q_{11} - q_{21})/2 \end{array} \right.$ |
| [100] | [100] | [010] | [001] | $\left\{ \begin{array}{l} q_{21} \\ q_{31} = q_{12} \\ -Ln^3(q_{21} - q_{12})/2 \end{array} \right.$ |
| [110] | [110] | [001] | $[1\bar{1}0]$ | $\left\{ \begin{array}{l} (q_{12} + q_{21})/2 \\ (2q_{11} + q_{12} + q_{21} - 4q_{66})/4 \\ -Ln^3(-2q_{11} + q_{12} + q_{21} + 4q_{66})/8 \end{array} \right.$ |
| [110] | [001] | $[1\bar{1}0]$ | [110] | $\left\{ \begin{array}{l} (2q_{11} + q_{12} + q_{21} - 4q_{66})/4 \\ (2q_{11} + q_{12} + q_{21} + 4q_{66})/4 \\ Ln^3 q_{66} \end{array} \right.$ |
| [110] | $[1\bar{1}0]$ | [110] | [001] | $\left\{ \begin{array}{l} (2q_{11} + q_{12} + q_{21} + 4q_{66})/4 \\ (q_{12} + q_{21})/2 \\ -Ln^3(2q_{11} - q_{12} - q_{21} + 4q_{66})/8 \end{array} \right.$ |
| [111] | [111] | $[1\bar{1}0]$ | $[11\bar{2}]$ | $\left\{ \begin{array}{l} (q_{11} + q_{12} + q_{21} - 2q_{66})/3 \\ (q_{11} + q_{12} + q_{21} - 2q_{66})/3 \\ 0 \end{array} \right.$ |
| [111] | [110]*) | [112]*) | [111] | $\left\{ \begin{array}{l} (q_{11} + q_{12} + q_{21} - 2q_{66})/3 \\ (q_{11} + q_{12} + q_{21} + 4q_{66})/3 \\ Ln^3 q_{66} \end{array} \right.$ |

*) The same result is obtained for arbitrary directions perpendicular to [111].

indices according to

$$\Delta n_{ij} = -(n_{ij})^3 \Delta a_{ij}/2.$$

The diffraction geometry is determined by the conservation of the quasimomentum (see Section 4.5.6). Energy conservation induces a change in the frequency of the diffracted photons. The intensity of the diffracted light wave can be calculated in a similar manner as the diffraction of X-rays on a grating. It is

$$I = I_0 L^2 (\Delta n_{ij})_{\text{eff}}^2 K,$$

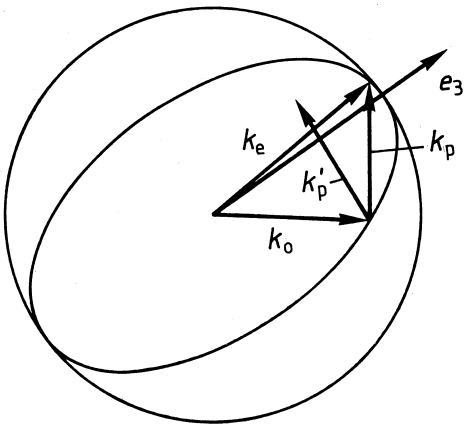


**Figure 4.54** Geometrical construction of the diffraction of a light wave with propagation vector $\boldsymbol{k}_0$ using phonons with a propagation vector $\boldsymbol{k}_p$ analogosly to the Ewald construction. Here, the propagation sphere is replaced by an index surface scaled by a factor of $1/\lambda_0$ (where $\lambda_0$ denotes the vacuum wavelength) which indicates the allowed propagation vectors for each direction. For quasi-infinite crystals, no diffraction is possible unless the propagation vector $\boldsymbol{k}_p$, starting at the tip of the vector $\boldsymbol{k}_0$, ends on this surface. The interference and dynamical effects observed for crystals with a sufficiently small ratio of transmission path length to acoustical wavelength are completely analogous to those in electron diffraction in thin crystals (see, e.g., *Kristallstrukturbestimmung*). The illustration shows an optically uniaxial crystal with an optical axis $\parallel \boldsymbol{e}_3$, $\boldsymbol{k}_0$ and $\boldsymbol{k}_p$ in the drawing plane.

where $(\Delta n_{ij})_{\text{eff}}$ is the effective Fourier coefficient of the optical phase grating and $L$ is the length of the optical path. $K$ is a constant taking into account the respective unique experimental arrangement.

In the concrete case of an arbitrary plane elastic wave strict conditions must be adhered to for the direction of the primary wave to even make diffraction possible. The propagation vectors $\boldsymbol{k}_0$ of the optic wave and $\boldsymbol{k}_p$ of the acustic wave define the diffraction plane. The intercept of this plane with the indicatrix shows whether a propagation direction exists at all which guarantees momentum conservation. The permissible vectors $\boldsymbol{k}_e$ of the diffracted wave must lie on the given sectional ellipse (Fig. 4.54). This corresponds to the Ewald construction. The calculation of the effective Fourier coefficients is only readily feasible in a few distinct cases. We will return to this experimentally important arrangement later.

First we have to clarify another aspect regarding the true symmetry of the elastooptical tensors. Nelson & Lax (1970) have pointed out that the generally accepted valid relationship $\Delta a_{ij} = p_{ijkl}\varepsilon_{kl}$ must be amended. Namely, in certain cases, the general relation

$$\Delta a_{ij} = p_{ijkl}\frac{\partial \xi_k}{\partial x_l}$$

is written, i.e., the rotational part

$$r_{ij} = \frac{1}{2}\left(\frac{\partial \xi_i}{\partial x_j} - \frac{\partial \xi_j}{\partial x_i}\right)$$

of the distortion vector

$$\frac{\partial \xi_i}{\partial x_j} = \varepsilon_{ij} + r_{ij}$$

may not be neglected. In pure longitudinal waves $r_{ij} = 0$. In contrast, elastic waves with strong transverse components cause a periodic rotational motion of the volume element, which can lead to a periodic change of the effective refractive indices for certain propagation directions. This contribution to the elastooptical effect can be calculated directly from the refractive indices as follows. A rigid rotation of the indicatrix is linked to the rotation of the volume element. The rotation of a vector $\boldsymbol{x}$ is described by $x_i' = x_i + r_{ik}x_k = u_{ik}x_k$ with $u_{ik} = \delta_{ik} + r_{ik}$ ($\delta_{ik}$ is the Kronecker symbol). The rotation of the polarization tensor $\{a_{ij}\}$, noted in the crystal-physical coordinate system, is obtained by tensor transformation with the transformation matrix $(u_{ik})$ : $a_{jj}' = u_{ik}u_{jl}a_{kl}$. The contribution to the elastooptical effect is then

$$\Delta_r a_{ij} = a_{ij}' - a_{ij} = u_{ik}u_{jl}a_{kl} - a_{ij}.$$

With $u_{ik} = \delta_{ik} + r_{ik}$ we get

$$\Delta_r a_{ij} = (\delta_{ik} + r_{ik})(\delta_{jl} + r_{jl})a_{kl} - a_{ij} = r_{ik}a_{kj} + r_{jl}a_{il},$$

whereby the quadratic term with the factor $r_{ik}r_{jl}$ was neglected. Due to the fact that $r_{ik} = -r_{ki}$ and with the help of the index commutation relation $r_{ki} = \delta_{il}r_{kl}$, we come to the following representation:

$$\Delta_r a_{ij} = (a_{il}\delta_{jk} - a_{kj}\delta_{il})r_{kl}.$$

In order to estimate the consequence of this change, we go into the optical principal axis system where $a_{ij} = 0$ for $i \neq j$. This gives $\Delta_r a_{ii} = 0$ and for $i \neq j$:

$$\Delta_r a_{ij} = (a_{jj} - a_{ii})r_{ij} = \left(\frac{1}{n_{jj}^2} - \frac{1}{n_{ii}^2}\right)r_{ij},$$

where $n_{jj}$ and $n_{ii}$ are the principal refractive indices. We then obtain for the general elastooptical effect in this coordinate system

$$\Delta a_{ij} = p_{ijkl}\varepsilon_{kl} + (a_{jj} - a_{ii})r_{ij}.$$

The second term, in the meantime designated as optorotation, delivers only in certain cases a measurable contribution. In cubic crystals and in crystals with small double refraction, optorotation is not or hardly measurable. Pure longitudinal waves do not generate optorotation.

Accordingly, optorotational effects are only expected with waves possessing strong transverse components in crystals with large double refraction. In such crystals, as seen in the examples of rutile and calcite, they can exceed the usual elastooptical effects a multiple of times. In any case the allowance of optorotation with knowledge of the distortion vector is unproblematic. Optorotation then plays a subordinate role for the measurement of elastooptical constants when the light wave is transmitted within a principal plane of the indicatrix and one stays in the range of small diffraction angles of maximum one degree. The orientation of the sectional ellipses for the primary and diffracted light waves then remain unaltered. Because $\Delta_r a_{ii} = 0$ the respective refractive indices do not experience any measurable change due to optorotation.

Another complication appears in piezoelectric crystals when elastic waves are accompanied by an electric field producing an electrooptical effect. As we have seen in Section 4.5.5, the electric field of an elastic wave can be described to sufficient approximation by

$$E_m = -(\text{grad}\,\phi)_m = -2\pi i k_m \phi \quad \text{mit} \quad \phi = \phi_0 e^{2\pi i(\boldsymbol{k}\cdot\boldsymbol{x}-\nu t)}.$$

$\boldsymbol{E}$ then runs parallel to the propagation direction $\boldsymbol{g} = \boldsymbol{k}/|\boldsymbol{k}|$. From the conditions

$$D_l = e_{lmn}\varepsilon_{mn} + \epsilon^{\varepsilon}_{lm} E_m \quad \text{and} \quad \boldsymbol{D}\cdot\boldsymbol{k} = 0$$

we obtain

$$D_l g_l = e_{lmn}\varepsilon_{mn} g_l - \epsilon^{\varepsilon}_{lm} 2\pi i k_m g_l \phi = 0$$

and hence, an expression for f $\phi$ and

$$E_k = -2\pi i (g_k/\lambda)\phi = -e_{lmn}\varepsilon_{mn} g_l g_k / \epsilon^{\varepsilon}_{rs} g_r g_s.$$

The expression $\epsilon^{\varepsilon}_{rs} g_r g_s$ represents the effective dielectric constant in the propagation direction $\boldsymbol{g}$. With this electric field we expect an electrooptical effect superimposed on the normal elastooptical effect:

$$\Delta a''_{ij} = r_{ijk} E_k = -r_{ijk} e_{lmn}\varepsilon_{mn} g_l g_k / \epsilon^{\varepsilon}_{rs} g_r g_s.$$

This contribution can be calculated from the dielectric, piezoelectric and electrooptical tensors when the propagation direction is given and the distortion vector is known. It is proportional to the amplitude of the elastic wave and

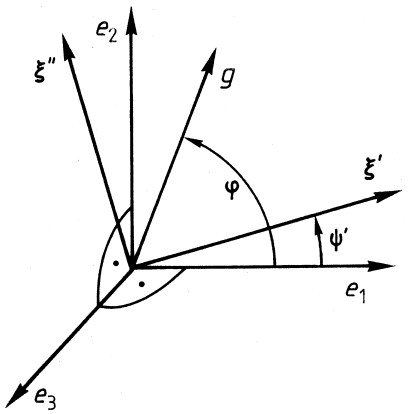


**Figure 4.55** Derivation of the change of the indicatrix of cubic crystals under the influence of sound waves. $g$ is the direction of propagation of the sound wave, and $\xi'$ and $\xi''$ are the corresponding distortion vectors in the plane perpendicular to $e_3$.

thus superimposes itself with the respective fixed part of the normal elastooptical effect. An estimation for $\alpha$-quartz with its small piezoelectric and electrooptical constants shows that the contribution in this case remains far under 1% of the normal elastooptical effect for each propagation direction. In crystals with high piezoelectric and electrooptical effects, as, for example, $\alpha$-iodic acid or $\alpha$-$LiIO_3$, one can count on substantial contributions of the elastooptical effect. This can be of advantage in practice (see below).

We now want to discuss some proven methods. Mueller (1938) showed that one can derive statements on the elastooptical constants from the state of polarization of the diffracted light. These methods are mainly suited for cubic crystals and for directions of optical axes of anisotropic crystals.

Let us consider the concrete case of an optical inactive cubic crystal cut in the form of a rectangular parallelepiped with light transmitted in approximately perpendicular incidence parallel [001]. The elastic waves generated by the elastooptical effect shall propagate in the plane (001), hence perpendicular to the light ray. The normalized propagation vector of the elastic wave is $\boldsymbol{g} = g_i \boldsymbol{e}_i = \cos\varphi \boldsymbol{e}_1 + \sin\varphi \boldsymbol{e}_2$ (Fig. 4.55). The direction of the distortion vectors of the elastic waves is gained, as discussed, from the electrodynamic basic equations when we insert the associated propagation velocities. From

$$(-\rho v^2 \delta_{ik} + c_{ijkl} g_j g_l)\xi_k = 0$$

we obtain for cubic crystals

$$\begin{vmatrix} -\rho v^2 + c_{11}g_1^2 + c_{44}g_2^2 & (c_{12}+c_{44})g_1 g_2 & 0 \\ (c_{12}+c_{44})g_1 g_2 & -\rho v^2 + c_{11}g_2^2 + c_{44}g_1^2 & 0 \\ 0 & 0 & -\rho v^2 + c_{44} \end{vmatrix} = 0.$$

As a result we get

$$\rho v'^2 \quad \text{or} \quad \rho v''^2 = \frac{c_{11}+c_{44}}{2} \pm \frac{1}{2}\sqrt{(c_{11}-c_{44})^2(g_1^2-g_2^2)^2 + 4(c_{12}+c_{44})^2 g_1^2 g_2^2}$$

and $\rho v'''^2 = c_{44}$.

For the associated distortion vectors, one finds

$$\left(\frac{\xi_1}{\xi_2}\right)' \quad \text{resp.} \quad \left(\frac{\xi_1}{\xi_2}\right)'' = \frac{\rho v'^2 \ (\text{or } \rho v''^2) \ - c_{11}g_2^2 - c_{44}g_1^2}{(c_{12}+c_{44})g_1 g_2}$$
$$= \cot\psi' \quad \text{resp.} \quad \cot\psi'', \qquad \text{with} \quad \psi = \angle(\boldsymbol{\xi}, \boldsymbol{e}_1),$$

furthermore,

$$\xi_3' = \xi_3'' = 0 \quad \text{as well as} \quad \xi_1''' = \xi_2''' = 0,$$

Since $\boldsymbol{\xi}'$ and $\boldsymbol{\xi}''$ are mutually perpendicular, $\tan\psi'' = -\cot\psi'$. The notation $'$ or $''$ specifies the faster or slower of both waves, respectively. We require the associated components of the deformation tensor to calculate the elastooptical effect. Let

$$\boldsymbol{\xi}' = \boldsymbol{\xi}_0' e^{2\pi i(\boldsymbol{k}\cdot\boldsymbol{x}-\nu t)} = C'\cos\psi'\boldsymbol{e}_1 + C'\sin\psi'\boldsymbol{e}_2$$

the same applies with $\boldsymbol{\xi}''$.

With

$$k_1 = \frac{1}{\lambda}\cos\varphi \quad \text{and} \quad k_2 = \frac{1}{\lambda}\sin\varphi$$

we have

$$\begin{aligned}
\varepsilon_{11}' &= \frac{\partial\xi_1}{\partial x_1} = 2\pi i k_1'\xi_1' = A'\cos\varphi\cos\psi',\\
\varepsilon_{22}' &= A'\sin\varphi\sin\psi',\\
\varepsilon_{12}' &= \frac{1}{2}\left(\frac{\partial\xi_1'}{\partial x_2} + \frac{\partial\xi_2'}{\partial x_1}\right) = \frac{A'}{2}(\cos\psi'\sin\varphi + \sin\psi'\cos\varphi) = \frac{A'}{2}\sin(\varphi+\psi'),\\
\varepsilon_{11}'' &= -A''\cos\varphi\sin\psi',\\
\varepsilon_{22}'' &= A''\sin\varphi\cos\psi',\\
\varepsilon_{12}'' &= \frac{A''}{2}\cos(\varphi+\psi'),\\
\varepsilon_{23}' &= \varepsilon_{13}' = \varepsilon_{23}'' = \varepsilon_{13}'' = 0,\\
\varepsilon_{22}''' &= \varepsilon_{12}''' = 0.
\end{aligned}$$

The sectional ellipse perpendicular [001] experiences the following change:

$$\begin{aligned}
\Delta a'_{11} &= p_{1111} A' \cos\varphi \cos\psi' + p_{1122} A' \sin\varphi \sin\psi', \\
\Delta a'_{22} &= p_{2211} A' \cos\varphi \cos\psi' + p_{1111} A' \sin\varphi \sin\psi', \\
\Delta a'_{12} &= p_{1212} A' \sin(\varphi + \psi'), \\
\Delta a''_{11} &= -p_{1111} A'' \cos\varphi \sin\psi' + p_{1122} A'' \sin\varphi \cos\psi' \\
\Delta a''_{22} &= -p_{2211} A'' \cos\varphi \sin\psi' + p_{1111} A'' \sin\varphi \cos\psi' \\
\Delta a''_{12} &= p_{1212} A'' \cos(\varphi + \psi').
\end{aligned}$$

The wave $\rho v^2 = c_{44}$, distortion vector parallel [001], does not contribute to the elastooptical effect for this sectional ellipse. We now inquire as to the position of the principal axes of this sectional ellipse noted in our crystal–physical coordinate system. The plane principal axis transformation (see Section 4.3.2) delivers

$$\tan 2\vartheta' = \frac{2\Delta a'_{12}}{a'_{11} - a'_{22}} = 2p_{1212} \sin(\varphi + \psi') / (p_{1111} \cos(\varphi + \psi') + p_{1122} \sin\varphi \sin\psi' - p_{2211} \cos\varphi \cos\psi')$$

and

$$\tan 2\vartheta'' = -2p_{1212} \cos(\varphi + \psi') / (p_{1111} \sin(\varphi + \psi') - p_{1122} \sin\varphi \cos\psi' - p_{2211} \cos\varphi \sin\psi').$$

In crystals of PSG 43, $\bar{4}3$ and 4/m3 we have $p_{1122} = p_{2211}$, so that

$$\tan 2\vartheta' = 2p_{1212} \tan(\varphi + \psi') / (p_{1111} - p_{1122})$$

and

$$\tan 2\vartheta'' = -2p_{1212} \cot(\varphi + \psi') / (p_{1111} - p_{1122}).$$

If one knows the angles $\vartheta'$ and $\vartheta''$ for both elastic waves belonging to an arbitrary angle $\varphi$, then the product of both equations delivers

$$\tan 2\vartheta' \tan 2\vartheta'' = -4p_{1212}^2 (p_{1111} - p_{1122})^{-2},$$

an expression independent of the angles $\varphi$ nd $\psi'$, and hence, amenable to observation without their knowledge.

The position of the sectional ellipse does not depend on the amplitude of the elastic waves. The diffracted light waves possess directions of vibration parallel to the principal axes of the respective sectional ellipse. If one selects the direction of vibration of the incoming light wave parallel to one of the principal axes, then the diffracted light wave also has the same direction of

vibration. This allows the measurement of the direction of vibration. If the crystal is placed between a pair of rotatable crossed polarizers the extinction position directly yields the angles $\vartheta'$ and $\vartheta''$. If one works with the Schaefer–Bergmann method, then all elastic waves with arbitrary propagation directions perpendicular to the direction of transmission are virtually continuously excited at the same time. It is especially advantageous to furnish the probe with a "gothic arch" grind as mentioned in Section 4.5.6, so as to generate a sufficiently intensive sound field with a minimum of sound power. For each angle $\varphi$ one then has the two diffraction spots with the angles of the semiaxes $\vartheta'$ and $\vartheta''$. The associated angles $\psi'$ and $\psi''$ of the distortion vectors are found from the angle $\varphi$ and the elastic constants taken from the formula above. Hence, all the coefficients of the above-mentioned homogeneous linear equations for $p_{1212}$, $p_{1111}$, $p_{1122}$ and $p_{2211}$ may be determined.

A second assertion on elastooptical coefficients is easily accessible with the observation of pure longitudinal waves propagating in the directions [100] or [110]. These longitudinal waves generate, as seen in the derivation above, a sectional ellipse whose principal axes run parallel and perpendicular to the propagation directions $\boldsymbol{g}$ of the longitudinal wave. Consequently, we obtain two components of the diffracted light, one parallel to the propagation direction and one vibrating perpendicular to this. Both components combine to form a linear polarized wave, whose direction of vibration arises from the amplitudes of the components. It is

$$\cot\zeta = A_{\mathrm{I}}/A_{\mathrm{II}},$$

whereby both directions of vibration are specified by $\boldsymbol{e}_{\mathrm{I}}$ and $\boldsymbol{e}_{\mathrm{II}}$. If the light wave is incident, as before, perpendicular to the propagation direction of the longitudinal wave and a polarizer is placed in front of the crystal in a position diagonal to $\boldsymbol{e}_{\mathrm{I}}$ and $\boldsymbol{e}_{\mathrm{II}}$ so that the components of the primary wave vibrating in $\boldsymbol{e}_{\mathrm{I}}$ and $\boldsymbol{e}_{\mathrm{II}}$ have the same amplitude, one obtains the following $A_{\mathrm{I}}/A_{\mathrm{II}}$-values for the diffracted waves:

| $\boldsymbol{e}_{\mathrm{I}} \parallel$ | $\boldsymbol{e}_{\mathrm{II}} \parallel$ | $\boldsymbol{g} \parallel$ | $A_{\mathrm{I}}/A_{\mathrm{II}} = \cot\zeta$ |
|---|---|---|---|
| [100] | [010] | [100] | $p_{1111}/p_{2211}$ |
| [100] | [001] | [100] | $p_{1111}/p_{1122}$ |
| [110] | [$\bar{1}$10] | [110] | $\dfrac{(2p_{1111}+p_{1122}+p_{2211}+4p_{1212})}{(2p_{1111}+p_{1122}+p_{2211}-4p_{1212})}$ |

The extinction position of the light diffracted due to the pure longitudinal wave is measured with the help of a rotatable analyzer. Thus one has $\zeta$ and the associated $A_{\mathrm{I}}/A_{\mathrm{II}}$-values when the polarizer is in the diagonal position. Again, one must ensure that no higher order diffraction effects come into play which superimpose on the first order diffraction. The method can also be applied along the directions of optical isotropy in noncubic crystals, whereby the valid electrooptical relationships are to be employed.

A useful method based on the measurement of the intensity of the diffracted light wave was first presented by Bergmann and Fues (1936). The incident light wave, before entering the probe, is decomposed into two mutually perpendicular vibrating components of equal intensity with the aid of a Wollaston prism, whereby both partial waves experience a spatial separation. The directions of vibration are adjusted parallel to the semiaxes of the sectional ellipse. Simultaneous measurements of the intensity of both diffracted waves—using a photographic plate or photo detector—ensure that during the measurement the same sound amplitude is effective in both directions of vibration. Hence, $I_\mathrm{I}/I_\mathrm{II} = (A_\mathrm{I}/A_\mathrm{II})^2$. For cubic crystals, the values $A_\mathrm{I}/A_\mathrm{II}$ given above apply. The method can also be employed for noncubic crystals when the position of the semiaxes of the sectional ellipse is independent of the amplitude of the elastic wave. In this case the intensity ratio is

$$\frac{I_\mathrm{I}}{I_\mathrm{II}} = \left(\frac{\Delta n_\mathrm{I}}{\Delta n_\mathrm{II}}\right)^2 = \frac{n_\mathrm{I}^6}{n_\mathrm{II}^6}\frac{p_\mathrm{I}^2}{p_\mathrm{II}^2},$$

where $n_\mathrm{I}$, $n_\mathrm{II}$ and $p_\mathrm{I}$, $p_\mathrm{II}$ are the effective refractive indices and effective elastooptical constants respectively, which for the given elastic wave and the effective sectional ellipse are calculated by tensor transformation.

The measurement accuracy can be decisively increased by employing lock-in amplifiers. Instead of the Wollaston prism it is convenient to use a switchable mechanical or electrooptical polarizer, to alternately drive the polarization of the primary light wave with a fixed frequency in both directions of vibration. in this manner, it is possible to measure the intensity ratio of both diffracted light waves to an accuracy of around 1 per mill without further measures. A related method, which even enables the direct determination of individual elastooptical coefficients referred to a standard crystal, was developed by Dixon & Cohen (1966). A standard crystal, for example, a plane parallel rectangular plate of quartz glass is attached to the test object by means of a suitable liquid. Short sound pulses with a fixed repetition rate are first transmitted through the test object then through the standard crystal and after reflection on the free face again back into the test object (Fig. 4.56). Now, if a light wave is sent into the test object and simultaneously another light wave into the standard crystal one obtains, per transit path of the elastic wave train 4 diffracted light flashes: 1. from the test object, 2. from the standard crystal, 3. again from the standard crystal after the reflection and 4. from the test object after the wave train re-enters. The length of the elastic wave train is so adjusted that the incoming wave and the reflected wave do not superimpose. From the ratio of the intensities of the 1. and 4. flashes of light one can determine the attenuation coefficient $Z$ of the amplitude of the wave train passing through the boundary faces test object-standard crystal using $I_4/I_1 = Z^4$. This assumes that $I_2 = I_3$, that is, no reflection losses appear at the free faces of the

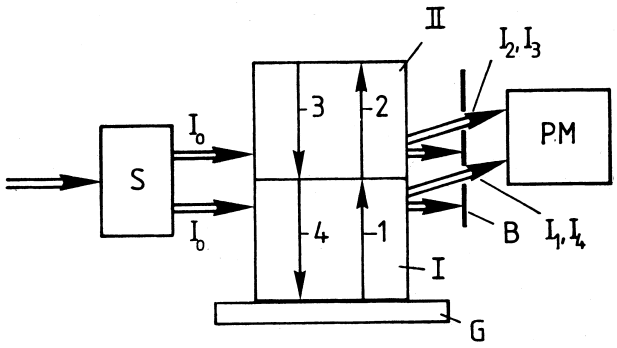


**Figure 4.56** Illustration of the Dixon & Cohen method for approximately perpendicular incidence (low acoustic frequency). G Sound generator, I crystal, II standard crystal (e.g., quartz), S beam splitter, B aperture to eliminate primary light rays, PM photomultiplier. 1, 2, 3, and 4 denote the paths of the acoustic pulse through the arrangement of test object and standard crystal.

standard crystal. For test object (I) and standard crystal (II) we then have

$$I_{\mathrm{I}} = K I_{\mathrm{I}0} n_{\mathrm{I}}^6 p_I^2 \xi_{\mathrm{I}0}^2 / \rho_{\mathrm{I}} v_{\mathrm{I}}^3$$

and

$$I_{\mathrm{II}} = K I_{\mathrm{II}0} n_{\mathrm{II}}^6 p_{\mathrm{II}}^2 \xi_{\mathrm{II}0}^2 / \rho_{\mathrm{II}} v_{\mathrm{II}}^3,$$

where $I_{\mathrm{I}0}$ and $I_{\mathrm{II}0}$ are the intensities of the primary light waves in test object (I) and in standard crystal (II). $|\boldsymbol{\xi}_{\mathrm{II}0}| = Z|\boldsymbol{\xi}_{\mathrm{I}0}|$ is true for amplitudes of the elastic waves in I and II. Hence, one obtains for the effective elastooptical coefficients

$$\frac{p_{\mathrm{I}}^2}{p_{\mathrm{II}}^2} = \frac{I_{\mathrm{I}}(I_1/I_4)^{1/2} I_{\mathrm{II}0} \rho_{\mathrm{I}} v_{\mathrm{I}}^3 n_{\mathrm{II}}^6}{I_{\mathrm{II}} I_{\mathrm{I}0} \rho_{\mathrm{II}} v_{\mathrm{II}}^3 n_{\mathrm{I}}^6}.$$

The assumption is made here that the transmission lengths in I and II are the same and that the wave type does not change during its travel through I and II. This only applies to pure longitudinal- and transverse waves, whose wave normal is perpendicular on the boundary face. At higher diffraction angles, the dependence of the transmission length on the angle of diffraction must be taken into account (Dixon, 1967).

As indicated above, the combination of static piezooptical and dynamic elastooptical methods opens the possibility for the complete determination of tensors, with high accuracy, even in crystals of low symmetry. Thus one can forgo measurements difficult to access or afflicted with large errors, as, for example, "absolute measurements."

To estimate elastooptical and piezooptical constants of cubic crystals, and to a certain extent crystals of low symmetry, we can draw upon the Lorentz–Lorenz relationship

$$\frac{(n^2-1)}{(n^2+2)} = \frac{\rho}{M}R,$$

where $R$ designates the specific refraction (mole refraction) of the substances (see Section 4.3.6.9).

From experiments it is found that the specific refraction is a combination of the quasiadditive contributions of the ions or atoms, which are only weakly dependent on the structural surroundings. Since $\rho =$ mole weight/mole volume, one can crudely estimate the change in the refractive index due to a change of the mole volume brought about by hydrostatic pressure. We will return to this question in Exercise 13.

Finally, we wish to point out the technological importance gained by elastooptical devices as deflectors or modulators of light. The deflection of light can be controlled by diffraction on elastic waves with variable frequency because the diffraction angle is a function of the wavelength and hence the frequency of the elastic wave. One can control a light beam in any arbitrary angle within a certain angular range with an arrangement of two deflectors connected one after another. The areas of application are mainly material processing with laser light, fast light pens and in combination with several colors, the reproduction of large-area color pictures in video technology. A measure of the efficiency of such devices is the elastooptical scattering factor $n^6p^2/\rho v^3$ containing the material properties contributing to the elastooptical effect. Especially important is the strong dependence on the refractive index. The response time of elastooptical devices is about a factor $10^5$ longer than with the electrooptical effect (ratio of the velocity of light to the velocity of sound).

Closely related to the piezooptical tensor is the piezodielectric tensor, which reproduces the change of the components of the dielectric tensor due to external mechanical stress

$$\Delta\epsilon_{ij} = Q_{ijkl}\sigma_{kl}.$$

The symmetry properties fully correspond to those of the piezooptical tensor. For the measurements, which so far have only been successful in a few cubic crystals, one uses the method discussed in Section 4.3.3 where the change in the capacity of a crystal plate is measure under the influence of mechanical stress. As we shall see in Section 5, there exists a close relationship between the piezodielectric and the quadratic electrostrictive tensor as well as the dependence of the elastic constants on the electric field.

### 4.5.10
### Second-Order Electrostrictive and Electrooptical Effects

The relationships

$$\varepsilon_{ij} = d_{ijkl} E_k E_l \quad \text{and} \quad \Delta a_{ij} = r_{ijkl} E_k E_l$$

describe, to a first approximation, the *electrostrictive* and the *electrooptical* effects respectively, not covered by the linear effects previously discussed. Both second-order effects appear in all substances since in contrast to the linear effects, there is no total existence constraint. The number and type of independent components of the tensors $\{d_{ijkl}\}$ and $\{r_{ijkl}\}$ was already discussed in Section 4.5.

Up until lately the opinion was that second-order electrostrictive effects were too small to be measured. Such effects were known only in the case of ferroelectric crystals or close to a phase transition. By using dynamic measurement techniques, employing lock-in amplification, the complete second-order electrostrictive tensors of numerous cubic crystals as well as that of rhombic calcium formate were recently determined (Bohatý & Haussühl, 1977). In doing so, the change in the length of the crystal in the longitudinal as well in the transverse arrangement, induced by double the frequency of the electric field was converted into a change in capacitance of a capacitor working as the frequency determining element in a high frequency oscillating circuit. Using an auxiliary crystal exhibiting a linear electrostrictive effect to which a voltage of double the frequency was applied in phase to the voltage at the test object, detuning of the capacitor could be compensated for by the quadratic effect. In this manner it was possible to detect changes in length of around $10^{-13}$m on probes with lengths of approximately 1 cm. All independent tensor components can be determined from longitudinal and transverse measurements in different orientations similar to first-order effects. The observed effects on a large collective of crystals were, in fact, found to be extremely small. Nevertheless, some interesting regularities could be uncovered, as, for example, the general phenomena of longitudinal dilatation and also volume expansion in an electric field. We will talk about the connection between second-order electrostriction and the pressure dependence of the dielectric tensor in due course. Second-order electrostriction also plays a decisive role in stimulated Brillouin scattering and in electrooptical effects.

The second-order electrooptical effect, also called the electrooptical Kerr effect, is in all details closely related to the piezooptical effect. The tensors of both effects have the same symmetry properties and the measurement arrangements are similar. In the absence of a linear effect, the change in the optical path difference of a plane parallel plate of thickness $L$, irradiated in

perpendicular incidence obeys

$$\Delta G = -\frac{L}{2}(n'^3_{jj} r'_{jjlm} - n'^3_{kk} r'_{kklm}) E'_l E'_m + (n'_{jj} - n'_{kk}) d'_{iilm} E'_l E'_m.$$

Propagation direction $\boldsymbol{e}'_i$ and the directions of vibration $\boldsymbol{e}'_j$ and $\boldsymbol{e}'_k$ are selected as in the corresponding relations of the piezooptical effect. An evaluation of the measurements of the change of the optical path under the action of an electric field, which are carried out in a manner completely analogous to the methods discussed for piezooptical measurements in Section 4.5.9.1, demand a knowledge of the second-order electrostrictive effect. The belief that this correction may be neglected was refuted by the investigations mentioned above. Rather, one observes that the electrostrictive contribution is of the same order of magnitude as the actual second-order electrooptical effect.

Simple measurement arrangements can be specified for crystals of the subgroup 22 which allow a reliable determination of the complete tensors with a minimum of effort. Table 4.15 presents the corresponding relations for cubic crystals.

Crystals with large coefficients of the second-order electrooptical effect can also be employed for the linear modulation of light. In this regard, one applies a high electrical dc voltage to the given crystal and superimposes this on the control voltage of the modulation. A $\Delta G$ then appears corresponding to the linear electrooptical effect, as is directly seen on the basis of the relationship given above for the optical path difference. This means that the second-order electrooptical effect may also be interpreted as a neutralization of the inversion center by the electric field.

### 4.5.11 Electrogyration

Optical activity can be induced or changed by external fields. In particular, certain crystals can first be optically active under the influence of an external field. We start from the relationship

$$D_i = \epsilon_{ij} E_j + g_{ijk} \frac{\partial E_j}{\partial x_k}$$

for optical activity (see Section 4.3.6.7) and assume a dependence of the components $g_{ijk}$ on the electric field strength given by $\Delta g_{ijk} = g_{ijkl} E_l$.

The *electrogyration tensor* $\{g_{ijkl}\}$ is, just as $\{g_{ijk}\}$, antisymmetric in both first index positions. Thus, it can be carried over to a third-order axial tensor as in $g_{ijkl} \rightarrow \gamma_{mkl}$ or $-\gamma_{mkl}$ with $m \neq i, j$ and $i, j, m$ cyclic or anticyclic in 1, 2, 3. Hence, the formulae derived in Section 4.3.6.7 can be used here when one writes the quantity $\gamma_{ij} + \gamma_{ijk} E_k$ instead of $\gamma_{ij}$.

The effects of electrogyration are most easily accessible in the propagation direction of optical isotropy. The situation is especially simple in crystals not possessing natural optical activity. The only cubic PSG in which a pure electrogyration effect appears is m3. In the cubic PSGs with fourfold axes, all components $g_{ijkl}$ vanish as one can directly establish by symmetry reduction. Both independent components $g_{1212}$ and $g_{2121}$ can exist in m3. Since, however, only the scalar product $\boldsymbol{G} \cdot \boldsymbol{g} = \gamma_{ij} g_i g_j$ or $\gamma_{ijk} g_i g_j E_k$ (see Section 4.3.6.7) enters into the equation for the refractive indices of optically active crystals in quasi-isotropy, both components cannot be separately determined by experiments measuring the refractive indices or related phenomena. This means only one independent component is effective. It is convenient to set $g_{1212} = \gamma_{312} = -g_{2121} = +\gamma_{321}$. The electrogyration effects a rotation of the plane of polarization of polarized light. The angle of rotation is given by the relation $\rho = \pi(n' - n'')/\lambda n$, discussed in Section 4.3.6.7, where $n' = n + \boldsymbol{g} \cdot \boldsymbol{G}$ and $n'' = n - \boldsymbol{g} \cdot \boldsymbol{G}$. The gyration vector is given by $G_i = \gamma_{ijk} g_j E_k$ when, as here, natural optical activity is missing. The following table presents some arrangements to be discussed for the measurement of electrogyration in PSG m3 ($q = \boldsymbol{E} \cdot \boldsymbol{a}$):

| $\boldsymbol{g} \parallel$ | $\boldsymbol{E} \parallel \boldsymbol{a}$ | $\boldsymbol{G}$ | $\boldsymbol{g} \cdot \boldsymbol{G}$ |
|---|---|---|---|
| [110] | [001] | $\frac{\sqrt{2}}{2} E_3 \gamma_{123} (\boldsymbol{e}_1 + \boldsymbol{e}_2)$ | $\gamma_{123} E_3$ |
| [001] | [$ab$0] | $\frac{1}{\sqrt{a^2+b^2}} \gamma_{123} \lvert\boldsymbol{E}\rvert \operatorname{sign} q (b\boldsymbol{e}_1 + a\boldsymbol{e}_2)$ | 0 |
| [1$\bar{1}$0] | [111] | $\frac{\sqrt{2}}{2} E_3 \gamma_{123} (-\boldsymbol{e}_1 + \boldsymbol{e}_2)$ | $-\frac{\sqrt{3}}{3} \gamma_{123} \lvert\boldsymbol{E}\rvert \operatorname{sign} q$ |
| [111] | [111] | $\frac{2}{\sqrt{3}} \gamma_{123} E_3 (\boldsymbol{e}_1 + \boldsymbol{e}_2 + \boldsymbol{e}_3)$ | $\frac{2}{\sqrt{3}} \gamma_{123} \lvert\boldsymbol{E}\rvert \operatorname{sign} q$ |
| [111] | [$ab.\bar{a} + b$] | *see* Exercise 33 | 0 |

If the propagation vector and the electric field lie parallel ($\boldsymbol{g} = \boldsymbol{E}/|\boldsymbol{E}|$), one obtains $\boldsymbol{g} \cdot \boldsymbol{G} = 6\gamma_{123} g_1 g_2 g_3 |\boldsymbol{E}|$. This means electrogyration vanishes in crystals of PSG m3 under longitudinal observation when $\boldsymbol{g}$ is normal to a twofold axis.

The measurement is best performed using a dynamic method in which an electric alternating field is applied to the crystal. The vibration of the plane of polarization oscillating with the same frequency as the field is measured with a lock-in amplifier (Weber & Haussühl, 1974). The effects observed on alums lie in the order of magnitude of $10^{-6}$ degree rotation of the plane of polarization per cm of irradiated length at a field strength of 1 V/cm. In isotypic crystals one observes marked changes of the coefficients $\gamma_{123}$ when one replaces symmetrical particles with antisymmetrical one, as, for example, in the $\beta$-alums of caesium and methyl ammonium (Weber & Haussühl, 1976). Little is known as yet concerning the electrogyration of other crystals.

### 4.5.12
### Piezoconductivity

The electric conductivity changes under the influence of an external mechanical stress. the relation is specified by

$$\Delta s_{ij} = w_{ijkl}\sigma_{kl}.$$

If one writes

$$\sigma_{mn} = c_{mnkl}\varepsilon_{kl}$$

for the stress tensor then

$$\Delta s_{ij} = w_{ijmn}c_{mnkl}\varepsilon_{kl} = y_{ijkl}\varepsilon_{kl}.$$

The tensors $\{w_{ijkl}\}$ and $\{y_{ijkl}\}$ are of type A and exist in all PSGs.

The corresponding effects also occur in thermal conductivity and in bulk conductivity.

The measurement of piezoconductivity is best performed with the help of longitudinal and transverse effects, whereby the change in the current density is observed as a function of hydrostatic or uniaxial pressure. The measurement scheme, even with triclinic crystals, is so simple that it can be effortlessly educed by the reader. If periodic changes in pressure are employed, one achieves, through lock-in amplification of the resulting change in current density, a high sensitivity.

Up to now, complete tensors have only been found for a few materials.

The effect also appears naturally in polycrystalline materials. The change in resistance of metal wires, as used in strain gauges, is based on piezoconductivity. High pressure sensors, where a change in the electrical resistance provides information on the prevalent pressure are also examples of the application of piezoconductivity.

## 4.6
## Higher Rank Tensors

### 4.6.1
### Electroacoustical Effects

Analogous to the electrooptical effect, an electrically induced change in the propagation direction of elastic waves may appear: *electroacoustical effect*. The tensorial description is

$$\Delta c_{ijkl} = z_{ijklm}E_m + z_{ijklmn}E_mE_n + \cdots$$

The polar tensor $\{z_{ijklm}\}$ only exists in acentric crystals except in PSG 43, whereas the tensor $\{z_{ijklmn}\}$ appears in all PSGs. The change of the elastic constants $\Delta c_{ijkl}$ leads, via the elastodynamic basic equations, to a change in the propagation velocities of the elastic waves. The measurement of this very small effect is exacerbated by the fact that first- or second-order electrostriction becomes effective, which may cause a change in the dimensions and density of the crystal. These contributions can be calculated with knowledge of the elastic, piezoelectric or electrostrictive coefficients and used for correction of the measured change of the propagation velocities according to the method discussed in Section 4.5.6. So far only isolated measurements of this type have been successful. The connection between the coefficients of the electroacoustical effect and the second-order piezoelectric effect, represented by

$$D_i = d_{ijklm}\sigma_{jk}\sigma_{lm}$$

is referred to in Section 5. $\sigma_{ij}$ are the components of the mechanical stress tensor.

### 4.6.2 Acoustical Activity

Analogous to optical activity, there also exists the phenomenon of *acoustical activity*, specified by the fifth-rank tensor $\{c_{ijklm}\}$, the gyration tensor, which can be represented by the following relationship:

$$\sigma_{ij} = c_{ijkl}\varepsilon_{kl} + c_{ijklm}\frac{\partial \varepsilon_{kl}}{\partial x_m}.$$

Just as with optical activity, we also set the condition that wave propagation progresses without additional energy terms. The elastic energy content is then

$$\Delta W = \sum_{i,j}\int \sigma_{ij}d\varepsilon_{kl} = \sum_{i,j}\int c_{ijkl}\varepsilon_{kl}d\varepsilon_{ij} + \sum_{i,j}\int c_{ijklm}\frac{\partial \varepsilon_{kl}}{\partial x_m}d\varepsilon_{ij}.$$

The second term, in the case of plane waves

$$\xi = \xi_0 e^{2\pi i(\boldsymbol{k}\cdot\boldsymbol{x}-\nu t)} \quad \text{with} \quad \varepsilon_{ij} = \frac{1}{2}\left(\frac{\partial \xi_i}{\partial x_j} + \frac{\partial \xi_j}{\partial x_i}\right)$$

takes the form

$$\sum_{i,j}\int 2\pi i k_m c_{ijklm}\varepsilon_{kl}d\varepsilon_{ij}.$$

This expression vanishes when $c_{ijklm} = -c_{ijlkm}$, i.e., when the gyration tensor is antisymmetric with respect to the 3. and 4. index position. Since the gyration tensor is an odd-rank polarer tensor, there exists no acoustical activity in

centrosymmetric crystals. With pure transverse waves, in certain preferential directions, a rotation of the plane of vibration is observed, namely along the so-called acoustic axes in which two transverse waves of equal velocity can propagate, similar to optical activity. From this rotation one can determine individual components of the gyration tensor. The measurement of rotation is possible with the help of pulsed ultrasound methods, whereby the pulses are recorded with a piezoelectric transverse oscillator, connected as a detector, after traveling through the crystal. The rotation can be determined, after making corrections for reflection and damping losses, from the amplitude of the signals generated by the pulses. The amplitudes are functions of the setting of the direction of vibration of the decor to the direction of vibration of the primary transverse sound generator. In arbitrary directions, the effects of acoustical activity are largely masked by anisotropy and optical activity. In this case the elastic waves take on a rather complicated form so that an analysis of this effect is experimentally laborious.

### 4.6.3 Nonlinear Elasticity: Piezoacoustical Effects

Hooke's law, i.e., the linear relationship between stress and deformation is a sufficient approximation for most elastic interactions as long as the stress is kept adequately small. Contrary to the long held opinion that deviations from Hooke's law are difficult to measure, the situation in the meantime has completely changed. The methods described in Section 4.5.6 allow observations of deviations from Hooke's law already with mechanical stresses of a few Newton/cm$^2$. We use the Lagrangian deformation tensor as an inducing quantity to describe these elastic nonlinearities and specify the following relationship:

$$\sigma_{ij} = c_{ijkl}\eta_{kl} + c_{ijklmn}\eta_{kl}\eta_{mn} + c_{ijklmnop}\eta_{kl}\eta_{mn}\eta_{op} + \cdots$$

For small deformation, $c_{ijkl}$ are identical with the components of the elasticity tensor defined in Section 4.5.1.

The components of the sixth-rank tensor are designated as *third-order elastic constants* and those of the eighth-rank tensor as *fourth-order elastic constants*. We recall that

$$\eta_{kl} = \frac{1}{2}\left(\frac{\partial\xi_k}{\partial x_l} + \frac{\partial\xi_l}{\partial x_k}\right) + \frac{1}{2}\frac{\partial\xi_m}{\partial x_k}\frac{\partial\xi_m}{\partial x_l}.$$

The first term corresponds to the components of the ordinary deformation tensor. Here, the pair-wise permutability of the indices follows from the reversibility of the deformation work, just as with the elasticity tensor, hence, for example,

$$c_{ijklmn} = c_{klmnij} = c_{mnklij} = \cdots$$

**Table 4.16** Number of independent components of the elasticity tensors of fourth, sixth, and eighth rank.

| Laue group | $\bar{1}$ | 2/m | 2/mm | $\bar{3}$ | $\bar{3}$m | 4/m | 4/mm |
|---|---|---|---|---|---|---|---|
| $Z(c_{ijkl})$ | 21 | 13 | 9 | 7 | 6 | 7 | 6 |
| $Z(c_{ijklmn})$ | 56 | 32 | 20 | 20 | 14 | 16 | 12 |
| $Z(c_{ijklmnop})$ | 126 | 70 | 42 | 42 | 28 | 36 | 25 |
| Laue group | 6/m, $\infty/m$ | 6/mm, $\infty$/mm | m3 | 4/m3 | $\infty$/m$\infty$ | | |
| $Z(c_{ijkl})$ | 5 | 5 | 3 | 3 | 2 | | |
| $Z(c_{ijklmn})$ | 12 | 10 | 8 | 6 | 3 | | |
| $Z(c_{ijklmnop})$ | 24 | 19 | 14 | 11 | 4 | | |

The indices within the pairs are naturally permutable due the the symmetry of the stress- and deformation tensor. Symmetry reduction in the individual PSGs is performed in a manner similar to the procedures discussed earlier. Table 4.16 presents the number $Z$ of independent components of the tensor $\{c_{ijklmn}\}$ for the eleven Laue groups.

Cubic crystals with fourfold axes are distinguished from those with twofold axes. In abbreviated notation, the independent components are

- m3, 23 (Laue group m3): $c_{111}$, $c_{112}$, $c_{113}$, $c_{123}$, $c_{144}$, $c_{155}$, $c_{166}$, $c_{456}$
- 4/m3, 43, $\bar{4}3$ (Laue group 4/m3): $c_{111}$, $c_{112}$ $c_{123}$, $c_{144}$, $c_{166}$, $c_{456}$.

Only three independent components exist in isotropic substances $c_{111}$, $c_{112}$, $c_{123}$. Furthermore, $c_{144} = (c_{111} - c_{123})/2$, $c_{166} = (c_{111} - c_{112})/4$ and $c_{456} = (c_{111} - 3c_{112} + 2c_{123})/8$, as is established from the condition of invariance of an arbitrary rotation about an arbitrary axis, for example, $\boldsymbol{e}_3$ (see Exercise 35).

One important aspect of nonlinear elastic behavior is exhibited by the dependence of the elastic constants on hydrostatic pressure, described by the coefficients $dc_{ij}/dp$ (see Section 4.5.8). The connection of these coefficients with the third-order elastic constants is found from the relationships to be discussed below.

The complete determination of third-order elasticity tensors requires a carefully prepared strategy. A method, since found to be successful, was proposed by Thurston & Brugger (1964). An exposition of this method is found in an overview article by Wallace (1970). One measures changes in delay times or shifts in the resonance frequencies of plane parallel plates under the influence of external hydrostatic and uniaxial stress. These effects correspond to those of piezooptics, whereby here, however, only "absolute measurements," i.e., measurements of the absolute changes in velocity are taken into consideration, because a quantitative analysis of the interference of elastic waves would require a much too higher effort.

We now want to outline the considerations establishing a connection between piezoacoustical effects and nonlinear elastic properties. In an experiment we compare the delay time of a sound pulse or the resonance frequencies of plane parallel plates with and without a state of external stress characterized by $\{\sigma_{ij}^0\}$. In both situations, the elastodynamic basic equations in the form

$$\frac{\partial \sigma_{ij}}{\partial x_j} = \rho \frac{\partial^2 \xi_i}{\partial t^2}$$

are valid. The familiar equations $(-\rho^0 v^{02}\delta_{ik} + c_{ijkl}^0 g_j g_l)\xi_k = 0$ $(i = 1, 2, 3)$ result from the prestress-free state. Furthermore, the coordinates of a mass point in the stress-free state are specified by $x_i^0$ and in the prestressed crystal by $x_i$. The same applies to all other quantities. The prestresses $\sigma_{ij}^0$ induce the deformations $\eta_{ij} = s_{ijkl}^0 \sigma_{kl}^0$. The deformations carry over the fixed material position vector $\boldsymbol{x}^0$ into a position vector $\boldsymbol{x}$, referred to the same Cartesian coordinate system, according to

$$x_i = x_i^0 + \frac{\partial x_i}{\partial x_j^0} x_j^0 = (\delta_{ij} + \eta_{ij}) x_j^0 = u_{ij} x_j^0.$$

We assume that no rotational components appear. Formally, we can interpret this relationship as a coordinate transformation from a Cartesian base system to a nonlinear coordinate system among others. The components of the elasticity tensor are now to be transformed in accordance with this transformation. However, when we wish to keep the original Cartesian system as the coordinate system, we must guarantee the invariance of the density of the elastic deformation work. This is accomplished by furnishing all transformed quantities with the factor $V^0/V = |u_{ij}|^{-1}$. $|u_{ij}|$ are also called the Jacobian determinants. Accordingly, the components of the elasticity tensor are then

$$c'_{ijkl} = |u_{ij}|^{-1} u_{ir} u_{js} u_{kt} u_{lv} c_{rstv}^0.$$

Writing $u_{ij} = (\delta_{ij} + \eta_{ij})$ and expanding the deformation tensor $\eta_{ij}$ to first order, taking into account $|u_{ij}|^{-1} = (1 + \eta_{11} + \eta_{22} + \eta_{33} + \cdots)^{-1} = (1 - \eta_{11} - \eta_{22} - \eta_{33} \cdots)$, gives

$$c'_{ijkl} = (1 - \delta_{rs}\eta_{rs}) c_{ijkl}^0 + c_{ijkr}^0 \eta_{lr} + c_{ijrl}^0 \eta_{kr} + c_{irkl}^0 \eta_{jr} + c_{rjkl}^0 \eta_{ir}.$$

The corresponding transformation of the components $c_{ijklmn}$ delivers, for the effective components $c_{ijkl}$, the contribution $c_{ijklmn}\eta_{mn}$ as the lowest order term in $\eta_{ij}$. Hence, we have

$$c_{ijkl} = c'_{ijkl} + c_{ijklmn}\eta_{mn}.$$

Thus the deformations generated by an elastic wave $\boldsymbol{\xi} = \boldsymbol{\xi}_0 e^{2\pi i(\boldsymbol{k}\cdot\boldsymbol{x}-\nu t)}$ superimpose on the deformations generated by the prestresses. We require the resulting total stress $\sigma_{ij}$. This is calculated in an analogous fashion to $c_{ijkl}$, employing, however, that transformation describing the change of the coordinates of the position vector of the prestressed state to the effective state described by the deformation resulting from the elastic waves. It is

$$x_i' = x_i + \Delta\xi_i = x_i + \frac{\partial \xi_i}{\partial x_j} x_j = \left(\delta_{ij} + \frac{\partial \xi_i}{\partial x_j}\right) x_j = u_{ij}' x_j.$$

Hence, $\sigma_{ij}' = |u_{ij}'|^{-1} u_{ir}' u_{js}' \sigma_{rs}^0$, where $\sigma_{ij}^0$ is the prestress. Expanding again, to a first approximation with respect to the deformation quantities $\partial\xi_i/\partial x_j$, one finds

$$\sigma_{ij}' = \left(1 - \frac{\partial \xi_k}{\partial x_k}\right)\sigma_{ij}^0 + \frac{\partial \xi_j}{\partial x_k}\sigma_{ik}^0 + \frac{\partial \xi_i}{\partial x_k}\sigma_{kj}^0.$$

Together with the deformation of the elastic waves gives

$$\sigma_{ij} = \sigma_{ij}' + c_{ijkl}\varepsilon_{kl}.$$

The elastodynamic basic equations then take on the following form:

$$\frac{\partial \sigma_{ij}}{\partial x_j} = (\sigma_{lj}^0 \delta_{ik} + c_{ijkl}) \frac{\partial^2 \xi_k}{\partial x_j \partial x_l} = \rho \frac{\partial^2 \xi_i}{\partial t^2}.$$

Using the plane wave approach results in

$$-\rho v^2 \xi_i + (\sigma_{lj}^0 \delta_{ik} + c_{ijkl}) g_j g_l \xi_k = 0.$$

To an approximation, one may assume that the position of the propagation vector and the deformation vector depend on the prestress $\sigma_{ij}^0$. Multiplying the above equation with $\xi_i$ and summing over $i$ gives

$$\rho v^2 = (\sigma_{lj}^0 \delta_{ik} + c_{ijkl}) g_j g_l \xi_i \xi_k / \boldsymbol{\xi}^2.$$

The values derived above are inserted for $c_{ijkl}$. Substituting the deformation $\eta_{ij}$ by $s_{ijkl}^0 \sigma_{kl}^0$, which is approximately correct, explicitly gives $\rho v^2$ as a function of the prestress $\sigma_{ij}^0$ and hence

$$\begin{aligned}\frac{\partial \rho v^2}{\partial \sigma_{pq}^0} &= g_p g_q + \frac{\partial c_{ijkl}}{\partial \sigma_{pq}^0} g_j g_l \xi_i \xi_k / \boldsymbol{\xi}^2 \\ &= g_p g_q + (-c_{ijkl}^0 s_{rspq}^0 \delta_{rs} + c_{ijkr}^0 s_{lrpq}^0 + c_{ijrl}^0 s_{krpq}^0 + c_{irkl} s_{jrpq}^0 \\ &\quad + c_{rjkl}^0 s_{irpq}^0 + c_{ijklmn} s_{mnpq}) g_j g_l \xi_i \xi_k / \boldsymbol{\xi}^2.\end{aligned}$$

With the help of these relationships, the components of the third-order elasticity tensor can be determined in a given propagation direction and position of the deformation tensor and with known elastic constants. If one works with static prestresses, which can be of hydrostatic or uniaxial nature, the isothermal constants must be inserted for $s^0_{ijkl}$. For sound propagation, one employs the adiabatic constants $c^0_{ijkl}$. The connection between isothermal and adiabatic quantities is discussed in Section 5.2. The third-order constants are a mixture of isothermal–adiabatic types. However, a closer inspection has shown that the difference between isothermal and adiabatic or third-order mixed constants is so small that they are hardly measurable (Guinan & Ritchie, 1970). Conveniently one employs computer programs to evaluate measurements performed under hydrostatic pressure and uniaxial stress. A direct evaluation is possible with cubic crystals. From the equation above, one obtains the following relationship for the pressure dependence of the elastic constants ($-p = \sigma^0_{11} = \sigma^0_{22} = \sigma^0_{33}$) of cubic crystals

$$\frac{dc_{11}}{dp} = -1 - (K^0/3)(c^0_{11} + c_{111} + c_{112} + c_{113}) \quad \text{with} \quad g_1 = \xi_1/|\boldsymbol{\xi}| = 1,$$

$$\frac{dc_{44}}{dp} = -1 - (K^0/3)(c^0_{44} + c_{144} + c_{155} + c_{166}) \quad \text{with} \quad g_1 = \xi_2/|\boldsymbol{\xi}| = 1,$$

$$\frac{d(c_{11} - c_{12})/2}{dp} = -1 - (K^0/3)(c^0_{11} - c^0_{12} + c_{111} - c_{123})/2 \quad \text{with}$$

$$g_1 = g_2 = \xi_1/|\boldsymbol{\xi}| = -\xi_2/|\boldsymbol{\xi}| = \sqrt{2}/2,$$

and hence,

$$\frac{dc_{12}}{dp} = 1 - (K^0/3)(c^0_{12} + c_{112} + c_{113} + c_{123}),$$

where $K^0$ is the volume compressibility

$$K^0 = 3(s^0_{11} + 2s^0_{12}) = 3(c^0_{11} + 2c^0_{12})^{-1}.$$

Similar relationships result for the dependence of the constants $c_{11}$ and $c_{44}$ on uniaxial pressure parallel or normal to the propagation direction [100] (see Exercise 36). It follows that the pressure dependence of the reciprocal volume compressibility, an important scalar invariant, is given by

$$\frac{dK^{-1}}{dp} = \frac{d(c_{11} + 2c_{12})}{3dp} = -(K^0/9)(c_{111} + 3c_{112} + 3c_{113} + 2c_{123})$$

whereby the difference between isothermal and adiabatic compressibility was neglected. The above expression is identical, except for the factor $-K^0/27$, to the invariants $c_{ijklmn}\delta_{ij}\delta_{kl}\delta_{mn}$.

Elastic nonlinearity, analogous to dielectric nonlinearity, generates, from an incident wave a frequency doubled secondary wave which can be used to a certain extent to measure nonlinear elastic properties. However, acoustic frequency doubling does not come into consideration as a precise measurement of routine nonlinear elastic properties.

If one takes into account higher order deformations in the relationships derived above, then fourth and higher order elasticity tensors come into play which are only partially and with low accuracy accessible to measurement.